

พฤติกรรมการ์ดของโครงถักเหล็กอัดแรงภายหลัง ด้วยคอนกรีตสมรรถนะสูงเป็นพื้นเชิงประกอบ



นาย กนกพัฒน์ ชาญไวยวิทย์

ศูนย์วิทยพัทยากร  
จุฬาลงกรณ์มหาวิทยาลัย

วิทยานิพนธ์นี้เป็นส่วนหนึ่งของการศึกษาตามหลักสูตรปริญญาวิศวกรรมศาสตรดุษฎีบัณฑิต

สาขาวิชาวิศวกรรมโยธา ภาควิชาวิศวกรรมโยธา

คณะวิศวกรรมศาสตร์ จุฬาลงกรณ์มหาวิทยาลัย

ปีการศึกษา 2553

ลิขสิทธิ์ของจุฬาลงกรณ์มหาวิทยาลัย

FLEXURAL BEHAVIOR OF POST-TENSIONED STEEL TRUSSES WITH  
HIGH PERFORMANCE CONCRETE COMPOSITE DECKS



Mr. Kanokpat Chanvaivit

ศูนย์วิทยทรัพยากร  
จุฬาลงกรณ์มหาวิทยาลัย  
A Dissertation Submitted in Partial Fulfillment of the Requirements  
for the Degree of Doctor of Philosophy Program in Civil Engineering

Department of Civil Engineering

Faculty of Engineering

Chulalongkorn University


Academic year 2010

Copyright of Chulalongkorn University

Thesis Title FLEXURAL BEHAVIOR OF POSTTENSIONED STEEL  
TRUSSES WITH HIGH PERFORMANCE CONCRETE  
COMPOSITE DECKS  
By Mr. Kanokpat Chanvaivit  
Field of Study Civil Engineering  
Thesis Advisor Professor Ekasit Limsuwan, Ph.D


---

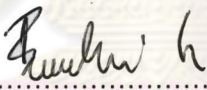
Accepted by the Faculty of Engineering, Chulalongkorn University in Partial  
Fulfillment of the Requirements for the Doctoral Degree

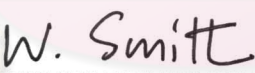
  
..... Dean of the Faculty of Engineering  
(Associate Professor Boonsom Lerthirunwong, Dr.Ing.)

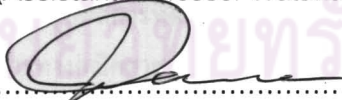
THESIS COMMITTEE

  
.....Chairman  
(Professor Thaksin Thepchatr, Ph.D)

  
.....Thesis Advisor  
(Professor Ekasit Limsuwan, Ph.D)

  
.....Examiner  
(Associate Professor Boonchai Stitmannathum, D.Eng)

  
.....Examiner  
(Assistant Professor Watanachai Smittakorn, Ph.D)

  
.....External Examiner  
(Professor John L. Dawe, Ph.D)

ศูนย์วิทยทรัพยากร  
จุฬาลงกรณ์มหาวิทยาลัย

กนกพัฒน์ ชาญไวยวิทย์ : พฤติกรรมการคดของโครงถักเหล็กอัดแรงภายหลัง ด้วยคอนกรีตสมรรถนะสูงเป็นพื้นเชิงประกอบ. (FLEXURAL BEHAVIOR OF POSTTENSIONED STEEL TRUSSES WITH HIGH PERFORMANCE CONCRETE COMPOSITE DECKS) อ. ที่ปรึกษาวิทยานิพนธ์หลัก : ศ.ดร.เอกสิทธิ์ ลิ้มสุวรรณ , 163 หน้า.

สมมติฐานการประยุกต์ใช้วิธีการคึงลวดอัดแรงภายหลังเพื่อเสริมสมรรถภาพ โครงถักเหล็กด้วยคอนกรีตสมรรถนะสูงเป็นพื้นเชิงประกอบ ได้มีการทดสอบและประเมินค่าทั้ง โดยการทำกรทดลองและการวิเคราะห์ทางทฤษฎี หลักการของวิธีการนี้คือการคึงลวดอัดแรงกำลังสูงภายนอกเพื่อสร้างหน่วยแรงอัดในโครงสร้างในทิศทางที่หักล้างกันกับหน่วยแรงคึงที่เกิดจากน้ำหนักบรรทุกภายนอกและศึกษาผลทางด้านพฤติกรรมการรับแรงคดของโครงสร้าง ส่วนทฤษฎีหลักที่ใช้ในการวิเคราะห์คือทฤษฎีหน้าตัดแปลง ทฤษฎีงานสมมติ และทฤษฎีพฤติกรรมเชิงเส้นและหลักการของการรวมผล การทดลองประกอบไปด้วยโครงถักเหล็กขนาดเท่าของจริงจำนวน 2 ชุด วางอยู่บนที่รองรับช่วงเดียวที่ปลายทั้งสองด้านและทดสอบด้วยน้ำหนักบรรทุกที่เพิ่มขึ้นด้วยอัตราคึงที่ ณ ที่จุดหนึ่งในสาม และสองในสาม ของช่วงที่รองรับทั้งสองด้านแบบสมมาตรกัน ตัวแปรต้นที่ใช้ในการทดลองคือปริมาณ และแรงคึงภายในลวดอัดแรงที่กระทำกับโครงถักเหล็กอันมีพื้นเชิงประกอบ และ โครงถักเหล็กขนาดเท่ากันแต่ไม่มีพื้นเชิงประกอบ ผลการทดสอบปรากฏว่า สำหรับการเพิ่มลวดอัดแรงเข้ากับ โครงถักเหล็กอันมีพื้นเชิงประกอบจำนวน 7.9% ของพื้นที่หน้าตัดขององค์อาคารหลักรับแรงคึงของ โครงถักเหล็ก ส่งผลให้สามารถรับน้ำหนักบรรทุกทุกระยะได้เพิ่มขึ้นถึง 20.4% เมื่อเทียบกับกรณีของ โครงถักเหล็กอันมีพื้นเชิงประกอบแต่ไม่มีลวดอัดแรง ทั้งนี้การวิบัติของ โครงถักเหล็กอันมีพื้นเชิงประกอบและมีลวดอัดแรงภายหลังนั้นเกิดขึ้นเมื่อหน่วยแรงคึงในองค์อาคารหลักรับแรงคึงของ โครงถักเหล็กถึงจุดคราก ในขณะที่หน่วยแรงคึงในลวดอัดแรงนั้นยังอยู่ในช่วงสภาวะอีลาสติกส่งผลให้การวิบัติเป็นไปแบบที่โครงสร้างมีการเสียรูปได้มากก่อนเกิดการวิบัติแบบฉับพลัน อันจะสามารถใช้เป็นสัญญาณเตือนภัยได้เป็นอย่างดี สรุปผลการทดลองสอดคล้องกับการวิเคราะห์ทางทฤษฎีเป็นอย่างดี และสามารถนำเอาทฤษฎีและสมการทางคณิตศาสตร์ที่ได้จากการวิเคราะห์ต่างๆซึ่งผ่านการสนับสนุนจากผลการทดลองนี้ไปใช้ในการคาดการณ์และอธิบายพฤติกรรมการคดทั้งด้านกำลังและสภาวะการใช้งาน รวมไปถึงสามารถใช้ในการหาปริมาณลวดอัดแรงที่ต้องการ ในการซ่อมหรือเสริมสมรรถภาพ โครงถักเหล็กที่มีพื้นเชิงประกอบ ทั้งโครงสร้างแบบสะพานหรือ โครงสร้างในอาคาร โดยคำนึงถึงสภาวะการใช้งาน ความสามารถในการเสียรูปได้มากก่อนเกิดการวิบัติ และความคงทนต่อสภาวะแวดล้อมของโครงสร้างนั้น

ภาควิชาวิศวกรรมโยธา ลายมือชื่อนิติ.....  
 สาขาวิชาวิศวกรรมโยธา ลายมือชื่อ.ที่ปรึกษาวิทยานิพนธ์หลัก.....  
 ปีการศึกษา.....2553

# # 4671801721 : MAJOR CIVIL ENGINEERING

KEYWORDS : POST-TENSIONING / COMPOSITE / STEEL TRUSSES / CONCRETE DECKS / UNBONDED MONO STRAND TENDONS

KANOKPAT CHANVAIVIT : FLEXURAL BEHAVIOR OF POSTTENSIONED STEEL TRUSSES WITH HIGH PERFORMANCE CONCRETE COMPOSITE DECKS. THESIS ADVISOR: PROF. EKASIT LIMSUWAN, Ph.D, 163 pp.

The hypothesis of using post-tensioning techniques in strengthening in situ steel trusses built compositely with high performance concrete decks is examined and evaluated experimentally and theoretically. In realizing the proposed technique, unbonded high-strength tendons are prestressed externally to provide axial compression to counteract tensile stresses caused by external loading. The effects of post-tensioning on composite truss systems are investigated as related to flexural strength and behavior. The analytical portion of the research utilizes a technique which incorporates the concepts of transformed section, principle of virtual work, and principle of superposition. In the experimental portion of the study, two full size truss specimens were simply supported at their ends and subjected to third-point monotonically increasing loads. Experimental parameters included the level of post-tensioning as applied to a complete composite system and a nominally identical truss only, without a concrete slab. Test results indicated that for the extra partial prestressing ratio (PPR) of 6.12%, the post-tensioned composite truss resisted a maximum total load 20.4% higher than that in the case of a composite truss without prestressing. The failure mode of the posttensioned composite truss occurred by yielding of the bottom chord while the tendon was still within the elastic range. This behavior resulted in a ductile failure mode displaying detectable warning deformation and is therefore preferred to sudden failure occurring without any noticeable ductile deformations. Good agreement between experimental and theoretical results was attained. The successfully developed and verified mathematical model is capable of evaluating the strength and stability of in situ structures similar to the type studied herein. The model can also be used to establish the maximum amount of post-tensioning required for structural rehabilitation as well as to evaluate the associated serviceability, and ductility factors. Such information can then be used for upgrading existing composite spans such as may be found in bridges or buildings and thereby to upgrade the flexural capacity of such linear structures by taking advantage of the high strength tendons.

Department : Civil Engineering

Student's Signature 

Field of Study : Civil Engineering

Advisor's Signature 

Academic Year : 2010

## ACKNOWLEDGEMENTS

First I would like to thank my research advisor, Prof. Dr. Ekasit Limsuwan for giving me opportunity, his experience suggestion and understanding while doing research. I wish to express to him all my gratitude.

Great appreciation goes to Thailand Research Fund (TRF) for the Royal Golden Jubilee Ph.D. Program scholarship (Grant No. PHD/0257/2545) With this fund, I had a chance to study at the University of Texas at Austin, Texas, U.S.A. with Professor Richard E. Klingner with a good laboratory experience for five months and also the return tickets and three month expenses while I studied at the University of New Brunswick at Fredericton, New Brunswick, Canada.

For my full scale experimental study, It was conducted in the structural laboratory, at the Department of Civil Engineering, University of New Brunswick, Fredericton, Canada. Funding by the National Sciences and Engineering Research Council of Canada (NSERC) is greatly appreciated along with contributions from DSIAmerica for tendons, LaFarge for the high performance concrete and PCA.

I would like to sincerely thank Prof. Dr. John L. Dawe from the Department of Civil Engineering, UNB Fredericton for continuous support since we knew each other in 2006, for helpful guidance, for reviewing all of my research papers, for helping me fight through all obstructions and for encouraging me for a long time.

I also wish to express my gratitude to all of my teachers, friends, laboratory colleagues, machinists and technicians for their help in studying, living and conducting experiments.

Finally, special thanks go to my beloved family for their support, my wife and my precious baby daughter for standing with me throughout this endeavor.

# CONTENTS

	Page
Abstract (Thai).....	iv
Abstract (English).....	v
Acknowledgements.....	vi
Contents.....	vii
List of Tables.....	xi
List of Figures.....	xii
Chapter I: Introduction.....	1
1.1 Research Background.....	1
1.2 Literature Reviews.....	2
1.3 Research Objectives.....	5
1.4 Research Scope.....	5
1.5 Research Significance.....	6
1.6 Research Program.....	6
1.7 Research Overview.....	7
Chapter II: Theoretical Study of Prestressed Composite Trusses.....	8
2.1 Composite Structures.....	8
2.1.1 Composite Action.....	8
2.1.2 Degree of Composite Action.....	14
2.1.3 Composite Truss.....	15
2.2 Posttensioned Composite Structures.....	17
2.3 Behavior of Posttensioned Composite Truss.....	30
2.3.1 Flexural Behavior.....	30
2.3.2 Semi Rigid Joint Behavior.....	34
2.3.3 Lateral Stability of Bottom Chords.....	36
2.3.4 Losses of Prestress.....	39
2.3.4.1 Shrinkage.....	39

	Page
2.3.4.2 Creep.....	41
2.3.4.3 Anchorage Seating.....	43
2.3.4.4 Relaxation.....	43
Chapter III: Experimental Study.....	44
3.1 Test Program.....	44
3.2 Test Specimens.....	45
3.3 Test Materials.....	54
3.4 Test Instrumentations.....	61
3.5 Test Procedures.....	63
3.6 Test Results.....	64
3.6.1 Overview of the Test Results.....	64
3.6.2 Measured Pre Camber.....	70
3.6.3 Measured Load and Mid Span Deflection Curves.....	71
3.6.4 Measured Load and Member Stress Curves.....	75
3.6.5 Measured Load and Slip Curves.....	85
3.6.6 Measured Load and Horizontal Movement Curves.....	88
3.6.7 Test Summary.....	89
Chapter IV: Analytical Study.....	91
4.1 Comparison of Theoretical and Experimental Results.....	91
4.1.1 Pre Camber .....	91
4.1.2 Load vs. Mid Span Deflection Curves.....	93
4.1.3 Load and Element Stress Analysis.....	99
4.1.4 Moment and Curvature Curves.....	101
4.1.5 Load and Slip Curves.....	103
4.1.6 Load and Lateral Movement Curves.....	104
4.2 Analysis of Semi Rigid Joint Behavior.....	106
4.3 Analysis of Concrete Strength Effects.....	111



	Page
4.4 Analysis of Percentage of Tendon Reinforcement Effects.....	115
4.4.1 Effect of percentage of Tendon Reinforcement to the ultimate moment capacity.....	115
4.4.2 Effect of percentage of Tendon Reinforcement to rotation capacity.....	117
4.4.3 Effect of percentage of Tendon Reinforcement to cracking of the concrete top surface.....	119
4.4.4 Effect of percentage of Tendon Reinforcement to the effective moment of inertia of the composite truss.....	120
4.5 Analysis of Shrinkage, Creep, Anchorage Seating and Relaxation Effects.....	122
4.5.1 Analysis of Shrinkage Effect.....	122
4.5.2 Analysis of Creep Effect.....	126
4.5.3 Analysis of Anchorage Seating Effect.....	128
4.5.4 Analysis of Relaxation Effect.....	129
Chapter V: Model of Prestressed Composite Truss.....	130
5.1 Strength and Stability.....	130
5.1.1 Flexural Strength.....	130
5.1.1.1 Ultimate Moment Capacity.....	130
5.1.1.2 Ultimate Shear Capacity.....	132
5.1.1.3 Ultimate Shear Stud Connector Capacity.....	132
5.1.2 Maximum of Posttensioning Tendon.....	134
5.1.2.1 Yielding of Bottom Chord Criteria.....	134
5.1.2.2 Yielding of Web Member Criteria.....	134
5.1.2.3 Cracking of Top Surface Concrete Criteria.....	135
5.1.2.4 Buckling of Bottom Chord Criteria.....	135
5.1.2.5 Buckling of Web Member Criteria.....	136
5.1.2.6 Buckling of Top Chord Criteria.....	136

	Page
5.1.2.7 Tendon Strength Criteria.....	137
5.1.2.8 Pre Camber Criteria.....	137
5.1.2.9 Losses of Prestress Criteria.....	137
5.2 Ductility .....	139
5.3 Serviceability.....	141
Chapter VI: Conclusions.....	145
6.1 General Observations.....	145
6.2 Research Conclusions.....	146
References.....	148
Appendix.....	152
Biography.....	163



ศูนย์วิทยทรัพยากร  
 จุฬาลงกรณ์มหาวิทยาลัย

## LIST OF TABLES

Tables	Page
3.1 Test program.....	44
3.2 Concrete compressive strength tests of 7 day concrete.....	54
3.3 Coupon tensile strength test data.....	57
3.4 Coupon tensile strength test results.....	58
3.5 Precamber and the yield loads at various prestress levels.....	70
3.6 Summary of test results.....	89
4.1 Theoretical and experimental precamber at various levels of prestress.	92
4.2 Plot data for the theoretical load-deflection curve.....	97
4.3 Shear stud strength.....	103
4.4 The free and restrain shrinkage calculation.....	124
4.5 Free shrinkage strain and shrinkage deflection.....	124
A.1 Precamber from the prestressing force at 460MPa on composite truss.	153
A.2 Precamber from the prestressing force at 690MPa on composite truss.	154
A.3 Precamber from the prestressing force at 920MPa on composite truss.	155
A.4 Vertical deformation from the steel dead load.....	156
A.5 Vertical deformation from the concrete dead load.....	157
A.6 Total elongation of the steel truss at the same level of the tendon due to the external load from the external ram load of 58ton(yield load), $\delta_{1p}$	158
A.7 Total elongation of the steel truss at the same level of the tendon due to the unit load in tendon, $\delta_{11}$ .....	159
A.8 Vertical deformation due to increase of tendon load, $\Delta T$ .....	160
A.9 Vertical deformation due to the external ram loads.....	161
A.10 Precamber from the prestressing force at 920MPa by fixed joint assumption.....	162

## LIST OF FIGURES

Figures	Page
2.1 Composite truss stress diagrams.....	8
2.2 Interface shearing stress of the composite truss section of length $dx$ ...	9
2.3 Push-out test specimens.....	11
2.4 Typical load and slip curve.....	12
2.5 Degree of the composite action.....	14
2.6 Flexural capacity of a composite truss.....	15
2.7 Typical posttensioned composite trusses.....	17
2.8 Typical posttensioned composite truss member designations.....	21
2.9 Uniform distributed load on a posttensioned composite truss.....	21
2.10 Tendon load on a posttensioned composite truss.....	23
2.11 Increase in tendon force due to the external load $P_{ext}$ .....	24
2.12 Compatibility condition for an increase in tendon force due to load $P_{ext}$ .....	25
2.13 External load on posttensioned composite truss.....	27
2.14 Ultimate stage of the posttensioned composite truss.....	28
2.15 Typical moment and curvature relationship for a posttensioned composite truss and a conventional composite truss.....	30
2.16 Flow chart for analyzing of a posttensioned composite truss.....	31
2.17 Strain and stress diagrams at balanced condition.....	32
2.18 Sign convention for the internal moments.....	35
2.19 Loaded configuration of ideal column with elastic bracing.....	36
2.20 Loaded configuration of horizontal imperfect column with bracing.....	37
2.21 Loaded configuration of bottom chord under prestressing force with web member as lateral bracing.....	38
2.22 Shrinkage strain diagram.....	39
2.23 Deflection from the shrinkage moments.....	41
3.1 Test specimens : Dimensions with drape down point and end anchorage details.....	46

Figures	Page
3.2	Plan view and end elevation view on the reaction load frame..... 48
3.3	Section view of a test specimen in the loading frame..... 49
3.4	Shear stud connectors and slab rebars..... 50
3.5	Curing under cover of wet burlap and plastic sheet..... 51
3.6	Posttensioning of Truss Series A..... 51
3.7	End anchorage of prestress tendons..... 52
3.8	Twin-ram jack with pump and pressure gauge..... 52
3.9	Two 1000kN load-rams with the load cells..... 53
3.10	Elevation view of the Truss Series A..... 53
3.11	Compressive strength tests of 28-day concrete..... 55
3.12	Compressive strength tests of 75-day concrete..... 55
3.13	Concrete compressive strength tests..... 56
3.14	Concrete modulus of rupture tests..... 56
3.15	Steel coupon tests..... 58
3.16	Monostrand unbonded tendon tension tests..... 59
3.17	Tendon tension load and time relation curves..... 59
3.18	Tension tests of the slab rebars..... 60
3.19	Load and elongation curves of the slab rebar..... 60
3.20	Strain gage and LSC locations..... 61
3.21	Data Acquisition System (DAQ)..... 62
3.22	Vertical and horizontal LSC..... 62
3.23	Steel and concrete strain gages..... 62
3.24	Truss series A showing Specimen A3 at ultimate..... 66
3.25	Cracks in concrete slab - Specimen A3..... 66
3.26	Shear stud connectors - inelastic deformed shape..... 66
3.27	Complete fracture of the bottom chord of Specimen A4..... 67
3.28	Specimen B1 – steel truss only without tendon..... 68
3.29	Specimen B1 – lateral buckling of compression chord..... 69
3.30	Specimen B2 – steel truss with posttensioned tendons..... 69

Figures	Page
3.31 Specimen B2 – lateral buckling at the ultimate stage.....	69
3.32 Measured precamber and prestress levels for Specimen A1, A2 and A3.....	70
3.33 Photograph of Specimen A3 at ultimate stage.....	71
3.34 Load-mid span deflection curves for Specimen A1, A2, A3, A4, B1 and B2.....	72
3.35 Load-mid span deflection curves for Specimen A1 and A2.....	73
3.36 Load-mid span deflection curves for Specimen A3 and A4.....	73
3.37 Load-mid span deflection curves for Specimen B1 and B2.....	74
3.38 Load-bottom chord stress curves for Specimen A1.....	75
3.39 Load-bottom chord stress curves for Specimen A2.....	75
3.40 Load-bottom chord stress curves for Specimen A3.....	76
3.41 Load-bottom chord stress curves for Specimen A4.....	76
3.42 Load-2 <sup>nd</sup> panel bottom chord B2N and B2S stress curves for Specimen A1.	77
3.43 Load-2 <sup>nd</sup> panel bottom chord B2N and B2S stress curves for Specimen A2.	77
3.44 Load-2 <sup>nd</sup> panel bottom chord B2N and B2S stress curves for Specimen A3.	78
3.45 Load-2 <sup>nd</sup> panel bottom chord B2N and B2S stress curves for Specimen A4.	78
3.46 Load-top chord stress curve for Specimen A1.....	79
3.47 Load-top chord stress curve for Specimen A2.....	79
3.48 Load-top chord stress curve for Specimen A3.....	80
3.49 Load-top chord stress curve for Specimen A4.....	80
3.50 Load-diagonal member stress curves for Specimen A1.....	81
3.51 Load-diagonal member stress curves for Specimen A2.....	81
3.52 Load-diagonal member stress curves for Specimen A3.....	82
3.53 Load-diagonal member stress curves for Specimen A4.....	82
3.54 Load-top surface concrete strain at mid span curves for Specimen A1.	83
3.55 Load-top surface concrete strain at mid span curves for Specimen A2.	83
3.56 Load-top surface concrete strain at mid span curves for Specimen A3.	84
3.57 Load-top surface concrete strain at mid span curves for Specimen A4.	84

Figures	Page	
3.58	Shear force and slip curves on the north side of the specimen including the unloading branch for Specimen A1.....	85
3.59	Shear force and slip curves on the north side of the specimen including the unloading branch for Specimen A2.....	85
3.60	Shear force and slip curves on the north side of the specimen including the unloading branch for Specimen A3.....	86
3.61	Shear force and slip curves on the south side of the specimen including the unloading branch for Specimen A3.....	86
3.62	Shear force and slip curves on both the north side and the south side of the specimen for Specimen A3.....	87
3.63	Shear force and slip curves on both the north side and the south side of the specimen for Specimen A4.....	87
3.64	Load and horizontal movement curves for Specimen B1.....	88
3.65	Load and horizontal movement curves for Specimen B2.....	88
4.1	Precamber chart from theory and experiment.....	92
4.2	Load-deflection curves from the theoretical and experimental data.....	98
4.3	Comparison of experimental results and calculated load and bottom chord stress a mid span curves.....	99
4.4	Comparison of experimental results and calculated load and bottom chord stress at 2 <sup>nd</sup> panel member curves.....	100
4.5	Comparison of experimental results and calculated load and diagonal member stress curves.....	100
4.6	Comparison of experimental results and calculated load and top fiber concrete strain curves.....	101
4.7	Moment and curvature curves from experimental results and theoretical calculation.....	102
4.8	Theoretical and experimental load slip curves.....	103
4.9	Critical buckling loads for steel Specimen B1 and B2.....	106

Figures	Page
4.10 Precamber based on fix and pinned joints compared to experimental results.....	108
4.11 Load and mid span deflection calculated from fixed and pinned joints compared to the experimental results.....	109
4.12 Moment and curvature as calculated from fixed and pinned joints compared to the experimental results.....	110
4.13 Effect of concrete strength to neutral axis location.....	111
4.14 Effect of concrete strength on transformed moment of inertia.....	111
4.15 Effect of concrete strength to the yield load.....	112
4.16 Effect of concrete strength to the ultimate load.....	112
4.17 Effect of concrete strength to the yield deflection.....	113
4.18 Effect of concrete strength to on shear stud strength.....	114
4.19 Effect of percentage of tendon on ultimate load.....	116
4.20 Effect of the total percentage of tendon on rotation capacity.....	117
4.21 Effect of partial prestress ratio percentage of tendon on rotation capacity.....	118
4.22 Mid span deflection of and SSB with third point loads, $P_{ext}$ .....	120
4.23 Effective to transformed moment of inertia - relative prestressing ratio.	121
4.24 Shrinkage strain diagram.....	122
4.25 The free shrinkage strains and shrinkage deflections.....	125
4.26 The free shrinkage strains and strains in members.....	125
4.27 Creep deflection and creep coefficient curves.....	127
4.28 Downward deflection and anchorage seating curves.....	128
4.29 Downward deflection and relaxation in tendon curves.....	129



## CHAPTER 1

### INTRODUCTION

#### 1.1 Research Background

In structural engineering, composite construction refers to a system which incorporates two or more essentially different materials in such a way as to take advantage of their particular structural characteristics. For example, a composite concrete and steel beam, which depends on the steel to sustain tension stresses and on the concrete to sustain compressive stresses, is much more effective than concrete or steel acting alone in flexure. The mechanical property of the concrete material has a very high resistance in compression and a much lower resistance in tension. The mechanical property of the steel material on the other hand is very efficient in resisting tension. It is efficient in compression only if buckling is either not a problem or if there is adequate lateral support to prevent compression buckling both locally and globally. In composite construction, both the cost as well as the structural efficiency may be optimized. The overall objective of using composite construction is to improve the mechanical performance in flexure as well as to reduce the cost of construction.

Composite construction also enables structural designers to significantly reduce the depth-to-span ratio thus achieving additional economic and design benefits. In the case of the research reported herein, a steel truss was topped off with a reinforced concrete slab to form an efficient bridge girder. The shear transfer between the concrete and the steel truss was affected by using shear studs welded to the upper chord of the truss. For this type of composite structure, the concrete deck slab provides sufficient lateral stability to the top flange of the steel girder which lies near the compressive zone in the immediate vicinity of the neutral axis. This type of structural system is referred to as a steel truss with composite concrete deck or simply as a composite truss. When the concrete deck is cast from a high strength or high

performance concrete, it is referred to as a composite girder with a high performance concrete slab.

One possible problem of existing older flexural composite trusses under long periods of service loads is that of large span deformations. The concept of external post-tensioning is introduced in this research to alleviate this problem. Moreover, such a prestressing concept can improve the flexural behavior in both strength and serviceability. The type of post-tensioned steel truss studied herein utilizes slab post-tensioning and steel stud shear connectors to ensure full integration of the steel truss acting compositely with the slab. Most commonly used composite trusses are one-way simply supported systems. Shear stud connectors are distributed along the top chord to enable a uniform shear transfer between the concrete slab and the steel top chord. The high-strength tendons are prestressed externally to provide axial compression which counteracts the tensile stresses caused by the external load.

## 1.2 Literature Review

Viest et al. (1958) found that if the concrete slab is perfectly connected to the steel section, which is called fully composite, they both act together in carrying the service load. Slip between the slab and steel section is greatly reduced and the compressive and tensile stresses are effectively balanced through the use of shear connectors between the steel and concrete.

For a non-composite section with no shear connectors the steel girder alone must carry the load acting on the floor plus the self weight of the slab and truss. Experimental studies also show that the friction between the concrete deck and the steel section without shear connectors is very low compared to the shear resistance developed when shear stud connectors are used. The friction may be increased by encasing the upper chord in the concrete slab. This method was studied by Watson et al. (1974). The method is applicable when at least 2.0 inches of concrete is provided

over the side and the bottom of the chord and at least 1.5 inches of cover is provided for composite action.

The concrete which experiences higher local stresses near the interface may crush at the shear connector base while some deformations of the shear connectors occur. Lam and El-Lobody (2005) found that the head zone of the shear connector where the confining concrete stress is lower than in the base zone remains in its original orientation; i.e. there is translation occurs while rotation is suppressed. The result is bending deformation in the connector corresponding to its bending stiffness. Long connectors are more likely to deform into the double curvature characteristic while maintaining ductility whereas short connectors tend to be brittle and are therefore undesirable.

Most codes of practice require stud connectors to be at least 3 or frequently 4 times longer than their diameters (AISC 1994 and BSI 1994). If the overall length of a stud is shorter than 4 times its diameter, a reduction factor of ultimate shear capacity of the stud of less than 1 is applicable

It has been reported by several researchers according to Viest (1960), Slutter (1965) and the Joint ASCE-ACI Committee (1960), that while the slip of a shear connector does not significantly affect the ultimate capacity of the composite beam, there is some reduction in stiffness of beam being approximately 15% in the elastic range. Furthermore, Wang (1998), Topkaya, Yura and Williamson (2004) proposed that the ultimate capacity of a shear stud connector be based on an interface slip limit of 0.8 mm (0.03 inches).

As reported by Slutter (1965), flexibility of shear connectors allows more ductility and a variation in the distribution of the longitudinal shear between the slab and steel section. Due to the flexibility of the connectors, it is not essential to distribute the shear connector according to the shear diagram. Experimental work in this area has shown that when a higher load is applied to the composite beam, redistribution will occur. Thus leading to a more uniform shear distribution.

Currently, there is no design specification for the post-tensioned composite truss concept. However, some research papers such as Hoadley (1963) and Saadatmanesh et al. (1989) mention external prestressing in the composite beam. They found that the use of the prestressing principle in the composite steel-concrete structure is not to overcome the tensile deficiencies of the material, as in the case of prestressed concrete, but to build opposite stresses into the composite beam in order to counteract the stresses caused by the external load. Furthermore, for the sufficient provision of high-strength tendons, Hoadley (1963) found that the tendon can upgrade the flexural strength and ductility of the composite beam. It was concluded that the effect of prestressing is significant to the ductility of the structure by increasing the ratio of ultimate to yield moment while the effect of variation in slab dimension to the ductility of the structure is not significant. He also found that the variation in the span length did not change the ductility property.

Post-tensioned trusses were also studied by Ayyub et al. (1990). They studied non composite steel trusses post-tensioned by the tendons anchored at truss joints and treated as a separate member. They performed the superposition of the two stages of analysis; first, the dead load and the prestressing force without considering the stiffness of the tendons and second, the live load considering the stiffness matrices of the tendons to be in effect. They found that if a tendon coincides with a truss member then only that member is affected by the post-tensioning force, but if a tendon does not coincide with a truss member, then most of the truss members are affected by post-tensioning. According to this study, for the case of post-tensioned steel trusses with a high performance concrete (HPC) composite deck, the stiffness and the slip of an externally unbonded tendon should be taken into consideration.

The use of a HPC composite deck is also adopted in this research to provide higher strength to resist the additional pre-compressed stress. Due to the higher elastic modulus in HPC, the transformed effective width of the slab is wider than the normal concrete strength deck slab. Crack problems due to the tensile stress from

prestressing will be reduced due to the higher modulus of rupture associated with HPC as reported in the research of Seri (1994)

The research reported herein is focused on two major aspects which are: (1) composite action between the concrete slab and steel truss, and; (2) the flexural behavior of the post-tensioned composite truss as related to strength and serviceability.

### 1.3 Research Objectives

The objective of this research is to study the flexural behavior of post-tensioned steel trusses with high performance concrete composite decks. Experimental study of the full-scale posttensioned steel trusses with high performance concrete composite decks is conducted along with the theoretical analysis to study the actual behavior of the real structure and to observe the problems that may occur in the real application. Moreover, the research aims to develop a model of the post-tensioned composite truss considering the stiffness and the effect of unbonded tendons. This model is intended to analyze the flexural behavior and the shear behavior in strength, stability and the ductility of the structure to accomplish the service life under the strength limit state and the serviceability limit state.

### 1.4 Research Scope

This study is limited to monotonically loaded simply support trusses. The bond between concrete deck and steel truss is perfectly bonded so that the fully composite action is achieved. The members of the trusses used in the analysis are not considered part of the lateral load-resisting system. All the truss members are connected to the truss joints without any eccentricity. The high strength prestressing tendons are draped down at the applied load points and there is no friction at those points as the unbonded prestressing tendon behavior is applied. Relaxation of the prestressing tendons is not considered as the time of the prestressing occurs

immediately before conducting the experiment. The material characteristics used in the analysis were determined for use in the theoretical analysis.

### 1.5 Research Significance

Currently there is no design specification for post-tensioned composite trusses. However, there are a few research papers that mention external prestressing for composite beams. This study aims to introduce the innovation of the use of the prestressing concept as applied to composite steel truss and concrete slab structures to upgrade the flexural strength as well as the stability, serviceability and ductility of both new and existing structures.

### 1.6 Research Program

A theoretical approach is established through a consideration of the various parameters affecting the shear transfer boundary between steel and concrete, this includes assessment of the shear stud connector strength as influenced by stud diameter, concrete strength, stud length, thickness of the flange of the shear-connected chord member and the deformed shape of the shear stud. The range of composite action considered includes: (1) fully composite action; (2) partially composite action, and; (3) non-composite action. The second phase of the theoretical study includes a consideration of posttensioned composite beams and the post-tensioned composite trusses. In the third phase of the study, the full flexural behavior of post-tensioned composite trusses is considered for flexural strength and stiffness as related by load - deflection curves. The study includes the stress distribution behavior in the composite truss, the maximum amount of tendon used, stiffness of the unbonded tendon, buckling behavior of both the element buckling (chord elements and web element) and overall buckling. Also included are losses due to tendon relaxation, creep, shrinkage, and anchorage seating. The possibility of the semi-rigid behavior of truss joints is also included. The study also considers the serviceability deformation of the post-tensioned composite truss.

An experimental study is conducted to evaluate the actual behavior of the real structure and to observe the problems that may occur in actual applications. Load-deformation response, tendon strains, element stresses and failure loads are also recorded. A model of the post-tensioned composite truss considering the stiffness and the effect of unbonded tendons is developed for analyzing the structural behavior as related to the flexural and shear behavior in strength, stability and the ductility of the structure to accomplish the service life under the strength and serviceability limit states.

### 1.7 Research Overview

In Chapter 2 the theoretical approach for a post-tensioned composite truss is presented. Included for consideration are composite action behavior, shear stud connector behavior, degree of composite action, flexural behavior of post-tensioned composite beams and post-tensioned composite trusses, member stresses, buckling behavior, loss behavior due to tendon relaxation, creep, shrinkage, and anchorage seating and as well as semi rigid behavior of the truss joints.

In Chapter 3 the experimental study considering the actual behavior of a real structure is presented along with observations of problems that may occur in real applications. Load-deformations, tendon strains, element stresses, and actual failure loads are recorded.

In Chapter 4 analyses are illustrated as outlined in Chapter 2 and results are plotted against experimental results to illuminate and verify theoretical approaches.

In Chapter 5 a model of the posttensioned composite truss considering the stiffness and effect of the unbonded tendon is developed for the flexural and shear behavior as related to strength, stability and the ductility of the structure.

In chapter 6 the conclusions of the research are stated and a summary of the dissertation is presented.

## CHAPTER 2

### THEORETICAL APPROACH

#### 2.1 Composite Structure

The general theories and principles as used in the analysis and evaluation of composite structural behavior and currently available in the literature are applied in the study of post-tensioned composite trusses with high performance concrete composite decks as investigated herein.

##### 2.1.1 Composite Action

A composite structure is formed with a concrete slab and steel truss connected together with top chord shear stud connectors. If the concrete slab is perfectly connected to the steel section the resulting structure is called fully composite with both structures acting together in carrying service loads. Relative slip between the interconnected surfaces is prevented and the connection fully resists longitudinal shear forces as transferred through the shear stud connectors.

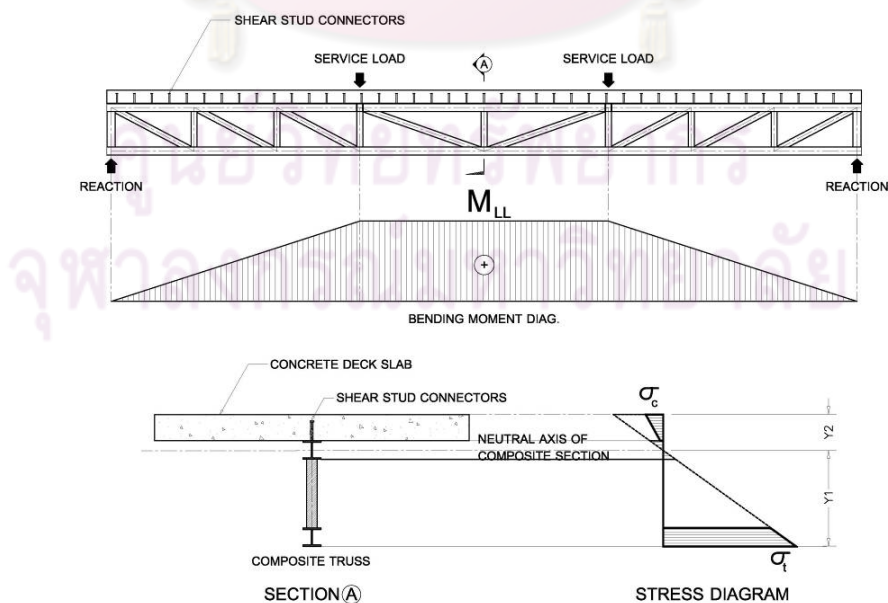


Figure 2.1 Composite truss stress diagrams



From Figure 2.1, the flexural stresses for the service load condition may be obtained from:

$$\begin{aligned}\sigma_t &= \frac{M_{LL} \cdot y_1}{I_t} \\ \sigma_c &= \frac{M_{LL} \cdot y_2}{n \cdot I_t}\end{aligned}\quad (2.1)$$

Where  $\sigma_t$  is the tensile stress in the steel member of the composite truss and  $\sigma_c$  is the compressive stress in the concrete deck slab.  $M_{LL}$  is the service load moment in the composite truss,  $I_t$  is the transformed section moment of inertia of the composite section to all steel material, and  $n$  is the modular ratio of the steel elastic modulus to the concrete elastic modulus,  $y_1$  and  $y_2$  are the distance from the neutral axis to the tensile surface and to the compressive surface respectively.

For the shear stress, as referring to Figure 2.2, consider the following part of the composite truss of length  $dx$  subjected to a flexural stress  $\sigma_1$  at section 1 from moment  $M_1$  which is assumed to be less than the flexural stress  $\sigma_2$  at section 2 as caused by moment  $M_2$ . The differential force between  $\sigma_1 dA$  and  $\sigma_2 dA$  is the net shearing force,  $dF$ , between the concrete slab and the steel member.

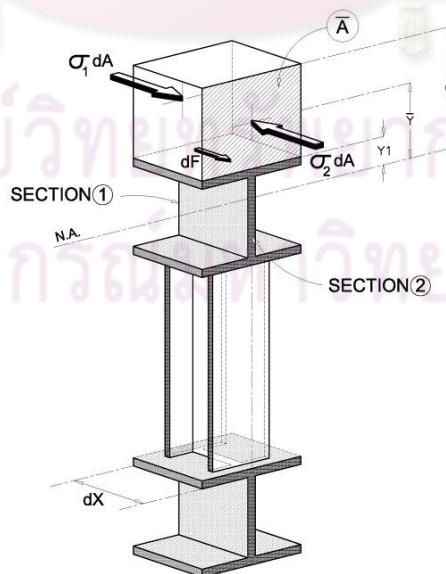


Figure 2.2 Interface shearing stress of the composite truss section of length  $dx$ .

Equilibrium of the longitudinal force acting on concrete slab from  $y_1$  to  $c$  (see Fig. 2.2)

$$\begin{aligned}
 dF &= \int_{y_1}^c \sigma_2 dA - \int_{y_1}^c \sigma_1 dA \\
 &= \frac{M_2}{I} \int_{y_1}^c y dA - \frac{M_1}{I} \int_{y_1}^c y dA \\
 dF &= \frac{M_2 - M_1}{I} \int_{y_1}^c y dA \quad (2.2)
 \end{aligned}$$

Substitute  $dF$  by  $v \cdot b$  where  $v$  is the shearing stress and  $b$  is the width of the interface.

$$v \cdot b = \frac{dM}{I \cdot dx} \int_{y_1}^c y dA \quad (2.3)$$

From mechanics of materials, the derivative of moment with respect to longitudinal axis equals the shear force  $V$  at the section considered.

$$v \cdot b = \frac{V}{I} \int_{y_1}^c y dA \quad (2.4)$$

Thus the shearing stress of the composite structure can be computed by,

$$v = \frac{V(\bar{A} \cdot \bar{Y})}{I \cdot b} \quad (2.5)$$

where  $\bar{A} \cdot \bar{Y}$  is the first moment of area above the interface about the composite neutral axis. Composite construction commonly uses shear connectors to prevent slip between the two materials. If it is assumed that the fully connected composite beam acts in an elastic way then the shear flow (shear force per unit length) between the concrete slab and the steel section may be calculated as:

$$shear\ flow = \frac{V(\bar{A} \cdot \bar{Y})}{I} \quad (2.6)$$

The spacing,  $s$ , of the shear connectors required for resisting the horizontal shear flow as calculated from equation (2.6) is:

$$s = \frac{Q_a}{\text{shear flow}} \quad (2.7)$$

Where  $Q_a$  is the allowable service load capacity of a shear connector which is calculated from  $Q_u$ , the ultimate load capacity of the shear connector, divided by an appropriate safety factor. For research purposes, the ultimate capacity of a connector is determined by direct testing. Since full beam tests are prohibitively expensive, a model test, known as the push-out test (Figure 2.3), is often used to determine ultimate strength and the load-slip behavior.

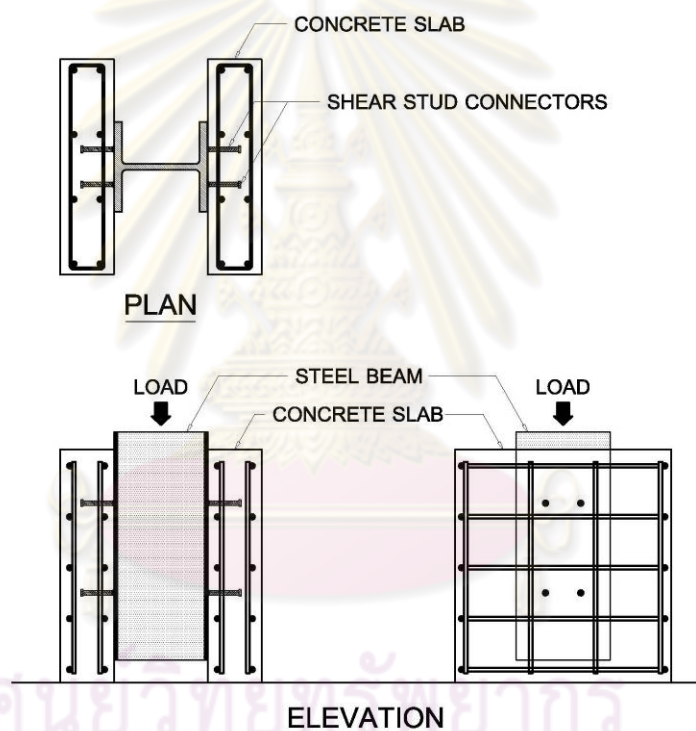


Figure 2.3 Push-out test specimens

Most specifications suggest steel properties for stud shear connectors. In addition to a high yield value the studs must be ductile and a minimum elongation is often specified. From the push-out experiments of shear stud connectors, Ollgaard et al. (1971) proposed a load-slip model as:

$$Q = (Q_u) \cdot (1 - e^{-18\Delta})^{\frac{2}{5}} \quad (2.8)$$

$$Q_u = 1.106 \cdot A_s f_c^{0.3} E_c^{0.44} \quad (2.9)$$

where  $Q$  is the shear load required of a connector at a given slip,  $Q_u$  is the shear capacity of the shear connector,  $A_s$  is the cross-sectional area of the shear stud connector,  $f_c$  is the concrete cylinder strength, and  $E_c$  is the elastic modulus of concrete while  $\Delta$  is the shear stud connector slip in inches, and  $e$  is the natural logarithm  $\sim 2.718281829$ . A typical load-slip curve is shown in Figure 2.4

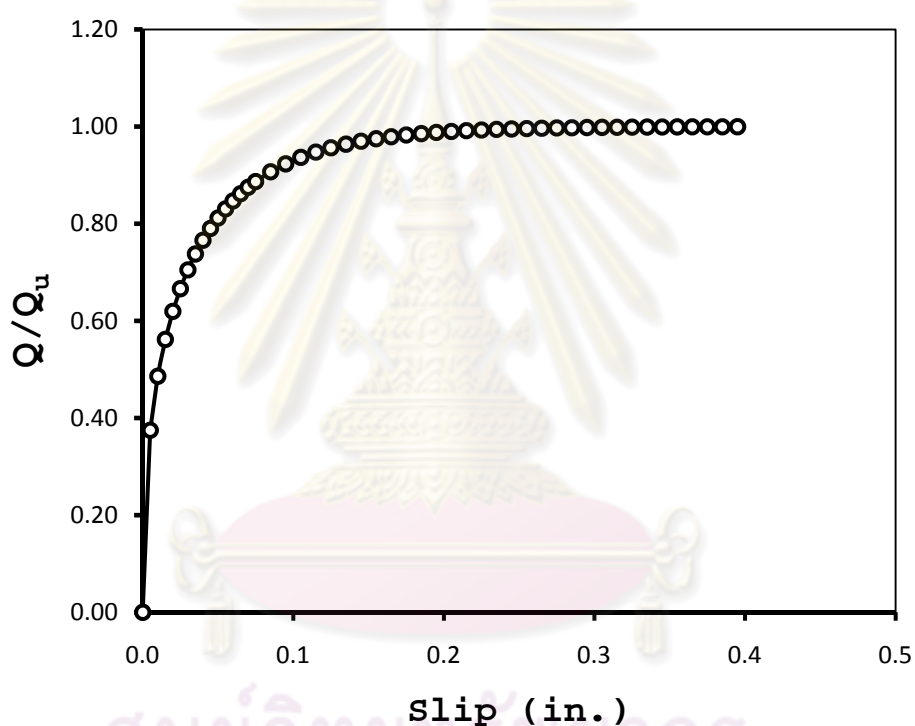


Figure 2.4 Typical load-slip curve

AISC (1993) specifies the shear capacity of a shear stud connector as,  
(in metric unit)

$$Q_u = 0.5 \cdot A_s \sqrt{f_c' E_c} \quad (2.10)$$

where  $A_s$  is the cross sectional area of a shear stud connectors,  $f_c'$  and  $E_c$  are the concrete cylinder compressive strength and the modulus of elasticity of the concrete,

respectively. The stud strength also must not be higher than its tensile strength, i.e.  $Q_u$  is not more than the tensile strength times  $A_s$ .

EC4 (1994) recommends the shear connector strength to be the minimum of:

$$P_R = 0.29 \cdot \alpha \cdot d^2 \sqrt{f_{ck} E_c} \quad (2.11)$$

$$P_R = 0.80 \cdot f_u \cdot \frac{\pi d^2}{4} \quad (2.12)$$

$$\alpha = 0.20 \cdot \left( \frac{h}{d} + 1 \right) < 1.0 \quad (2.13)$$

where  $P_R$  is the shear stud connector strength in EC4,  $d$  is the diameter of the shear stud connector,  $f_{ck}$  is the concrete cylinder compressive strength,  $f_u$  is the ultimate tensile strength of the shear stud material, and  $h$  is the overall length of the stud.

The ratio of the stud diameter to the base material thickness,  $\tau$ , shall not exceed 4.0. If  $\tau$  exceeds 2.5, the stud resistance shall be multiplied by a reduction factor,  $R_f$ , given by

$$R_f = 2.67 - 0.67\tau \leq 1.0 \quad (2.14)$$

Studs shall not be placed closer than the height of the stud to the edge of the concrete slab since otherwise it may exhibit a reduction in strength. Moreover, a uniform distribution of the shear studs along the top chord is applicable for shear studs of length greater than 4 times their diameter. The stud bending deformation leads to equal redistribution of shear stress to all of the studs along the point of the maximum moment to the zero moment of the composite structure, regardless of the shear force diagram along the span length.

### 2.1.2 Degree of Composite Action

In case of an insufficient number of shear stud connectors which leads to reduced shear connection between the two materials, there will be some differential deformation at the interface resulting in partially composite action.

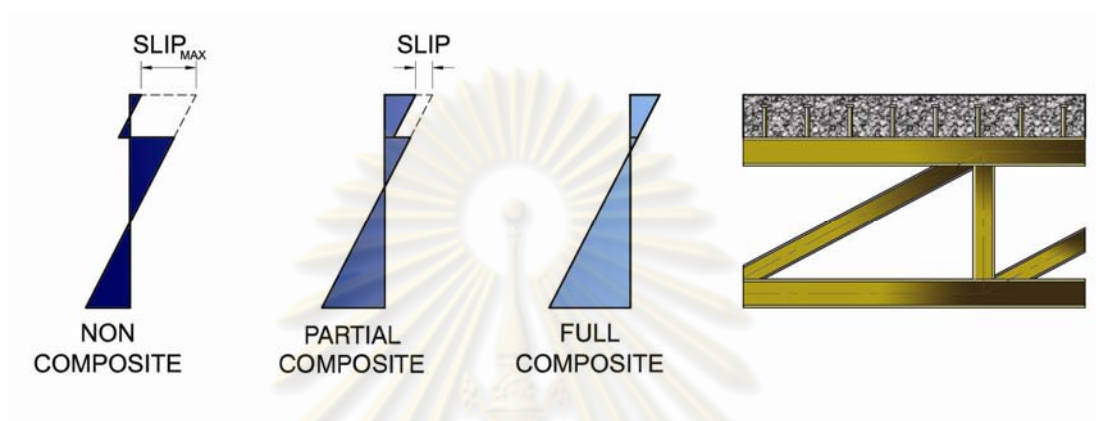


Figure 2.5 Degree of the composite action

Full composite action is the condition that shear stud connectors provide sufficient strength so that the full yield strength of the material used on the tension side of the composite structure can occur at the ultimate load stage.

Non-composite action is the condition that there is no shear transfer between the two material contact surfaces such as the concrete deck slab and the steel member. The slab and steel section deflect with respect to their own neutral axis and at the same level of deflection. The slip at the interface occurs freely and the maximum slip occurs at the support for a simple span structure.

Partial composite action is the condition between full composite action and complete non-composite action. It is obtained when the shear transfer strength between the interfaces governs the flexural strength of the composite beam or truss. This implies that the tensile zone of the structure is not able to develop the full yield strength of the material and the failure mode of the overall structure occurs in an abrupt mode which is not preferred in the normal situation.

However, for full composite action, even the slip between the surfaces is assumed to be zero. In reality however, all the tests, both from other researchers and in this research, there is always some measureable slip that occurs in proportion to applied loads.

### 2.1.3 Composite Trusses

A composite truss consists of a steel truss connected to a concrete deck slab via the shear stud connectors welded to the truss and embedded in the slab. Normally composite trusses are simple span supported structures used widely both in building structures and in highway bridge structures. Full composite action is preferred to provide a ductile failure mode due to yielding of the tension chord of the truss rather than the brittle failure mode due to crushing or shearing of the concrete deck slab. In this respect, AISC (1993) specifically requires a ductility factor of at least 3.

The ASCE Task Committee on Design Criteria for Composite Structures in Steel and Concrete (1996) stated that the possible failure mechanisms of the composite truss are: (1) yielding of the tensile stress region of the truss; (2) crushing of the concrete slab; (3) failure of the shear connectors; (4) yielding of the web; or (5) instabilities occurring during and after construction; (6) buckling of the web elements; and (7) buckling of the top chord during construction.

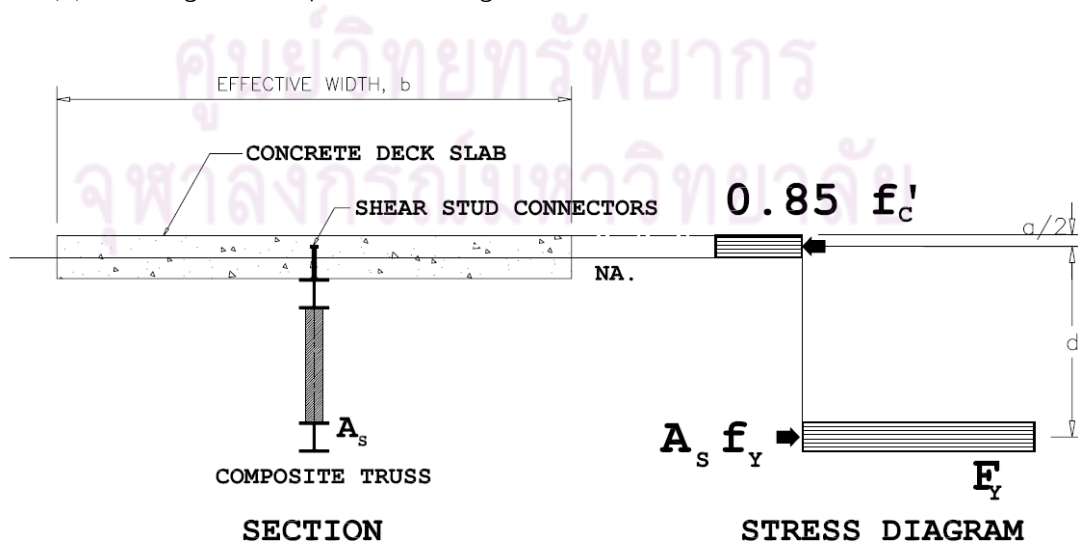


Figure 2.6 Flexural capacity of a composite truss

Referring to Figure 2.6, the flexural capacity of a conventional composite truss can be computed as:

$$\phi M_n = \phi A_s f_y d \quad (2.15)$$

$$A_s f_y \leq 0.85 f_c' b t_c \quad (2.16)$$

$$A_s f_y \leq 0.80 A_e f_u \quad (2.17)$$

where  $\phi$  is a resistance factor for steel yielding in tension and equals 0.9;  $A_s$  is the cross-sectional area of the steel bottom chord;  $f_y$  is the specified minimum yield stress of steel bottom chord;  $d$  is the distance from the centroid of the steel bottom chord to the center of resistance of the concrete in compression;  $b$  is the effective width of the slab;  $t_c$  is the minimum thickness of the concrete slab;  $A_e$  is the effective net area of the steel bottom chord; and  $f_u$  is the tensile strength of steel bottom chord. The distance between the centroid of the tension chord and the centroid of the compression block,  $d$ , shall be computed using a concrete stress of  $0.85f_c'$ , and an equivalent slab width on either side of the truss taken as the smallest of (1) one-eighth of the member span; (2) one-half of the distance to the adjacent composite truss; (3) the distance from the member center line to the edge of the slab; as shown in the Equations 2.18 and 2.19, and in figure 2.6 where 'a' is the depth of the concrete stress block and 'h' is the distance from the centroid of the bottom chord to the top surface of the concrete slab:

$$a = \frac{A_s f_y}{0.85 f_c' b} \quad (2.18)$$

$$d = h - \frac{a}{2} \quad (2.19)$$

For the overall vertical shear capacity of a composite truss, the small contribution to shear capacity of the concrete slab and steel top and bottom chords as compared to the much higher shear capacity from the web elements is ignored.

When considering composite action, the top chord is not assumed to contribute to the flexural capacity of the structure due to its nearness to the neutral axis of the composite member. Experiments conducted by Alsamsam (1988) and Curry



(1988) confirmed that relatively small axial forces exist in the top chord when the maximum flexural capacity is reached.

## 2.2 Post-tensioned Composite Trusses

General post-tensioned composite trusses consist of composite trusses with the application of high strength prestressing tendons to provide opposite stresses to counter balance external load effects. The prestressing concept presented herein is aimed at the repair of existing composite structures by providing uplift displacement and additional flexural capacity. The pre-compression stresses in the tensile zone of composite beams or trusses can increase the ductility of the overall structure more efficiently than can be done using additional plates or beams welded to the existing structure.

For the case of post-tensioned composite trusses, the high-strength tendon will be used externally to provide the axial compression and the uplift moment as shown in Figure 2.7.

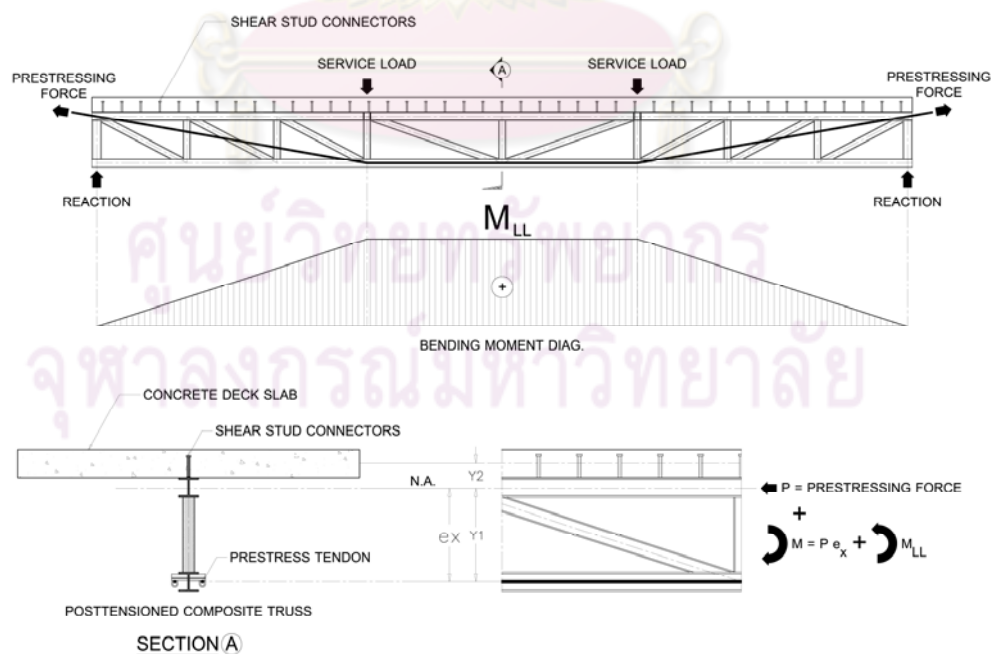


Figure 2.7 Typical posttensioned composite trusses

From Figure 2.7, the elastic flexural stresses can be computed by the following equations where  $\sigma_{x(\text{bottom chord})}$  and  $\sigma_{x(\text{top chord})}$  are the horizontal stresses in the bottom chord and in the top chord respectively.  $P(x)$  and  $e(x)$  are the prestressing force and the eccentricity or at the section  $x$ .  $y_1(x)$  and  $y_2(x)$  are the vertical distance from the neutral axis to the center of the bottom chord and the top chord at the section  $x$ .  $M_{LL}(x)$  is the service moment at the section  $x$ .  $A_t(x)$  and  $I_t$  are the transformed cross sectional area and the transformed moment of inertia at the section  $x$ . The effect of tendon stiffness and slip of the external prestressing tendon is neglected in this step.

$$\begin{aligned}\sigma_{x(\text{bottom chord})} &= -\frac{P(x)}{A_t(x)} - \frac{P(x) \cdot e(x) \cdot y_1(x)}{I_t} + \frac{M_{LL}(x) \cdot y_1(x)}{I_t} \\ \sigma_{x(\text{top chord})} &= -\frac{P(x)}{A_t(x)} + \frac{P(x) \cdot e(x) \cdot y_2(x)}{I_t} - \frac{M_{LL}(x) \cdot y_2(x)}{I_t}\end{aligned}\quad (2.20)$$

$$I_t = \sum_{i=1}^n (I_{t,i} + A_{t,i} d_i^2) \quad A_t = \frac{b \cdot t_c}{n} + \sum_{i=1}^n (A_s) \quad (2.21)$$

For more accurate behavior analysis, the stiffness and the slip of the externally unbonded tendon should be taken into consideration.

According to the principle of virtual work for particles and rigid bodies (J.T. Oden, 1967), There are two concepts of the works which are (1) the virtual work,  $\delta W$ , or the work done by the system of equilibrium true force  $P$  in moving through the virtual displacement  $\delta u$  and (2) the complementary virtual work,  $\delta W^*$ , or the work done by the system of equilibrium virtual force,  $\delta P$ , in moving through the true displacement,  $u$ . Under the equilibrium condition, the principle of virtual work states that both  $\delta W$  and  $\delta W^*$  are also equal to 0.

In this study, the case of the principle of complementary virtual work,  $\delta W^*$ , is utilized for determining the displacement of the structure under the system of the true equilibrium force, i.e. the true displacements of a system of particles and rigid bodies in reaching an equilibrium configuration are such that the virtual work is zero for every system of virtual forces satisfying the equilibrium conditions.

For deformable bodies, the continuous functions of all the internal stresses,  $\delta\sigma_x$ ,  $\delta\sigma_y$ ,  $\delta\sigma_{xy}$ , the body forces,  $\delta X_b$ ,  $\delta Y_b$ , and the surface tractions  $\delta X_s$  and  $\delta Y_s$ , are regarded as a system of self-equilibrating virtual forces and stresses which are independent of the true forces and stresses existing in the structures.

$$\begin{aligned}\delta W^* &= \iint_A \left[ \left( \frac{\partial \delta\sigma_x}{\partial x} + \frac{\partial \delta\tau_{xy}}{\partial y} + \delta X_b \right) u + \left( \frac{\partial \delta\sigma_y}{\partial y} + \frac{\partial \delta\tau_{xy}}{\partial x} + \delta Y_b \right) v \right] dx dy \\ \delta W^* &= - \iint_A \left[ \delta\sigma_x \frac{\partial u}{\partial x} + \delta\sigma_y \frac{\partial v}{\partial y} + \delta\tau_{xy} \left( \frac{\partial u}{\partial y} + \frac{\partial v}{\partial x} \right) \right] dA \\ &+ \iint_A (\delta X_b \cdot u + \delta Y_b \cdot v) dA + \oint_c [(\delta\sigma_x \cdot l + \delta\tau_{xy} \cdot m)u + (\delta\sigma_y \cdot m + \delta\tau_{xy} \cdot l)v] ds\end{aligned}\quad (2.22)$$

Where the  $\delta W^*$  is the complementary virtual work which equals to the negative virtual strain energy  $-\delta U^*$  plus the virtual work done by the external force,  $\delta W_e^*$ ;

$$\begin{aligned}-\delta U^* &= - \iint_A \left[ \delta\sigma_x \frac{\partial u}{\partial x} + \delta\sigma_y \frac{\partial v}{\partial y} + \delta\tau_{xy} \left( \frac{\partial u}{\partial y} + \frac{\partial v}{\partial x} \right) \right] dA \\ \delta W_e^* &= + \iint_A (\delta X_b \cdot u + \delta Y_b \cdot v) dA + \oint_c [(\delta\sigma_x \cdot l + \delta\tau_{xy} \cdot m)u + (\delta\sigma_y \cdot m + \delta\tau_{xy} \cdot l)v] ds\end{aligned}\quad (2.23)$$

These virtual stresses satisfy the equilibrium equations;

$$\begin{aligned}\frac{\partial \delta\sigma_x}{\partial x} + \frac{\partial \delta\tau_{xy}}{\partial y} + \delta X_b &= 0 \\ \frac{\partial \delta\sigma_y}{\partial y} + \frac{\partial \delta\tau_{xy}}{\partial x} + \delta Y_b &= 0\end{aligned}\quad (2.24)$$

$$\delta\sigma_x \cdot l + \delta\tau_{xy} \cdot m = \delta X_s$$

$$\delta\sigma_y \cdot m + \delta\tau_{xy} \cdot l = \delta Y_s$$

Thus  $\delta W^*$  is automatically equal to zero, regardless of the interpretation for any given  $u$  and  $v$ ;

$$\delta W^* = -\delta U^* + \delta W_e^* = 0$$

$$\delta U^* = \delta W_e^* \quad (2.25)$$

Therefore the virtual strain energy,  $\delta U^*$ , equals the virtual work done by the external forces,  $\delta W_e^*$ . For the truss members, the virtual strain energy,  $\delta U^*$ , can be determined by:

$$\delta U^* = \sum_{i=1}^n \int_0^L \left( \frac{F_i(x) \cdot \delta F_i(x)}{E_i(x) A_i(x)} \right) dx \quad (2.26)$$

where  $i$  is the number of the element from 1 up to  $n$  and  $L$  is the length of the member  $i$ .  $F_i(x)$  and  $\delta F_i(x)$  denote the internal force in member  $i$  and the virtual internal force.  $E_i(x)$  and  $A_i(x)$  are the modulus of elasticity and cross sectional area of member  $i$ . While the virtual work done by the external forces,  $\delta W_e^*$  equals:

$$\delta W_e^* = \delta P_{ext} \cdot \Delta \quad (2.27)$$

Thus the deformation  $\Delta$  in the direction of  $\delta P_{ext}$  can be computed by the following equation;

$$\Delta = \left( \frac{1}{\delta P_{ext}} \right) \sum_{i=1}^n \int_0^L \left( \frac{F_i(x) \cdot \delta F_i(x)}{E_i(x) A_i(x)} \right) dx \quad (2.28)$$

The application of the energy theorem above is used to solve the problem of the increase in tendon force due to the external load.

Given the member names for a typical posttensioned composite truss are shown in figure 2.8. Please be noted that “TL” refers to “top member on the left half of the composite truss”, “VL” refers to “vertical member on the left half of the composite truss”, “DL” refers to “diagonal member on the left half of the composite truss” and “BL” refers to “bottom chord member on the left half of the composite truss”.

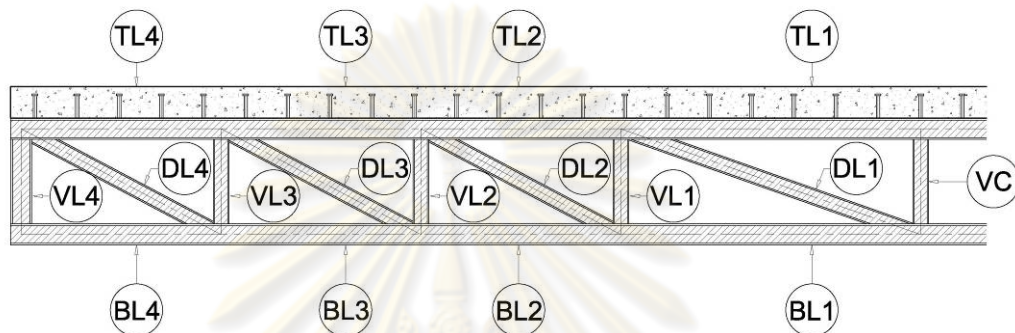


Figure 2.8 Typical posttensioned composite truss member designations

The first step of the analysis is to find the stress in each member due to  $w$ , comprised of uniformly distributed dead load (DL), and superimposed dead load (SDL) of both the steel truss and the concrete deck slab. These loads act on the posttensioned composite truss neglecting the high strength prestressing tendon according to the actual stage of stresses as shown in Figure 2.9. Please be noted that  $a$ ,  $b$ ,  $\alpha$  and  $\beta$  are the member lengths and the internal angles as variables in the analysis.

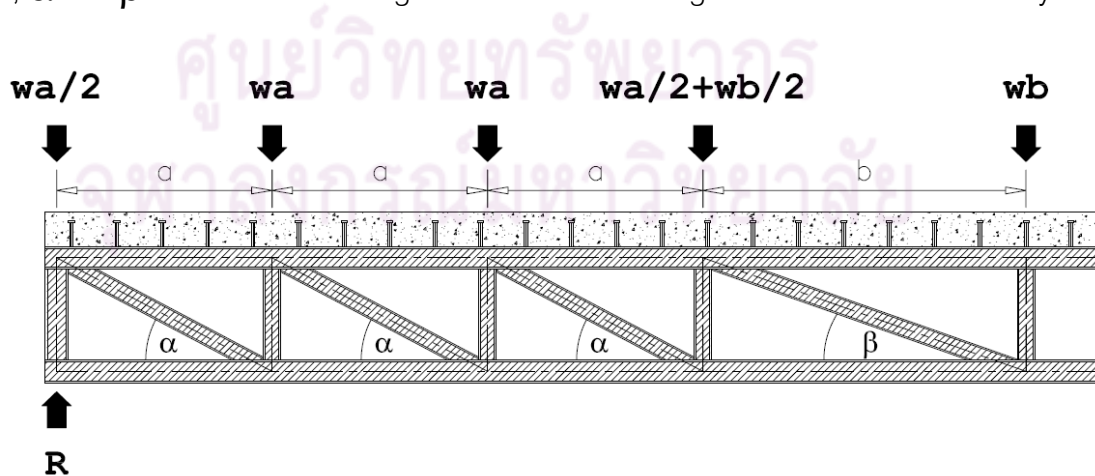


Figure 2.9 Uniform distributed load on a posttensioned composite truss

The member stresses from the uniformed distributed dead load  $w$  are as follows;

$$\begin{aligned}
 \sigma_{TL_4} &= \frac{\left( \frac{\frac{5}{2}wa + wb}{\tan \alpha} \right)}{A_{TL_4}}; \quad \sigma_{TL_3} = \frac{\left( \frac{-4wa + 2wb}{\tan \alpha} \right)}{A_{TL_3}}; \\
 \sigma_{TL_2} &= \frac{\left( \frac{\frac{9}{2}wa + 3wb}{\tan \alpha} \right)}{A_{TL_2}}; \quad \sigma_{TL_1} = \frac{\left( \frac{\frac{9}{2}wa + 3wb}{\tan \alpha} - \frac{\frac{1}{2}wb}{\tan \beta} \right)}{A_{TL_1}}; \\
 \sigma_{BL_4} &= 0; \quad \sigma_{BL_3} = \frac{\left( \frac{\frac{5}{2}wa + wb}{\tan \alpha} \right)}{A_{BL_3}}; \quad \sigma_{BL_2} = \frac{\left( \frac{+4wa + 2wb}{\tan \alpha} \right)}{A_{BL_2}}; \quad \sigma_{BL_1} = \frac{\left( \frac{\frac{9}{2}wa + 3wb}{\tan \alpha} \right)}{A_{BL_1}}; \\
 \sigma_{VL_4} &= \frac{-(3wa + wb)}{A_{VL_4}}; \quad \sigma_{VL_3} = \frac{-\left( \frac{5}{2}wa + wb \right)}{A_{VL_3}}; \quad \sigma_{VL_2} = \frac{-\left( \frac{3}{2}wa + wb \right)}{A_{VL_2}}; \\
 \sigma_{VL_1} &= \frac{-\left( \frac{1}{2}wa + wb \right)}{A_{VL_1}}; \quad \sigma_{VC} = -wb; \\
 \sigma_{DL_4} &= \frac{\left( \frac{\frac{5}{2}wa + wb}{\sin \alpha} \right)}{A_{DL_4}}; \quad \sigma_{DL_3} = \frac{\left( \frac{\frac{3}{2}wa + wb}{\sin \alpha} \right)}{A_{DL_3}}; \\
 \sigma_{DL_2} &= \frac{\left( \frac{\frac{1}{2}wa + wb}{\sin \alpha} \right)}{A_{DL_2}}; \quad \sigma_{DL_1} = \frac{\left( \frac{\frac{1}{2}wb}{\sin \beta} \right)}{A_{DL_1}};
 \end{aligned} \tag{2.29}$$

The second step of the analysis is to find the stresses due to the tendon load,  $P$ , acting on the posttensioned composite truss. It should be noted that the tendon internal force is detected by a hydraulic pressure gauge reading which is independent of the dead load of the structure, as shown in figure 2.10

**P = Prestressing force**

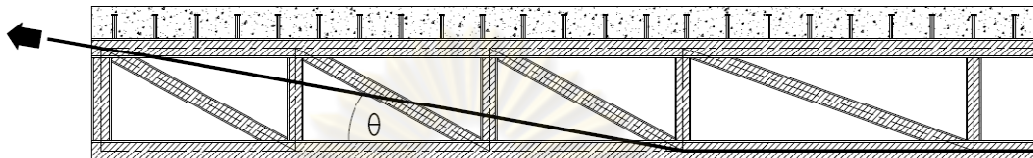


Figure 2.10 Tendon load on a posttensioned composite truss

The member stresses from the tendon load  $T$  are as follows ;

$$\begin{aligned} \sigma_{TL_4} &= \frac{-P \left( \cos \theta - \frac{\sin \theta}{\tan \alpha} \right)}{A_{TL_4}}; \sigma_{TL_3} = \frac{-P \left( \cos \theta - \frac{2 \sin \theta}{\tan \alpha} \right)}{A_{TL_3}}; \sigma_{TL_2} = 0; \sigma_{TL_1} = 0; \\ \sigma_{BL_4} &= 0; \sigma_{BL_3} = \frac{\left( -\frac{P \sin \theta}{\tan \alpha} \right)}{A_{BL_3}}; \sigma_{BL_2} = \frac{\left( -2 \frac{P \sin \theta}{\tan \alpha} \right)}{A_{BL_2}}; \sigma_{BL_1} = \frac{-P}{A_{BL_1}}; \\ \sigma_{VL_4} &= 0; \sigma_{VL_3} = \frac{\left( +P \sin \theta \right)}{A_{VL_3}}; \sigma_{VL_2} = \frac{\left( +P \sin \theta \right)}{A_{VL_2}}; \sigma_{VL_1} = 0; \sigma_{VC} = 0; \\ \sigma_{DL_4} &= \frac{\left( -\frac{P \sin \theta}{\sin \alpha} \right)}{A_{DL_4}}; \sigma_{DL_3} = \frac{\left( -\frac{P \sin \theta}{\sin \alpha} \right)}{A_{DL_3}}; \sigma_{DL_2} = \frac{\left( -\frac{P \sin \theta}{\sin \alpha} \right)}{A_{DL_2}}; \sigma_{DL_1} = 0; \end{aligned} \quad (2.30)$$

From the principle of superposition, the stresses corresponding to each element can be imposed directly at this step before the external load is applied.

When an external load,  $P_{ext}$ , acts on the posttensioned composite truss considering the stiffness and the slip of the unbonded tendon, the resulting stresses occur in the truss members and also inside the posttensioned tendon itself. This leads to an increase in the tendon force,  $\Delta P$ , as indicated in Figure 2.11.

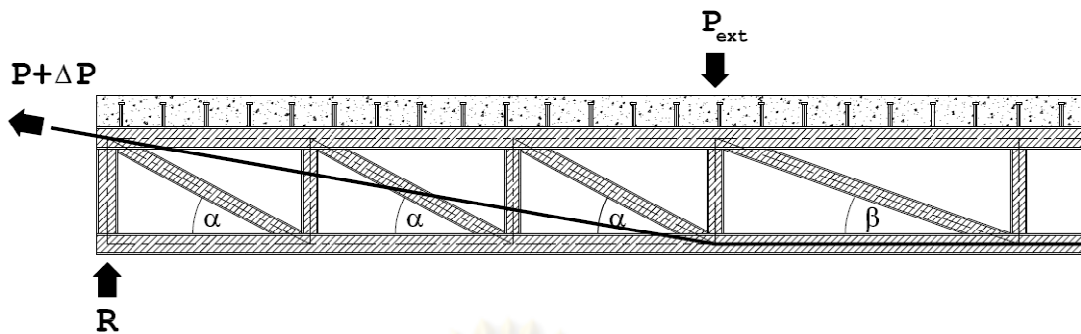


Figure 2.11 Increase in tendon force due to the external load  $P_{ext}$

Strain compatibility as used in a bonded prestressing system cannot be applied in this step because the change in tendon strain is not the same as the change in steel structure strain at the same level. The behavior in the elastic range can be analyzed by using the transformed section, the principle of virtual work, and the principle of superposition to investigate the change in tendon strain. Since the structure is statically indeterminate internally, the redundant is assumed to be the increase in tendon force due to the external load.

To solve this problem first the post-tensioned composite truss is made determinate by cutting the tendon. Then the relative displacement at the cut  $\delta_{1p}$ , or the total elongation of the composite truss along the whole alignment of the tendon due to the external load  $P_{ext}$  by applying a unit virtual force in the direction and location of the tendon, is calculated as shown in figure 2.12. The relative displacement at the cut  $\delta_{11}$ , or the shortening of the composite truss along the whole alignment of the tendon due to the unit virtual force in the tendon by applying a unit virtual force in the direction and location of the tendon is then calculated. At this point, a tendon force increment,  $\Delta P$ , is applied to close the gap by the compatibility condition that the gap must be zero.



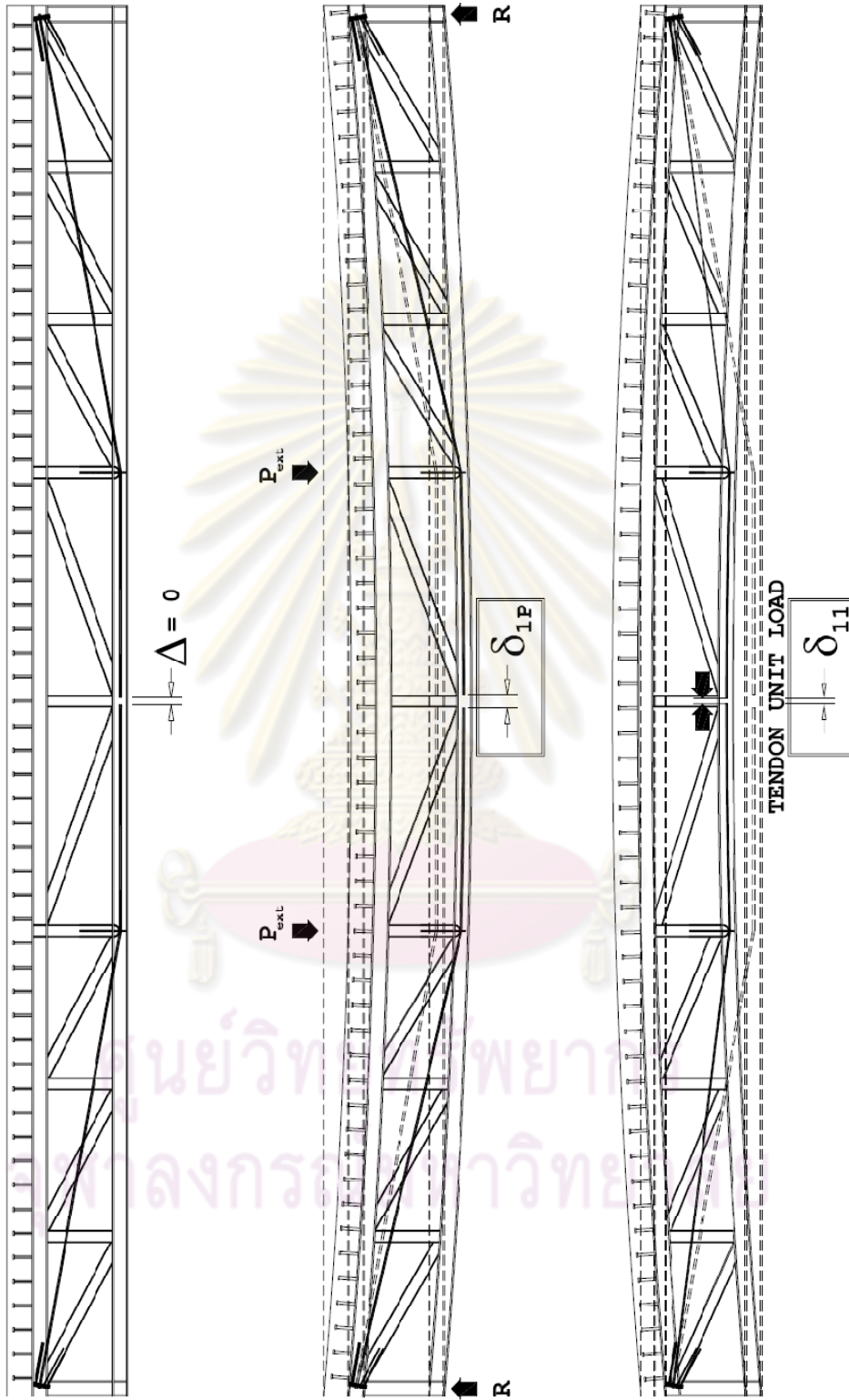


Figure 2.12 Compatibility condition for an increase in tendon force due to external load  $P_{ext}$

The compatibility condition requires that the relative displacement at the cut ends of the tendon must be zero:

$$\delta_{11}\Delta P - \delta_{1P} = 0 \quad (2.31)$$

where  $\delta_{11}$  denotes the shortening due to unit virtual tendon force and  $\delta_{1P}$  represents the elongation due to the applied external load. The elongation and the shortening can be calculated by the principle of complementary virtual work;

$$\begin{aligned} \delta_{1P} &= \sum_{i=1}^n (\delta F_i) \left( \frac{F_{si} \cdot L_i}{A_i E_i} \right) \\ \delta_{11} &= \sum_{i=1}^n (\delta F_i) \left( \frac{F_{si} \cdot L_i}{A_i E_i} \right) + \sum_{j=1}^m (\delta F_j) \left( \frac{F_{sj} \cdot L_{Tj}}{A_{Tj} E_{Tj}} \right) \end{aligned} \quad (2.32)$$

where  $\delta F_i$  and  $\delta F_j$  represent the virtual force in member  $i$  and in tendon  $j$ , respectively.  $F_{si}$  and  $F_{sj}$  represent the internal axial force from external load in member  $i$  and in tendon  $j$ , respectively.  $E_i$  and  $E_{Tj}$  are the modulus of elasticity of steel truss member  $i$  and tendon  $j$ , respectively.  $L_i$  and  $L_{Tj}$  are the length of the steel truss member  $i$  and tendon  $j$ , respectively.  $A_i$  and  $A_{Tj}$  are the cross sectional area of the steel truss member  $i$  and tendon  $j$ , respectively.

Thus the increase in tendon force due to the external load can be computed by:

$$\Delta P = \frac{\left[ \sum_{i=1}^n (\delta F_i) \left( \frac{F_{si} \cdot L_i}{A_i E_i} \right) \right]}{\left[ \sum_{i=1}^n (\delta F_i) \left( \frac{F_{si} \cdot L_i}{A_i E_i} \right) + \sum_{j=1}^m (\delta F_j) \left( \frac{F_{sj} \cdot L_{Tj}}{A_{Tj} E_{Tj}} \right) \right]} \quad (2.33)$$

The strain compatibility equation is used to find the increase in tendon force due to the applied external load. The total force in the tendon is then equal to the initial prestressing force plus the increments in tendon force due to dead-load and live-load. When all of the internal forces are known, the load-deformation curves can be determined.

At the first step, the member stresses due to the external load  $P_{ext}$  are computed individually regardless of the posttensioned tendon as shown in figure 2.13;

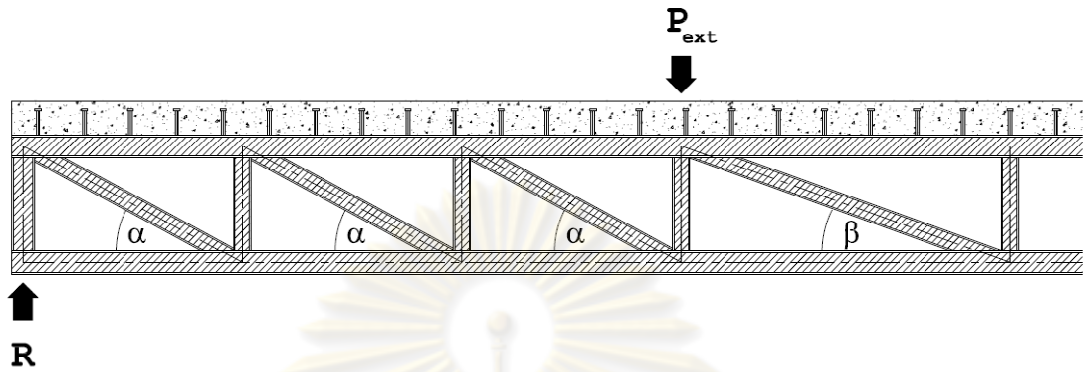


Figure 2.13 External load on posttensioned composite truss

$$\begin{aligned}
 \sigma_{TL_4} &= \frac{\left(-\frac{P_{ext}}{\tan \alpha}\right)}{A_{TL_4}}; \quad \sigma_{TL_3} = \frac{\left(-\frac{2P_{ext}}{\tan \alpha}\right)}{A_{TL_3}}; \quad \sigma_{TL_2} = \frac{\left(-\frac{3P_{ext}}{\tan \alpha}\right)}{A_{TL_2}}; \quad \sigma_{TL_1} = \frac{\left(-\frac{3P_{ext}}{\tan \beta}\right)}{A_{TL_1}}; \\
 \sigma_{BL_4} &= 0; \quad \sigma_{BL_3} = \frac{\left(+\frac{P_{ext}}{\tan \alpha}\right)}{A_{BL_3}}; \quad \sigma_{BL_2} = \frac{\left(+\frac{2P_{ext}}{\tan \alpha}\right)}{A_{BL_2}}; \quad \sigma_{BL_1} = \frac{\left(+\frac{3P_{ext}}{\tan \alpha}\right)}{A_{BL_1}}; \\
 \sigma_{VL_4} &= \frac{\left(-P_{ext}\right)}{A_{VL_4}}; \quad \sigma_{VL_3} = \frac{\left(-P_{ext}\right)}{A_{VL_3}}; \quad \sigma_{VL_2} = \frac{\left(-P_{ext}\right)}{A_{VL_2}}; \quad \sigma_{VL_1} = \frac{\left(-P_{ext}\right)}{A_{VL_1}}; \quad \sigma_{VC} = 0; \\
 \sigma_{DL_4} &= \frac{\left(+\frac{P_{ext}}{\sin \alpha}\right)}{A_{DL_4}}; \quad \sigma_{DL_3} = \frac{\left(+\frac{P_{ext}}{\sin \alpha}\right)}{A_{DL_3}}; \quad \sigma_{DL_2} = \frac{\left(+\frac{P_{ext}}{\sin \alpha}\right)}{A_{DL_2}}; \quad \sigma_{DL_1} = 0; \quad (2.34)
 \end{aligned}$$

Second step, the applied external load  $P_{ext}$  also causes the tendon to be deformed; i.e. the tendon stress is increasing due to the external load  $P_{ext}$ . Thus, the composite truss members are affected by the increase in tendon force,  $\Delta P$ . These stresses can be computed as follows:

$$\sigma_{TL_4} = \frac{-\Delta P \left( \cos \theta - \frac{\sin \theta}{\tan \alpha} \right)}{A_{TL_4}}; \quad \sigma_{TL_3} = \frac{-\Delta P \left( \cos \theta - \frac{2 \sin \theta}{\tan \alpha} \right)}{A_{TL_3}}; \quad \sigma_{TL_2} = 0; \quad \sigma_{TL_1} = 0;$$

$$\sigma_{BL_4} = 0; \sigma_{BL_3} = \frac{\left(-\frac{\Delta P \sin \theta}{\tan \alpha}\right)}{A_{BL_3}}; \sigma_{BL_2} = \frac{\left(-2\frac{\Delta P \sin \theta}{\tan \alpha}\right)}{A_{BL_2}}; \sigma_{BL_1} = \frac{-\Delta P}{A_{BL_1}};$$

$$\sigma_{VL_4} = 0; \sigma_{VL_3} = \frac{\left(+\Delta P \sin \theta\right)}{A_{VL_3}}; \sigma_{VL_2} = \frac{\left(+\Delta P \sin \theta\right)}{A_{VL_2}}; \sigma_{VL_1} = 0; \sigma_{VC} = 0;$$

$$\sigma_{DL_4} = \frac{\left(-\frac{\Delta P \sin \theta}{\sin \alpha}\right)}{A_{DL_4}}; \sigma_{DL_3} = \frac{\left(-\frac{\Delta P \sin \theta}{\sin \alpha}\right)}{A_{DL_3}}; \sigma_{DL_2} = \frac{\left(-\frac{\Delta P \sin \theta}{\sin \alpha}\right)}{A_{DL_2}}; \sigma_{DL_1} = 0; \quad (2.35)$$

Finally, the combined total stresses acting on each of the posttensioned composite truss members can be written as;

$$\sigma_{\text{total}} = (\sigma_{DL} + \sigma_{SDL}) + \sigma_{\text{TENDON}} + \sigma_{\text{EXT.LOAD}} + \sigma_{\Delta P} \quad (2.36)$$

where  $\sigma_{DL}$  and  $\sigma_{SDL}$  are the stresses from the dead load and the superimposed dead load;  $\sigma_{\text{TENDON}}$  is the stress due to the prestressing tendon load;  $\sigma_{\text{EXT.LOAD}}$  is the stress due to the external load; and  $\sigma_{\Delta P}$  is the increase in tendon stress due to the external load considering the stiffness and the slip of the unbonded prestressing tendon.

For the flexural capacity of the posttensioned composite truss, the method of static equilibrium of internal forces for each element in the cross section that has reached the ultimate limit state is considered in the analysis.

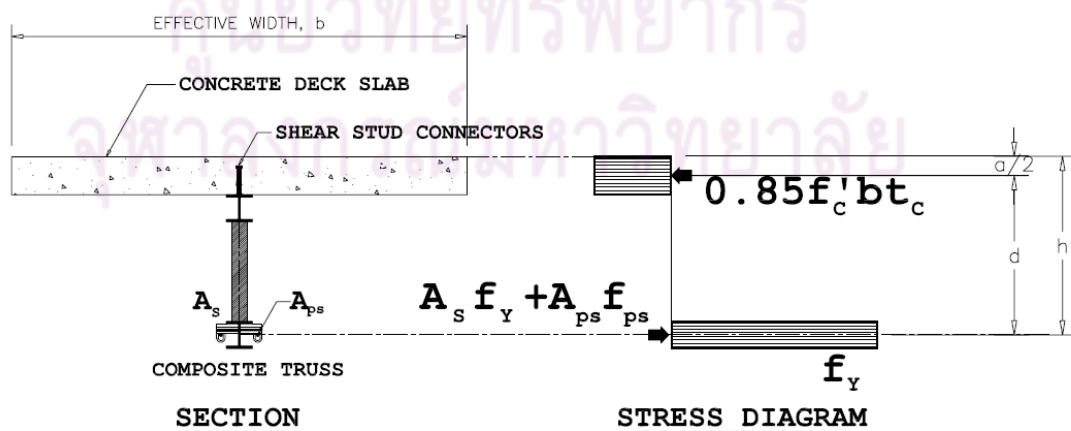


Figure 2.14 Ultimate stage of the posttensioned composite truss

From Figure 2.14, the maximum tensile force results from the combination of the tensile stress in the bottom chord member and the tensile stress in the tendon but not more than the cases of the summation of the shear stud connectors strength from the maximum point of moment to the zero point of moment or the maximum compressive force in the top concrete slab. The maximum flexural strength comes from this maximum tensile force times the moment arm length.

$$F_{\max} = \min \left[ \left( A_s \cdot f_y + A_{ps} \cdot f_{ps,\max} \right), \sum Q_u, 0.85f_c'bt_c \right]$$

$$M_u = F_{\max} \cdot \left( h - \frac{a}{2} \right) \quad (2.37)$$

The minimum boundary of the flexural capacity can be computed if the value of the prestressing force is placed equal to that obtained at the beginning of yielding in the bottom chord of the truss.

$$f_{ps,\max} = f_{jacking} + \Delta f_{ps,yield} \quad (2.38)$$

The maximum boundary for the moment capacity in the inelastic range would be that moment capacity if the value of the prestressing force was set to the ultimate tensile load capacity of the cable. Therefore:

$$f_{ps,\max} = f_{pu} \quad (2.39)$$

The difference between the values of the ultimate moment computed at each bound for the prestressing force is on the order of 5% in which is not significant. For the ultimate deflection, it can be computed from the ductility index of 4 if the section analysis shows that the tensile strain is equal to or exceeds 0.005 when the maximum compressive strain in concrete reaches 0.003 (ACI 318-10.3.3).

## 2.3 Behavior of Posttensioned Composite Trusses

The behavior of a posttensioned composite truss is influenced by flexural behavior, semi-rigid joint behavior, the lateral stability and losses related to prestressing.

### 2.3.1 Flexural Behavior

The transformed section analysis, the principle of complementary virtual work method, and the principle of superposition can be applied to the posttensioned composite truss to investigate the change in tendon strain. The general flexural behavior exhibits an elastic moment vs. angle relationship until the beginning of the yielding of the bottom chord followed by an inelastic transition up to the ultimate load carrying capacity as shown in figure 2.15.

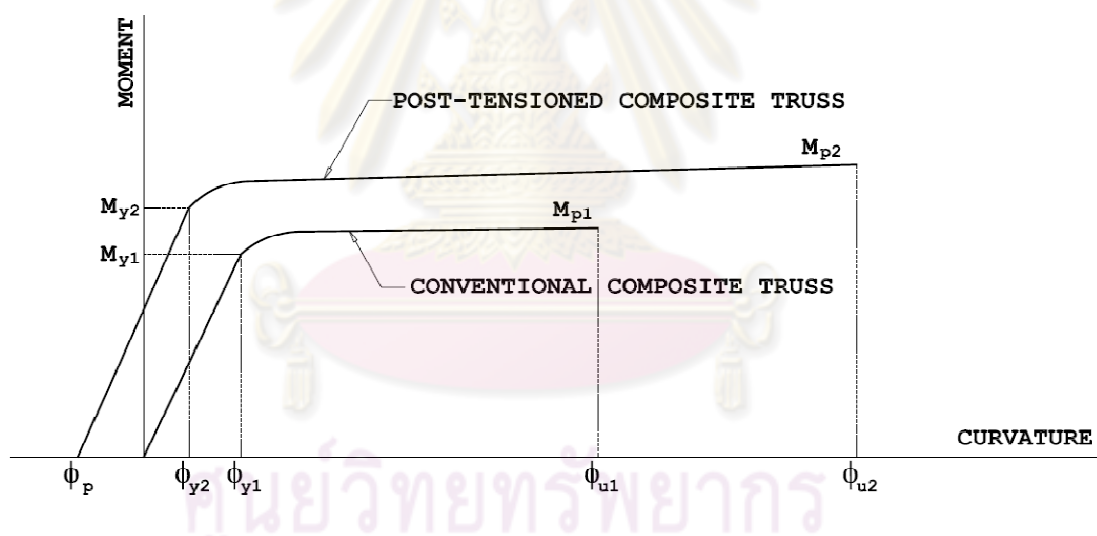


Figure 2.15 Typical moment and curvature relationship for a posttensioned composite truss and a conventional composite truss

According to the previous part of the research concerning the stiffness and the slip of the unbonded tendon, the unknown increase in the tendon force due to the external load is solved and all of the stresses in every truss element can be computed step by step. The procedural flow chart for determining the load-deflection curve of the posttensioned composite truss is shown in the figure 2.16.

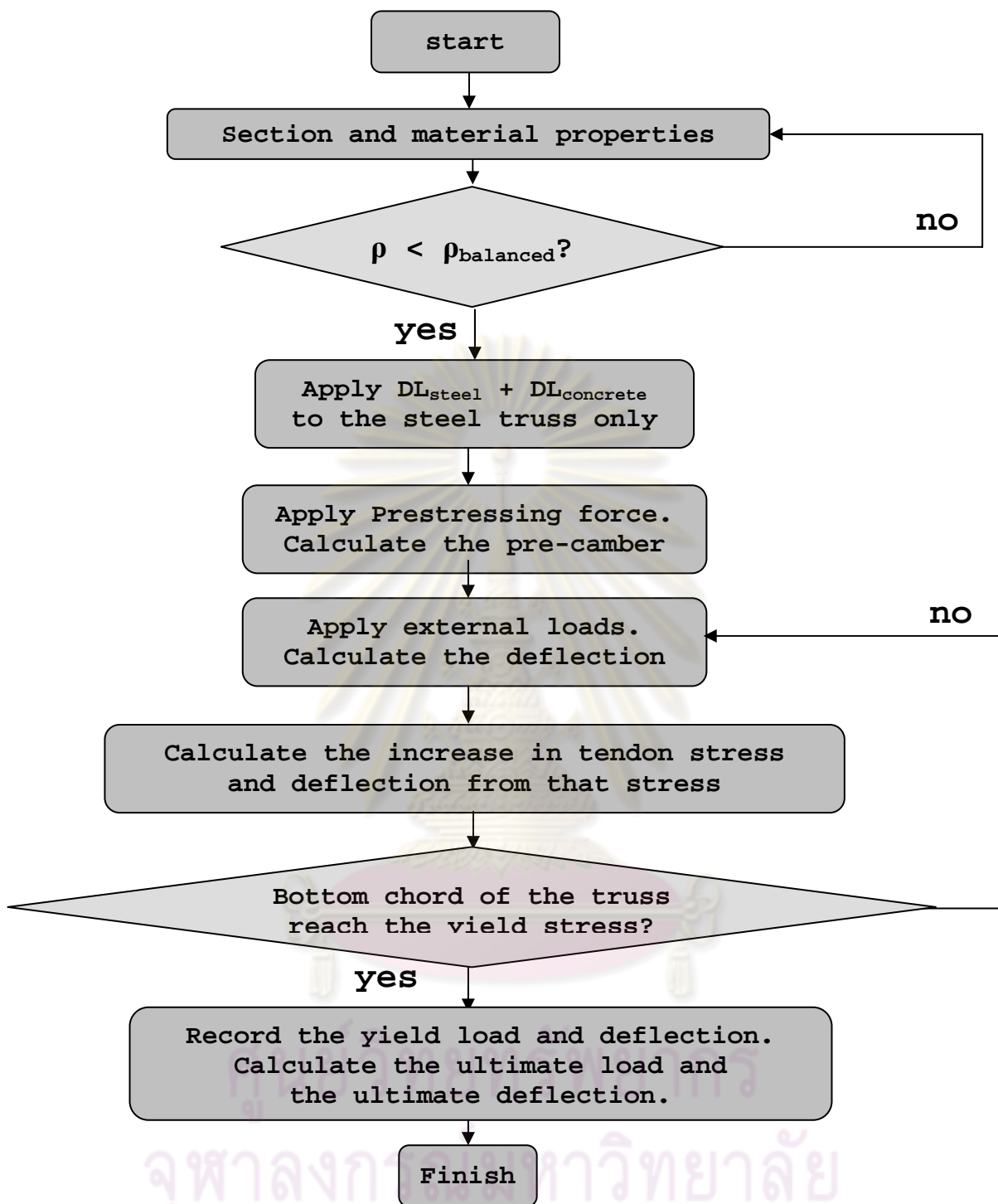


Figure 2.16 Flow chart for analyzing of a posttensioned composite truss.

The procedure starts with the material mechanical properties such as are determined from stress-strain curves of concrete, steel, shear stud connectors and the tendons. The truss configuration and cross-sectional dimensions must also be accurately determined.

Then a percentage of the steel truss bottom chord cross-sectional area plus the total cross-sectional area of the tendons in equilibrium with the area of the effective width of the concrete slab are considered. The distance from the top surface of the concrete slab to the centroid of the effective area of the steel truss bottom chord is computed. The results are compared with the balanced condition percentage,  $\rho_b$ , which is determined using a balanced failure theory. In a balanced failure analysis, the compressive strain in the top surface of the concrete reaches an ultimate compressive strain of 0.003 at the same time as the tensile stress in the bottom chord reaches the yield strength.

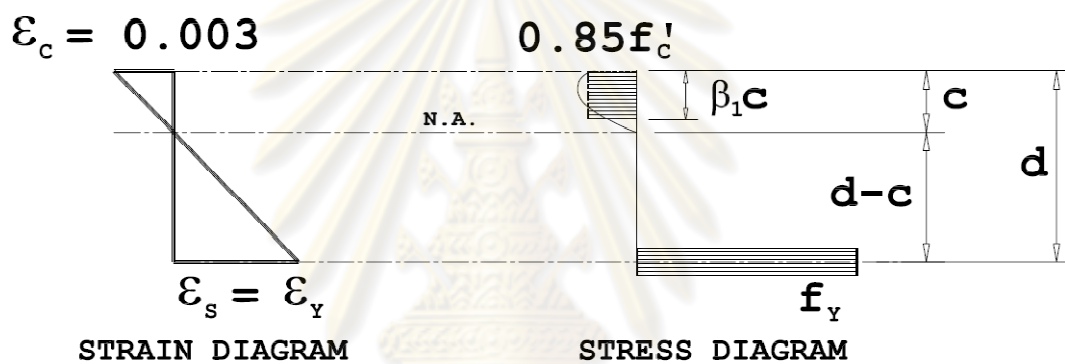


Figure 2.17 Strain and stress diagrams at balanced condition

From the strain compatibility as shown in Figure 2.17 and the constitutive law, using similar triangles for the distance  $c$  and  $(d-c)$ ;

$$\frac{\epsilon_{cu}}{c} = \frac{\epsilon_y}{(d-c)} = \left( \frac{F_y}{E} \right)$$

$$c = \frac{\epsilon_{cu} d}{\left( \frac{F_y}{E} - \epsilon_{cu} \right)} \quad (2.40)$$



From cross-section equilibrium;

$$0.85 f_c' \beta_1 c \cdot b = A_s F_y$$

$$0.85 f_c' \beta_1 \frac{\varepsilon_{cu} d}{\left(\frac{F_y}{E} - \varepsilon_{cu}\right)} \cdot b = A_s F_y$$

$$\frac{A_s}{b \cdot d} = \rho_b = 0.85 \frac{f_c'}{F_y} \beta_1 \frac{\varepsilon_{cu}}{\left(\frac{F_y}{E} - \varepsilon_{cu}\right)} \quad (2.41)$$

For the section that has both  $A_s$  for the bottom chord and  $A_{ps}$  for the tendon;

$$\rho_{total} = \rho_s + \rho_{ps}$$

$$\rho_{total} = \left(\frac{A_s}{b \cdot d}\right) + \eta \left(\frac{A_{ps}}{b \cdot d}\right) \quad (2.42)$$

$$\eta = \frac{F_{py}}{F_y}$$

where  $\eta$  is the yield strength ratio of the yield strength of the tendon to the yield strength of the bottom chord.

The limit of the percentage of  $\rho_{total}$  less than the balanced condition makes the structure fail in a ductile manner involving yielding of the bottom chord prior to the crushing of the concrete at a ductility ratio of 4 or greater.

The dead loads and the prestressing tendon force are applied to the composite truss without considering the stiffness and slip of the unbonded tendon. The pre-camber from the prestressing tendon load and the deflection from superimposed dead loads are also determined by the energy theorem using the actual stresses in all members. When the external loads are applied to the post-tensioned composite truss, the corresponding increase in tendon force is calculated using the strain compatibility condition and energy technique as described before. Deflections due to external loads

are calculated along with the camber from the increase in tendon load which acts in the opposite direction. The downward external loads tend to make the posttensioned composite truss move downward while the increasing tendon force tends to make the truss move upward.

The combinations of stresses due to all steps are calculated up to the beginning of the yielding in the bottom chord of the truss. The external loads which cause the first yielding of the bottom chord are recorded as the yield load with a corresponding yielding deflection.

The ultimate external loads are those that produce ultimate internal stresses in the bottom chord and in the tendons at the maximum flexural capacity of the posttensioned composite truss. The ultimate deflection  $\Delta_u$  is calculated base on the yielding deflection  $\Delta_y$  multiplied by the ductility ratio of 4.

All the data for the load deflection curve can be computed as described above. For the moment - curvature relationship can also be computed from the data that produce the load deflection curve; i.e. the internal moment can be found by the internal stresses and the curvature can be computed by the strain divided by the distance between the neutral axis to the strain line.

### 2.3.2 Semi-Rigid Joint Behavior

Although trusses are usually analyzed as assemblages of pin-ended elements, bending can occur in them as a result of joint eccentricities caused by eccentricities due to welding procedures. Member flexural stiffness,  $EI$ , also comes into play once joint eccentricity effects are activated by imposed loads. Even in the case of true pinned joints truss members may experience flexural action due to secondary effects. The local and global stability of the truss and its elements are also considered in the analysis.

The analysis considering effects of the semi-rigid joint behavior can be done by analyzing trusses as rigid joint frames considering both the axial forces and the bending moments inside each member. The results can then be plotted and then compared with similar load - deflection curves a simple truss analysis.

From the principle of virtual work the internal virtual strain energy within the structure is equated to the work done by external virtual loads;

$$\delta U^* = \delta W_e^* \quad (2.25)$$

The virtual strain energy,  $\delta U^*$ , can be calculated based on both axial as well as flexural action of the members using the relationship:

$$\delta U^* = \sum_{i=1}^n \int_0^L \left( \frac{F_i(x) \cdot \delta F_i(x)}{E_i(x) A_i(x)} + \frac{M_i(x) \cdot \delta M_i(x)}{E_i(x) I_i(x)} \right) dx \quad (2.43)$$

Where  $i$  is the number of an element from 1 up to  $n$  and  $L$  is the length of member  $i$ .  $F_i(x)$  and  $\delta F_i(x)$  denote the real internal force and the virtual internal force of member  $i$ .  $M_i(x)$  and  $\delta M_i(x)$  denote the real internal moment and the virtual internal moment of member  $i$ .  $E_i(x)$ ,  $A_i(x)$  and  $I_i(x)$  are respectively, the modulus of elasticity, cross sectional area, and moment of inertia of member  $i$ .

A member extending from node 1 to node 2 as shown in the figure 2.21 below is considered. The sign convention of the internal moments are positive in the compression zone, and ;

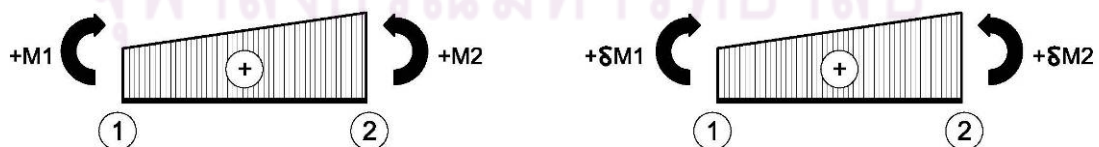


Figure 2.18 Sign convention for the internal moments.

$$\delta U^*_{bending} = \sum_{i=1}^n \int_0^L \left( \frac{M_i(x) \cdot \delta M_i(x)}{E_i(x) I_i(x)} \right) dx \quad (2.44)$$

$$\begin{aligned} \delta U^*_{bending} &= \sum_{i=1}^n \frac{1}{E_i I_i} \int_0^L \left[ \left( \frac{M_2 - M_1}{L} \right) x + M_1 \right] \cdot \left[ \left( \frac{\delta M_2 - \delta M_1}{L} \right) x + \delta M_1 \right] dx \\ &= \sum_{i=1}^n \frac{L_i}{E_i I_i} \left\{ \frac{(M_2 - M_1)(\delta M_2 - \delta M_1)}{3} + \frac{[(M_2 - M_1)(\delta M_1) + (\delta M_2 - \delta M_1)M_1]}{2} + M_1 \delta M_1 \right\} \end{aligned} \quad (2.45)$$

The analytical results for the semi-rigid joint compared to the experimental results along with the pin joint analysis are presented in Chapter 4.

### 2.3.3 Lateral Stability of Bottom Chords

The bracing systems may be considered as simplified models each consisting of a pinned end column with a horizontal spring at the top that is capable of developing a horizontal reaction equal to the spring stiffness,  $\beta$ , times the deflection,  $\Delta$ . For an ideal column, the member is perfectly straight and the loaded configuration is considered as shown below;

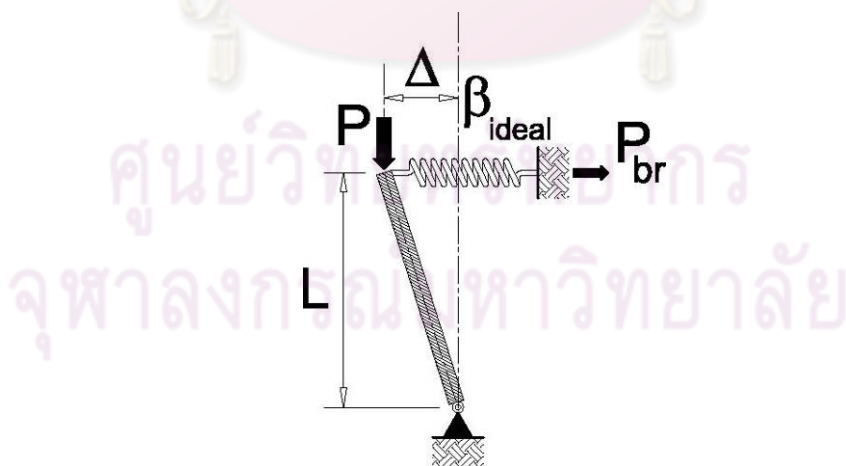


Figure 2.19 Loaded configuration of ideal column with elastic bracing

The equilibrium condition for the moment about the lower pinned end gives;

$$P \cdot \Delta = \beta_{ideal} \cdot \Delta \cdot L$$

$$\beta_{ideal} = \frac{P}{L} \quad (2.46)$$

The  $\beta_{ideal}$  is the required spring stiffness for the ideal straight column of length  $L$  to resist the axial load  $P$ . For the column with initial horizontal imperfection of  $\Delta_o$ , the moment about the lower pinned end from the loaded configuration shown below gives;

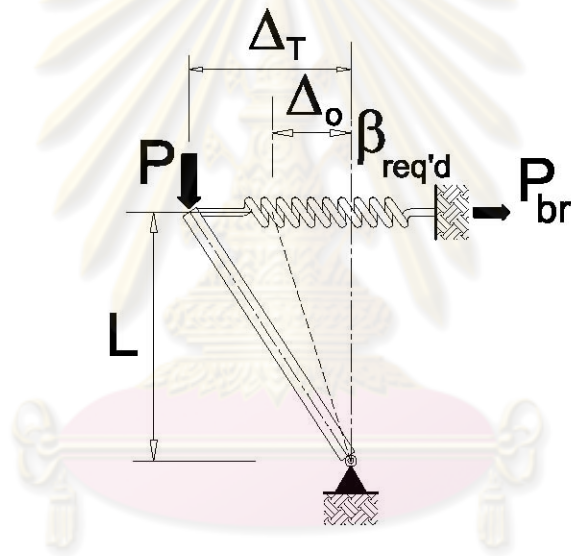


Figure 2.20 Loaded configuration of horizontal imperfect column with bracing

$$P \cdot \Delta_T = \beta_{req'd} \cdot (\Delta_T - \Delta_o) \cdot L$$

$$\beta_{req'd} = \frac{P}{L} \left( \frac{1}{1 - \frac{\Delta_o}{\Delta_T}} \right) = \beta_{ideal} \left( \frac{1}{1 - \frac{\Delta_o}{\Delta_T}} \right) \quad (2.47)$$

Winter (1958, 1960) found that the best suitable value for  $\Delta_o$  is  $L/500$  and that  $\Delta_T$  equals to  $2\Delta_o$ , thus,  $\beta_{req'd}$  equals  $2\beta_{ideal}$ .

Consider the bottom chord of the posttensioned composite truss under the prestressing force from tendon  $F_{ps}$ . The loaded configuration is shown in the following figure;

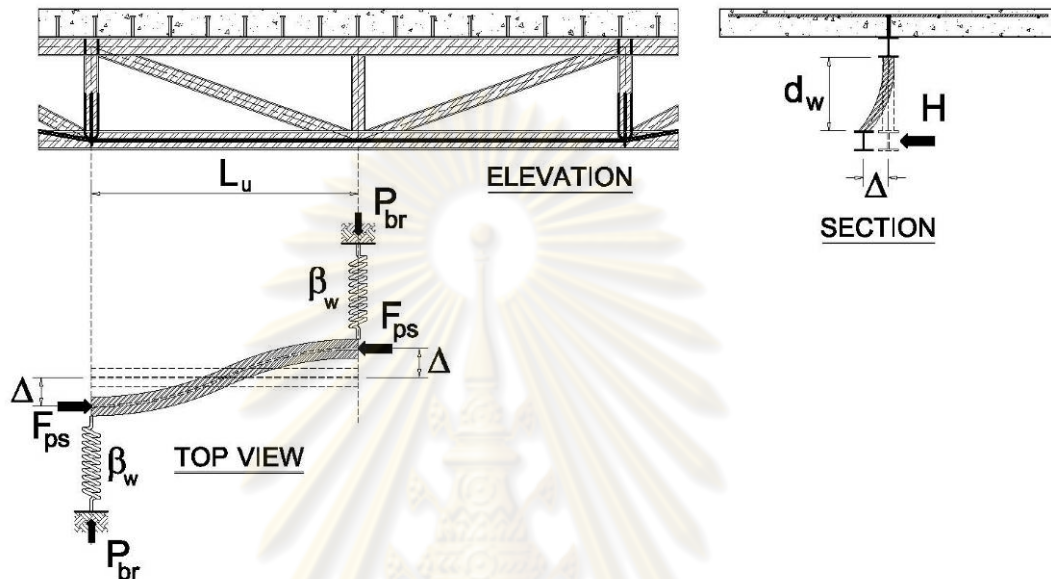


Figure 2.21 Loaded configuration of bottom chord under prestressing force with web member as lateral bracing

$$F_{ps} \cdot 2\Delta = \beta_w \cdot \Delta \cdot L_u$$

$$\beta_w = \frac{2F_{ps}}{L_u} \quad (2.48)$$

The lateral translation stiffness of the bottom chord considering the web member as the lateral bracing element is;

$$K_H = \frac{3 \cdot E_w \cdot I_w}{d_w^3} \quad (2.49)$$

Substitute the lateral translation stiffness in the required spring stiffness for  $F_{ps}$  and also considering the initial imperfection effect ( $\beta_{req'd}$  equals to  $2\beta_{ideal}$ ) gives;

$$F_{ps,max} = \frac{3 \cdot E_w \cdot I_w}{d_w^3} \left( \frac{L_u}{4} \right) \quad (2.50)$$

This is the equation to determine the maximum prestressing force considering lateral buckling of the bottom chord.

### 2.3.4 Losses of Prestress

#### 2.3.4.1 Shrinkage

Shrinkage causes the tensile strain developed inside the concrete slab. If the shrinkage can occur freely without any restraint, free shrinkage strain,  $\epsilon_f$  is the result. Referring to the study by Brattland and Kennedy (1986) For the type of composite truss studied herein, the shrinkage in the concrete slab is restrained by the steel truss to which the slab is attached by means of the shear studs. Therefore, the tensile strain in the concrete slab is less than the free shrinkage strain resulting in the restrained shrinkage strain,  $\epsilon_r$ . The actual tensile strain in the concrete slab is,  $\epsilon_s$ , which is equal to the difference between free shrinkage strain,  $\epsilon_f$  and the restrained shrinkage strain,  $\epsilon_r$ . These strains are illustrated as shown in the strain diagram of the composite truss in Figure 2.22.

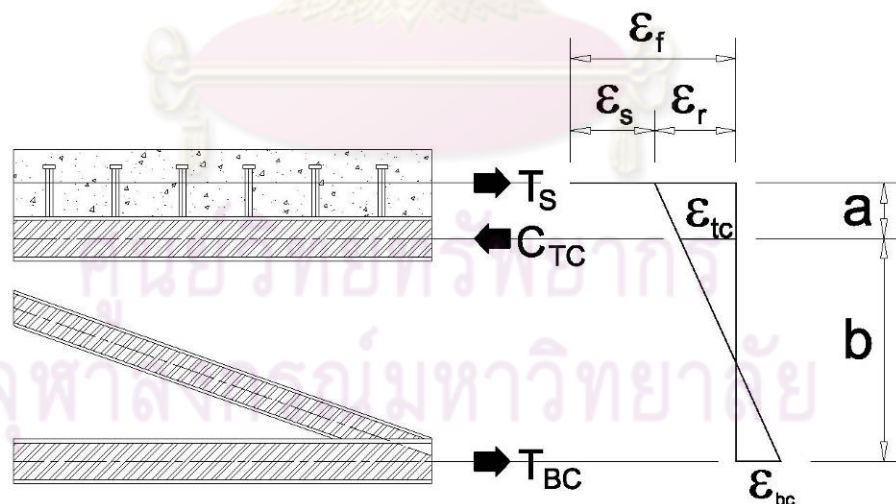


Figure 2.22 Shrinkage strain diagram

The shrinkage strain decreases rapidly from the free shrinkage strain at the ends and remains constant for most of the length of the concrete slab (approximately 90%) along the longitudinal. Thus, the distribution of longitudinal

shrinkage strains in the concrete slab is uniform. As a result the tensile force in the concrete is constant over most of the length. By equilibrium in the longitudinal direction, the compression in the top chord is equal to the combination of the tensile forces in the concrete slab and the bottom chord.

Referring the force, strain diagrams and the distance variables,  $a$  and  $b$  from Figure 2.22,

$$C_{TC} = T_s + T_{BC} \quad (2.51)$$

Summing moments about the mid depth of the steel top chord in the Figure 2.22 gives;

$$T_{BC} = \left(\frac{a}{b}\right) \cdot T_s \quad (2.52)$$

From the above two equations,

$$C_{TC} = \left(\frac{a+b}{a}\right) \cdot T_{BC} \quad (2.53)$$

Substituting the term of the internal forces by the internal strains and taking moments about the mid depth of the steel top chord gives:

$$\begin{aligned} \varepsilon_{tc} EA_{tc} - \varepsilon_{bc} EA_{bc} &= (\varepsilon_f - \varepsilon_r) E_c A_c \\ \varepsilon_{bc} EA_{bc} &= \left(\frac{a}{b}\right) (\varepsilon_f - \varepsilon_r) A_c E_c \end{aligned} \quad (2.54)$$

$$\left(\frac{a+b}{b}\right) \varepsilon_{tc} + \left(\frac{a}{b}\right) \varepsilon_{bc} = \varepsilon_r$$

Solving the above three equations gives the strain,  $\varepsilon_r$ , the strain in the bottom chord,  $\varepsilon_{bc}$  and the strain in the top chord member,  $\varepsilon_{tc}$ .

The deflection due to shrinkage,  $\Delta_{sh}$ , is calculated by applying the constant moments acting on the composite cross section in magnitude to a compressive force at the centroid of the concrete slab multiplied by the distance from its line of action to the centroid of the transformed section,  $e$ .



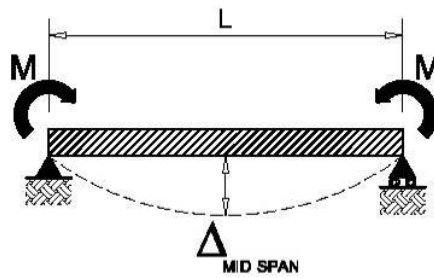


Figure 2.23 Deflection from the Shrinkage moments

For this calculation, the magnitude of the compressive force is the force required to shorten the concrete cover slab by an amount equal to the restrained shrinkage strain:

$$\Delta_{SH} = \frac{ML^2}{8EI_{transf}} \quad (2.55)$$

$$M = (\varepsilon_r E_c A_c)(e)$$

The shrinkage moments cause the prestressing tendons to be shortened leading to a decrease in tendon force of  $\Delta T_{sh}$ . This decrease in tendon force makes the truss deflect downward in the same direction as the creep deflection. In order to find the decrease in tendon force from shrinkage,  $\Delta T_{sh}$ , due to the shrinkage moment, the total elongation at the same level as the tendon is  $\delta_{1p}$ . The total elongation at the same level as the tendon due to the unit prestressing force,  $\delta_{11}$ , is determined resulting in:  $\Delta T_{sh} = \delta_{1p} / \delta_{11}$ .

#### 2.3.4.2 Creep

Creep strain is a time dependent strain in concrete that develops from sustained compressive stress. The strain at time  $t$  in a concrete member,  $\varepsilon_c(t)$ , uniaxially loaded with a constant stress  $\varepsilon_c(t_0)$  at time  $t_0$  is;

$$\varepsilon_c(t) = \varepsilon_{ci}(t_0) + \varepsilon_{cc}(t, t_0) \quad (2.56)$$

where  $\varepsilon_{ci}(t_0)$  is the initial elastic creep as determined from the stress  $\sigma_c(t_0)$  and the creep strain  $\varepsilon_{cc}(t, t_0)$  from time  $t_0$  to  $t$ , can be calculated from;

$$\varepsilon_{cc}(t, t_o) = \frac{\sigma_c(t_o)}{E_c(28)} \phi(t, t_o) \quad (2.57)$$

$E_c(28)$  is the concrete modulus of elasticity at 28 days and  $\phi(t, t_o)$  is the creep coefficient. Introducing  $\phi_o$  as the basic creep,  $\beta_c(t, t_o)$  is a coefficient to account for the development of creep with time,  $h_e$  is the effective thickness in inches to account for the volume to surface ratio equal to 2 times cross sectional area over perimeter of the cross section exposed to the atmosphere in inches;  $h_o$  is the original thickness in inches, RH is the relative humidity of the ambient atmosphere in percent,  $RH_o$  is 100%;  $f_{cm}$  is the mean compressive strength at 28 days in psi,  $f_{cmo}$  equals 1450 psi,  $t_1$  equals 1 day; and  $\phi_{RH}$  is the coefficient that accounts for the effect of relative humidity on shrinkage. Thus, the creep coefficient is computed as follows;

$$\begin{aligned} \phi(t, t_o) &= \phi_o \beta_c(t, t_o) \\ \phi_o &= \phi_{RH} \beta(f_{cm}) \beta(t_o) \\ \phi_{RH} &= 1 + \frac{1 - RH/RH_o}{0.46(h_e/h_o)^{1/3}} \\ \beta(f_{cm}) &= \frac{5.3}{(f_{cm}/f_{cmo})^{0.5}} \\ \beta(t_o) &= \frac{1}{0.1 + (t_o/t_1)^{0.2}} \\ \beta_c(t, t_o) &= \left[ \frac{(t - t_o)/t_1}{\beta_H + (t - t_o)/t_1} \right]^{0.3} \\ \beta_H &= 150 \left[ 1 + \left( 1.2 \frac{RH}{RH_o} \right)^{18} \right] \left( \frac{h_e}{h_o} \right) + 250 \leq 1500 \end{aligned} \quad (2.58)$$

Since shear stud connectors are provided uniformly over the truss length, the creep strain from the prestressing force is also restrained by the steel top chord member as in the case of shrinkage. The method of calculation follows that as in the shrinkage calculation. However, when the creep deflection is determined, the deflection equation changes to the following equation based on the different moment diagrams from the creep moments.  $M_1$  and  $M_2$  are the moments from the forces equal to

restrained strains times the elastic modulus and cross sectional areas of the concrete about the centroid of the transformed section for panel 1 and panel 2, respectively.

$$\begin{aligned}\Delta_{CR} &= \frac{M_1 L^2}{162EI_c} + \frac{M_2 L^2}{54EI_c} \\ M_1 &= [(\varepsilon_{cr,r} E_c A_c)(e)]_1 \\ M_2 &= [(\varepsilon_{cr,r} E_c A_c)(e)]_2\end{aligned}\quad (2.59)$$

The only unknown variable in the above equations is the concrete strain which is a function of the creep strain,  $\varepsilon_{cc}(t, t_0)$  and the creep strain is a function of the creep coefficient  $\phi(t, t_0)$ .

#### 2.3.4.3 Anchorage Seating

Anchorage seating loss occurs when the wedges move in to the anchorage seating pocket due to the prestressing force as the pressure is transferred from the prestressing jack. The amount of the anchorage seating depends on the type of the wedge and the stress in the tendon. An average value of the anchorage movement is 2 to 3 mm. For this type of loss the anchorage seating loss is distributed uniformly over the entire length of the tendon between the two tendon anchorage points. The stress loss can be calculated from the following equation;

$$\Delta f_{anch} = \frac{\Delta}{L_T} E_{tendon} \quad (2.60)$$

where  $\Delta$  is the anchorage movement,  $L_T$  is the total length of the tendon between two anchorage points and  $E_{tendon}$  is the elastic modulus of the tendon.

#### 2.3.4.4 Relaxation

The relaxation in a prestressing tendon refers to the gradual loss of prestress over a period of time. An important factor that governs the relaxation behavior is the stress ratio of the jacking stress to the yield strength of the tendon,  $f_{pi}/f_{py}$ :

$$\frac{f_p}{f_{pi}} = 1 - \left( \frac{\log t - \log t_1}{10} \right) \left( \frac{f_{pi}}{f_{py}} - 0.55 \right) \quad (2.61)$$

## CHAPTER 3

### EXPERIMENTAL APPROACH

#### 3.1 Test Program

To study the flexural behavior of the steel trusses with high performance concrete composite decks, an experimental approach is essential for the research procedure. The full scale specimens were constructed to observe several aspects of behavior including: the influence of post-tensioned tendons on flexural behavior; load and deflection relationships; ultimate moment capacity; failure modes; actual truss joint behavior; possible problems for posttensioned composite trusses, and; verification of the theoretical approach. Specimens were tested under monotonic loading conditions. Table 3.1 below is a summary of the test program. The depth-to-span ratio of 1/16 was selected as representative of conventional depth-to-span ratios found in practice for such composite trusses.

Table 3.1 Test Program

Series	Concrete Slab	Test Specimen	Tendon Details	Tendon Stress (MPa)
A	Yes	Specimen A1	2-Ø12.7mm.	460
		Specimen A2	2-Ø12.7mm.	690
		Specimen A3	2-Ø12.7mm.	920
		Specimen A4	-	-
B	No	Specimen B1	-	-
		Specimen B2	12.7	460

Two test series as summarized in Table 3.1 were tested under point loads applied at the third points along the length. Truss series A included a concrete composite deck and was subjected to prestress by two grade 250 DYWIDAG<sup>®</sup> monostrand tendons of 12.7 mm (1/2 in.) diameter at three different prestressing levels of: 460MPa (Specimen A1); 690MPa (Specimen A2), and; 920MPa (Specimen A3). Specimen A4 was performed on the remnant of the Specimen A3 after the cables were cut to eliminate the prestress. For the case of prestressing level at 920MPa (Specimen A3) the specimen was loaded up to ultimate failure. Truss series B had the same nominal member sizes and dimensions as Truss series A except that it had no concrete composite slab. Truss series B was used as two specimens, Specimen B1 and Specimen B2. For Specimen B1, just the steel truss with no prestressing was tested. For Specimen B2, the tendons were stressed up to 460 MPa and loads were applied up to ultimate.

### 3.2 Test Specimens

The span length of all test specimens were 8534mm (28 ft.) long with a top chord center to the bottom chord center depth of 500mm. Specimen A, as shown in Figure 3.1, had an 1800mm (6 ft.) wide by 150mm (6 in.) thick high performance reinforced concrete composite deck slab with a nominal concrete compressive 28-day strength of 50MPa. The concrete slab was connected to the top chord of the truss which consisted of a W100x19 shape ASTM A992 steel. The shear connection was formed using 57 welded standard Nelson shear stud connectors, 15.9 mm in shank diameter and 115mm long with a center spacing of 150mm. The bottom chord of the truss had the same size chord (W100x19 shape ASTM A992 steel) as the top. The W100x19 shape had a flange thickness of 8.8mm and a web thickness of 7.1 mm. The overall depth was 106mm and the overall width was 103mm with a cross sectional area of 2480mm<sup>2</sup> resulting in a self weight of 0.191kN/m. The sectional moments of inertia about the major and minor axes were  $4.77 \times 10^6 \text{ mm}^4$  and  $1.61 \times 10^6 \text{ mm}^4$ , respectively.

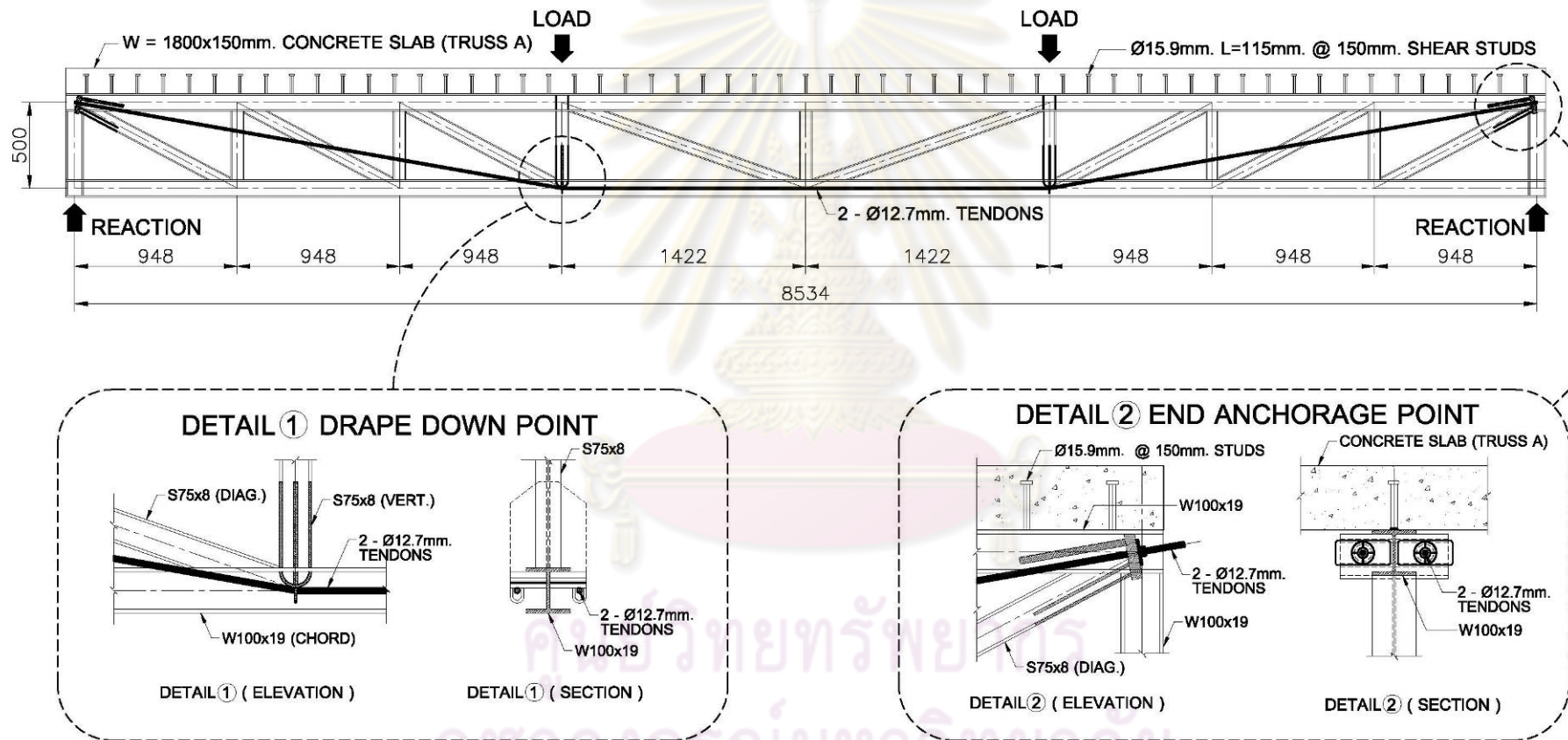


Figure 3.1 Test specimens: Dimensions with drape down points and end anchorage details

The vertical and diagonal web members consisted of S75x8 sections made of ASTM A992 steel with a flange thickness of 6.6 mm and a web thickness of 4.3 mm. The overall depth was 76mm. and the overall width was 59mm and a cross sectional area of  $1070\text{mm}^2$  resulting in a self weight of 0.083kN/m. This section has a moment of inertia about its major axis of  $1.04 \times 10^6 \text{mm}^4$  and about its minor axis of  $0.187 \times 10^6 \text{mm}^4$ .

Since all experiments were conducted in the structural laboratory at the Department of Civil Engineering, University of New Brunswick, Fredericton, Canada, all of the materials such as steel plates, concrete and shear studs are under Canadian specifications along with some of the materials from DSI America which are under American specifications. The rolled shapes available in Canada are produced either to CSA Standard G40.21 350W, to ASTM A572 grade 50, or to ASTM A992. All of these grades have similar specified minimum values of yield strength at 350MPa (min.) to 450MPa (max.) and the tensile strength at 450MPa (min.) to 650MPa (max.)

Test specimens were mounted in a self-equilibrating test frame for loading in the structural lab as shown the plan and elevation views in Figure 3.2 with a typical section view shown in Figure 3.3. The self-equilibrating load – reaction frame was constructed using four wide flange W200x59 steel sections with a flange thickness of 15mm used as columns fastened to the strong floor by 38mm diameter high strength bolts. Two W610x217 wide flange steel girders served as the main reaction load girders supported by W460x97 cross beams with a flange thickness of 20mm. Four 22mm ASTM A325 high tension bolts per support were used to connect the main girders to the cross beams. The frame was braced using steel angles 100x100x6mm connected to the strong floor using 38mm diameter bolts. Solid round steel bars of diameter 1 inch were used as roller supports located directly under the center of the end span vertical member. A translation slot and pivot plate permitted horizontal translation and rotation at the support. Concrete forms were designed especially for the research purpose to simulate the actual construction. The dead loads of the concrete and forms were applied to the steel truss directly with no dead load force being transferred to the laboratory floor.





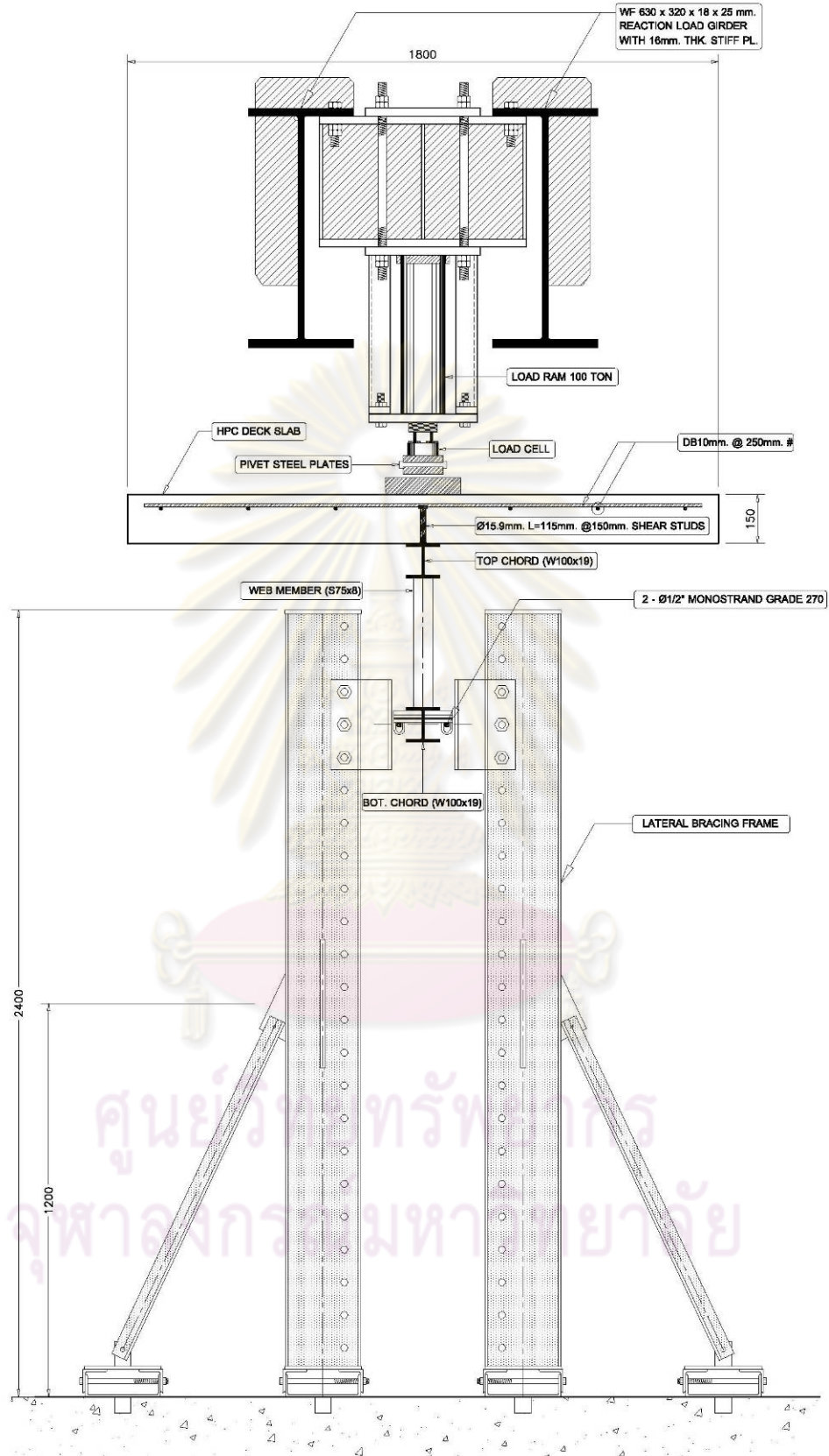


Figure 3.3 Section view of a test specimen in the loading frame

The temperature and shrinkage reinforcement used were 10mm (3/8 in.) diameter deformed bars with seven spaced longitudinally at 250 mm (10 in.) on centers and 35 placed transversely at 250mm (10 in.) on centers. The 100mm. (4 in.) rebar chairs were used to set the lowest level of the rebars at 100mm above the top surface of the concrete form. Thus, the highest level of the rebars was at 120mm above the top surface of the concrete forms resulting in a top cover of 30mm. Hooked bars were placed in the concrete slab for lifting and removal purposes after all the tests were done.

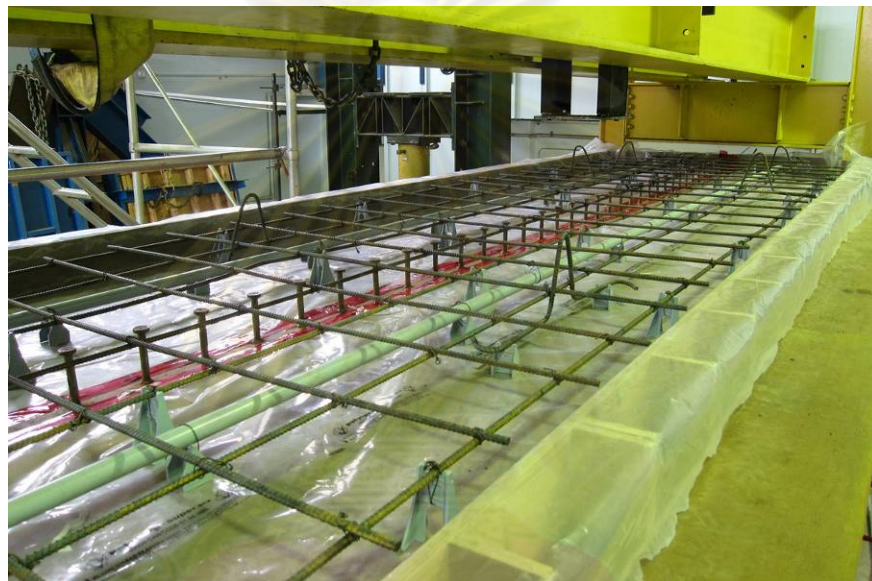


Figure 3.4 Shear stud connectors and slab rebars

The concrete bucket and the travelling crane inside the structural lab were used for the concrete casting procedure. A plastic sheet was provided on the top surface and also the side forms of the plywood to prevent the leaking of the cement paste and the water. A concrete vibrator was used during casting to assist in spreading the concrete. After the concrete was cast, curing was done in a moist atmosphere at room temperature by using wet burlap and plastic sheet covering to prevent water evaporation for a 7-day period. This ensured that the compressive strength would develop up to 80% of the 28-day design strength before removal of the concrete forms.



Figure 3.5 Curing under cover of wet burlap and plastic sheet.

After the concrete had reached the design compressive strength of 50MPa, the composite truss specimen was prestressed with the two 12.7mm diameter ( $\frac{1}{2}$  in.) unbonded monostrand posttensioning tendons. They were anchored at the ends with welded end anchorage plates designed specially to fit the two-piece DYWIDAG<sup>®</sup> wedge-anchor system.



Figure 3.6 Posttensioning of Truss A

The tendons were draped at the one-third points of the truss at 2845mm from the center of the end vertical member. The overall length of each tendon between two wedge anchor systems was 8620mm. Curved steel plates were used to locate the tendons to the level of the center of the bottom chord member with nearly frictionless surfaces. Referring to Figures 3.7 and 3.8, two hydraulic twin-ram jacks and the control system from DSI America along with the pressure gauge reading, the calibration chart, and wedge installation hammers were used to anchor and produce the tensile stresses in the tendons.



Figure 3.7 End anchorages of prestress tendons

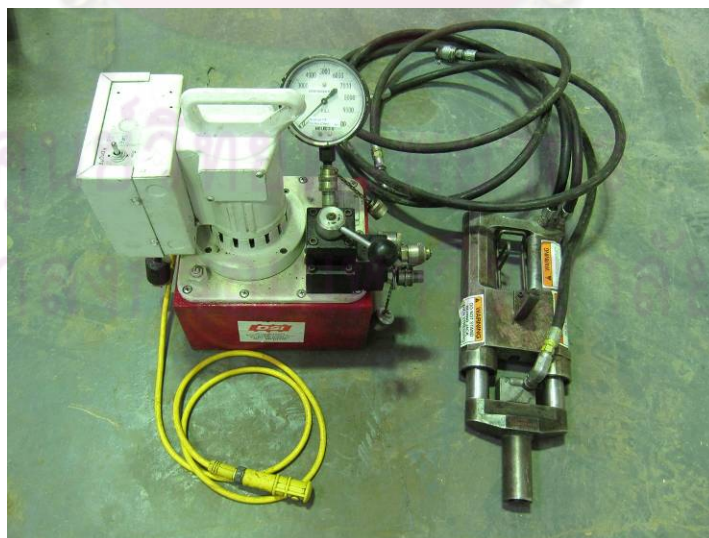


Figure 3.8 Twin-ram jack with pump and pressure gauge.

Referring to Figures 3.9 and 3.10, specimens were loaded at the third points by two load rams of 1000kN capacity with a stroke of 300mm. The hydraulic hoses were connected to the rams and hydraulic pumps. Carefully controlled apparatus ensured that tendon loads applied by the two rams remained equal as indicated by the reading values from the calibrated load cells. The two load cells were calibrated and installed between the rams and the concrete slab for measuring actual loads acting on the test specimens. Pivot plates were used to adjust the angle of the load to be perpendicular to the concrete slab at all times during a test.



Figure 3.9 Two 1000kN load-rams with the load cells.



Figure 3.10 Elevation view of the Truss series A.

### 3.3 Test Materials

#### Concrete

High performance concrete was used in the experiment to provide sufficiently high shear transfer strength via the shear stud connectors. The 28-day design compressive strength of the HPC mix was 50MPa with a slump of 150mm. The actual concrete had 2.6% air entrainment and a temperature of 60°F at the time of sampling.

Figures 3.11 to 3.14 illustrate test results as summarized in Table 3.2. Nine of the concrete cylindrical mould samples were incurred under the same conditions as the concrete slab. The first set of three cylinder moulds were tested for the compressive strength on the 7<sup>th</sup> day after the concrete had been cast before the concrete forms were stripped. The measured mean compressive strength of these three cylinders was 47.8MPa. The measured mean compressive strength of the three cylinders after 28 days was 55.7MPa. The measured mean compressive strength of the three cylinders after 75 days was 62.5MPa. The mean tensile strength test for the modulus of rupture was 5.6MPa by testing three two point loads on small rectangular beams of 150mm wide by 150mm thick and 450mm span length.

Table 3.2 Concrete compressive strength tests of 7 day concrete

Cylinder No.	Average diameter (cm)	Length (cm)	Failure Load (kg)	Concrete Compressive strength (kg/cm <sup>2</sup> )	7 day to 28 day design compressive strength ratio
1	15.10	30.10	85 299.46	476.32	0.953
2	15.00	30.20	85 072.60	481.41	0.963
3	14.90	30.00	83030.85	476.19	0.952
Average				477.97	0.96

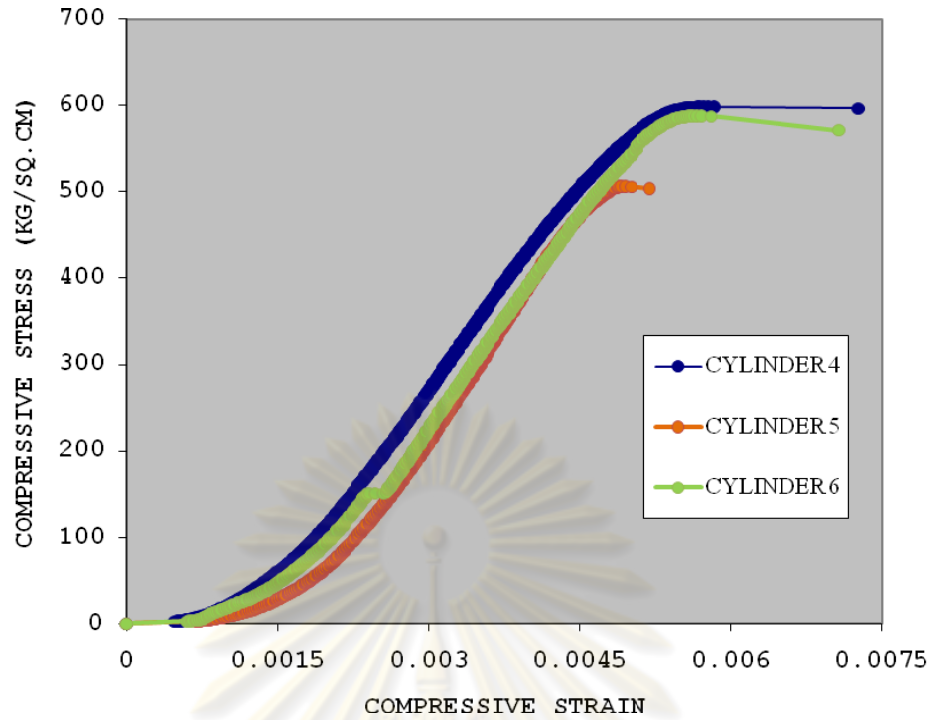


Figure 3.11 Compressive strength tests of 28-day concrete

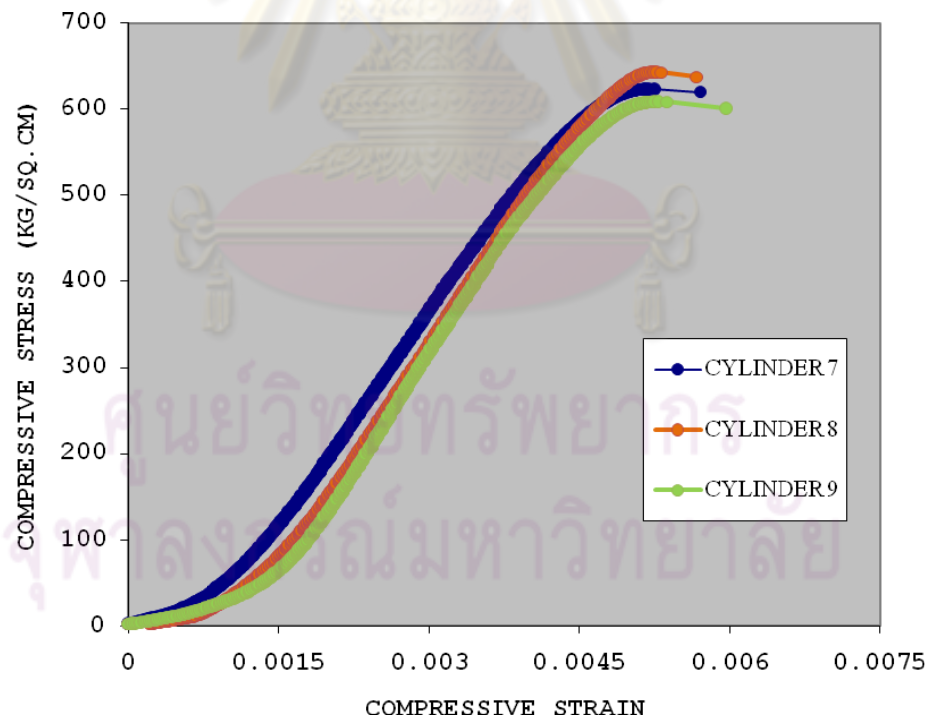


Figure 3.12 Compressive strength tests of 75- day concrete



Figure 3.13 Concrete compressive strength tests



Figure 3.14 Concrete modulus of rupture tests

### Steel Truss Members

The steel chord members were made of W100x19 sections while the vertical and diagonal web members were made of S75x8 sections, all conforming to ASTM A992 steel with a minimum tensile strength of 450MPa (65ksi) and minimum yield stress between 350MPa and 450MPa (50ksi to 65ksi). The gage length used was 50mm. (49.97mm.) with an applied strain rate of 11.5MPa/sec (690MPa/min.) conforming to the standard ASTM A370-03a for rectangular tension test specimens. The mean tensile strength of the W100x19 flange members from coupons 1, 3 and 4 tension tests was 587.3MPa and the mean yield stress level was 483.6MPa. The mean tensile strength of the W100x19 web members from coupons 2, 5 and 6 was 586.9MPa and the mean yield strength was 439.7MPa. The mean tensile strength of S75x8 web members



from coupons 7, 8 and 9 was 503.0MPa and the mean yield strength was 399.0MPa. The web member flange could not be cut and trim for the tension test specimen because the thickness of the flange was not constant.

The overall mean yield strength was 440.7MPa and the overall mean tensile strength was 559.1MPa regardless of the location the coupon was taken from. All the tensile strength test data are summarized in Tables 3.3 and 3.4 below and Figure 3.15 shows test coupon details..

Table 3.3 Coupon tensile strength test data.

Coupon	Width (mm)	Thickness (mm)	Yield Load (kg)	Yield Strength (kg/cm <sup>2</sup> )	Tensile Load (kg)	Tensile Strength (kg/cm <sup>2</sup> )	Elongation (%)	Location
1	12.51	8.55	5808	5430	6237	5831	20.97	Flange W100x19
2	12.48	6.90	3729	4330	5028	5839	37.48	Web W100x19
3	12.55	8.11	4551	4471	6014	5909	37.62	Flange W100x19
4	12.40	8.50	4854	4605	6196	5879	25.48	Flange W100x19
5	12.25	6.90	3764	4453	4980	5892	35.72	Web W100x19
6	12.45	6.90	3785	4406	5049	5877	24.97	Web W100x19
7	12.30	4.53	2226	3995	2780	4989	25.46	Web S75x8
8	12.31	4.50	2219	4006	2792	5040	24.99	Web S75x9
9	12.50	4.50	2232	3968	2847	5061	24.99	Web S75x10
Average				4407		5591	28.63	

Table 3.4 Coupon tensile strength test results.

Location	Average Yield Strength (kg/cm <sup>2</sup> )	Average Tensile Strength (kg/cm <sup>2</sup> )
Flange W100x19	4836	5873
Web W100x19	4397	5869
Web S75x8	3990	5030

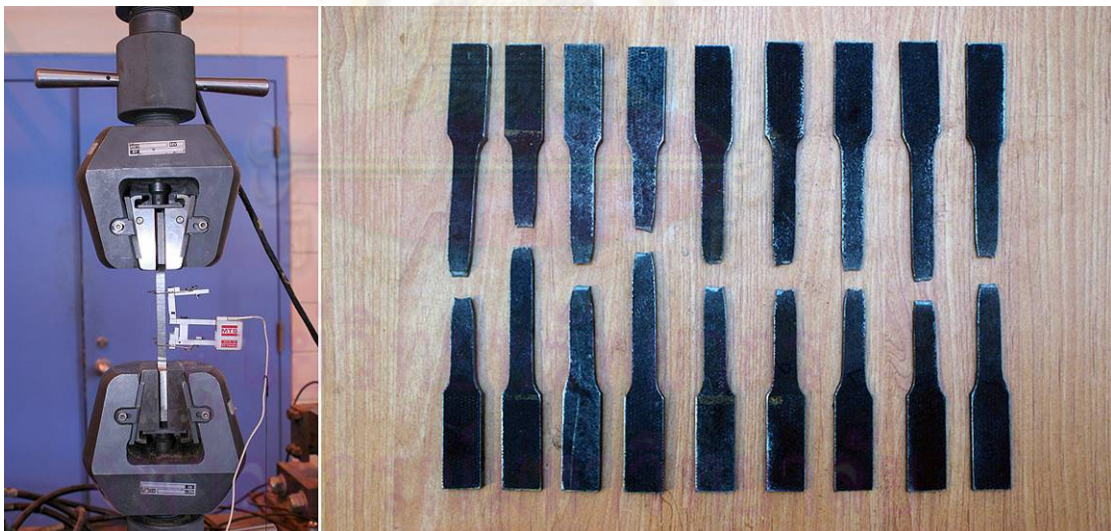
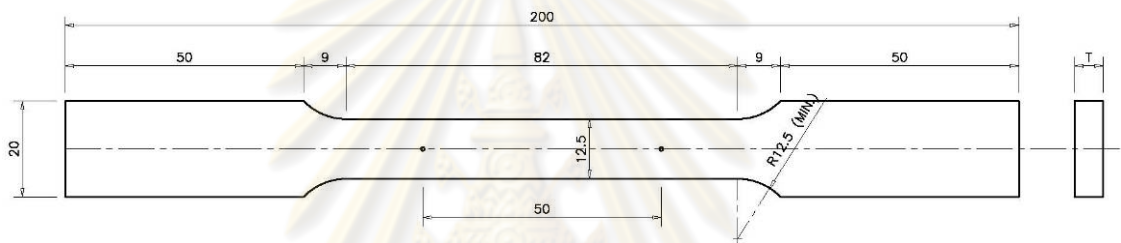


Figure 3.15 Steel coupon tests

### Prestressing Tendons

As shown in Figure 3.16 five samples of the 12.7 mm diameter prestressing tendons were subjected to tension tests to determine the ultimate tensile strength as well as the capacity of the anchorage wedge system. Tendons typically failed by rupture of the small wires one by one for the total number of 7 wires. The anchorage wedges showed a capacity much higher than the tendon itself. The average measured tensile strength was 1 715MPa. Load vs. time curves for four specimens are plotted in Figure 3.17.



Figure 3.16 Monostrand unbonded tendon tension tests

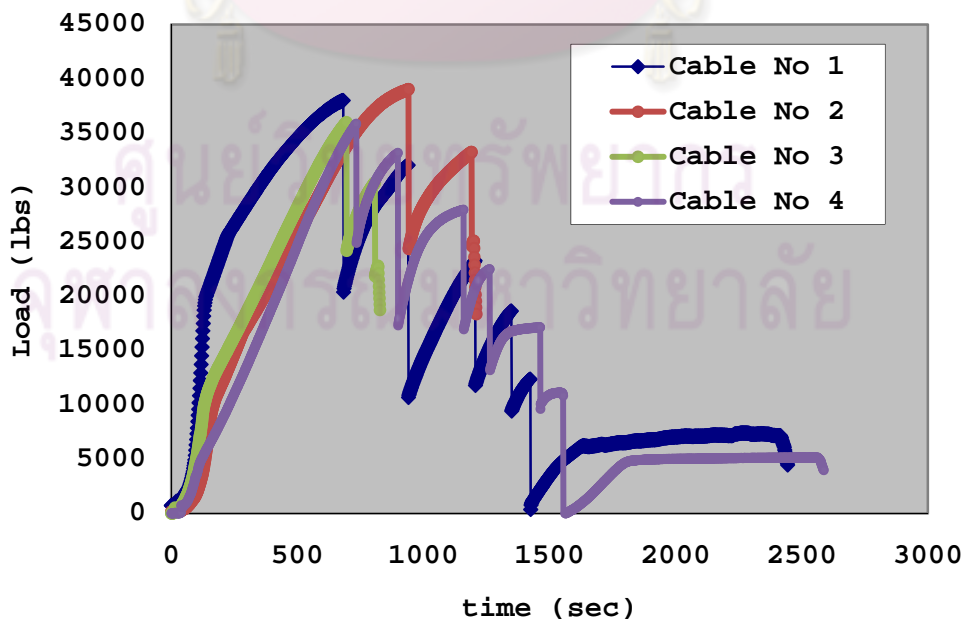


Figure 3.17 Tendon tension load and time relation curves.

## Rebars

Referring to Figures 3.18 and 3.19, five samples of the 10mm slab reinforcement rebars were subjected standard tension test procedures. The mean tensile strength was 860MPa and the mean yield strength was 510MPa with a mean elongation of 8.4%



Figure 3.18 Tension tests of the slab rebar.

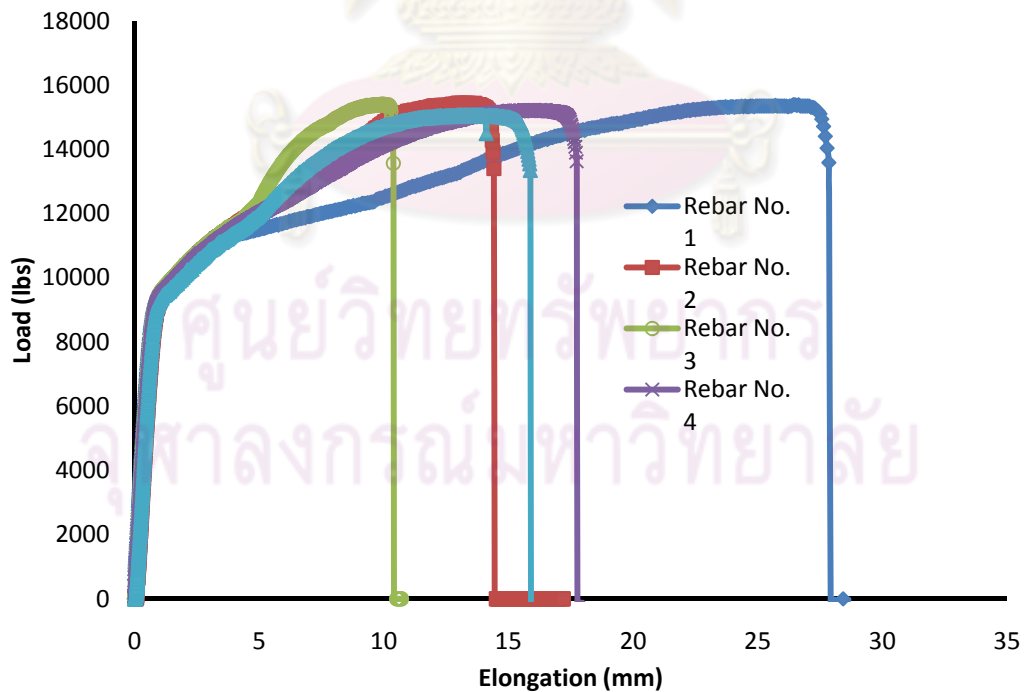


Figure 3.19 Load and elongation curves of the slab rebar.

### 3.4 Test Instrumentations

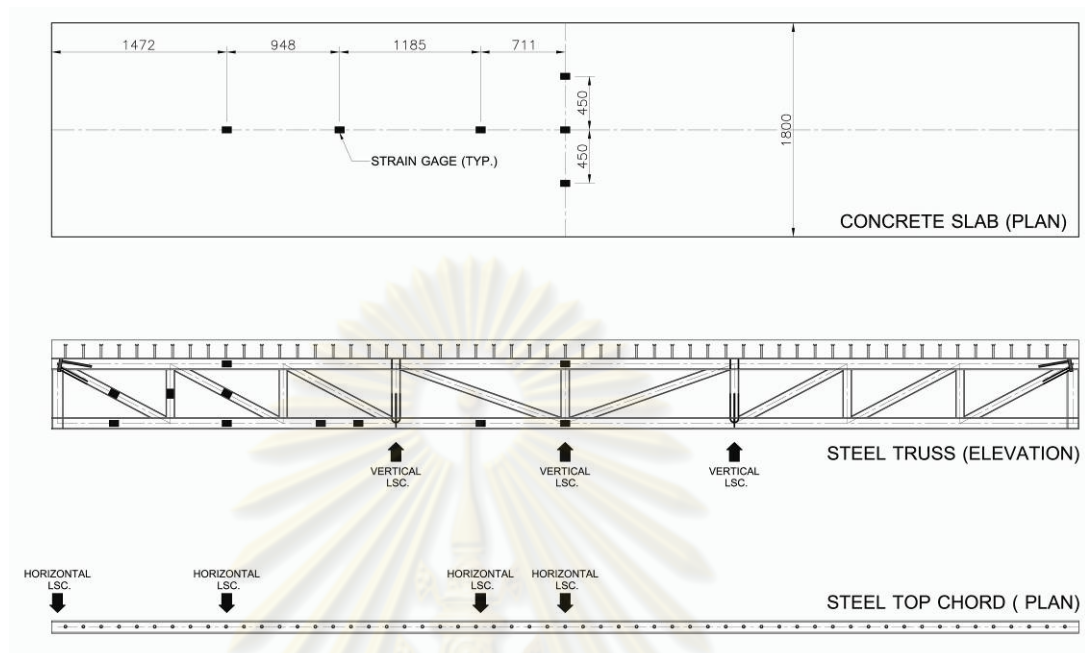


Figure 3.20 Strain gage and LSC locations

As shown in Figure 3.20, strain gages (Omega SGD-6/120-LY11 120 Ohm) were used on the steel members of the specimens. Strain gages (Omega KFG-30-120-C1-11L1M2R 120 $\Omega$ ) were used on the surface of the composite concrete deck. Deflections at mid-span and third points were measured using linear strain converters (LSC). For the lateral movement of the steel truss, LSCs were also used to observe the buckling behavior of the top chord.

At each strain gage attachment point the base materials were prepared carefully according to a specified procedure including solvent degreasing, surface abrading, application of gage layout lines, surface conditioning and neutralizing before each strain gage was placed. Electrical wires were soldered permanently and well controlled to plug in to the Data Acquisition System (DAQ) working with the computer program LABVIEW<sup>®</sup> to display and record the data. Instrumentation is illustrated in Figures 3.21 to 3.23.

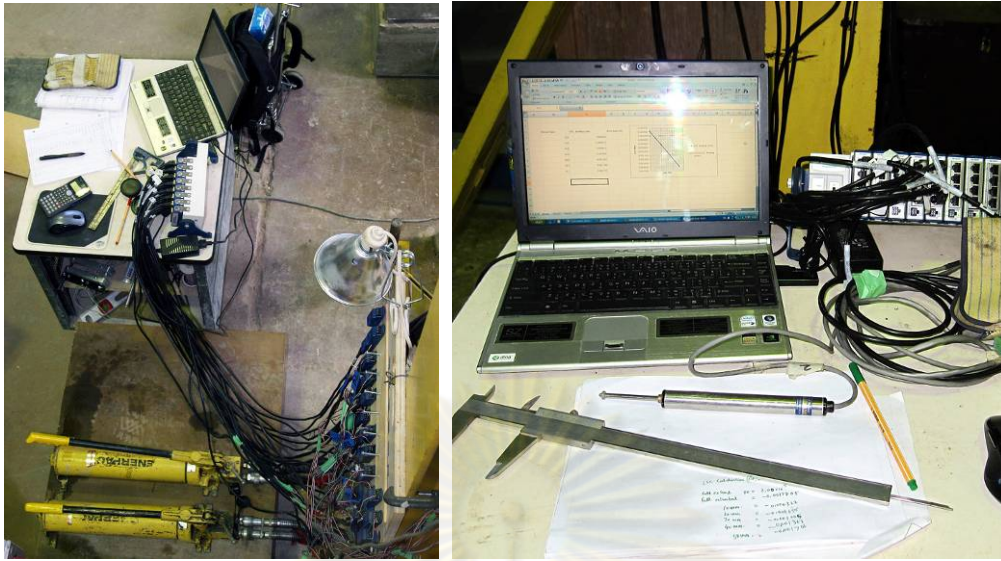


Figure 3.21 Data Acquisition System (DAQ)

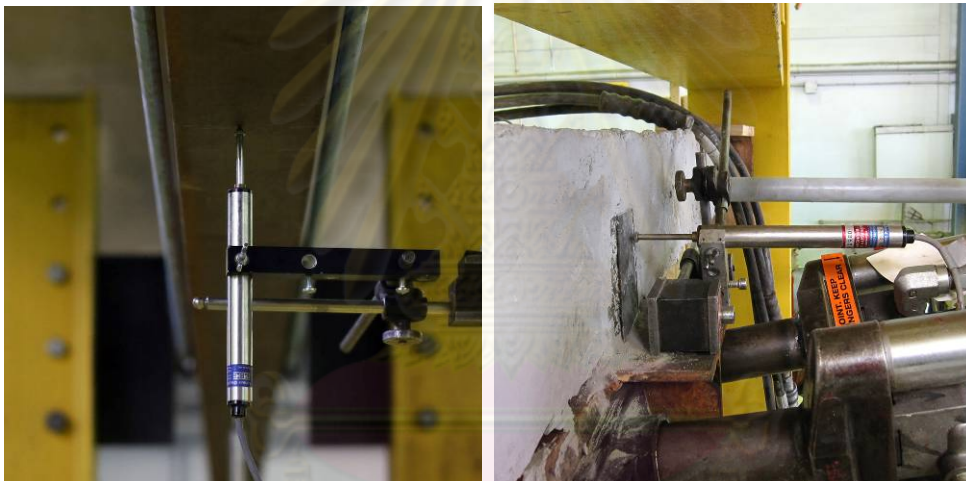


Figure 3.22 Vertical and horizontal LSC.

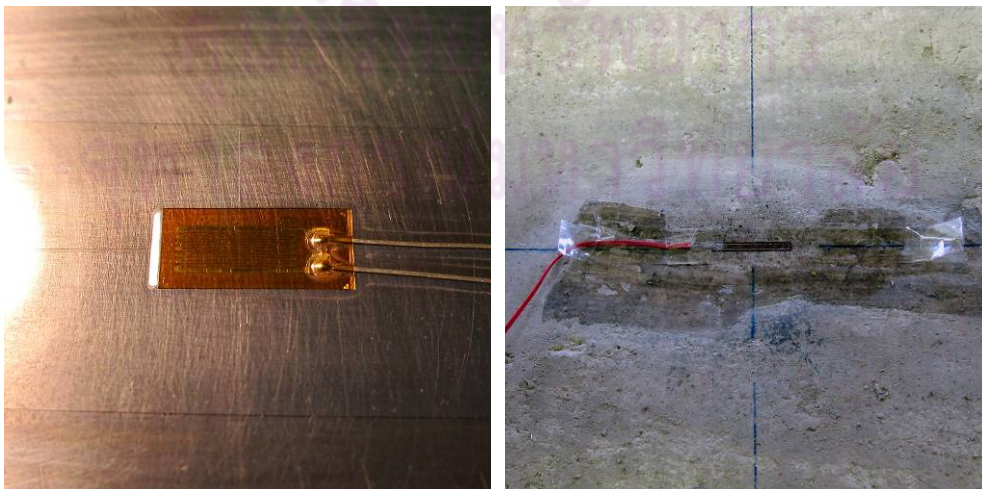


Figure 3.23 Steel and concrete strain gages.

### 3.5 Test Procedures

For truss series A, after the concrete had been cast and the concrete compressive strength had reached the expected design strength, the twin-ram jacks were used to prestress the tendons on the steel truss at the level of 20 kips (460 MPa) on the two high strength 12.7mm diameter ( $\frac{1}{2}$  in.) Grade 250 DYWIDAG® unbonded monostrand post-tensioning tendons. After the first 20kips (460MPa) was applied, the equal vertical load rams pushed downwards on the concrete slab a total of 50 tons (Specimen A1). In Specimen A2, the prestressing process was done again to increase the prestressing force to 30kips (690MPa). The same vertical load rams pushed down the concrete slab again in total of 50 tons for the second time. For Specimen A3 the prestressing force was increased up to 40kips (920MPa) on the tendons and the vertical load rams pushed down for the third time. In Specimen A3, the vertical load rams continually pushed down the concrete slab up to failure due to the yielding of the bottom chord of the truss and also the excessive deflection at the mid span. In Specimen A4, after the tendons were cut off, the vertical load rams also started pushing the slab down from the beginning up to the failure of the structure up to complete tensile rupture failure in the bottom chord.

Truss series B had similar member sizes and dimensions as the Truss series A except that it had no concrete composite slab. Truss series B was used as two test specimens, Specimen B1 and Specimen B2. For Specimen B1 the truss with no prestressing was tested from the vertical load rams at zero loaded up to the buckling load of the top chord. For Specimen B2, tendons were stressed up to 460 MPa and loads were applied up to ultimate in the same mode as for Specimen B1 causing buckling in the top chord of the truss. All the data such as loads, vertical displacements, horizontal displacements, strains and the slips of the shear stud connectors were recorded and stored from the DAQ with the computer program LABVIEW.

## 3.6 Test Results

### 3.6.1 Overview

Specimen A1: The steel and concrete composite truss series A was post-tensioned by two 12.7mm diameter ( $\frac{1}{2}$  in.) tendons at the prestressing force of 9,074kg (20kips, stressed at 460MPa). This resulted in moving the truss upward for the maximum amount at mid span of 1.8mm. The precamber chart was presented in Figure 3.32. The steel and concrete dead load stresses in every member changed by the prestressing force and the tensile stress in the bottom chord was reduced accordingly. Then the truss was pushed down by the two load rams up to 50 tons. The stress in the bottom chord member of the truss exactly at mid span increased due to the ram loads and reached the yield stress when the total ram loads reached 44 tons while all other member stresses were still within the elastic limit. The concrete stress at the top surface was also in the elastic limit on compressive side. There were some cracks in the concrete, but the sizes of the cracks were very small and barely detectable to the eye.

Specimen A2: After unloading the ram loads from Specimen A1, the post-tensioned force was applied to the Truss series A for the second time. The hydraulic pumps increased the pressure for the twin ram jacks to pull up the tendons from 1600psi for Specimen A1 to 2400psi for Specimen A2. This resulted in the prestressing force increasing to 13,612kg (30kips, stressed at 690MPa). The mid span upward deformation increased to 3.3mm. The dead load tensile stress in the bottom chord changed from tension to compression. The ram loads were applied again up to 50 tons as in Specimen A1, but this time the combined stress in the bottom chord from the stresses from dead loads, the stress from ram loads and the stress from the posttensioned force reached the yield stress at ram loads of 49.5 tons. As in the Specimen A1, there were some cracks in the concrete, but the sizes of the cracks were very small.



Specimen A3: After unloading the ram loads from Specimen A2, a post-tensioned force was applied to the Truss series A for the third time. The hydraulic pumps increased the pressure for the twin ram jacks from 2400psi for Specimen A2 to 3200psi for Specimen A3. This resulted in an increase of the prestressing force to 18149kg (40kips, stressed at 920MPa). The mid span precamber had increased to 4.4mm. The ram loads were applied again up to failure of the truss. The combined stress in the bottom chord member of the truss at mid span increased due to the ram loads and reached the yield stress when the total ram loads were to 55.7 tons. The ram continued to deflect the truss downwards until a failure load of 68.4 tons was reached. Beyond this point deflection increased with no increase in the ram loads. At this point cracks in the bottom of the slab were widespread and were generally in a direction perpendicular to the longitudinal direction of the slab. The cracks penetrated upward into the slab for an average of 100mm at mid-span and thence changed in direction towards the mid-span. At this point the mid-span deflection was 151.15mm which was 5.38 times the deflection of 28.09mm at the point of yielding of the bottom chord. Two loud noises were heard when the loads reached 65.9 tons and the mid span deflection was 63.16mm. The loads reached 67.3 tons at which point the mid span deflection was at 105.17mm. The snapping noises were suspected of being related to slippage of the tendon wedge anchorages or to the breaking of a shear stud connector which was later discovered. The load vs. mid-span deflection curves for Specimen A1, A2, A3, A4, B1 and B2 are discussed below in connection with Figure 3.34

ศูนย์วิทยทรัพยากร  
จุฬาลงกรณ์มหาวิทยาลัย



Figure 3.24 Truss series A showing Specimen A3 at ultimate.



Figure 3.25 Cracks in concrete slab - Specimen A3.



Figure 3.26 Shear stud connectors - inelastic deformed shape.

Specimen A4: Once both tendons were cut, the load rams were actuated and continued to deflect the specimen downwards. The bottom chord of the truss experienced tensile stress from the combined dead loads and the ram loads. For Specimens A1, A2, A3 and A4, the top chord of the truss had a relatively low stress as compared to the bottom chord. The ratio between the top chord stress and the bottom chord stress was approximately less than 0.10. After the bottom chord stress reached the yield point, the top chord stress increased dramatically due to the high intensity of curvature. The relationship between the load and top chord force is shown in Figure 3.46 to 3.49. The bottom chord reached yield stress at 40.8 Tons which was less than in Specimen A1 at 3.2Tons and less than in Specimen A3 at 14.9Tons. The specimen deflected downwards to an ultimate failure load of 56.8 tons with a corresponding mid-span deflection of 55.6mm. Characteristic concrete cracks extended in size and distribution as load level load and deflection increased. Diagonal member stress reached the yield point as did the bottom chord. For Specimen A4 the bottom chord member suddenly and completely fractured through its entire cross-section with a very loud snapping noise. This failure mechanism is shown in Figure 3.27 below.



Figure 3.27 Complete fracture of the bottom chord of Specimen A4

Specimen B1: Truss series B without prestressing was loaded until the top chord buckling was initiated. As expected, the stiffness of the structure was greatly reduced in comparison with Truss series A due to the absence of an attached concrete slab. This was reflected by a decreased slope of the load-deflection curves for Specimens B1 and B2 as compared to those involving Truss series A. For Specimen B1 failure occurred due to buckling of the compression chord at ram loads of 19.5 tons.

Specimen B2: Tendons were stressed up to 460 MPa and loads were applied up to ultimate in the same mode as for Specimen B1 as seen by buckling of the compression chord. The total ram load was 18.0Tons. The post-tensioned system cannot show any advantage to the structure because of the critical failure in the buckling mode as shown in the load and horizontal movement curves in Figure 3.64 and Figure 3.65.



Figure 3.28: Specimen B1 - Steel truss only without tendon.



Figure 3.29: Specimen B1 - Lateral buckling of compression chord.



Figure 3.30 Specimen B2 - Steel truss with posttensioned tendons.



Figure 3.31 Specimen B2 – Lateral buckling at the ultimate stage.

### 3.6.2 Pre-camber measurement

Specimen A1, A2, and A3 were performed on Truss series A at prestressing levels of 460MPa, 690MPa and 920MPa, respectively. This resulted in pre-cambers of 1.8 mm for Specimen A1, 3.3 mm for Specimen A2, and 4.4mm for Specimen A3 as shown in Figure 3.32.

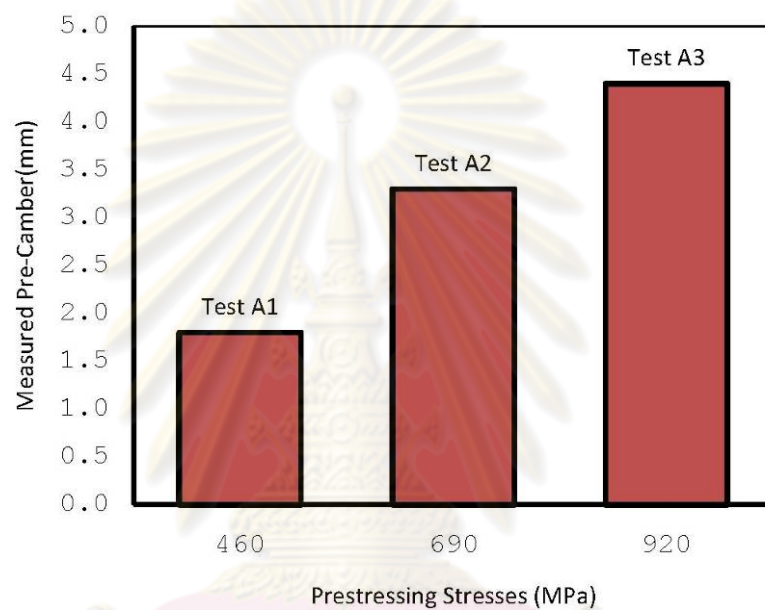


Figure 3.32 Measured pre-camber and prestress levels for Specimens A1, A2, and A3

Table 3.5: Precamber and the yield loads at various prestress levels

Prestressing Stresses (MPa)	Precamber (mm.)	Yield Load (Tons)
460	1.8	44.0
690	3.3	49.5
920	4.4	55.7

### 3.6.3 Measured Load and Mid Span Deflection Curves

For Specimens A3 and A4 failure was in a ductile flexural mode. The stress in the bottom chord of the steel truss reached yield strength while the top surface stress of the slab was less than the crushing strength. The structure continually deflected above the yield load in a very large deformed shape. Yielding started at an approximate load of 550kN which corresponded to a yield deflection of 30mm. After the yield load had been reached, the load rams were continually operated to push the structure downwards until the bottom of the composite deck slab reached a deflection of 150mm. This deflection was five times greater than the previous yield deflection at 30mm as shown in Fig. 3.33

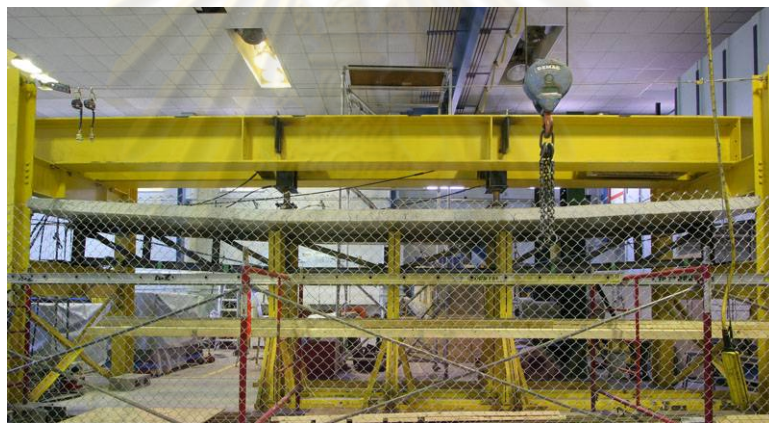


Figure 3.33 Photograph of Specimen A3 at ultimate stage.

The difference between the Specimens A3 and A4 was due to the prestressing tendons. Specimen A3 exhibited more ductility and was stronger than Specimen A4. The maximum total load was 684kN while the specimen of Specimen A4 failed in rupture mode of the bottom chord due to the ultimate tensile strain at the maximum load of 568kN. Adding the extra cross sectional area of 196mm<sup>2</sup> which was 7.9% of the sectional area of the bottom chord area of 2480mm<sup>2</sup> resulted in an increase in the total load capacity of 20.4%.

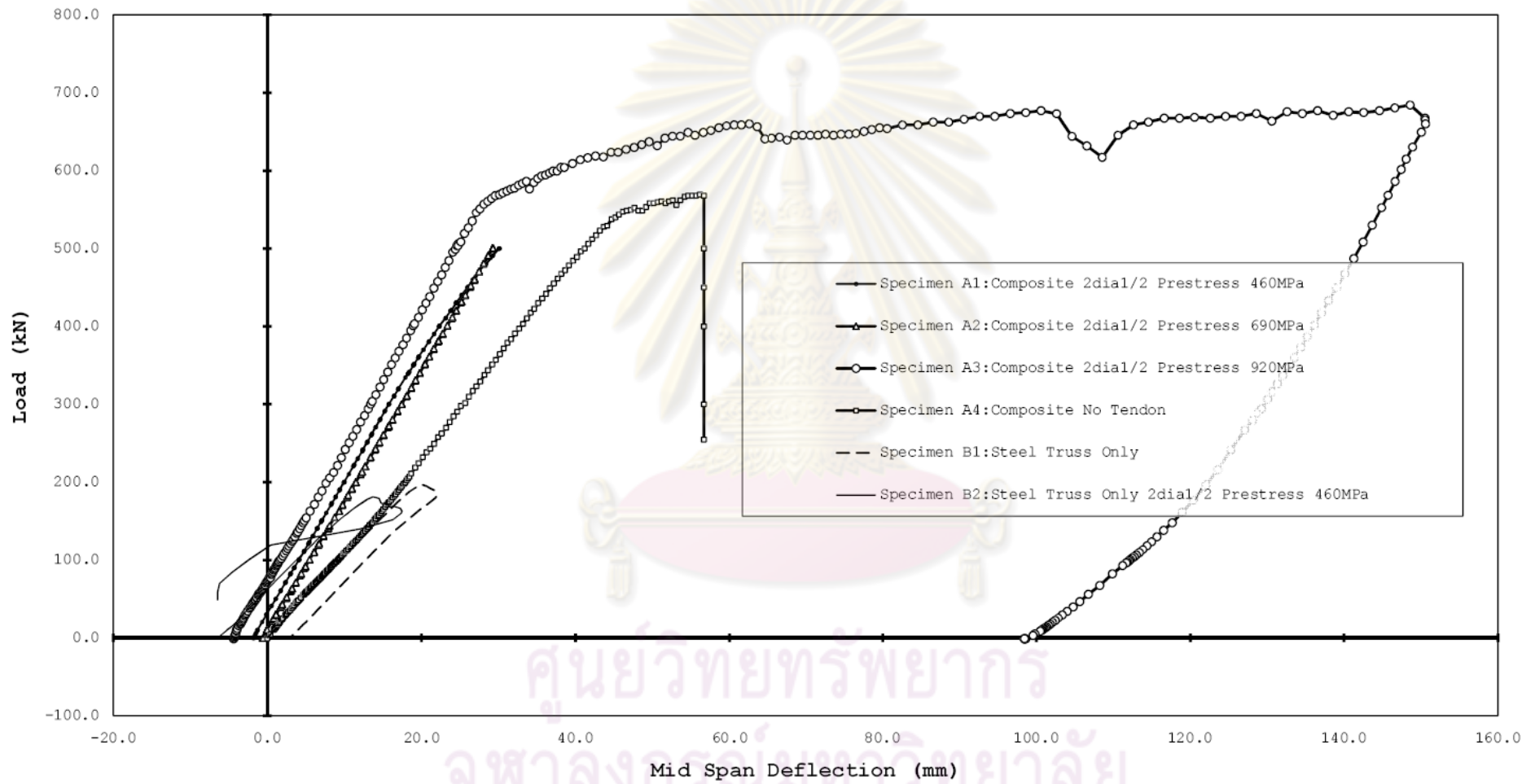


Figure 3.34 Load and mid span deflection curves for Specimens A1, A2, A3, A4, B1 and B2



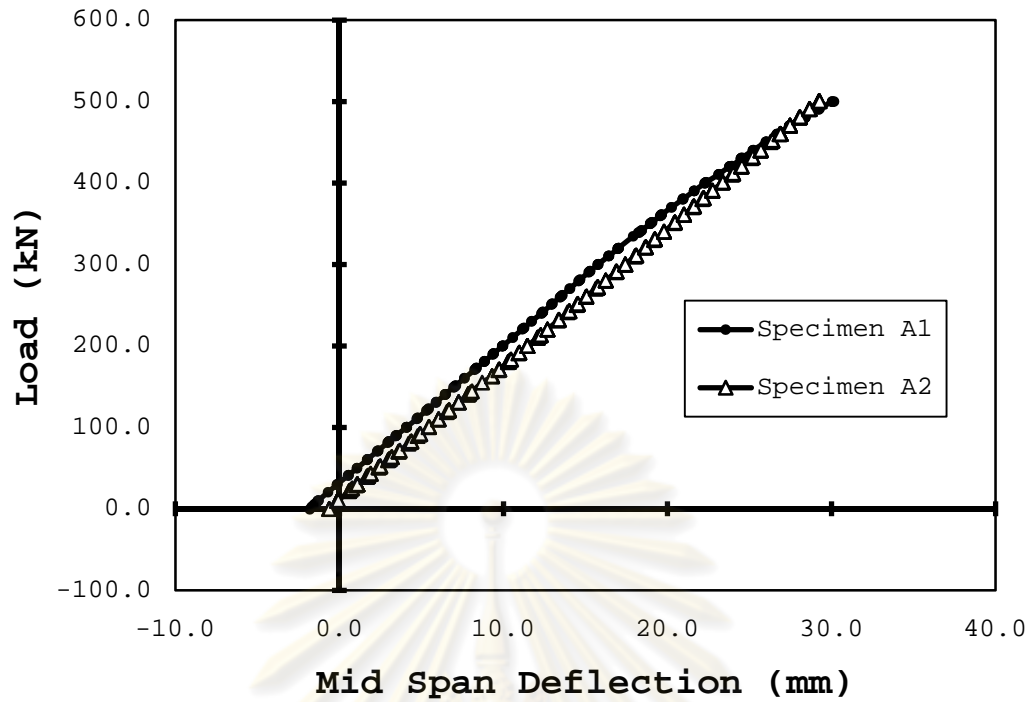


Figure 3.35 Load and mid span deflection curves (Specimens A1, A2)

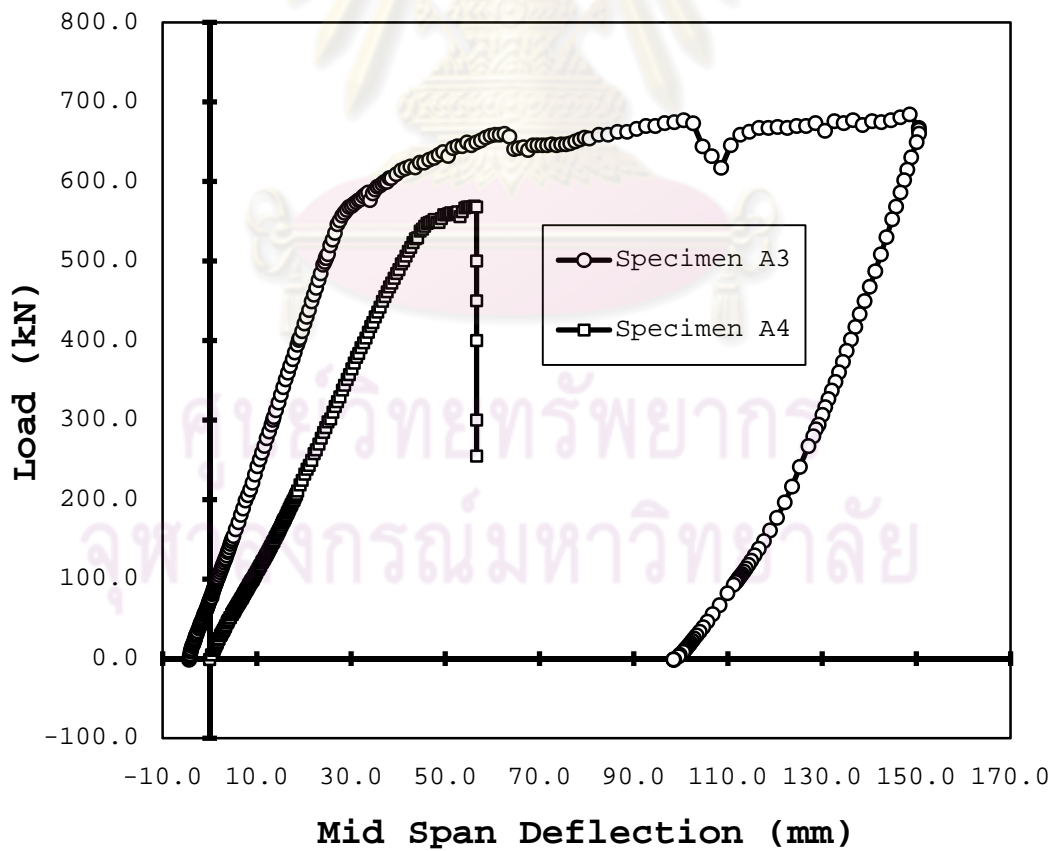


Figure 3.36 Load and mid span deflection curves (Specimens A3, A4)

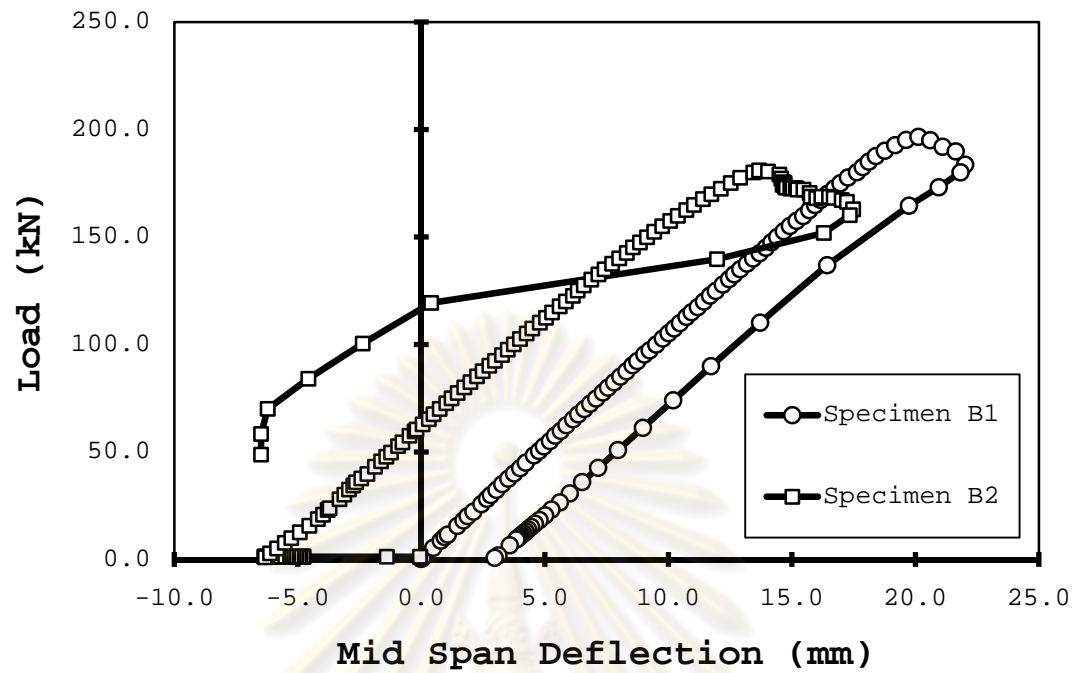


Figure 3.37 Load and mid span deflection curves (Specimens B1, B2)

ศูนย์วิทยทรัพยากร  
จุฬาลงกรณ์มหาวิทยาลัย

## 3.6.4 Measured Load and Member Stress Curves

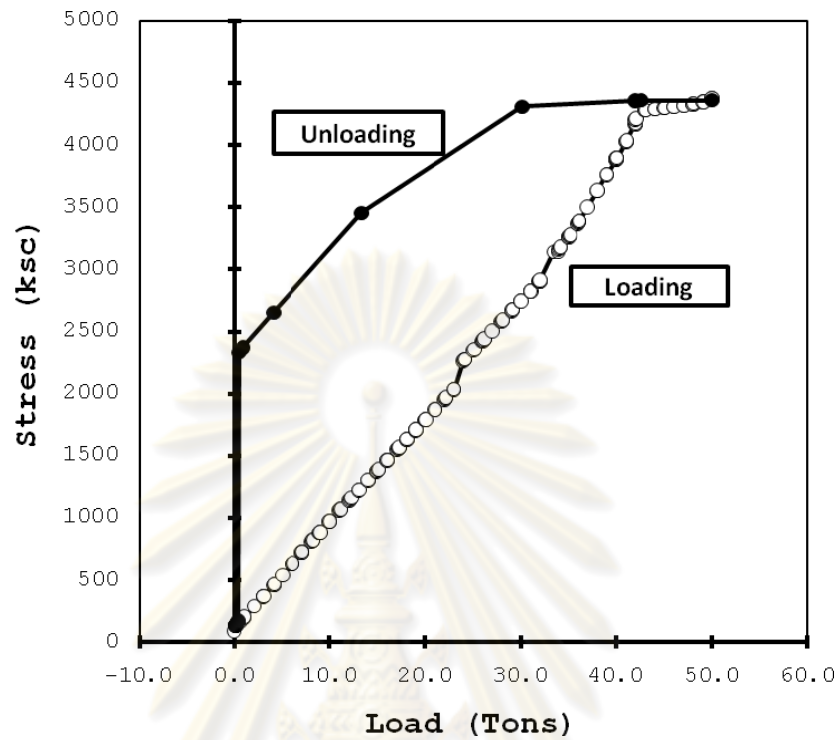


Figure 3.38 Load and bottom chord stress curves (Specimen A1)

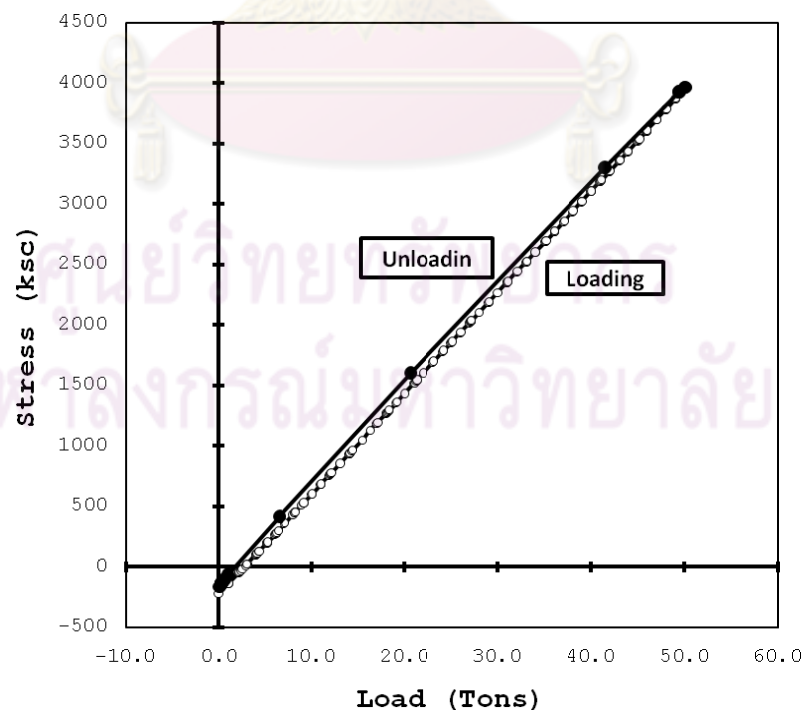


Figure 3.39 Load and bottom chord stress curves (Specimen A2)

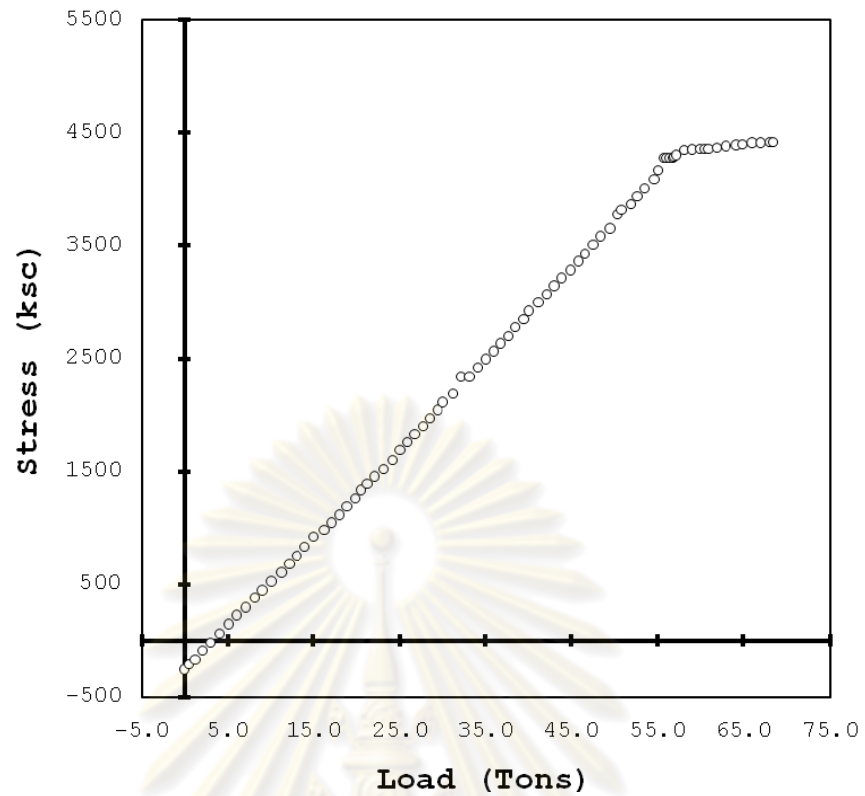


Figure 3.40 Load and bottom chord stress curve (Specimen A3)

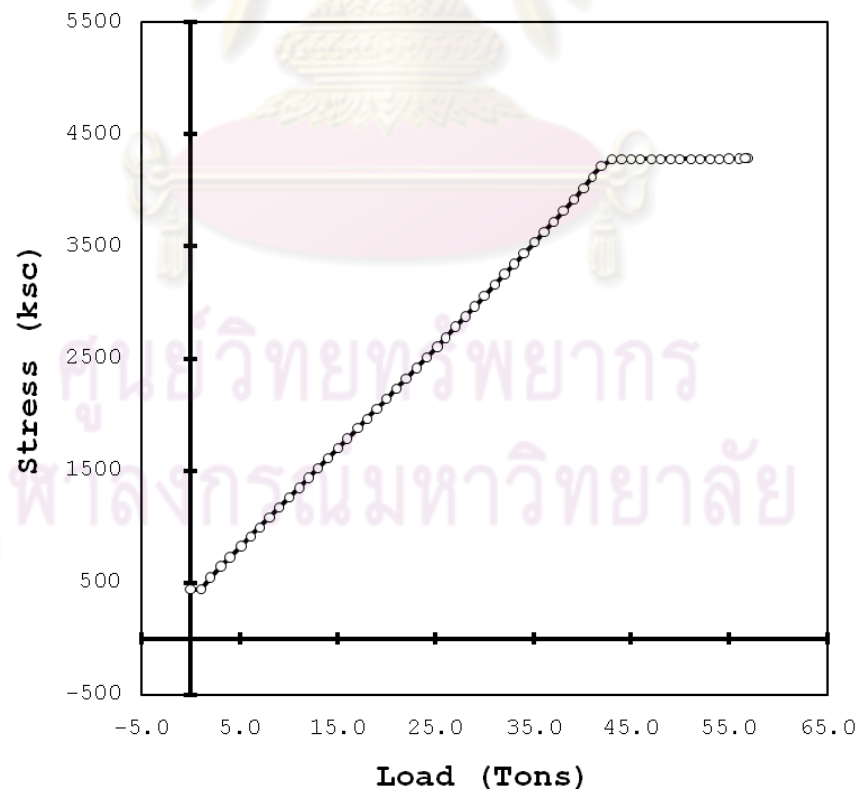


Figure 3.41 Load and bottom chord stress curve (Specimen A4)

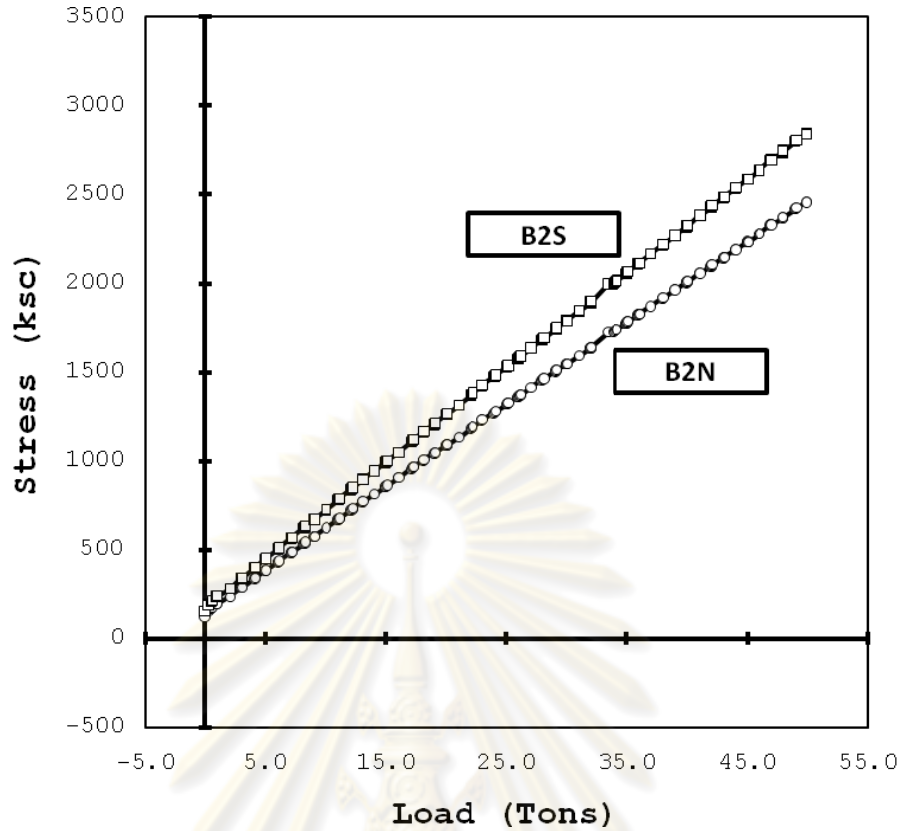


Figure 3.42 Load and 2<sup>nd</sup> panel bottom chord B2N & B2S stress curves (Specimen A1)

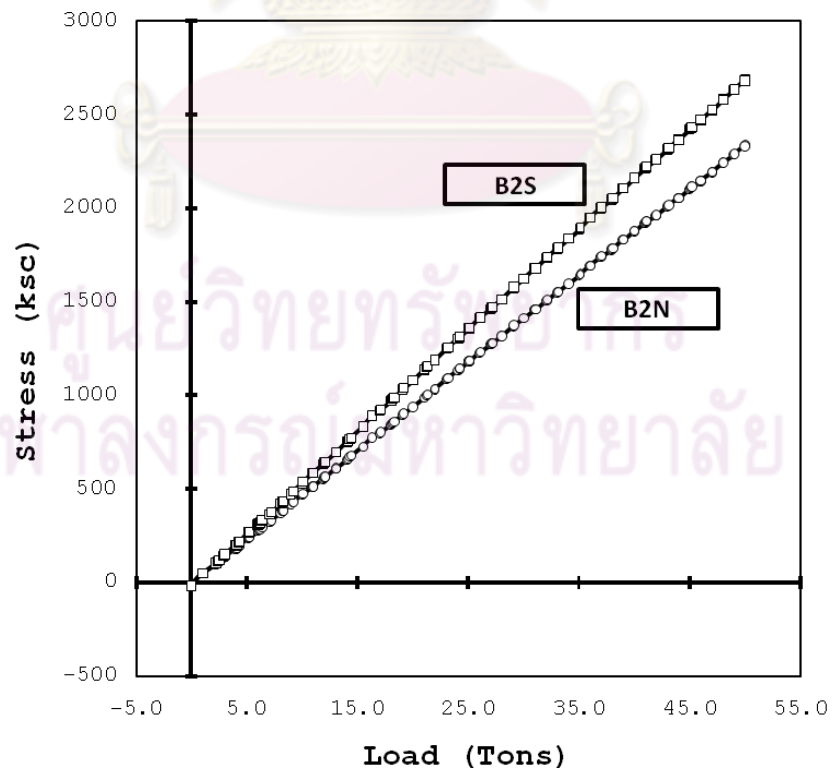


Figure 3.43 Load and 2<sup>nd</sup> panel bottom chord B2N & B2S stress curves (Specimen A2)

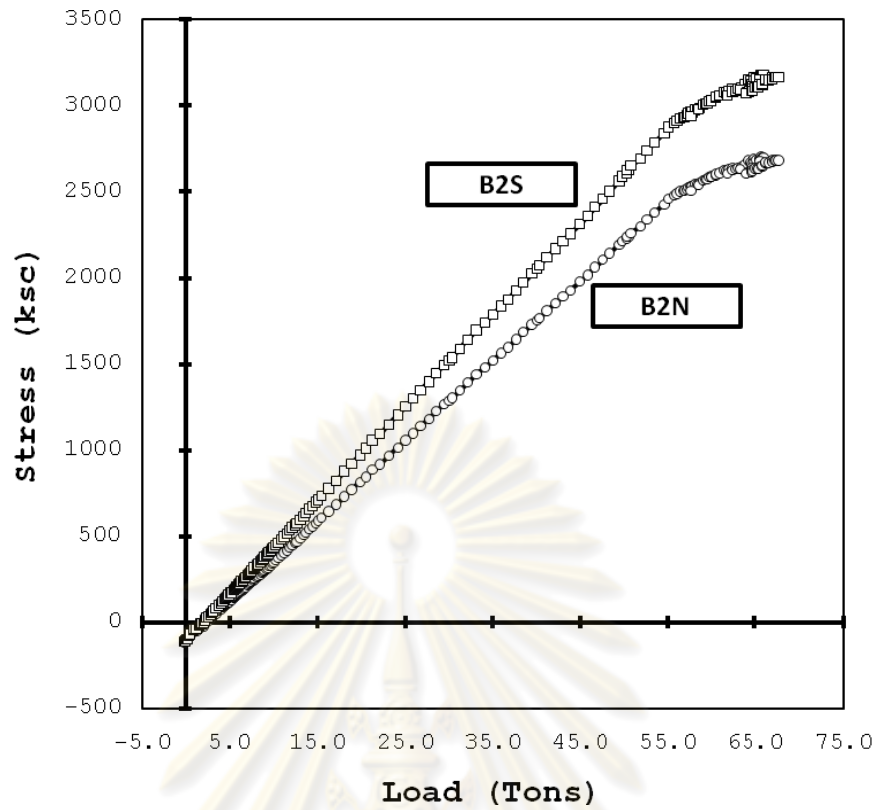


Figure 3.44 Load and 2<sup>nd</sup> panel bottom chord B2N & B2S stress curves (Specimen A3)

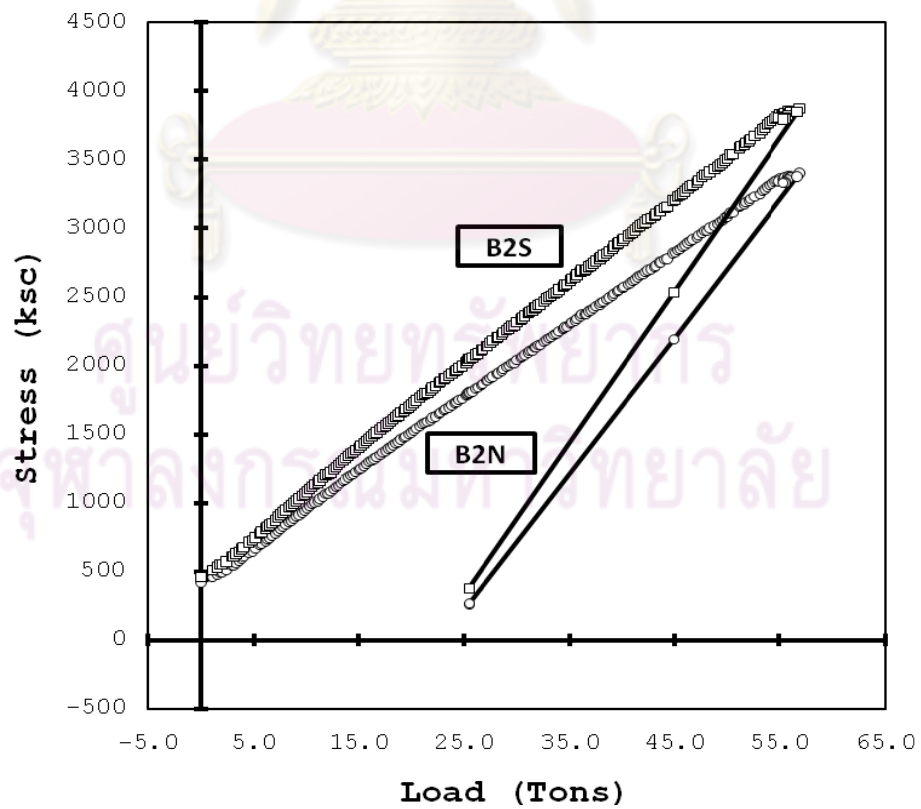


Figure 3.45 Load and 2<sup>nd</sup> panel bottom chord B2N & B2S stress curves (Specimen A4)

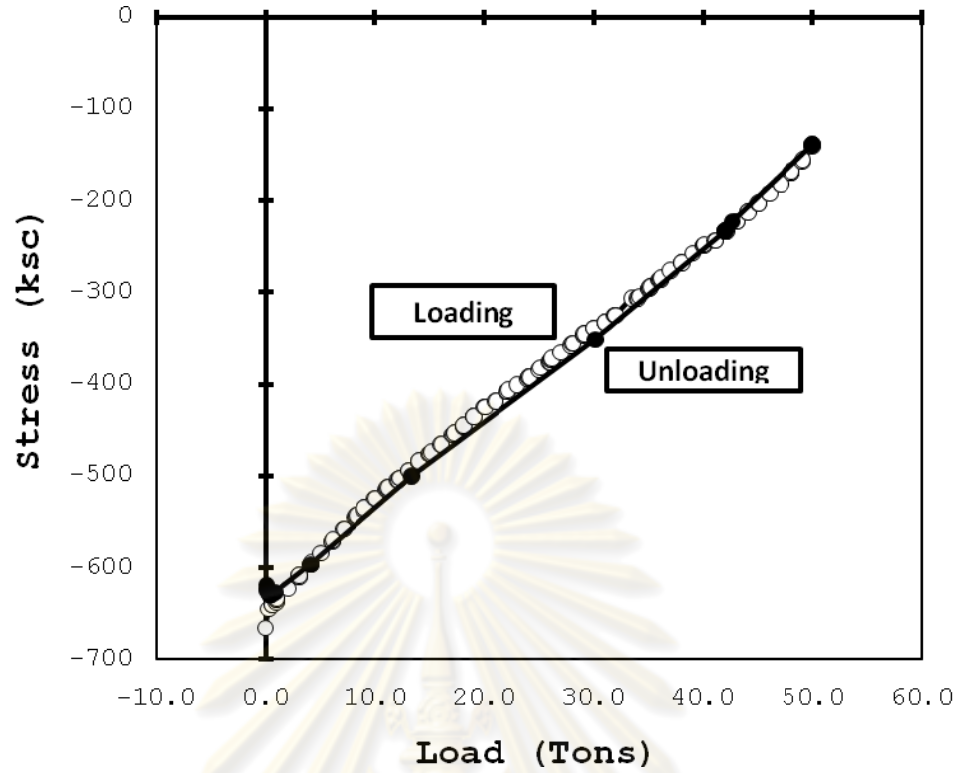


Figure 3.46 Load and top chord stress curve (Specimen A1)

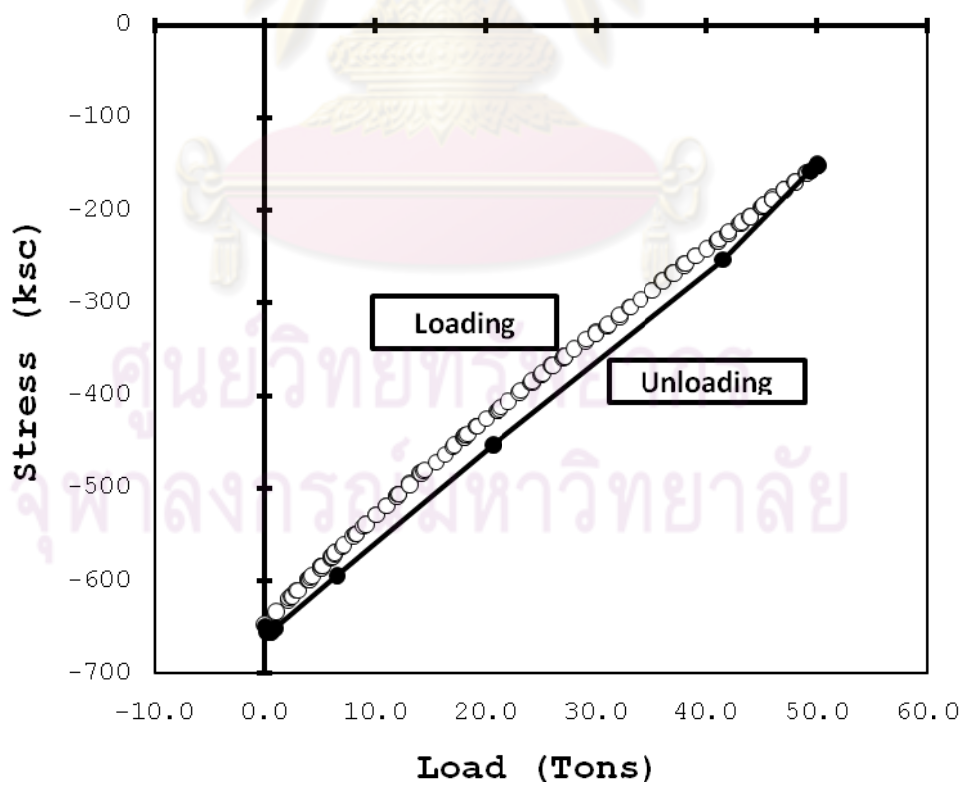


Figure 3.47 Load and top chord stress curve (Specimen A2)

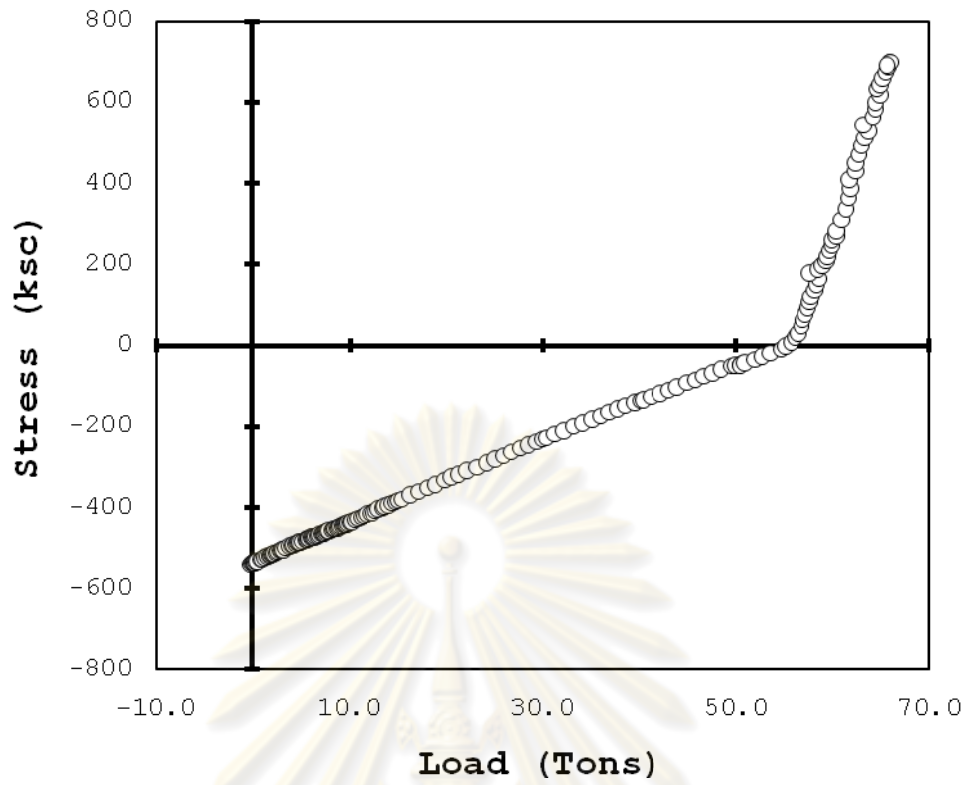


Figure 3.48 Load and top chord stress curve (Specimen A3)

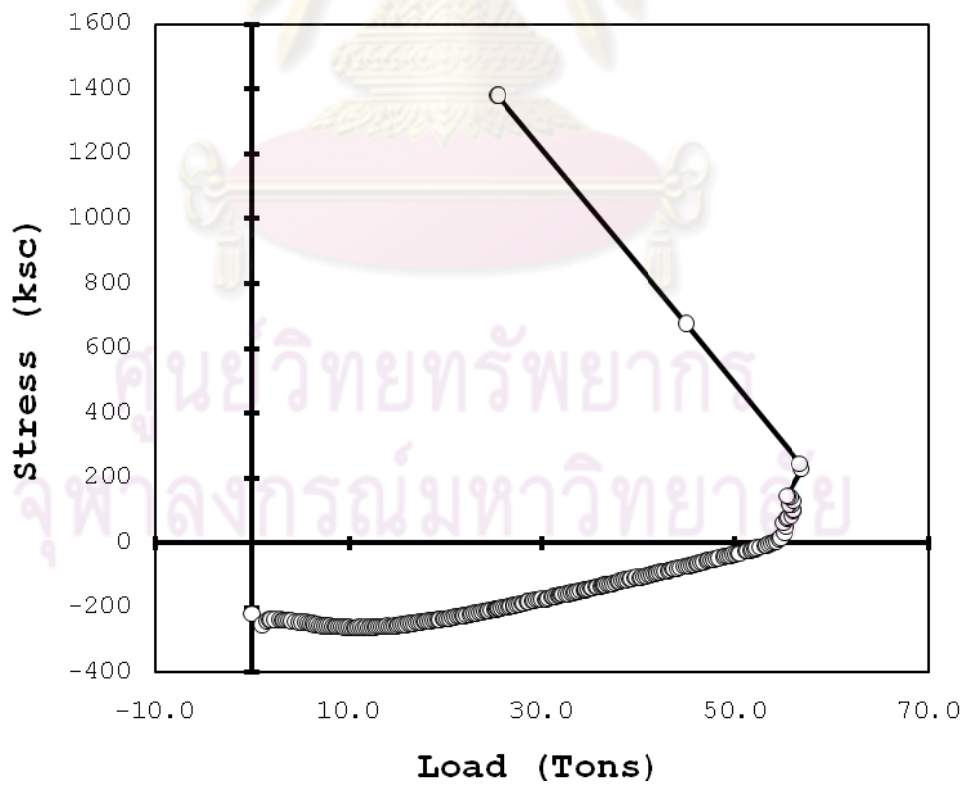


Figure 3.49 Load and top chord stress curve (Specimen A4)



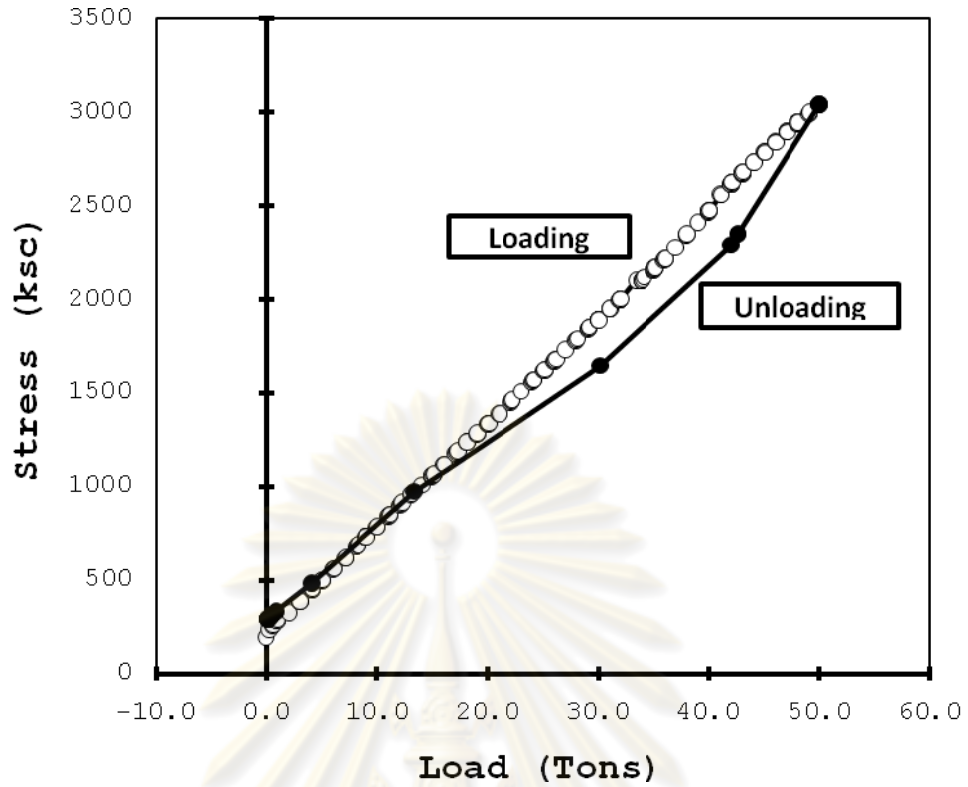


Figure 3.50 Load and diagonal member stress curves (Specimen A1)

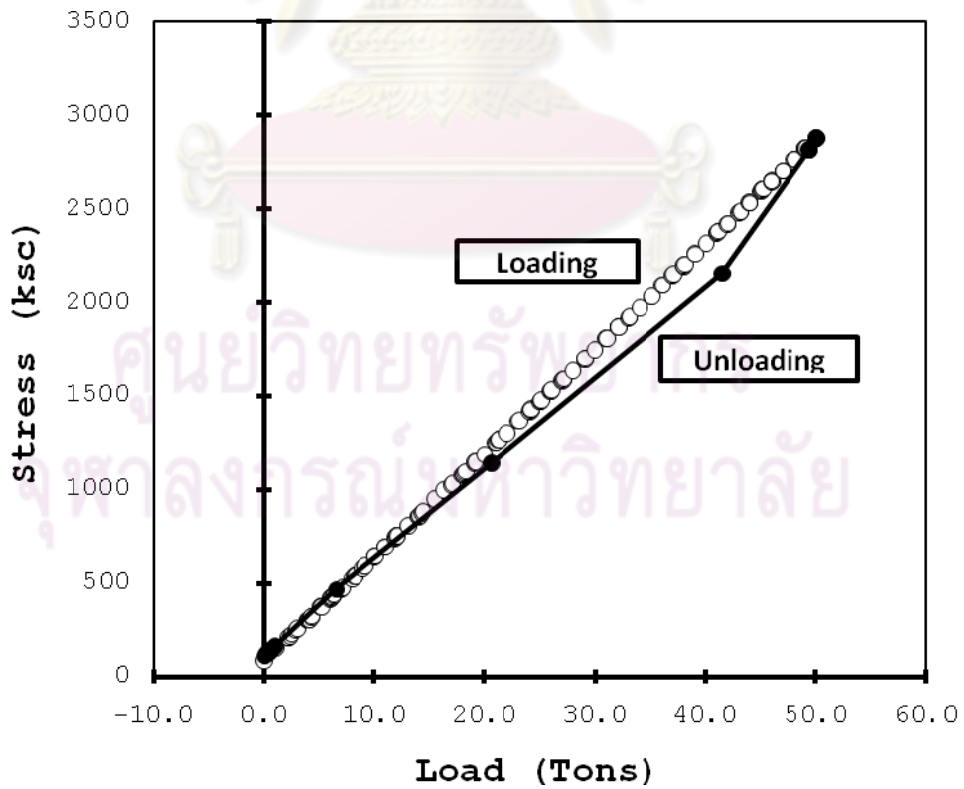


Figure 3.51 Load and diagonal member stress curves (Specimen A2)

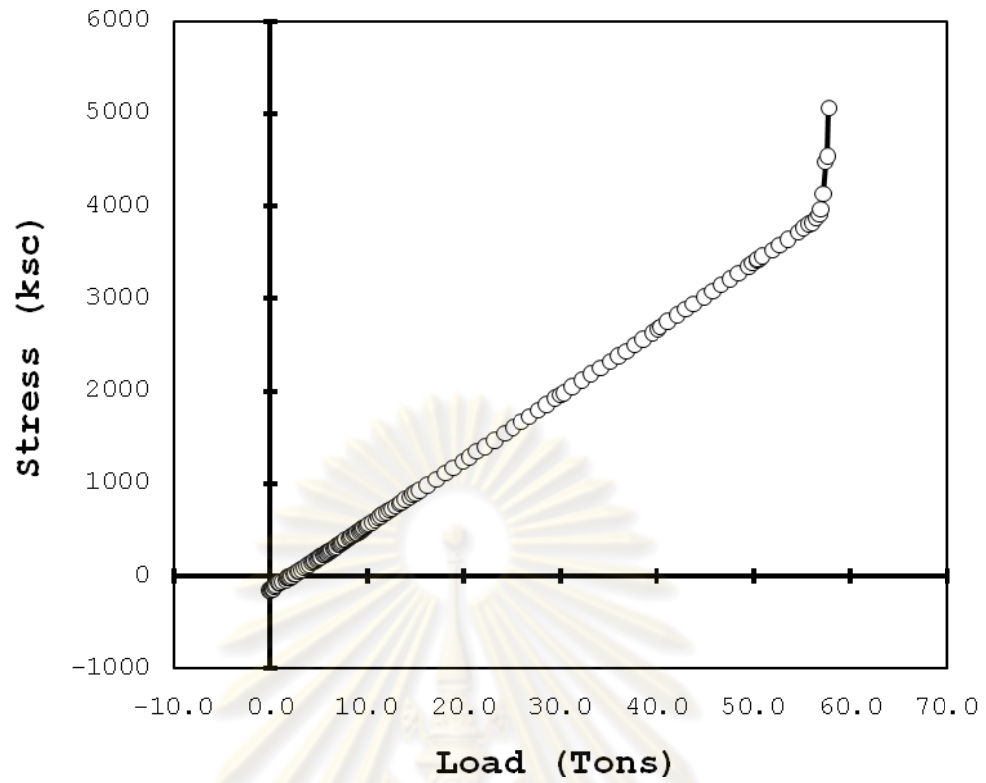


Figure 3.52 Load and diagonal member stress curves (Specimen A3)

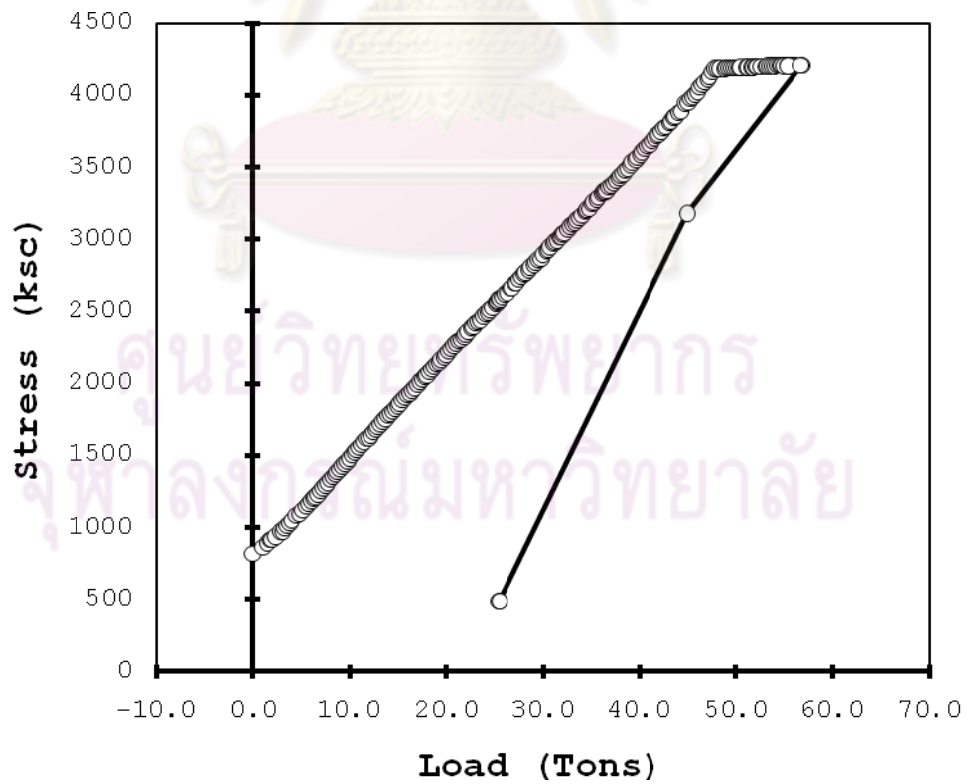


Figure 3.53 Load and diagonal member stress curves (Specimen A4)

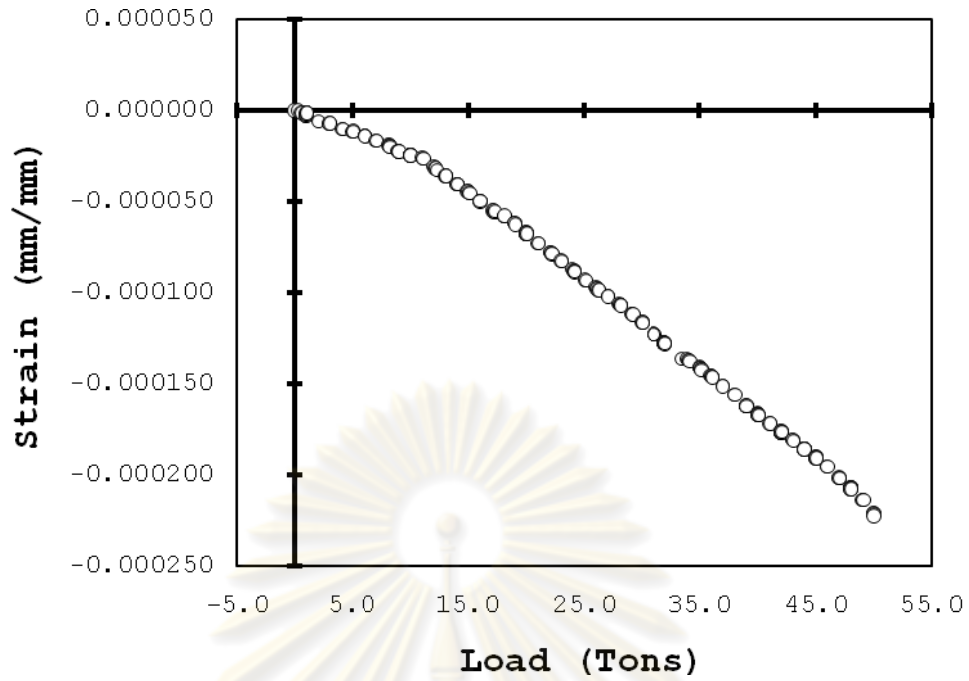


Figure 3.54 Load and top surface concrete strain at mid span curve (Specimen A1)

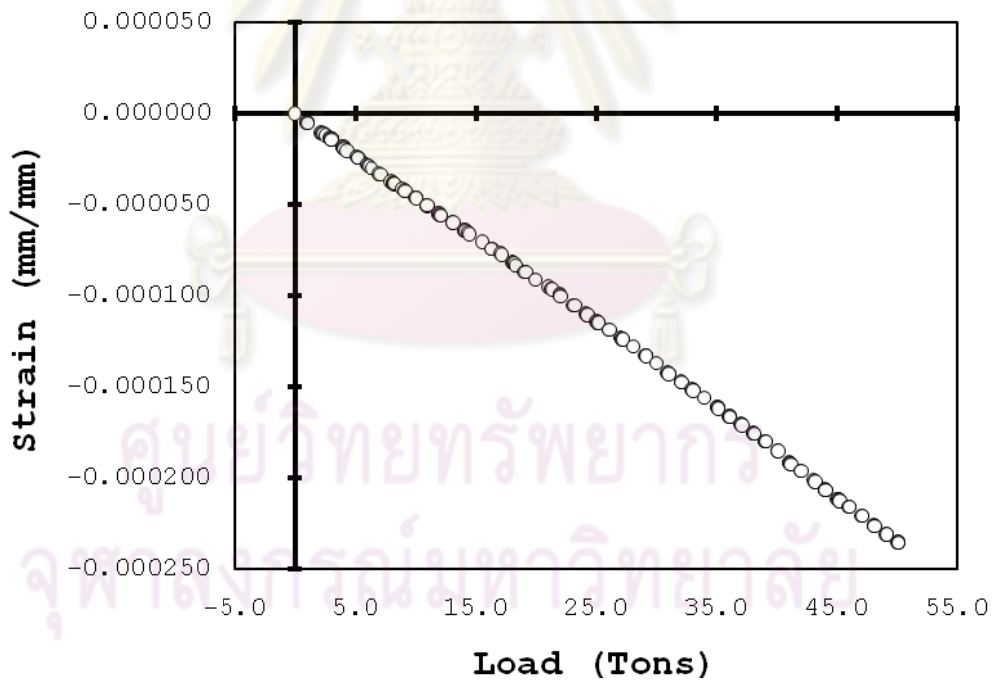


Figure 3.55 Load and top surface concrete strain at mid span curve (Specimen A2)

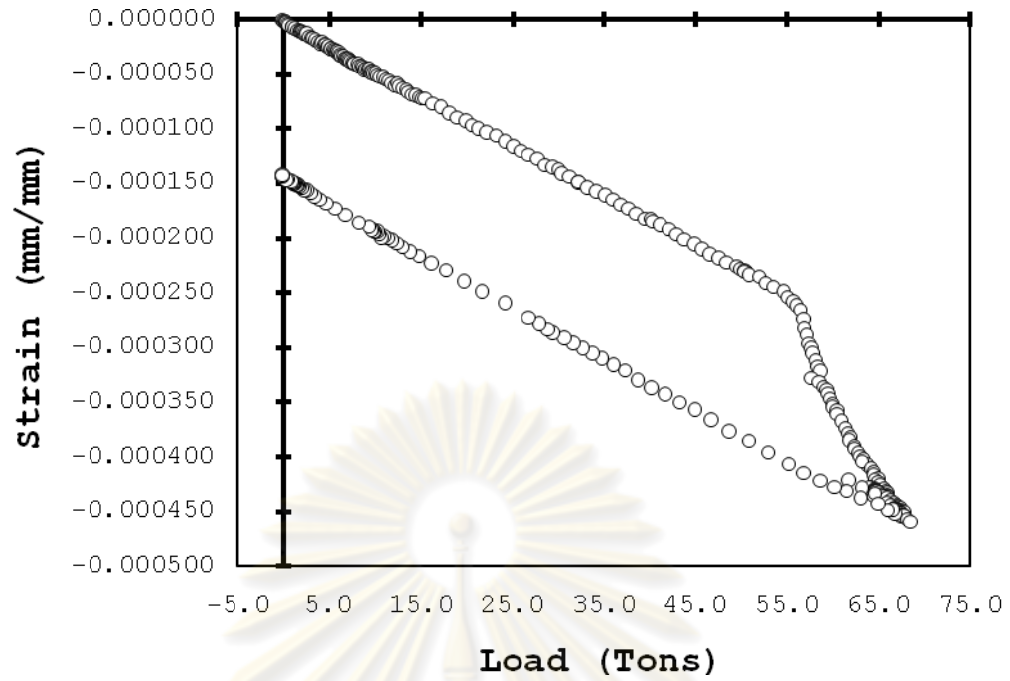


Figure 3.56 Load and top surface concrete strain at mid span curve (Specimen A3)

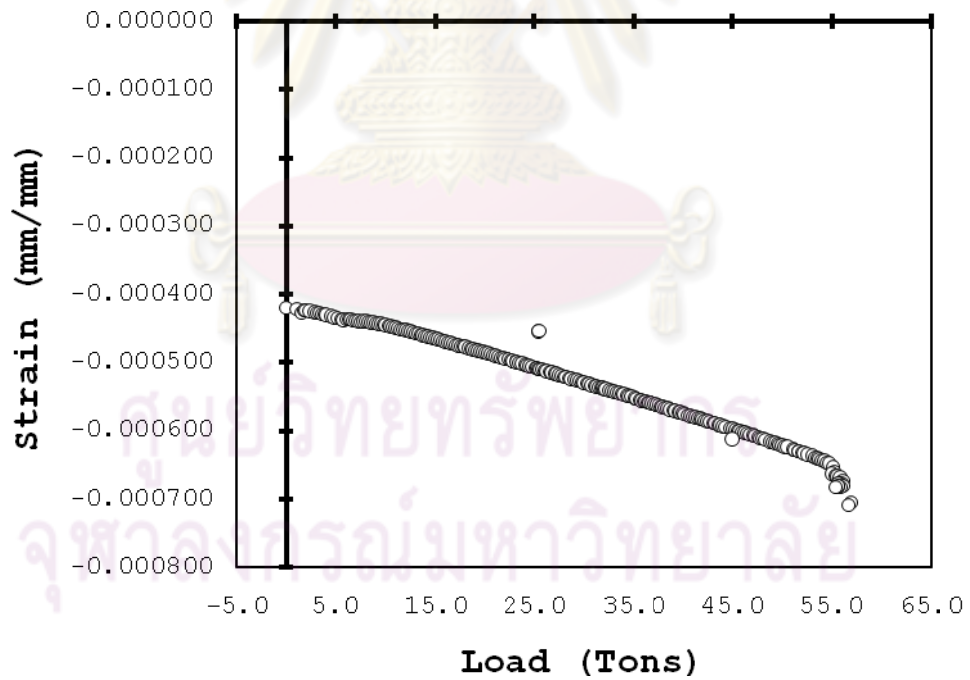


Figure 3.57 Load and top surface concrete strain at mid span curve (Specimen A4)

## 3.6.5 Measured Load Slip Curves

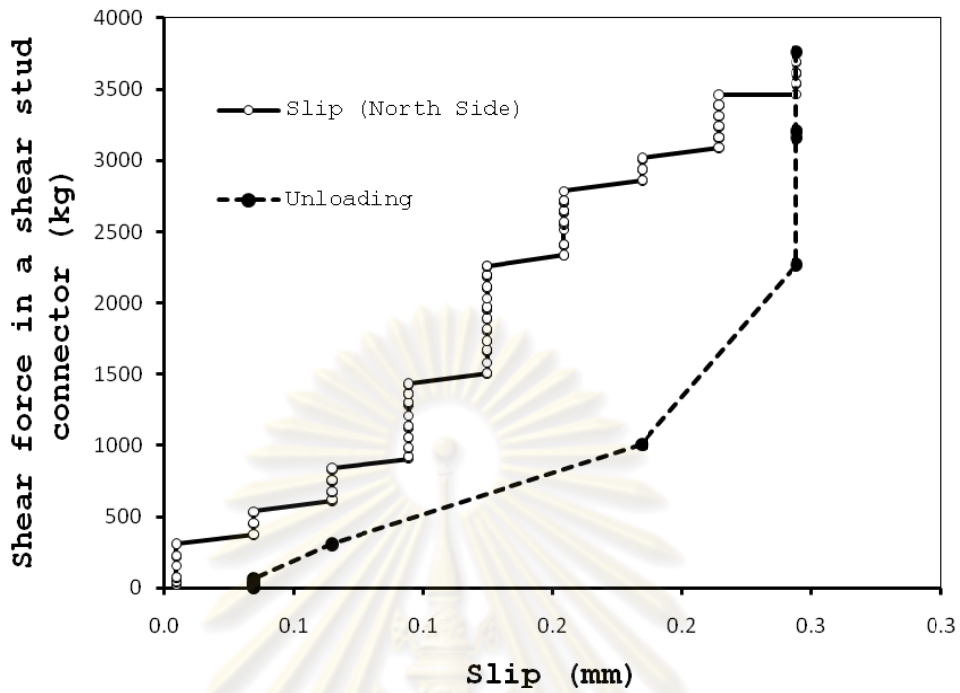


Figure 3.58 Shear force and slip curves on the North side of the specimen (Specimen A1) including the unloading branch.

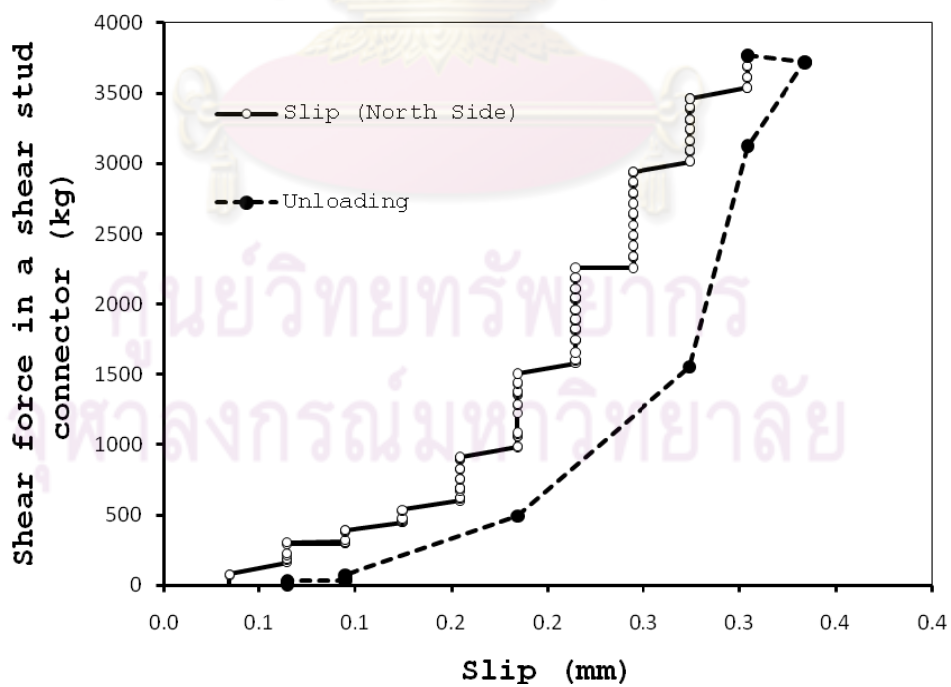


Figure 3.59 Shear force and slip curves on the North side of the specimen (Specimen A2) including the unloading branch.

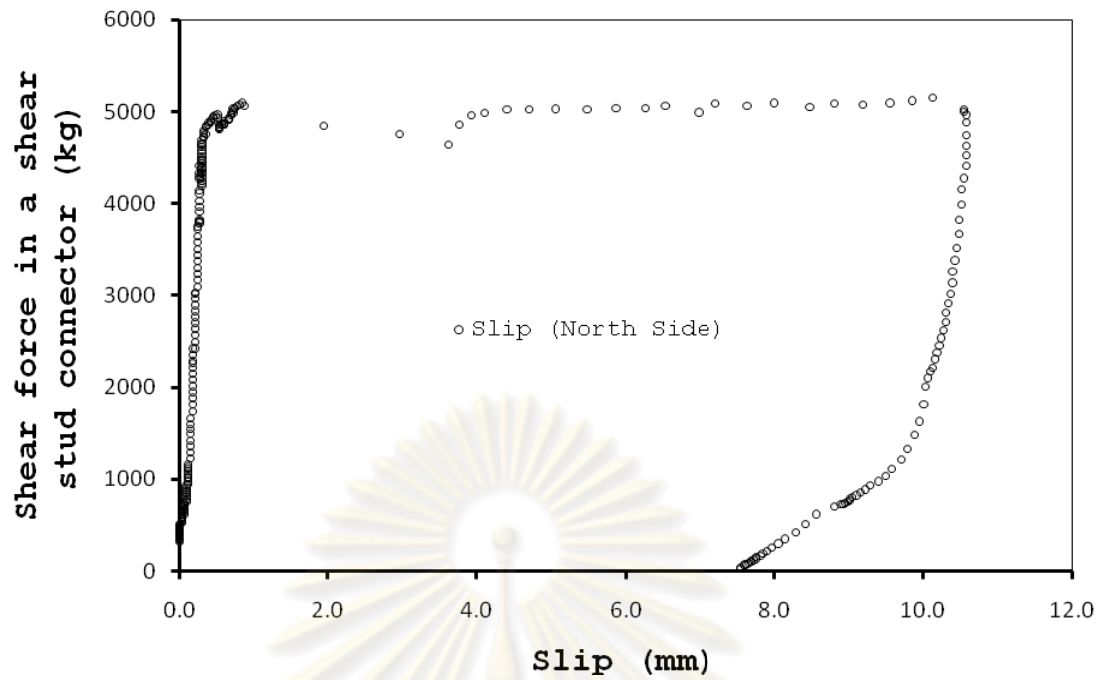


Figure 3.60 Shear force in a shear stud connector and slip curve on the North side of the specimen (Specimen A3)

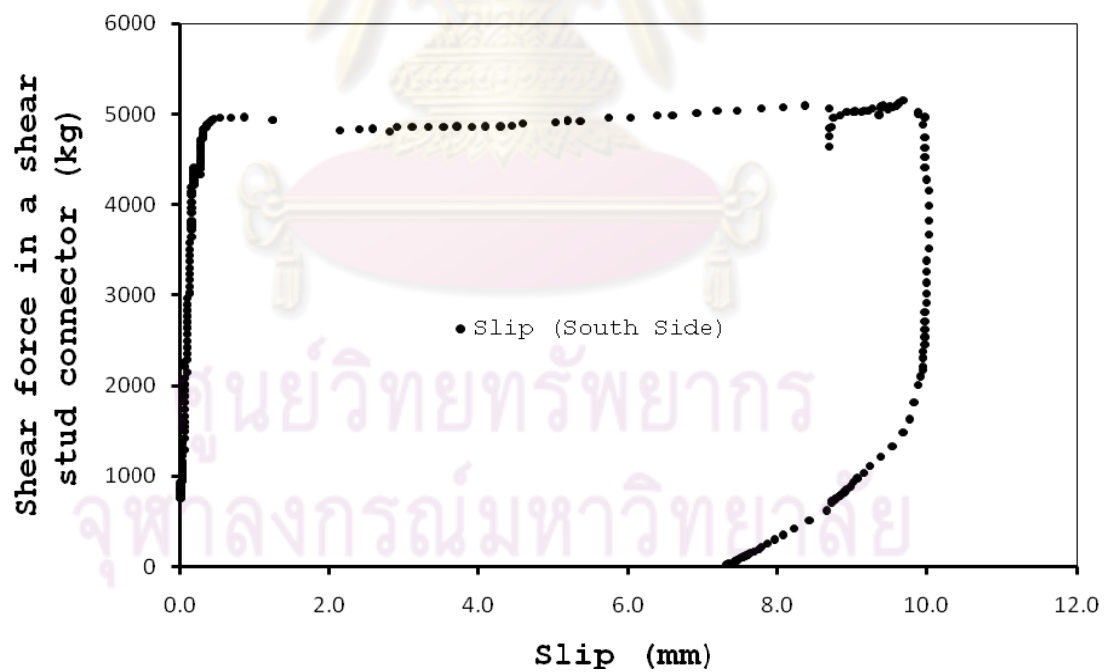


Figure 3.61 Shear force in a shear stud connector and slip curve on the South side of the specimen (Specimen A3)

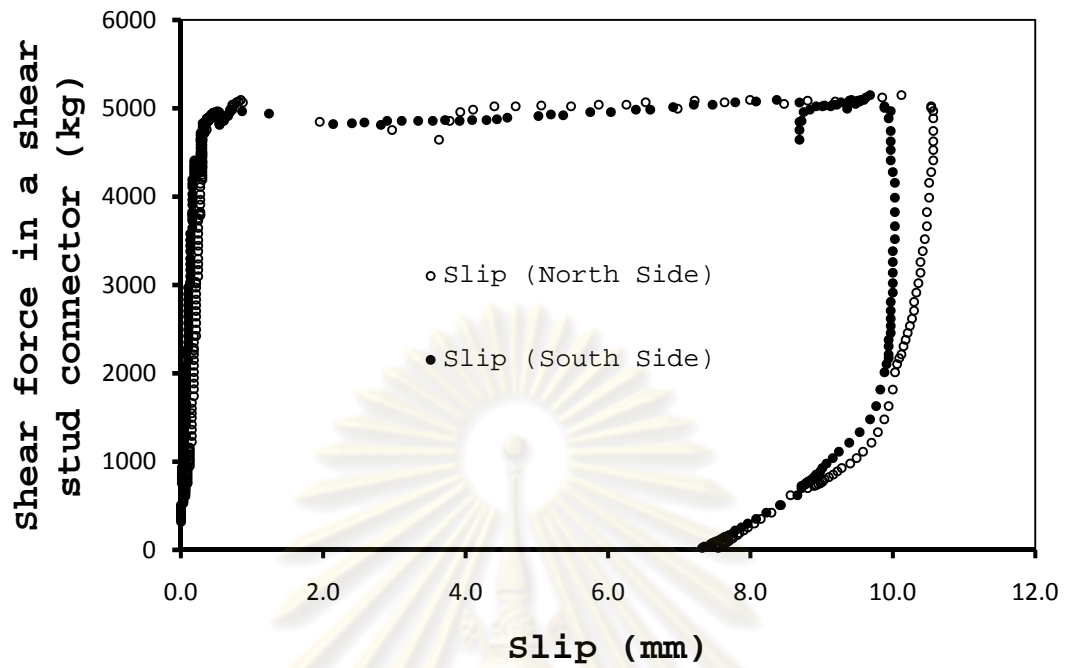


Figure 3.62 Shear force and slip curves on both the North side and the South side of the specimen (Specimen A3)

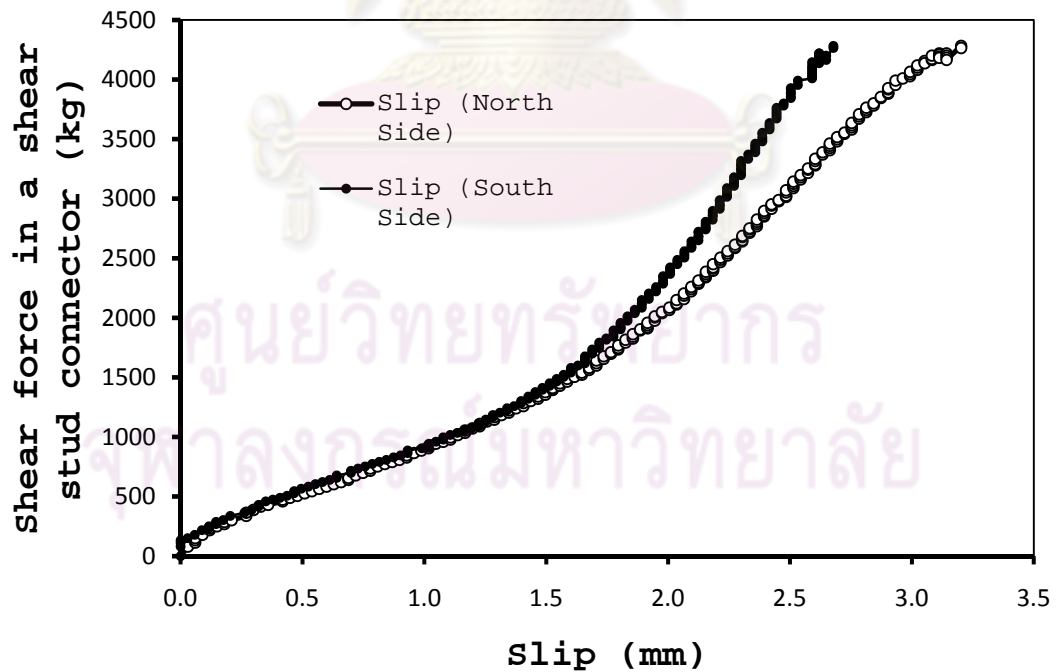


Figure 3.63 Shear force and slip curves on both the North side and the South side of the specimen (Specimen A4)

## 3.6.6 Measured Load Horizontal Movement Curves

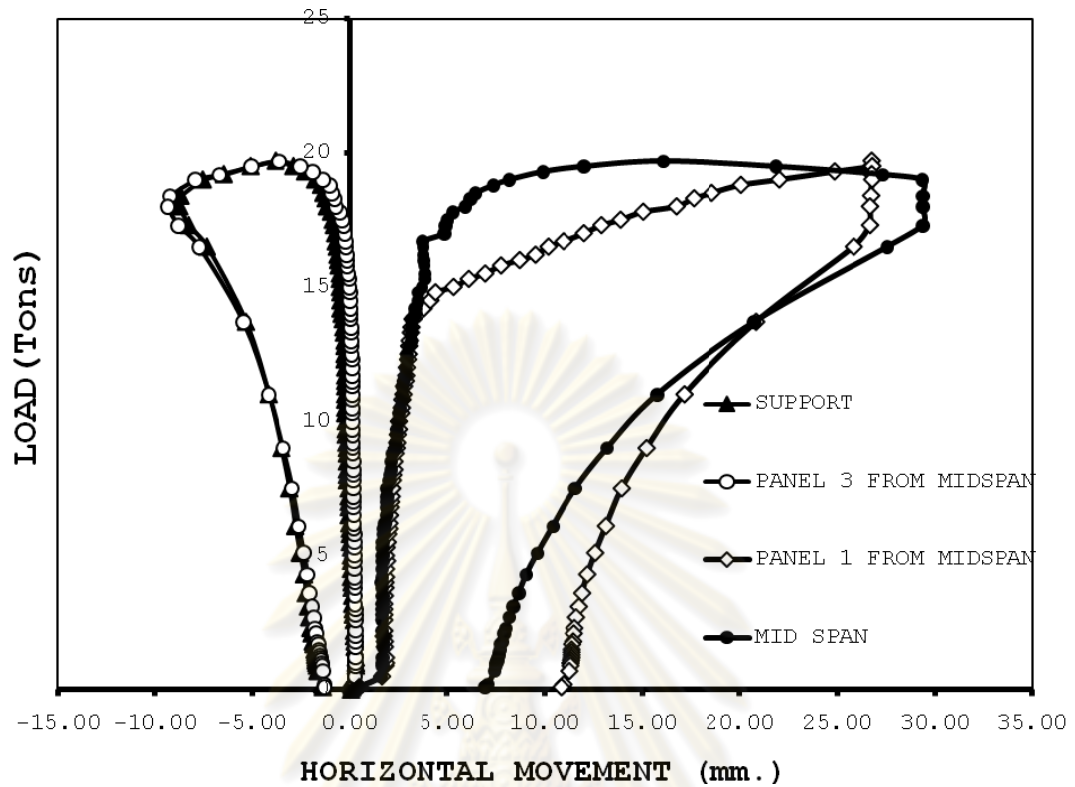


Figure 3.64 Load - horizontal movement curves (Specimen B1)

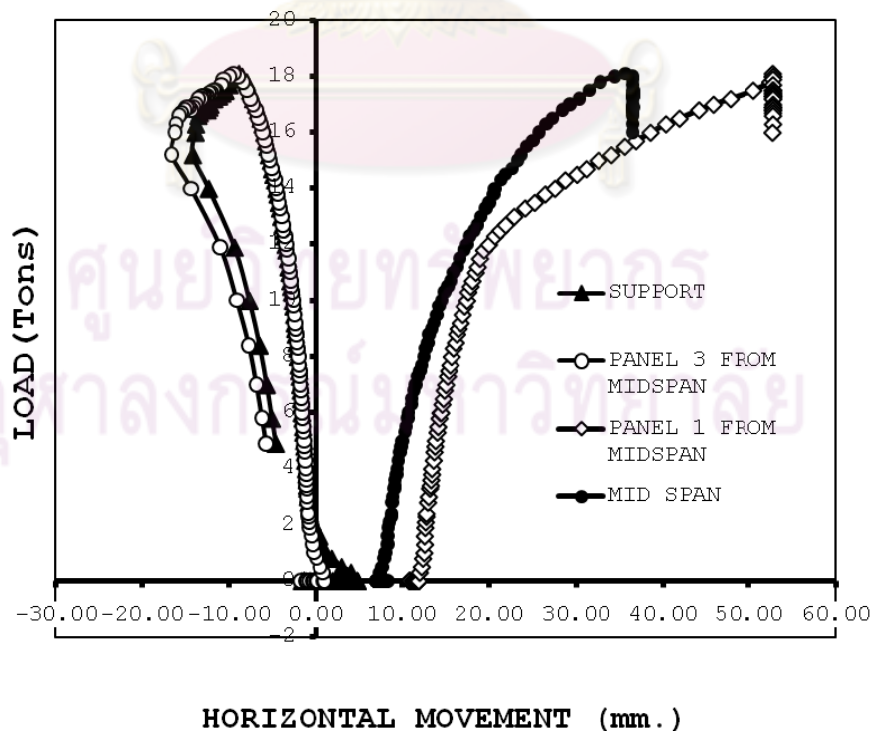


Figure 3.65 Load - horizontal movement curves (Specimen B2)



### 3.6.7 Test Summary

Test results are summarized in Table 3.6. Test specimen No. 1 (Truss series A), with a simple span of 8,534 mm, consisted of a 150mm thick, high performance concrete deck in composition with a 600 mm deep steel truss. The composite system also included two 12.7 mm diameter tendons extending from end to end of the structure and draped at the third points above which equal test loads were applied. Prestressing levels of 460MPa, 690MPa and 920MPa resulted in mid-span pre-cambers of 1.8mm, 3.3mm and 4.4mm, respectively. For the extra 7.9% of the tendon cross sectional area as compared to the bottom chord cross sectional area, the post-tensioned composite truss resisted a maximum total load of 68.4 Tons which was 20.4% higher than the total load of 56.8 Tons in the case of a composite truss without prestressing. However, for similar specimen No. 2 (Truss series B) with no composite slab, the use of post-tensioned tendons had no advantage on the steel non-composite truss because the specimen critically failed in the lateral buckling mode of the top chord.

Table 3.6 Summary of Test Results

Specimens	Pre camber (mm)	Prestress (MPa)	Yield Load (Ton)	Mid Span Deflection at Yield (mm)	Ultimate Load (Ton)	Mid Span Deflection at Ultimate (mm)	Slope of Load and Deflection Curve (kg/cm)
A1	1.8	460	44.0	25.0	-	-	16,418
A2	3.3	690	49.5	26.2	-	-	16,779
A3	4.4	920	55.7	28.1	68.4	151.2	17,144
A4	-	-	40.8	33.7	56.8	55.6	12,107
B1	-	-	-	-	19.5	19.6	9,949
B2	6.4	460	-	-	18.0	13.4	9,090

The pre-camber can be controlled by adjusting the prestressing level. The local buckling of the truss members should be prevented when the prestressing level is increased. Sufficient lateral bracings for the truss members are required to apply the posttensioning technique.

For this experiment, the posttensioning tendons must not be stressed more than 920MPa because when the ram loads applied the force to the structure, the tendons tended to have more stress due to the deflected shape of the truss. The maximum internal force of tendon must not exceed 14,972kg (33kips) or 85% of the ultimate tensile capacity of the tendon.

Shear stud connectors should provide sufficient shear transfer strength especially for the post-tensioned composite truss in which shear force is higher than the ordinary composite truss. High performance concrete should be used to increase the shear stud strength also.



ศูนย์วิจัยทรัพยากร  
จุฬาลงกรณ์มหาวิทยาลัย

## CHAPTER 4

### ANALYTICAL APPROACH

#### 4.1 Comparison of Theoretical and Experimental Results

##### 4.1.1 Pre Camber

In chapter 2, the theoretical approach for calculating the relation between the applied ram loads and the deflection of the posttensioned steel trusses with high performance concrete composite decks was presented. The transformed section, the principle of complementary virtual work, and the principle of superposition can be applied to the posttensioned composite truss to investigate the change in tendon strain. For a composite truss which has n members, the deformation  $\Delta$  in the direction of the virtual load,  $\delta P_{ext}$ , can be computed by the following equations;

$$\delta U^* = \delta W_e^* \quad (2.25)$$

$$\delta U^* = \sum_{i=1}^n \int_0^L \left( \frac{F_i(x) \cdot \delta F_i(x)}{E_i(x) A_i(x)} \right) dx \quad (2.26)$$

$$\delta W_e^* = \delta P_{ext} \cdot \Delta \quad (2.27)$$

Thus;

$$\Delta = \left( \frac{1}{\delta P} \right) \sum_{i=1}^n \int_0^L \left( \frac{F_i(x) \cdot \delta F_i(x)}{E_i(x) A_i(x)} \right) dx \quad (2.37)$$

Where i is the number of the element from 1 up to n and L is the length of member i.  $F_i(x)$  and  $\delta F_i(x)$  denote the internal force in member i and the virtual internal force.  $E_i(x)$  and  $A_i(x)$  are the modulus of elasticity and cross sectional area of member i.

The pre-cambers for the different prestressing forces are shown in table 4.1 below with the experimental data;

Table 4.1 Theoretical and experimental precamber at various levels of prestress

Prestressing Level (MPa)	Theoretical Values (mm.)	Experimental Results (mm.)	Error
460	2.4	1.8	23.4%
690	3.5	3.3	6.4%
920	4.7	4.4	6.4%

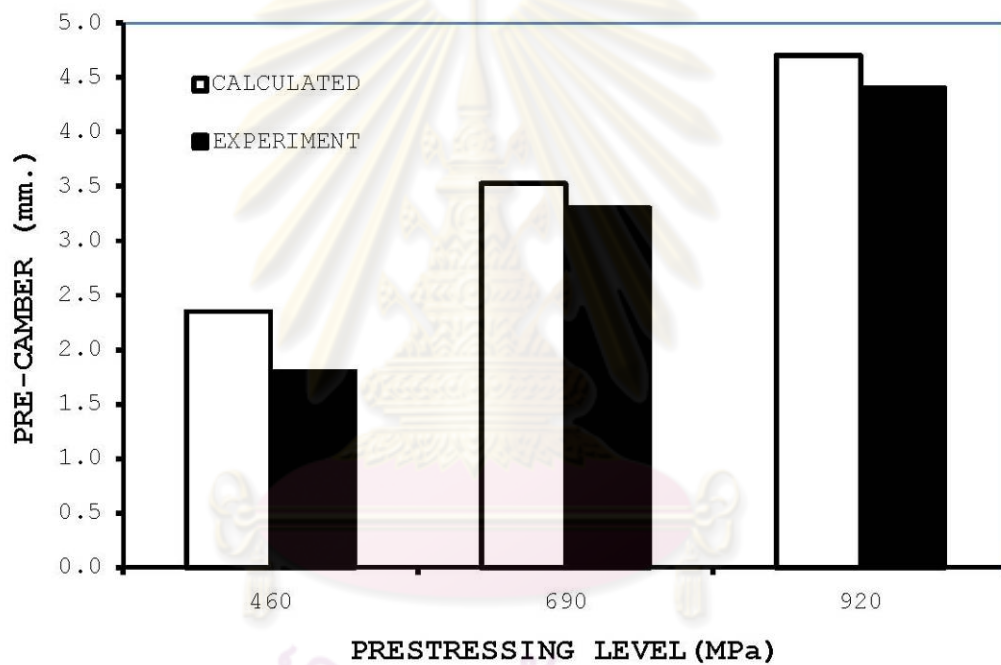


Figure 4.1 Precamber chart from theory and experiment.

The measured pre-camber amounts were different from the calculated values by 23.4%, 6.4% and 6.4% at the prestressing levels of 460 MPa, 690 MPa, and 920 MPa, respectively. The varying margins of error were attributed to varying levels of cracking of the concrete slab caused by prestressing.

#### 4.1.2 Load vs. Mid Span Deflection Curves

To construct the load vs. mid span deflection curve, the internal stresses in the posttensioned composite truss must be investigated. The first coordinates of the load and mid span deflection curves is the precamber deflection which corresponds to the zero external load.

For the next coordinates, the stress such as the bottom chord tensile stress and the top surface compressive stress are observed and used to calculate the mid span deflection which corresponds to the applied external load. These stresses are limited to its tensile or compressive yield strength or the ultimate compressive strength. From the equation 2.36 in chapter 2, the combined total stresses acting on each of the posttensioned composite truss members can be written down as;

$$\sigma_{\text{total}} = (\sigma_{\text{DL}} + \sigma_{\text{SDL}}) + \sigma_{\text{TENDON}} + \sigma_{\text{EXT.LOAD}} + \sigma_{\Delta P} \quad (2.36)$$

where  $\sigma_{\text{DL}}$  and the  $\sigma_{\text{SDL}}$  are the stresses from the dead load and the superimposed dead load;  $\sigma_{\text{TENDON}}$  is the stress due to the prestressing tendon load. This stress is both from the axial stress and the flexural stress;  $\sigma_{\text{EXT.LOAD}}$  is the stress due to the external load; and  $\sigma_{\Delta P}$  is the stress from the increase in tendon force due to the external load considering the stiffness and the slip of the unbonded prestressing tendon.  $\Delta P$  results from the axial and the flexural stress and can be computed as follows;

$$\Delta P = \frac{\left[ \sum_{i=1}^n (\delta F_i) \left( \frac{F_{si} \cdot L_i}{A_i E_i} \right) \right]}{\left[ \sum_{i=1}^n (\delta F_i) \left( \frac{F_{si} \cdot L_i}{A_i E_i} \right) + \sum_{j=1}^m (\delta F_j) \left( \frac{F_{sj} \cdot L_{Tj}}{A_{Tj} E_{Tj}} \right) \right]} \quad (2.33)$$

where  $\delta F_i$  and  $\delta F_j$  represent the virtual load in real member  $i$  up to  $n$  members and in tendon member  $j$  up to  $m$ , respectively.  $F_{si}$  and  $F_{sj}$  represent the internal axial force from external load in real member  $i$  and in tendon  $j$  respectively.  $E_i$ ,  $E_{Tj}$  are the modulus of elasticity of steel truss member  $i$  and tendon  $j$ , respectively.  $L_i$  and  $L_{Tj}$  are the

length of steel truss member  $i$  and tendon  $j$ , respectively.  $A_i, A_{Tj}$  are the cross sectional area of the steel truss member  $i$  and tendon  $j$ , respectively.

After all the internal stresses are known for the iteration of the applied external loads, the principle of virtual work is used to solve for the mid span deflection. As long as the stresses in the composite truss members and the tendon are within the limitation yield strength or the ultimate compressive strength for the concrete slab, the procedure for the load and deflection curve continues to the higher load level.

For the Specimen A3, The tendon conforming to grade 250 steel has an ultimate tensile strength of  $17,581\text{kg/cm}^2$  or  $1758\text{MPa}$  and also has the yield strength at  $15,822\text{kg/cm}^2$  or  $1582\text{MPa}$ . The initial prestressing force is  $18,149\text{ kg}$  or  $920\text{MPa}$  which causes the calculated precamber amount at  $4.73\text{mm}$  in the upward direction.

At the time of the application of the external load at  $58\text{ tons}$ , the total calculated elongation at the same level of the tendon due at the total external load of  $58\text{ tons}$ , which was the load that caused the bottom chord stress yield,  $\delta_{1p}$  equals to  $1.505145$  while the total elongation of the steel truss at the same level as the tendon due to the unit load,  $\delta_{11}$ , was  $0.000237$ . Consequently, the increase in tendon load from the external load can be calculated from the compatibility equation;

$$\delta_{11}\Delta T - \delta_{1P} = 0 \quad (2.31)$$

In which  $\delta_{1p}$  and  $\delta_{11}$  are;

$$\begin{aligned} \delta_{1P} &= \sum_{i=1}^n (\delta F_i) \left( \frac{F_{si} \cdot L_i}{A_i E_i} \right) \\ \delta_{11} &= \sum_{i=1}^n (\delta F_i) \left( \frac{F_{si} \cdot L_i}{A_i E_i} \right) + \sum_{j=1}^m (\delta F_j) \left( \frac{F_{sj} \cdot L_{Tj}}{A_{Tj} E_{Tj}} \right) \end{aligned} \quad (2.32)$$

Thus, the calculated increase in tendon load is;

$$\Delta P = \frac{[\delta_{1P}]}{[\delta_{11}]} = \frac{\left[ \sum_{i=1}^n (\delta F_i) \left( \frac{F_{si} \cdot L_i}{A_i E_i} \right) \right]}{\left[ \sum_{i=1}^n (\delta F_i) \left( \frac{F_{si} \cdot L_i}{A_i E_i} \right) + \sum_{j=1}^m (\delta F_j) \left( \frac{F_{sj} \cdot L_{Tj}}{A_{Tj} E_{Tj}} \right) \right]} = 6,350 \text{kg}$$

From theoretical analysis, after the external ram load of 58 tons was applied to the posttensioned composite truss, the increase in tendon force is 6,350kg. The total internal force for the prestressing tendon becomes 24,449kg. The actual stress in the tendon is  $12,347 \text{kg/cm}^2$  or 1235MPa or approximately 80% of the yield strength of the tendon. This external load makes the bottom chord stress starting to yield.

The final point on the load and mid span deflection curve is the ultimate strength point. The flexural capacity of the posttensioned composite truss can be computed by the following equation;

$$F_{\max} = \min \left[ \left( A_s \cdot f_y + A_{ps} \cdot f_{ps,\max} \right), \sum Q_u, 0.85 f_c' b t_c \right]$$

$$M_u = F_{\max} \cdot \left( h - \frac{a}{2} \right) \quad (2.37)$$

The maximum tensile force comes from the minimum of the three tensile forces: (1) the combination of the yield tensile strength of the bottom chord and the tendon force; (2) the summation of the shear stud connector strength from the point of the maximum moment to the zero moment, and: (3) the maximum compressive force in the concrete deck slab. For the tendon stress, the difference between the values of the ultimate moment computed from: (1) the tendon stress at the bottom chord yielding point,  $f_{ps}$ : (2) the yield strength of the tendon itself,  $f_{py}$ , and: (3) the ultimate strength of the tendon,  $f_{pu}$ . The difference between the values of the ultimate moment computed at each bound for the prestressing force is on the order of 5% in which is not significant.

For the minimum bound,  $f_{ps}$  equals the tendon force at the yield load, for the case that the tendon has not yielded;

$$F_{\max,1} = A_s f_y + A_{ps} f_{ps,yield} = 123,697 \text{ kg}$$

For the middle and the upper bound,  $F_{ps}$  equals the yield strength and the ultimate strength of tendon, respectively;

$$F_{\max,2} = A_s f_y + A_{ps} f_{py} = 129,761 \text{ kg}$$

$$F_{\max,3} = A_s f_y + A_{ps} f_{pu} = 133,157 \text{ kg}$$

The differences in the maximum tendon forces;  $F_{\max,1}$  and  $F_{\max,2}$  is 6,064kg (4.9%) and  $F_{\max,2}$  and  $F_{\max,3}$  is 3,396kg (2.6%). The difference between the values of the ultimate moment computed at each bound for the prestressing force is on the order of 5%. Normally, the tendon force from the yield strength,  $F_{\max,2}$  is appropriate for calculation of the upper bound ultimate moment is less than the ultimate tendon strength.

Moreover, for full composite action, the shear connector strength is adequate for the bottom chord to develop the full yield strength. Also the ultimate compression force in concrete is more than the tension force in the bottom chord plus the tendon force.

Thus, the calculated flexural capacity of the specimen A3 is

$$M_u = F_{\max} \cdot \left( h - \frac{a}{2} \right) \quad (2.45)$$

$$M_{u1} = (129,761)(0.675) = 87,588 \text{ kg-m}$$

$$P_{\text{ext}} = (2) 87,588 (0.351) = 61,573 \text{ kg/ram} = 61.6 \text{ ton}$$

For the ultimate deflection, for the under reinforce section or the  $\rho_{\text{total}}$  less than  $\rho_b$ . For the section that has both  $A_s$  for the bottom chord and  $A_{ps}$  for the tendon;



$$\frac{A_s}{b \cdot d} = \rho_b = 0.85 \frac{f_c'}{F_y} \beta_1 \frac{\varepsilon_{cu}}{\left(\frac{F_y}{E} - \varepsilon_{cu}\right)} \quad (2.49)$$

$$\rho_{total} = \rho_s + \rho_{ps}$$

$$\rho_{total} = \left(\frac{A_s}{b \cdot d}\right) + \eta \left(\frac{A_{ps}}{b \cdot d}\right) \quad ; \quad \eta = \frac{F_{py}}{F_y} \quad (2.50)$$

where  $\eta$  is the yield strength ratio calculated from the ratio between the yield strength of the tendon to the yield strength of the bottom chord. The limit of the percentage of  $\rho_{total}$  being not more than the balanced condition makes the structure fail in a ductile mode from the yielding of the bottom chord prior to the crushing of the concrete at the ductility ratio of 4 or greater. Thus, the yield deflection equals 4 times 29.91 which is 119.64mm (ACI 318-10.3.3). All of plot data are shown in Table 4.2.

Table 4.2 Plot data for the theoretical load-deflection curve

Deflection from Ext Load(mm)	Initial Precamber(mm)	Uplift from $\Delta T$ (mm)	Total Deflection (mm)	External Load (tons)
0	-4.73	0	-4.73	0
3.12	-4.73	-0.14	-1.74	5
6.24	-4.73	-0.27	1.24	10
9.37	-4.73	-0.41	4.23	15
12.49	-4.73	-0.54	7.21	20
15.61	-4.73	-0.68	10.20	25
18.73	-4.73	-0.82	13.19	30
21.86	-4.73	-0.95	16.17	35
24.98	-4.73	-1.09	19.16	40
28.10	-4.73	-1.23	22.15	45
31.22	-4.73	-1.36	25.13	50
34.35	-4.73	-1.50	28.12	55
36.22	-4.73	-1.58	29.91	58
			119.64	61.6

The plot of the load and deflection curve from the theoretical calculation and the experimental data is shown in figure 4.2 below;

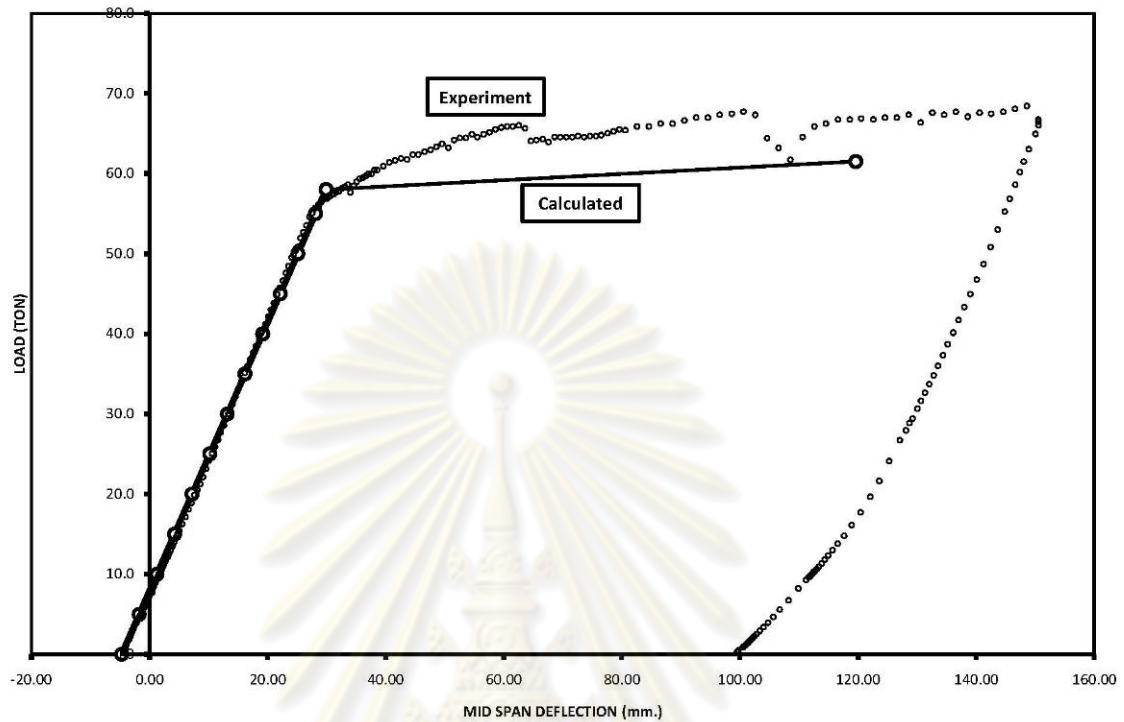


Figure 4.2 Load - deflection curves from the theoretical and experimental data

From figure 4.2, the calculated load and deflection shows a good prediction for the flexural behaviour of the posttensioned composite truss. This verifies that the energy theorem, the principle of complementary virtual work theory and the principle of superposition are applicable for the theoretical approach. For the elastic range the principle of superposition is valid, the slope of the experimental data and the theoretical calculation are almost the same. For the inelastic range, the ultimate flexural capacity of the posttensioned composite truss calculated by section analysis is on the conservative side but the trend of the slope is similar. The different points between the calculated value and the experiment data is due to slip of the anchorage wedges of the prestress tendons.

### 4.1.3 Load and Element Stress Analysis

The calculated load and member stress curves are plotted against the experimental load and stress curves from chapter 3. For the mid span bottom chord stress, the second panel bottom chord stress, the diagonal member and the top fibre concrete stress curves are shown below.

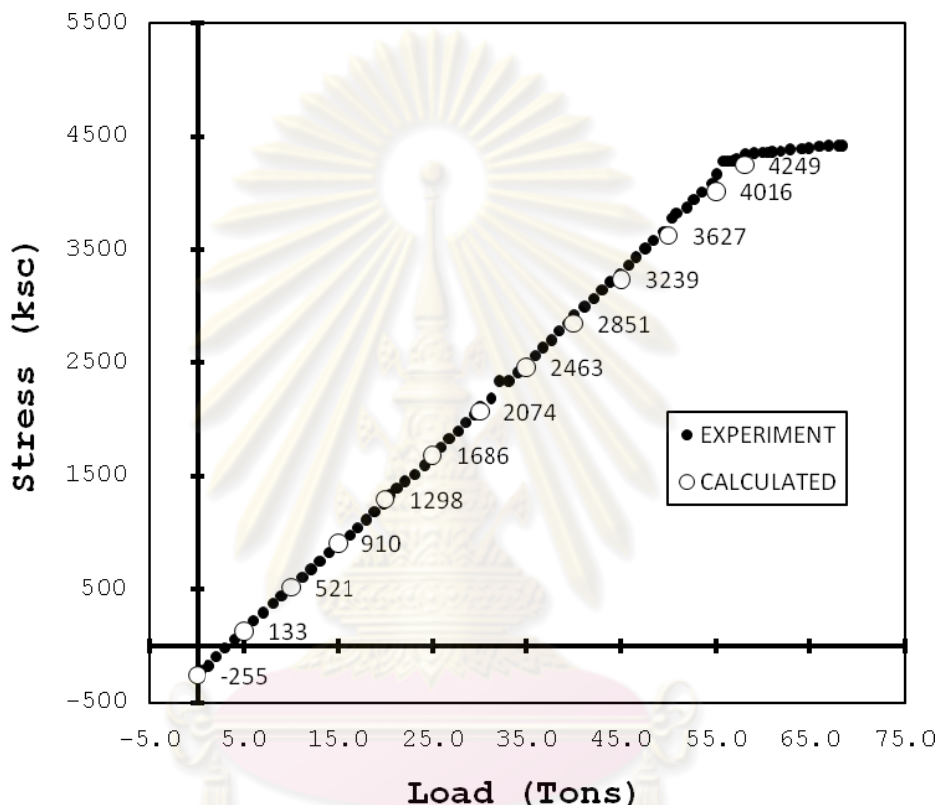


Figure 4.3 Comparison of experimental results & calculated load and bottom chord stress at mid span curves

ศูนย์วิจัยและพัฒนา  
จุฬาลงกรณ์มหาวิทยาลัย

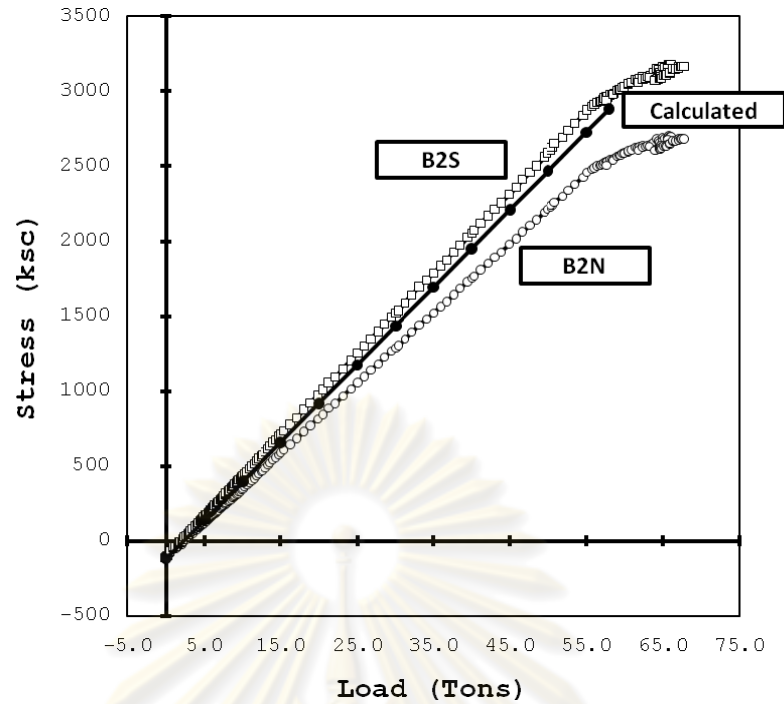


Figure 4.4 Comparison of experimental results & calculated load and bottom chord stress at 2<sup>nd</sup> panel member curves

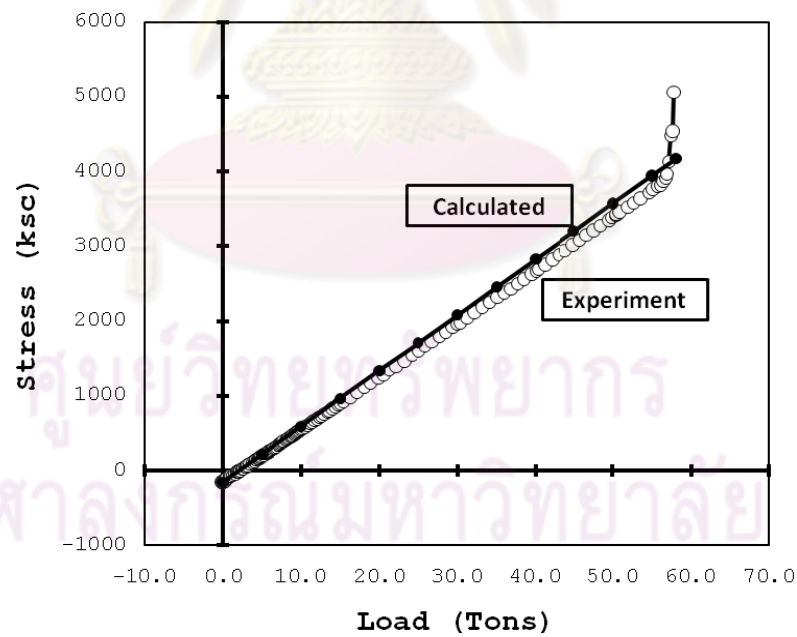


Figure 4.5 Comparison of experimental results & calculated load and diagonal member stress curves

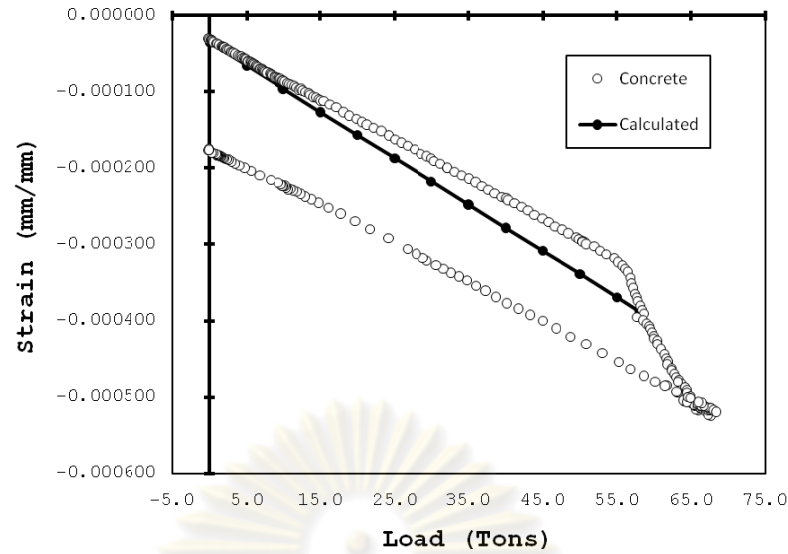


Figure 4.6 Comparison of experimental results & calculated load and top fibre concrete stress curves

#### 4.1.4 Moment and Curvature Curves

From the stress and strain readings from the strain gages in the experimental specimens, the plot of the moment and curvature curves are shown in comparison with the theoretical calculations. The calculated moment is computed from the ram loads and the span length where moment equals  $P_{\text{ext}}L/6$ . The corresponding curvature is calculated from the bottom chord strain,  $\epsilon_s$ , divided by the distance from the neutral axis to the centre of gravity of the bottom chord. The experimental moment is calculated the same way as the theoretical one while the curvature is then calculated from;

$$\phi = \left( \frac{\epsilon_s - \epsilon_c}{t_c + \frac{t_s}{2} + d} \right) \quad (4.2)$$

where  $\epsilon_s$  is the strain of steel bottom chord at mid span,  $\epsilon_c$  is the top surface concrete strain at mid span,  $t_c$  is the concrete thickness,  $t_s$  is the top chord thickness and  $d$  is the distance between the center of gravity of the top chord to the center of gravity of the bottom chord.

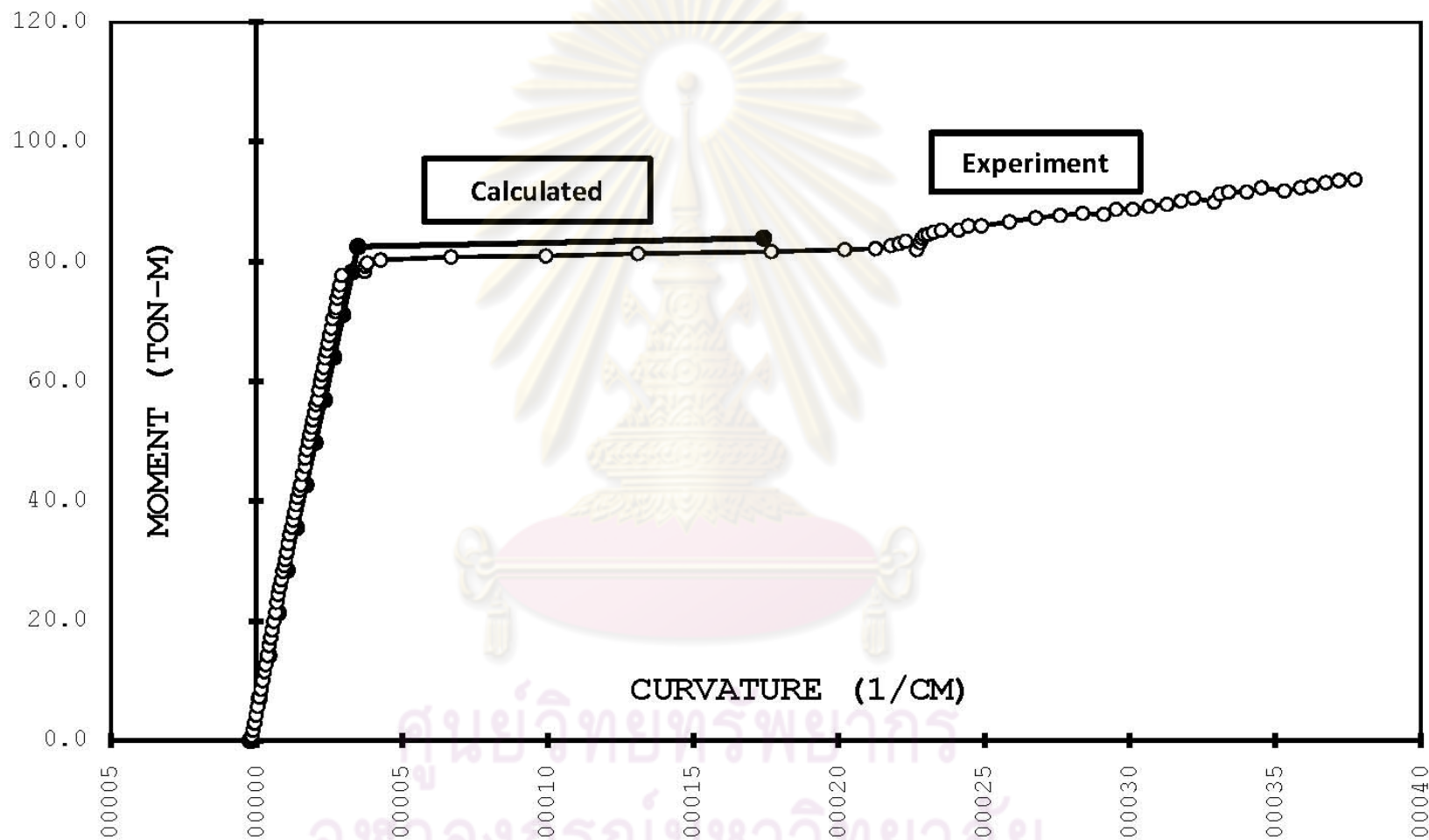


Figure 4.7 Moment and curvature curves from experimental results and theoretical calculation

#### 4.1.5 Load and Slip Curves

Shear stud connectors are an important part of the composite truss. The load and slip relation is an important part to study the behavior of the interface action. From the theoretical approach in chapter 2, the plot of the theoretical shear stud connector load slip curve with the experimental curve is shown below.

Table 4.3 Shear stud strength

Failure Modes	Equation	$Q_u$ (kg)
Concrete Crushing Mode	$Q_u = 0.5 \cdot A_s \sqrt{f_c' E_c}$	14,951
Tension Failure Mode	$Q_u = A_s F_u$	8,000
Direct Shear at Base Mode	Welding Strength at Base	4,655
$Q_u$ , Shear Stud Strength (kg)		4,655

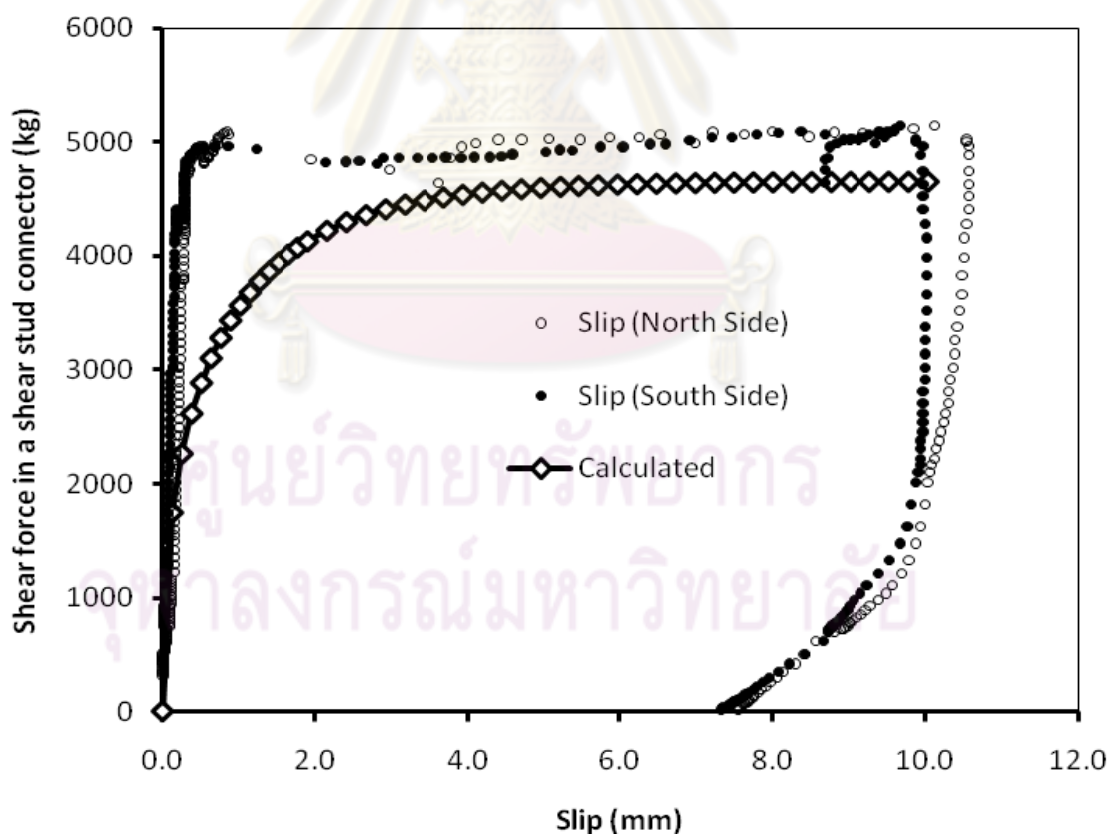


Figure 4.8 Theoretical and experimental load slip curves.  $Q = (Q_u) \cdot \left(1 - e^{-18\Delta}\right)^{\frac{2}{5}}$

The theoretical load and slip relation for the shear stud connectors is on the conservative side. The slip of the experiment behaved more rigid with the higher ultimate strength. The shear capacity was controlled by the direct shear mode of the shear stud itself which equals the shear stud cross sectional area times 0.67 and the tensile strength of the material.

#### 4.1.6 Load and Lateral Movement Curves

An important mode of failure of a conventional steel truss as seen for Truss B is lateral torsional buckling. Test B1 and Test B2 showed that the posttensioned technique has no advantage for the flexural load resistance because the controlling factor is the buckling load of the truss. In order to find the critical buckling load of the truss, the governing equation for lateral torsional buckling of a simply supported beam subjected to pure bending with rotation prevented at the support is;

$$EC_w \frac{d^4 \beta}{dz^4} - GJ \frac{d^2 \beta}{dz^2} - \frac{M_x^2 \beta}{EI_y} = 0 \quad (4.1)$$

The above equation is evaluated using boundary condition at  $z = 0$ ,  $\beta = 0$  and  $z = L$ ,  $\beta = 0$  for  $\beta = (\beta_{L/2}) \sin \frac{\pi z}{L}$  where  $\beta_{L/2}$  is the mid span rotation of the beam about longitudinal axis. Substituting the  $\beta$  equation into the governing equation yields:

$$\left( \frac{\pi^4}{L^4} EC_w + \frac{\pi^2}{L^2} GJ - \frac{M_x^2}{EI_y} \right) (\beta_{L/2}) \sin \frac{\pi z}{L} = 0 \quad (4.2)$$

The buckling occurs when the value in parentheses equals zero;

$$\left( \frac{\pi^4}{L^4} EC_w + \frac{\pi^2}{L^2} GJ - \frac{M_x^2}{EI_y} \right) = 0$$

$$M_{x,cr}^2 = \left( \frac{\pi^4}{L^4} EI_y EC_w + \frac{\pi^2}{L^2} EI_y GJ \right) \quad (4.3)$$



For the case that other moment diagrams acting on the beam, the critical moment is:

$$M_{x,cr}^2 = C_b^2 \left( \frac{\pi^4}{(KL)^4} EI_y EC_w + \frac{\pi^2}{(KL)^2} EI_y GJ \right)$$

$$I_{y,truss} = 2I_{y,chord}$$

$$C_{w,truss} = \frac{d^2}{4} (I_{y,truss}) \quad (4.4)$$

$$J_{truss} = \frac{1}{3} \sum bt^3$$

For a simply supported span with two third point loads the value for  $C_b$  and  $K$  are 1.04 and 1.00, respectively. For  $C_{w,truss}$ , the value of 'd' is the distance between the top chord and the bottom chord which is 50cm. Substituting values to calculate the critical moment and, critical load. The critical load is six times critical moment over  $L$  due to the arrangement of the load and span for Truss B.

$$I_{y,truss} = 2 I_y = 2(161) = 322 \text{cm}^4$$

$$C_{w,truss} = (50^2)(322)/4 = 201,250 \text{cm}^6$$

$$J_{truss} = 11.47 \text{cm}^4$$

$$M_{x,cr} = 3,007.4 \text{kg-m}$$

$$P_{cr} = 2,115 \text{kg}$$

The calculated critical load of the truss without any lateral bracing is very low. In the case of Truss A, three lateral braces were provided to Truss B at the distance from support of  $L/3$  and  $2L/3$ . For the unbraced length of 2.845m ( $L/3$ ), the calculated top chord elastic buckling load equals 34,904kg. The bending moment from this compression force is 17,452kg-m from the total vertical load equal to 12,270kg. All the critical loads are plotted against the critical load from Test B1 and Test B2 as shown below.

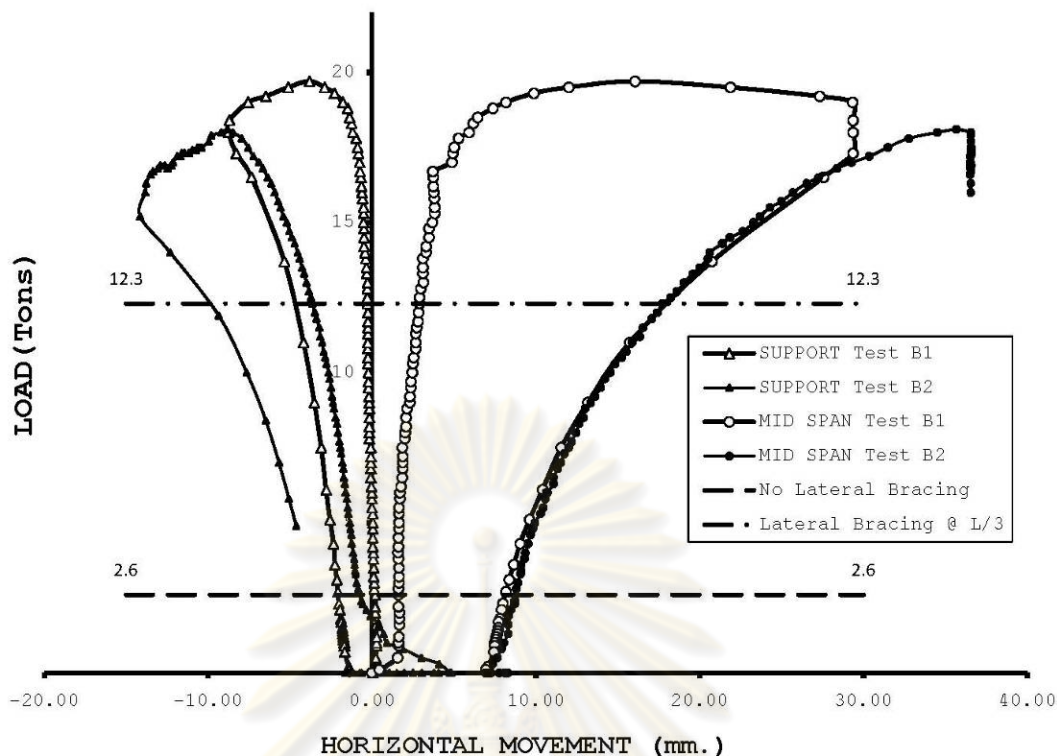


Figure 4.9 Critical buckling loads for Specimens B1 and B2

#### 4.2 Analysis of Semi Rigid Joint Behavior

As the steel members in a rigid frame are connected together at the joints from the welding method, the local flexural stiffness of the welding joints transfers the flexural bending moment from member to member. For a composite truss, the steel members are connected in the same way as the rigid frame. Hence, the posttensioned composite truss may behave between the cases of pin joint and fix joint, called semi rigid joint behavior. The analysis of semi rigid joint behavior is presented in this section.

The previous analyses in this research are based on pinned joint behavior. To study semi rigid joint behavior, the posttensioned composite truss is re-analyzed by assuming that all the joints are connected perfectly rigidly. The structural analysis is based on the fixed joint behavior as in the case of a rigid frame. The analysis considers both the axial forces and the bending moments acting on each member. The results are then compared to determine the different behaviors.

From the principle of the complementary virtual work;

$$\delta U^* = \delta W_e^* \quad (2.25)$$

The virtual strain energy,  $\delta U^*$ , considering the flexural stiffness of the member, can be determined by

$$\delta U^* = \sum_{i=1}^n \int_0^L \left( \frac{F_i(x) \cdot \delta F_i(x)}{E_i(x) A_i(x)} + \frac{M_i(x) \cdot \delta M_i(x)}{E_i(x) I_i(x)} \right) dx \quad (2.43)$$

Where  $i$  is the number of the element from 1 up to  $n$  and  $L$  is the length of member  $i$ .  $F_i(x)$  and  $\delta F_i(x)$  denote the internal force and the virtual internal force of member  $i$ .  $M_i(x)$  and  $\delta M_i(x)$  denote the internal moment and the virtual internal moment of member  $i$ .  $E_i(x)$ ,  $A_i(x)$  and  $I_i(x)$  are the modulus of elasticity, cross sectional area and the moment of inertia of member  $i$ .

The structural analyses for the steel truss only are done for (1) a uniformly distributed load 1kg/m and (2) the unit virtual load  $\delta P_{\text{ext}}=1.0\text{kg}$  at mid span. The uncracked concrete section of the posttensioned composite truss is analyzed for the unit tendon load  $\delta P=1\text{kg}$  in the same location and configuration as the prestressing tendon. The prestressing level of 920MPa can be resisted by the concrete modulus of rupture and no crack occurs in the concrete. (2) the unit virtual load  $\delta P_{\text{ext}}=1.0\text{kg}$  at mid span. The cracked section of the posttensioned composite truss is analyzed for (1) with two point loads equals to 1.0kg at  $L/3$  and  $2L/3$  of the span length and (2) the unit virtual load  $\delta P_{\text{ext}}=1.0\text{kg}$  at mid span. The noncracked section has  $A_t$  equal to  $518\text{cm}^2$ ,  $I_x$  equal to  $13,479\text{cm}^4$  and  $I_y$  equal to  $44,675\text{cm}^4$ . The cracked section has  $A_t$  equal to  $182\text{cm}^2$ ,  $I_x$  equal to  $7,427\text{cm}^4$  and  $I_y$  equal to  $14,346\text{cm}^4$ .

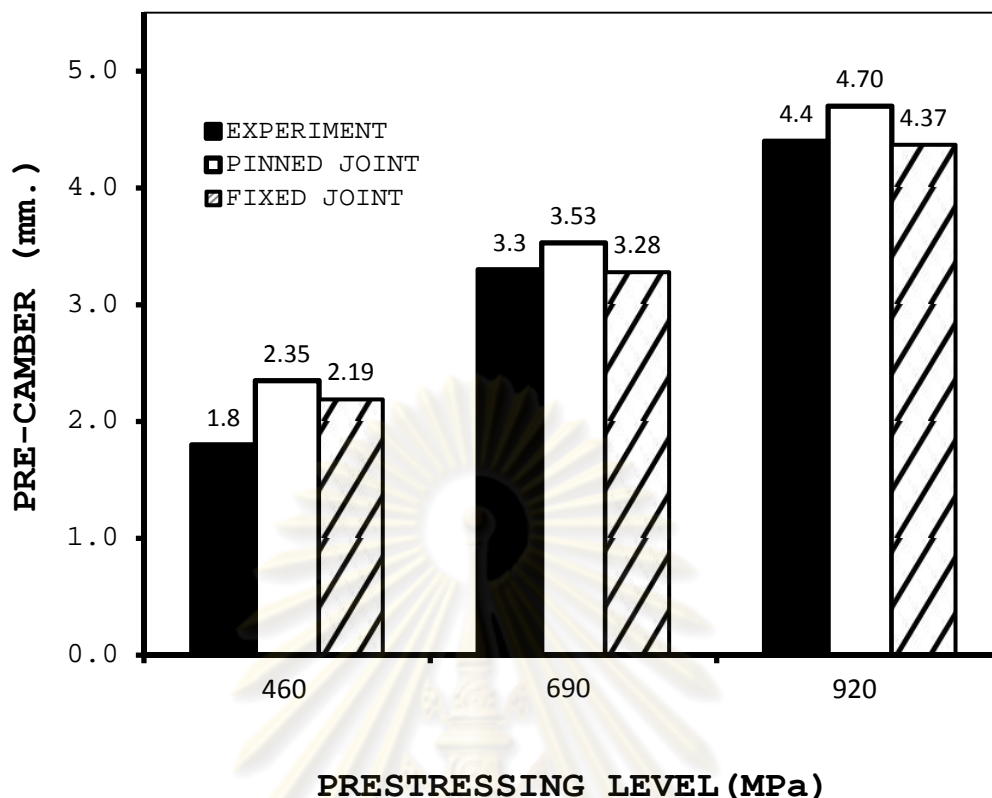


Figure 4.10 Precamber based on fixed and pinned joint assumptions compared to experimental results

Figure 4.10 shows the plot of the precamber calculated from both the pinned joint and the fixed joint assumptions compared to the experimental results. The precamber amounts calculated from the fixed joint assumption are 2.19mm for 460MPa prestressing level, 3.28mm for the 690MPa prestressing level and 6.56mm for the prestressing level of 920MPa. These precamber amounts are less than the precamber calculated from the pinned joint assumption but they are almost the same as the experimental precambers.

Calculations from the pinned joint assumption are slightly higher than the experimental precamber. The differences between the pinned joint assumption and the experiment are approximately 6.8% for the case that the concrete slab has cracked (Specimens A2 and A3). On the other hand, the differences from the fixed joint assumption and the experimental results are approximately 0.5% (Specimens A2 and A3) which is very low.

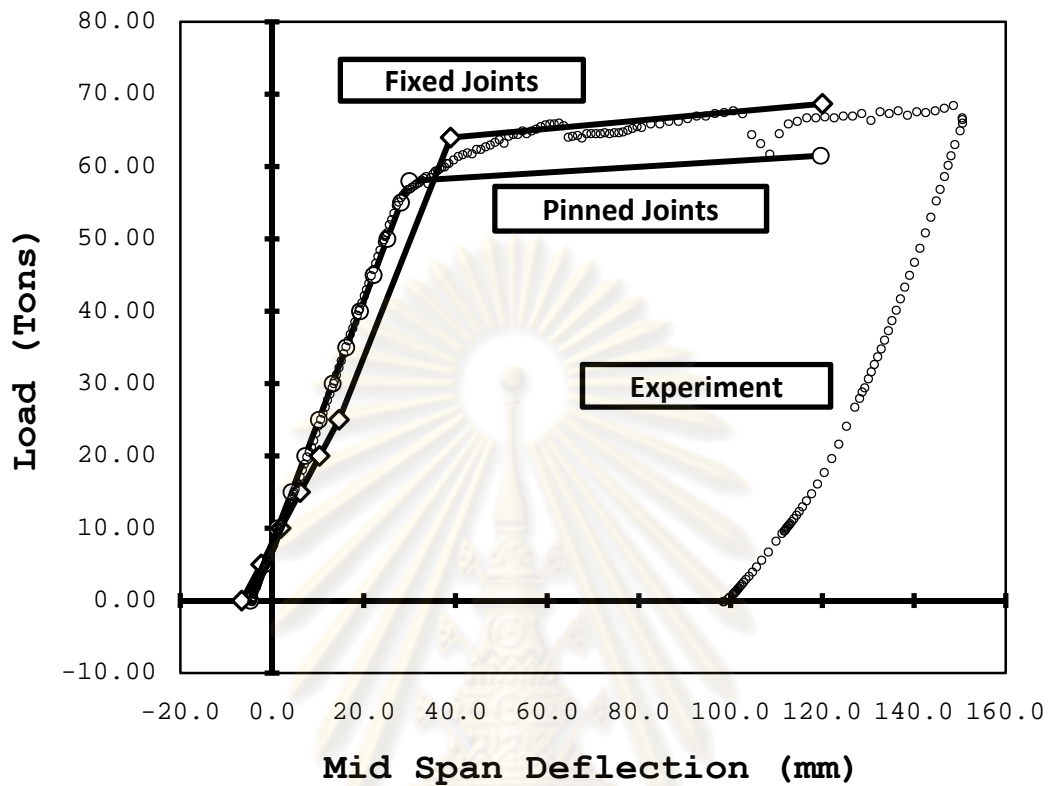


Figure 4.11 Load and mid span deflection calculated from fixed and pinned joints compared to the experimental results

From Figure 4.11, the load and deflection curve calculated from the pinned joint assumption is in good correlation to the experimental results compared to the load and deflection curve calculated from the fixed joint assumption. For ram loads at 25 Tons, the bottom flange of the steel top chord member begins to yield from the internal forces and high bending moments. After the steel top chord yields, the elastic modulus of the steel section is reduced and the overall structure tends to behave as in truss mode. The bottom chord stress calculated from the fixed joint assumption has less stress than the pin joint assumption at the same ram loads. Thus, the extra load can be applied to the truss before the bottom chord starts to yield. The yield load of the fixed joint assumption is higher than the pinned joint assumption because the truss can be

deflected more and hence the tendon stress is also higher than the pinned joint assumption and that at the ultimate load capacity.

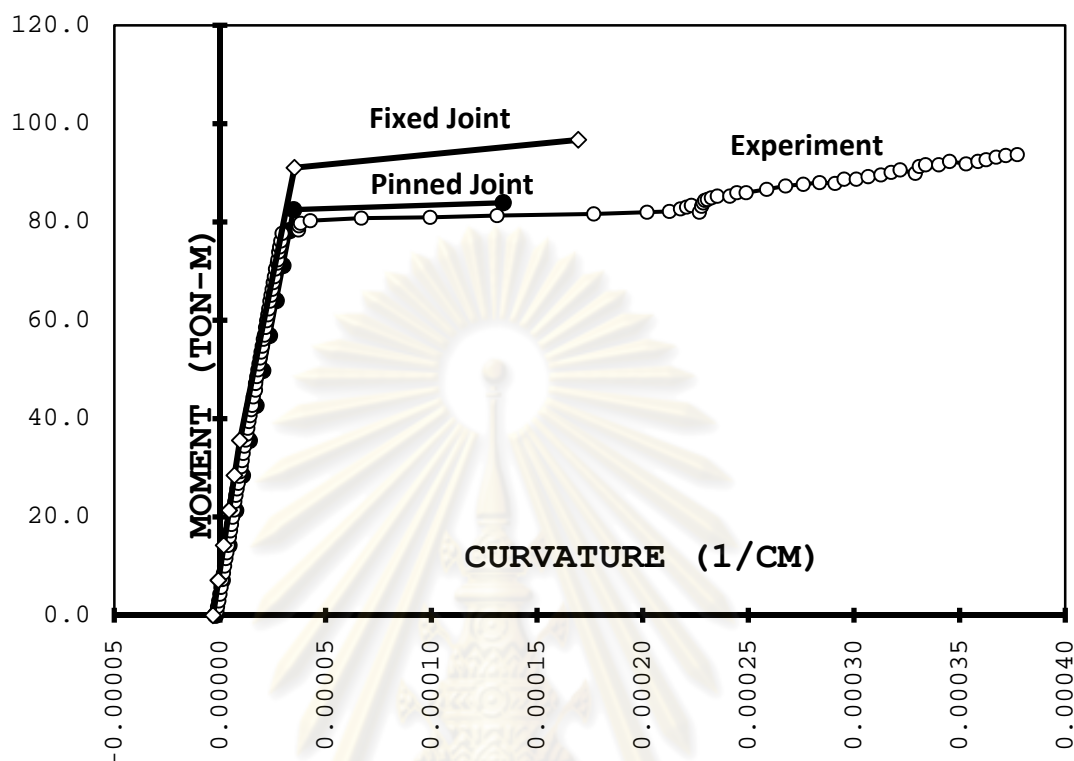


Figure 4.12 Moment vs. curvature as calculated from fixed and pinned joints and compared to the experimental results

From Figure 4.12, the moment - curvature curves, the three curves are almost the same in the elastic range. The experimental result tends to behave between the moment -curvature curves calculated from pinned and fixed joint assumptions. However, for the inelastic range the calculation from the pinned joint assumption shows better correlation with the experimental one.

For the higher load level, the actual welding joint flexural stiffness of the posttensioned composite truss is not rigid enough to resist the high flexural moment so the joint can be rotated and then the moment is reduced. Thus, for overall behavior, the member internal stresses and the tendon force tend to behave in the truss mode. It is reasonable to conclude that the pinned joint assumption can be used to calculate the stress, deflection, the increase in tendon force and also the ultimate capacity.

### 4.3 Analysis of Concrete Strength Effects

The effect of concrete strength for the flexural behavior is presented in this section. The higher concrete strength causes the neutral axis to be closer to the top surface of the concrete slab. This increases the transformed moment of inertia. The effect is significant for a compressive strength lower than 300kg/sq.cm as shown in the following figures.

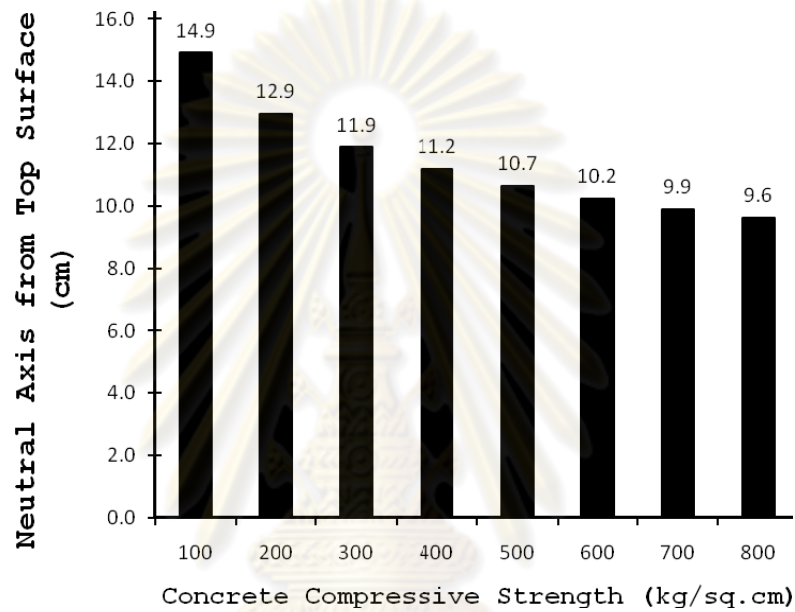


Figure 4.13 Effect of concrete strength to neutral axis location

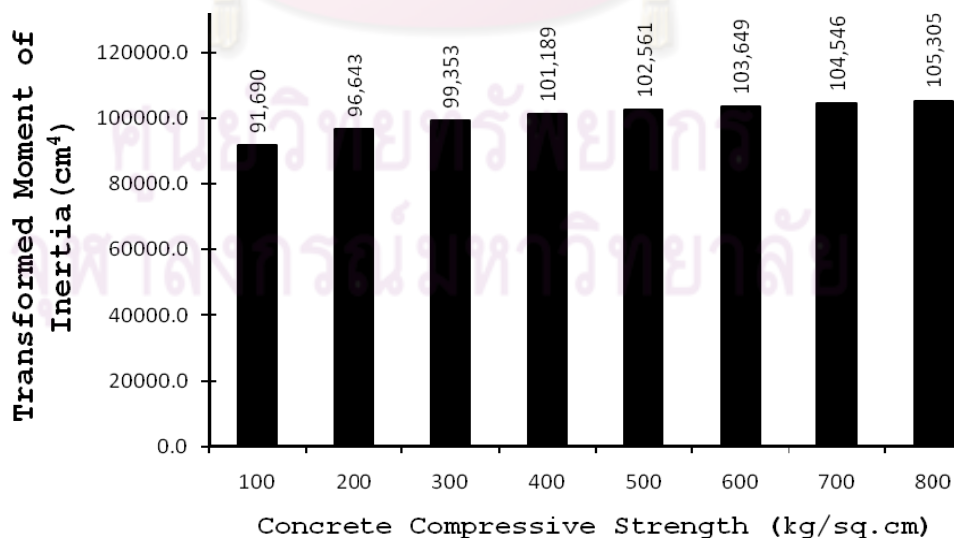


Figure 4.14 Effect of concrete strength on transformed moment of inertia

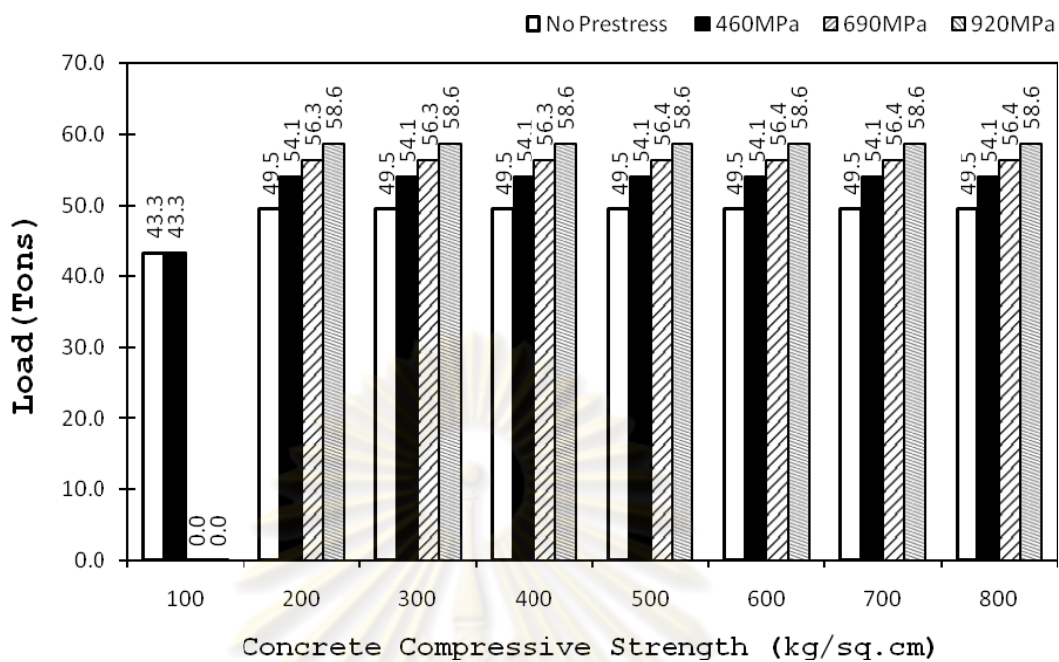


Figure 4.15 Effect of concrete strength to the yield load

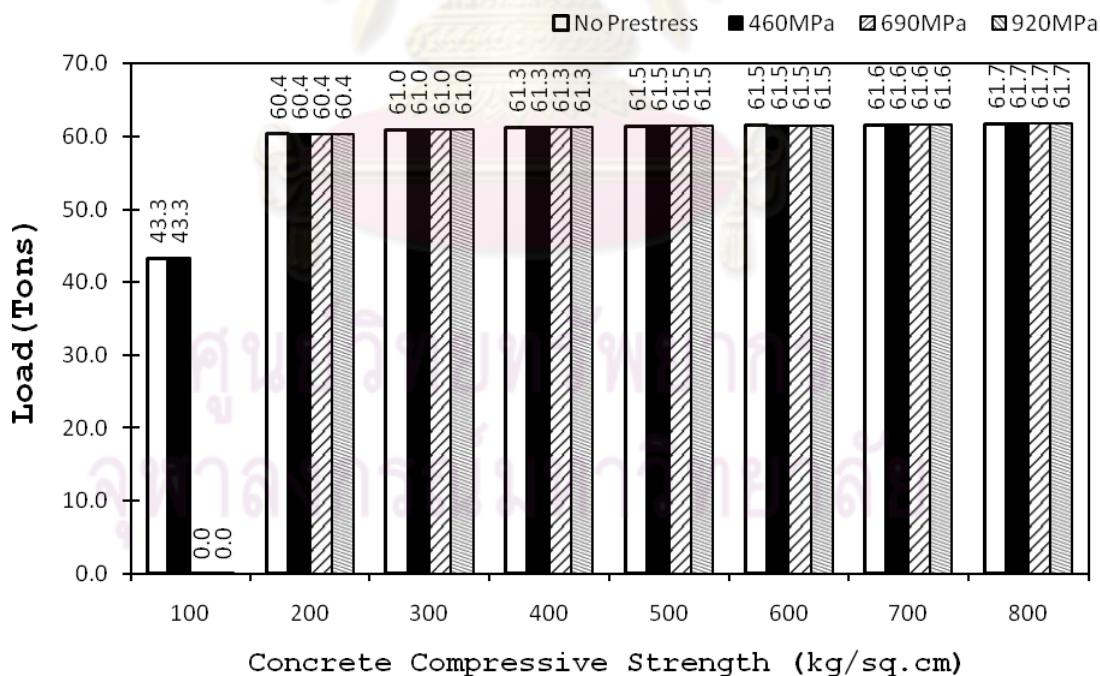


Figure 4.16 Effect of concrete strength to the ultimate load



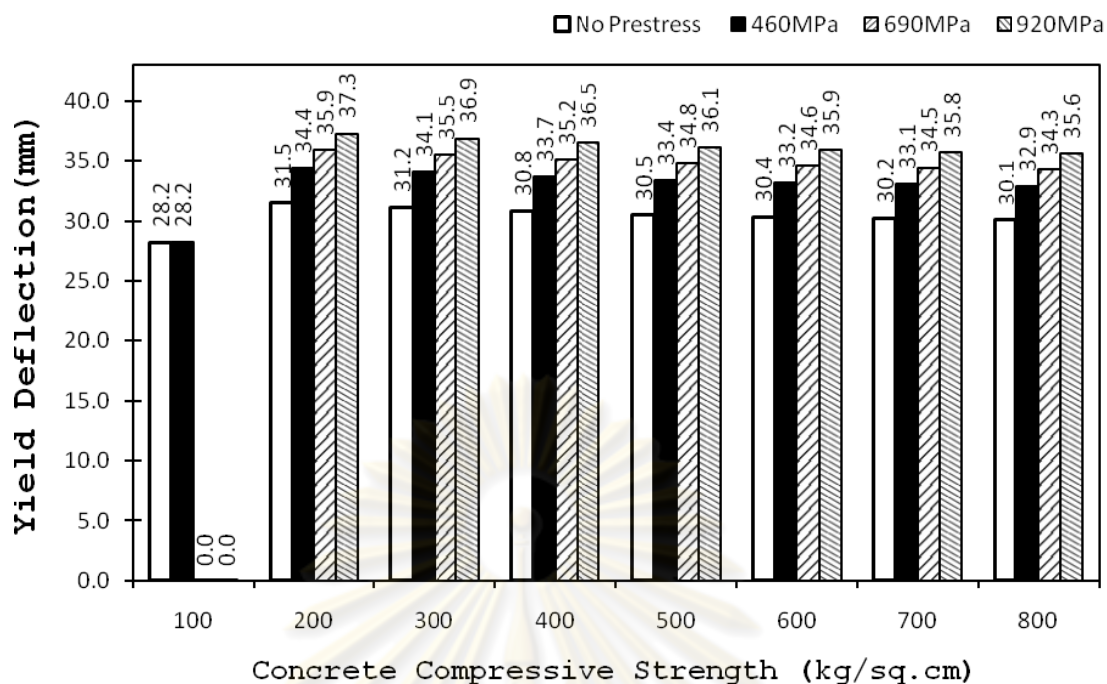


Figure 4.17 Effect of concrete strength to the yield deflection

Concrete strength has a significant effect on the failure mode of the posttensioned composite truss especially for the lower strength concrete as shown in Figure 4.18. A 100kg/sq.cm concrete strength causes the structure to fail by shear stud connector failure due to concrete crushing behind the studs.

For similar dimensions of concrete slab, steel truss and configuration of the truss members, support conditions and the prestressing tendons, the neutral axis moves closer to the top fibres of the slab. For a concrete strength of 100kg/sq.cm the neutral axis is very close to top surface. At a higher prestress of the top surface of the concrete slab undergoes tensile cracking failure and the modulus of rupture is exceeded.

For yielding of the bottom chord and the tendons the concrete strength has less effect on this behavior. This leads to a more ductile failure mode.

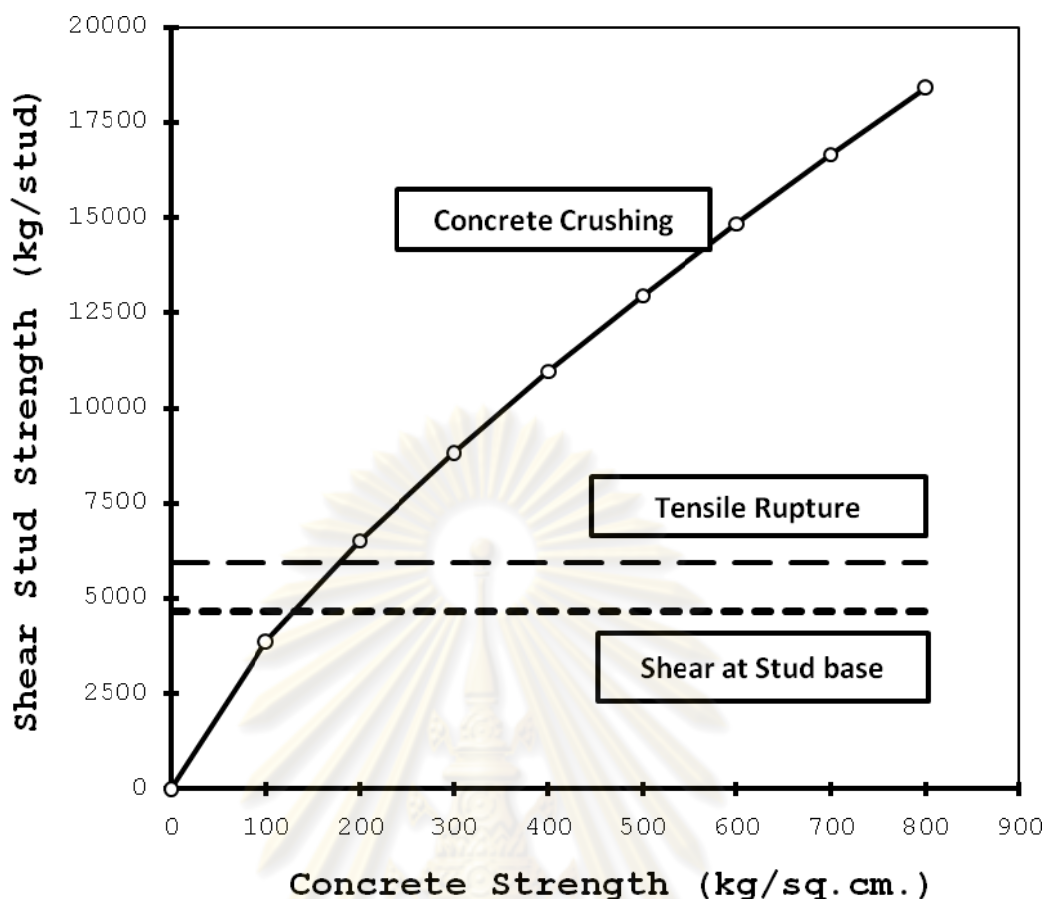


Figure 4.18 Effect of concrete strength on the shear stud strength

The concrete strength has the effect to the shear stud connector as shown in Figure 4.18. For a small diameter of shear stud connector, the failure mode of the shear stud is in the tensile rupture mode or direct shear at the stud base. Increasing concrete strength shows less effect for this case such as in the experiments Specimens A1, A2, A3 and A4 where the shear stud diameter is 15.9mm. The shear stud strength is controlled by the direct shear at base. For larger stud diameters, the concrete strength shows more influence since the failure load for the direct shear at the base and the tensile rupture are higher than the concrete crushing failure.

#### 4.4 Analysis of Percentage of Tendon Reinforcement Effects

##### 4.4.1 Effect of Percentage of Tendon Reinforcement to the Ultimate Moment Capacity

The effect of the prestressing tendon on the strength and behavior of a posttensioned composite truss is the major concern of this research. In order to study this effect, variation of the level tendon prestress is introduced.

Consider a posttensioned composite truss section that has a cross sectional area of  $A_s$  for the bottom chord and the cross sectional area of  $A_{ps}$  for the tendon. The total reinforcement ratio,  $\rho_{total}$  is the combination of the reinforcement ratio for the steel bottom chord,  $\rho_s$  and the reinforcement ratio for the tendon,  $\rho_{ps}$ :

$$\rho_{total} = \rho_s + \rho_{ps}$$

$$\rho_{total} = \left( \frac{A_s}{b \cdot d} \right) + \eta \left( \frac{A_{ps}}{b \cdot d} \right) \quad (2.42)$$

$$\eta = \frac{F_{py}}{F_y}$$

where  $\eta$  is the yield strength ratio calculated from the ratio between the yield strength of the tendon to the yield strength of the bottom chord.

The bottom chord of the truss is in compression from the prestressing force at the time of the posttensioning. The failure modes that govern the behavior of the structure are: (1) buckling of the bottom chord of the truss, and: (2) compressive yielding of the bottom chord of the truss providing lateral supports are adequate. If the structure is strong enough for the buckling and the compressive yielding of the bottom chord, then the next mode of failure is the tensile yielding of the bottom chord. Figure 4.19 shows the effect of the percentage of tendon reinforcement on the ultimate load for various modes of failure.

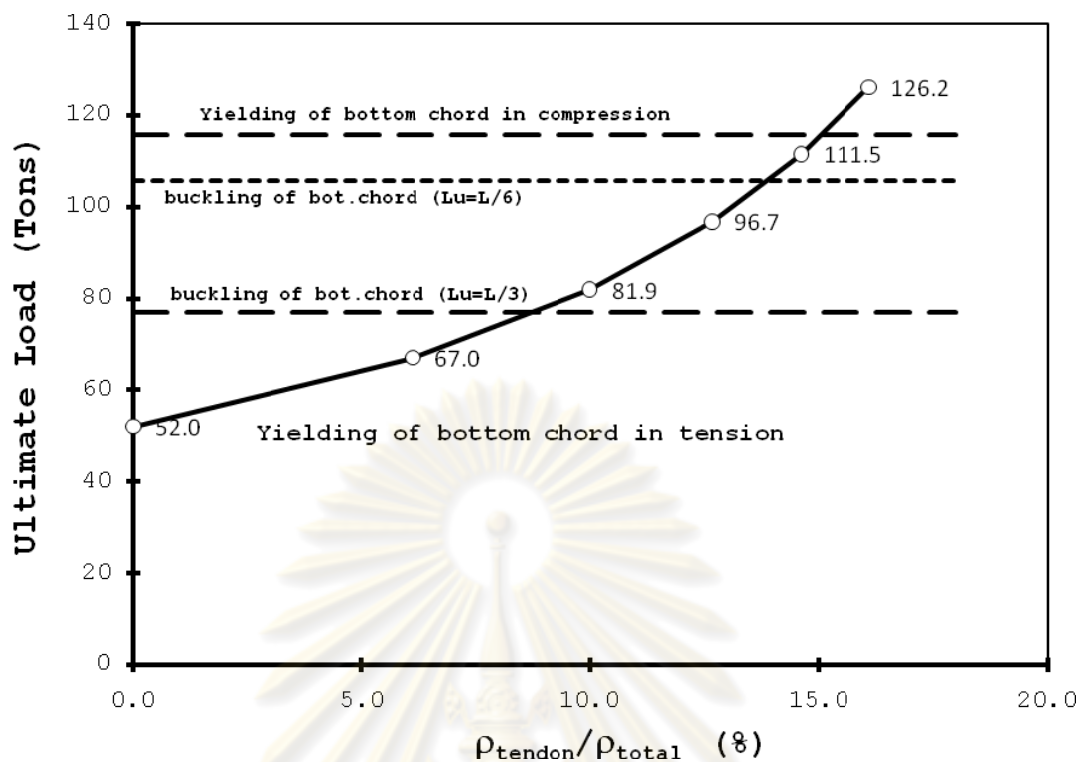


Figure 4.19 Effect of percentage of tendon on ultimate load

From the above figure, the prestressing force shows a significant effect on the ultimate load of the structure. The higher stress level of the tendon reinforcement improves the ultimate load capacity, but on the other hand the higher levels of the tendon reinforcement can cause buckling failure of the truss bottom chord. The lateral bracing is an important concern when the percentage of the tendon reinforcement is increased. As shown in the above figure, lateral bracing was provided at four locations, namely: at each of the two supports, and at  $L/3$  and  $2L/3$  from either support of the truss. The maximum percentage of tendon reinforcement was approximately 9%. If the number of the lateral brace points is increased to five locations, namely: at each of the two supports, and at  $L/3$ ,  $L/2$ , and  $2L/3$  where  $L$  is the length of the truss between end supports, the maximum percentage of the tendon reinforcement increases to 14%. If the bottom chord is continuously braced against buckling, the percentage of the tendon reinforcement can be increased to 15% approximately. Similar observations are also valid when the buckling of other truss elements is concerned.

#### 4.4.2 Effect of Percentage of Tendon Reinforcement to the Rotation Capacity

The effect of the prestressing tendon on the rotation capacity behavior of a posttensioned composite truss is also studied in this research. In order to study this effect, variations of the amount of the  $\rho_{total}$  are plotted against the rotation capacity as shown in Figure 4.20;

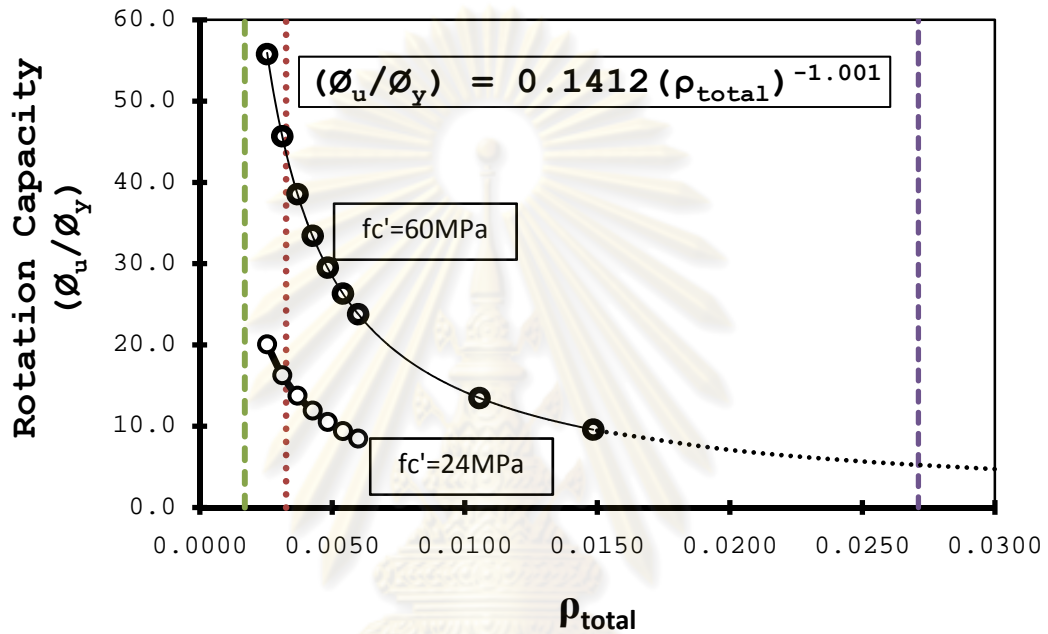


Figure 4.20 Effect of the total percentage of tendon on rotation capacity

From Figure 4.20, the relation between the total percentage of tendon  $\rho_{total}$  to the rotation capacity is  $(\phi_u/\phi_y) = 0.1412(\rho_{total})^{-1.001}$  for the concrete strength of 60MPa. This relation can be utilized to find the rotation capacity of the post-tensioned composite truss for the design purpose. Please be noted that in order to find the rotation capacity of the post-tensioned composite truss with the unbonded tendon attached, the strain compatibility are not applicable since the tendon strain are not follow the assumption of plane section remains plain for the loaded configuration. The method of trial and error is the only approach for the solution. By given the top surface concrete strain equals to the crushing strain and the tensile stress in the bottom chord and the tendon reach yield points, the trial and error of the neutral axis that produce the summation of the concrete compressive force equals to the total tensile force in the

bottom chord and tendon. The curvature at the ultimate stage then can be calculated from the top concrete strain divided by the distance from the top surface to the neutral axis.

The two dotted line shown in Figure 4.20 are the limitation from ACI318-05 code of practice for the minimum reinforcement. The less limitation comes from the minimum reinforcement ratio of 0.0017 for the reinforce concrete slab while the higher limitation comes from the minimum reinforcement ratio of  $14/f_y$  for the flexural member.

The another relation of the partial prestressing ratio, P.P.R. or the ratio of  $\rho_{tendon} / \rho_{total}$  are also plotted against the rotation capacity as shown in Figure 4.21.

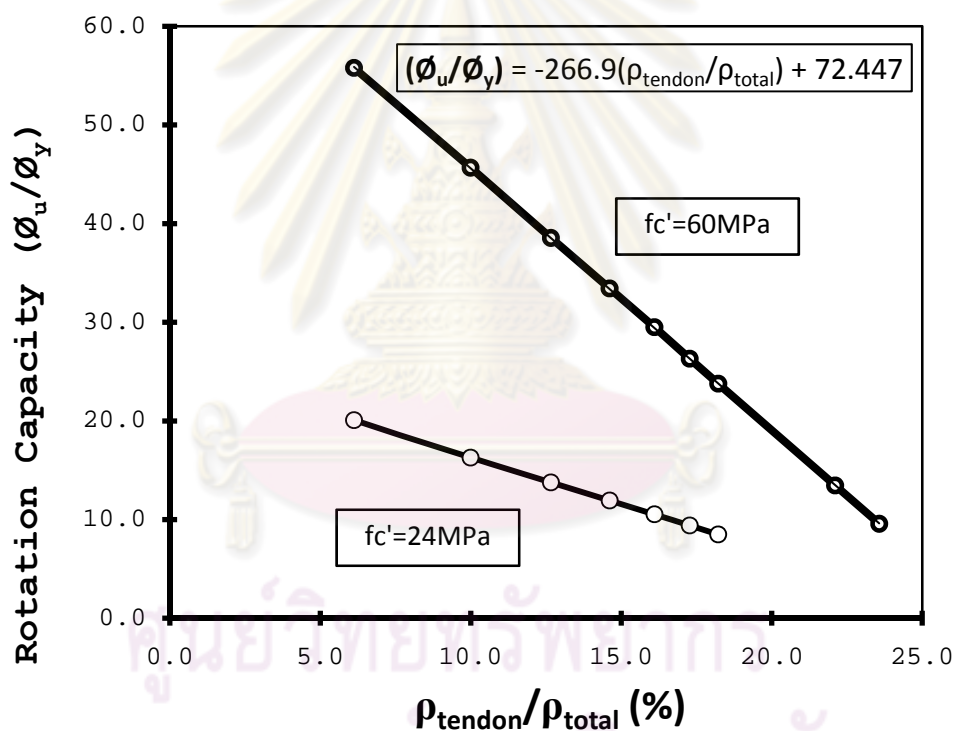


Figure 4.21 Effect of partial prestress ratio percentage of tendon on rotation capacity

From Figure 4.22, the relation between the total percentage of tendon  $\rho_{total}$  to the rotation capacity is  $(\phi_u/\phi_y) = -266.9(\rho_{tendon}/\rho_{total}) + 72.447$  for the concrete strength of 60MPa. This relation can be utilized to find the maximum percentage of tendon that can be applied to the post-tensioned composite truss when the required rotation capacity is known.

#### 4.4.3 Effect of Percentage of Tendon Reinforcement to Cracking of Concrete Top Surface

The prestressing force applied to the composite truss section produces direct compression and flexural tension stress in the concrete composite slab at the top surface. . The combined stress may be computed as;

$$\sigma_{conc,top} = \left( \frac{1}{n} \right) \left( -\frac{P}{A_t} + \frac{M_{ps} \cdot y_{N.A.}}{I_t} \right) \quad (4.5)$$

If the prestressing force reaches a value of P which produces a combined stress at the top surface of the concrete slab equal to the modulus of rupture,  $f_r$ , the concrete surface begins to crack from the high tensile stress. Substituting  $\sigma_{conc,top} = f_r$  in the above equation and solving for  $P_{max}$  results in;

$$f_r \cdot n = \left( P \right) \left( + \frac{e \cdot y_{N.A.}}{I_{transf}} - \frac{1}{A_{transf}} \right)$$

$$P_{max} = \frac{f_r \cdot n}{\left( + \frac{e \cdot y_{N.A.}}{I_t} - \frac{1}{A_t} \right)} \quad (4.6)$$

$P_{max}$  defines the maximum prestressing force that causes the top surface of the concrete slab to begin cracking and should be avoided. Substituting the values of  $f_r$ ,  $n$ ,  $e$ ,  $y_{N.A.}$ ,  $A_t$  and  $I_t$  to find the maximum prestressing force yields a specific value of;

$$P_{max} = \frac{2\sqrt{600} \cdot (5.475)}{\left( + \frac{59.75 \cdot (10.25)}{103648} - \frac{1}{386.5} \right)} = 80,759 \text{ kg}$$

This corresponds to a maximum permissible jacking stress of  $(0.8)(0.9)(f_{pu}) = 12,659 \text{ ksc}$ . This is the maximum prestressing tendon stress that results in  $F_{ps,max}$ . At this maximum jacking stress, the tendon area is  $(80,759)/(12,659) = 6.38 \text{ cm}^2$  which corresponds to approximately 6 of 12.7mm diameter Grade250 strands.

#### 4.4.4 Effect of Percentage of Tendon Reinforcement to the Effective Moment of Inertia of the Composite Truss

For a simply supported beam subjected to point loads  $P$  at  $L/3$  and  $2L/3$ , where  $L$  is the total span length of the beam the vertical mid-span deflection is:

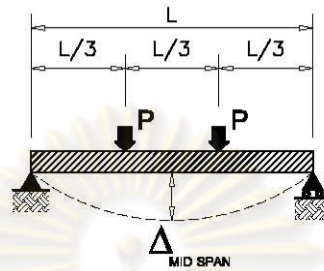


Figure 4.22 Midspan deflection of an SSB with third point loads,  $P$

$$\Delta_{midspan} = \frac{2P \cdot b}{48EI} (3L^2 - 4b^2) \quad (4.7)$$

Setting  $b$  equal to  $L/3$  the deflection becomes;

$$\Delta_{midspan} = \frac{2P \cdot \left(\frac{L}{3}\right)}{48EI} \left(3L^2 - 4\left(\frac{L}{3}\right)^2\right) \quad (4.8)$$

$$\Delta_{midspan} = \frac{23PL^3}{648EI}$$

Substituting the composite truss total span length,  $L$ , equal to 853.4cm,  $E$  of transformed section equal to  $2.04 \times 10^6$  kg/sq.cm,  $P$  equal to  $P/2$  and rearranging the variables gives:

$$\frac{P}{\Delta_{midspan}} = \frac{1296}{23L^3} EI = 0.185 \cdot I \quad (4.9)$$

The ratio of  $P/\Delta_{midspan}$  is the slope of the load vs. mid-span deflection curve. Let  $I_{eff}$  be the effective moment of inertia of the post-tensioned composite section including the effect of the truss as determined from the slope of the experimental curve. The calculation below results in a value,  $\zeta$  which is the ratio of  $I_{eff}$  to the moment of inertia of the transformed section,  $I_t$ . Thus:



$$\frac{P}{\Delta_{midspan}} = 0.185 \cdot I_{eff}$$

$$I_{eff} = \frac{P}{0.185 \cdot (\Delta_{midspan})} = \frac{\text{Slope of Load - Deflection Curve}}{0.185}$$

$$\zeta = \left( \frac{I_{eff}}{I_t} \right) \quad (4.10)$$

Experimental values for the slopes of the load vs. deflection curves for Specimens A1, A2, and A3 corresponding to jacking stresses of 460MPa, 690MPa and 920MPa, respectively, are readily determined. A graph of the relative prestressing ratio ( $A_{ps}F_{ps} / A_sF_y$ ) vs. the ratio of the  $I_{eff}$  to  $I_t$  may be plotted and extrapolated up to a value of  $\zeta = 1.0$ .

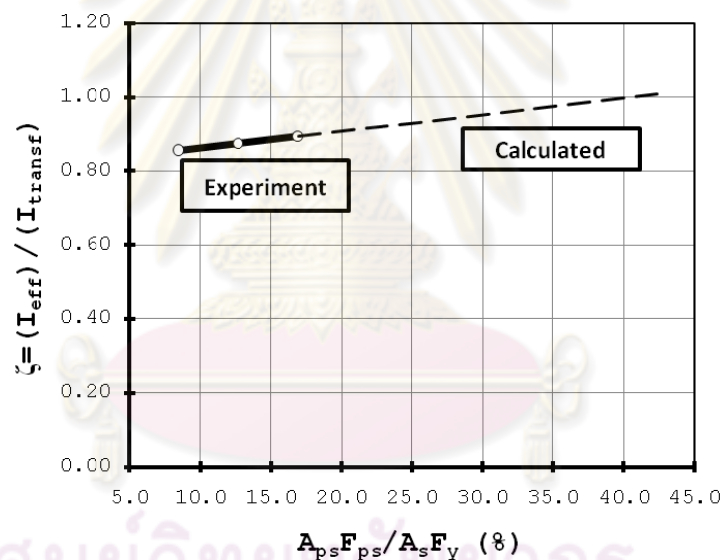


Figure 4.23  $I_{eff} / I_t$  vs. relative prestressing ratio

Interpolation of the above graph, for more relative prestressing ratios of ( $A_{ps}f_{ps} / A_s f_y$ ) up to 40%, and a ratio of  $\zeta = 1.0$  may be obtained. That means that the calculated transformed moment of inertia of the composite truss section can be represented as a constant moment of inertia of the overall structure and can be used in the deflection calculation without any reduction factor. The relationship between the percentage of the relative prestressing ratio ( $A_{ps}f_{ps} / A_s f_y$ ) and the reduction factor for the calculated transformed moment of inertia is;

$$R_{I,eff} = 0.0044 \left( \frac{A_{ps} f_{ps}}{A_s f_y} \right) + 0.826 \quad (4.11)$$

Thus, the effective moment of inertia is the transformed moment of inertia times reduction factor  $R_{I,eff}$  as in the equation below,

$$I_{eff} = R_{I,eff} \cdot I_t \quad (4.12)$$

In conclusion, the appropriate prestressing force improves the linearity of the load and deflection relation of the posttensioned composite truss. The effective moment of inertia can be used for more accurate deflection calculations.

## 4.5 Effects of Shrinkage, Creep, Anchorage Seating and Relaxation

### 4.5.1 Analysis of Shrinkage Effect

Shrinkage causes tensile strain to develop inside the concrete slab. If the shrinkage is permitted to occur freely without any restraint a free shrinkage strain,  $\epsilon_f$ , develops. For the composite truss, shrinkage in the concrete slab is restrained by the steel truss and the tensile strain in the concrete is less than the shrinkage strain. This results in the restrained shrinkage strain,  $\epsilon_r$ . The actual tensile strain in the concrete slab is the slab strain,  $\epsilon_s$ , which is equal to the difference between free shrinkage strain,  $\epsilon_f$ , and the restrained shrinkage strain,  $\epsilon_r$ . These strains can be illustrated as shown in the strain diagram of the composite truss in Figure 4.20.

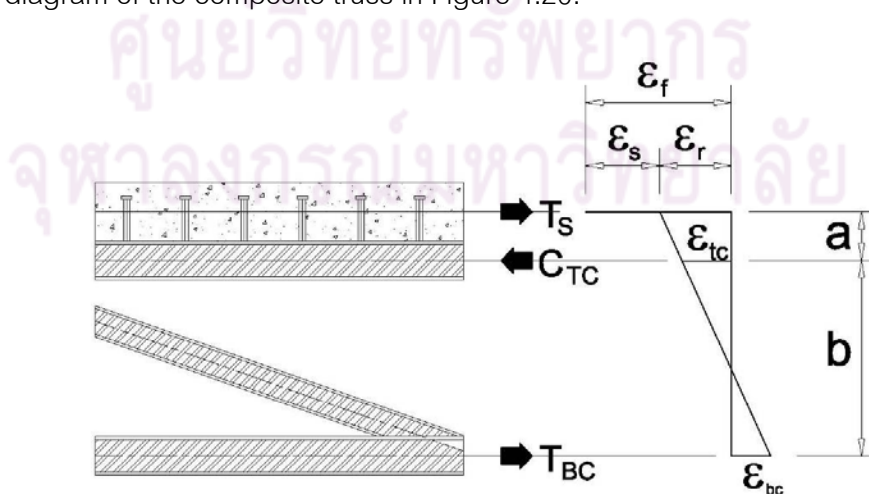


Figure 4.24 Shrinkage strain diagram

$$\begin{aligned}
\varepsilon_{tc} EA_{tc} - \varepsilon_{bc} EA_{bc} &= (\varepsilon_f - \varepsilon_r) E_c A_c \\
\varepsilon_{bc} EA_{bc} &= \left(\frac{a}{b}\right) (\varepsilon_f - \varepsilon_r) A_c E_c \\
\left(\frac{a+b}{b}\right) \varepsilon_{tc} + \left(\frac{a}{b}\right) \varepsilon_{bc} &= \varepsilon_r
\end{aligned} \tag{2.54}$$

The above three equations may be solved for the restrained strain,  $\varepsilon_r$ , the strain in the bottom chord,  $\varepsilon_{bc}$  and the strain in the top chord member,  $\varepsilon_{tc}$ .

The deflection due to shrinkage,  $\Delta_{sh}$ , is calculated from;

$$\begin{aligned}
\Delta_{SH} &= \frac{ML^2}{8EI_t} \\
M &= (\varepsilon_r E_c A_c)(e)
\end{aligned} \tag{2.55}$$

Shrinkage moments cause the prestressing tendons to be shortened which leads to a decrease in tendon force,  $\Delta P_{sh}$ . This decrease causes the truss to deflect downward. In order to find the decrease in tendon force from shrinkage,  $\Delta P_{sh}$ , the total elongation at the same level of the tendon due to the shrinkage moment,  $\delta_{1p}$ , and the total elongation at the same level of the tendon due to the unit prestressing force,  $\delta_{11}$  are determined and  $\Delta P_{sh}$  equals  $\delta_{1p}/\delta_{11}$ . The relevant results for a number of values are shown in Table 4.4, Table 4.5, Figures 4.23 and 4.24.

ศูนย์วิทยทรัพยากร  
จุฬาลงกรณ์มหาวิทยาลัย

Table 4.4 the free and restrain shrinkage calculation

a (cm)	b (cm)	$A_c$ (cm <sup>2</sup> )	$A_{bc}$ (cm <sup>2</sup> )	$A_{tc}$ (cm <sup>2</sup> )	$\epsilon_f$	$\epsilon_r$	$\epsilon_{bc}$	$\epsilon_{tc}$
12.5	50	2700	24.8	24.8	0.000100	0.000097	0.000015	0.000075
12.5	50	2700	24.8	24.8	0.000200	0.000194	0.000030	0.000149
12.5	50	2700	24.8	24.8	0.000300	0.000291	0.000045	0.000224
12.5	50	2700	24.8	24.8	0.000400	0.000388	0.000060	0.000298
12.5	50	2700	24.8	24.8	0.000500	0.000485	0.000075	0.000373
12.5	50	2700	24.8	24.8	0.000600	0.000582	0.000090	0.000448
12.5	50	2700	4.8	4.8	.000700	.000679	.000104	.000522
2.5	0	700	4.8	4.8	.000800	.000776	.000119	.000597
2.5	0	700	4.8	4.8	.000900	.000873	.000134	.000672
2.5	0	700	4.8	4.8	.001000	0.000970	0.000149	0.000746

Table 4.5 Free shrinkage strain and shrinkage deflection

$\epsilon_f$	$\Delta_{shrinkage}$ (mm)	$\Delta_{\Delta T}$ (mm)	$\Delta_{total}$ (mm)
0.000100	1.16	0.01	1.16
0.000200	2.31	0.01	2.33
0.000300	3.47	0.02	3.49
0.000400	4.62	0.03	4.65
0.000500	5.78	0.04	5.81
0.000600	6.93	0.04	6.98
0.000700	8.09	0.05	8.14
0.000800	9.24	0.06	9.30
0.000900	10.40	0.07	10.46
0.001000	11.55	0.07	11.63

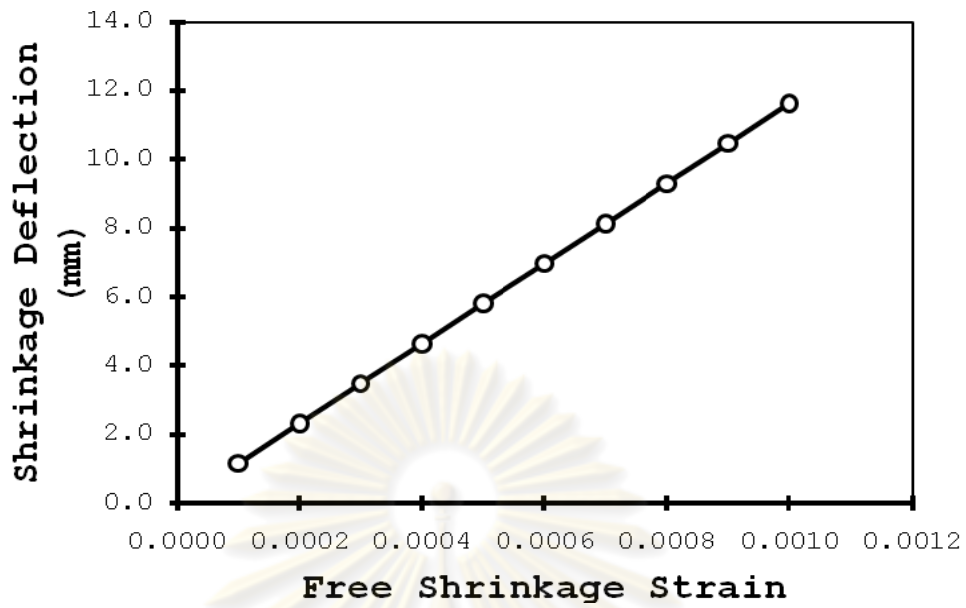


Figure 4.25 The free shrinkage strains and shrinkage deflections

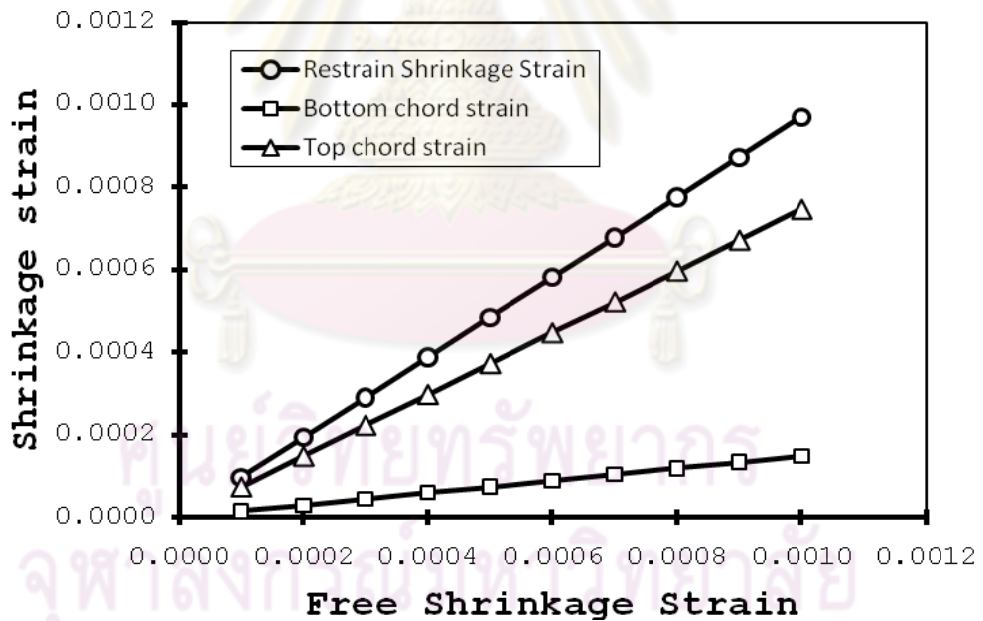


Figure 4.26 The free shrinkage strains and strains in members

From the shrinkage deflection and the free shrinkage strain relationship, if the free shrinkage strain is known, the deflection of the posttensioned composite truss can be determined. Free shrinkage behaves time dependently. Normally the free shrinkage is approximately 80% of the total shrinkage strain in the first year. The

modifying factors for volume-to-surface ration (V/S) and relative humidity (RH) are related as follows:

$$\varepsilon_f = 8.2 \times 10^{-6} \left( 1 - 0.06 \left( \frac{V}{S} \right) \right) (100 - RH) \quad (4.13)$$

In the case where the slab volume is  $2.304\text{m}^3$  and the surface area is  $33.823\text{m}^2$  the volume to surface ratio equals 0.0681. For a relative humidity of 70%, the free shrinkage strain is approximately 0.00025. The shrinkage deflection is 2.9mm downward. For more accurate behavior, the local shrinkage model or the actual measurement from the test specimens for the free shrinkage strain are preferred to predict the shrinkage deflection.

#### 4.5.2 Analysis of Creep Effect

For the posttensioned composite truss, the concrete slab was cast on top of the steel truss. Hence, the dead load of the steel truss and the dead load of the concrete slab are carried by the steel truss only. There is no creep behavior from the dead load of the steel truss and the dead load of the concrete.

The only constant compressive force inside the concrete slab comes from the prestressing force. This prestressing force in the concrete slab starts at the end anchorage points up to the second panel from the supports.

By the calculation procedure explained in chapter 2, the plot of creep coefficient,  $\phi(t, t_0)$ , vs. the creep deflection,  $\Delta_{CR}$  is given in Figure 4.25.

จุฬาลงกรณ์มหาวิทยาลัย

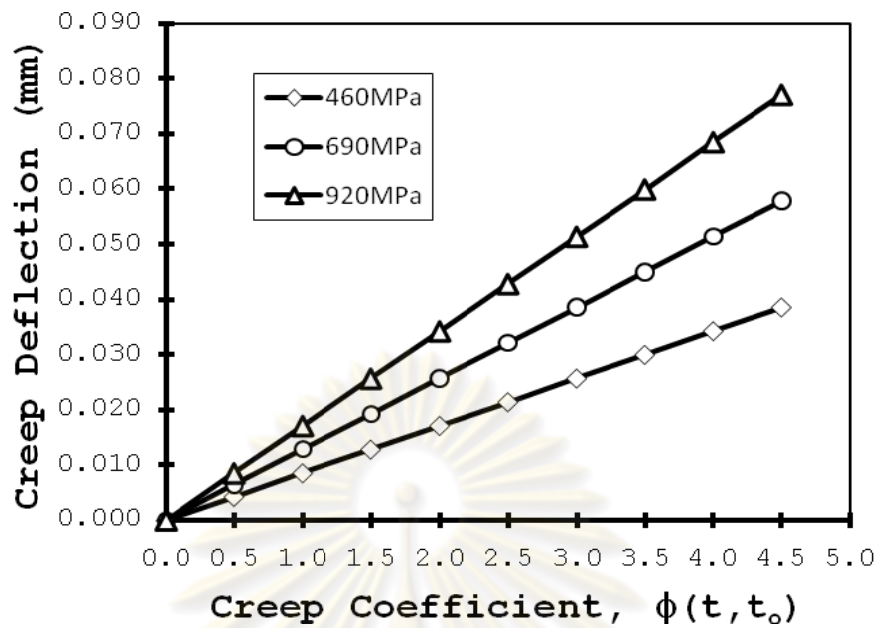


Figure 4.27 Creep deflection-creep coefficient curves

The above figure shows the relation between the creep coefficient and the creep deflection for the prestressing level of 460MPa, 690MPa and 920MPa. The higher prestressing force causes larger creep deflection due to the higher net stress inside the concrete slab. Normally at a lower level of accuracy, for an effective thickness of 6 in in dry atmosphere, the creep coefficient at 70 years of loading is 2.1 which results in a creep deflection of 0.018mm, 0.027mm and 0.036mm for prestressing levels of 460MPa, 690MPa and 920MPa, respectively.

This creep deflection is relatively low compared to the yield deflection and the ultimate deflection due to the low level of the remaining stress inside the concrete slab. However, the creep deflection is dependent on the creep coefficient. If the creep coefficient is more accurately determined the more accurate will be the creep deflection.

### 4.5.3 Anchorage Seating Effect

For the post-tensioned composite truss, the anchorage seating loss is distributed uniformly over the entire length of the tendon between the two anchorage points because of the unbonded posttensioning property.

$$\Delta f_{anch} = \frac{\Delta}{L_T} E_{tendon} \quad (2.60)$$

where  $\Delta$  is the anchorage movement,  $L_T$  is the total length of the tendon between two anchorage points and  $E_{tendon}$  is the elastic modulus of the tendon.

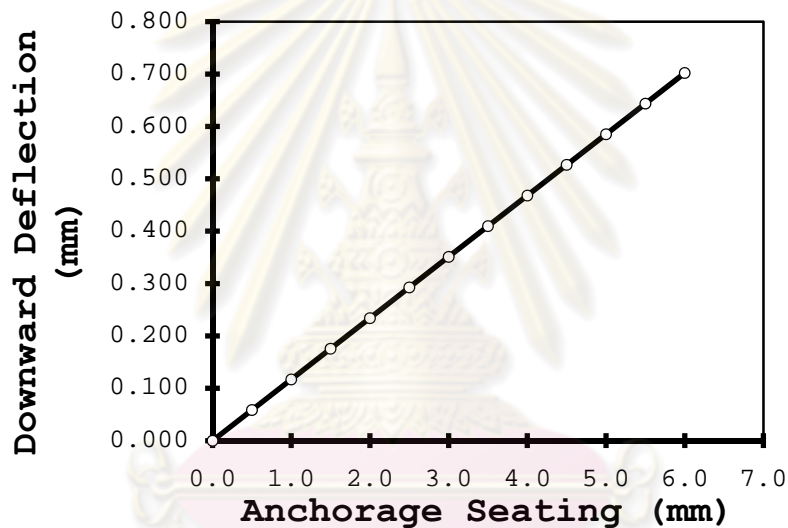


Figure 4.28 Downward Deflection vs. Anchorage Seating

From Figure 4.26, the anchorage seating reduces the level of prestressing force resulting in increased deflection. Normally for the wedge type anchorage the average anchorage seating is approximately 2-3mm. If the anchorage seating is 2.5mm the downward deflection at mid span is 0.3mm which is very low compared to the yield deflection and the ultimate deflection.



#### 4.5.4 Analysis of Relaxation Effect

For the posttensioned composite truss, the prestress tendon is unbonded. Thus, the relaxation of the prestressing tendon occurs uniformly over the entire length of the tendon.

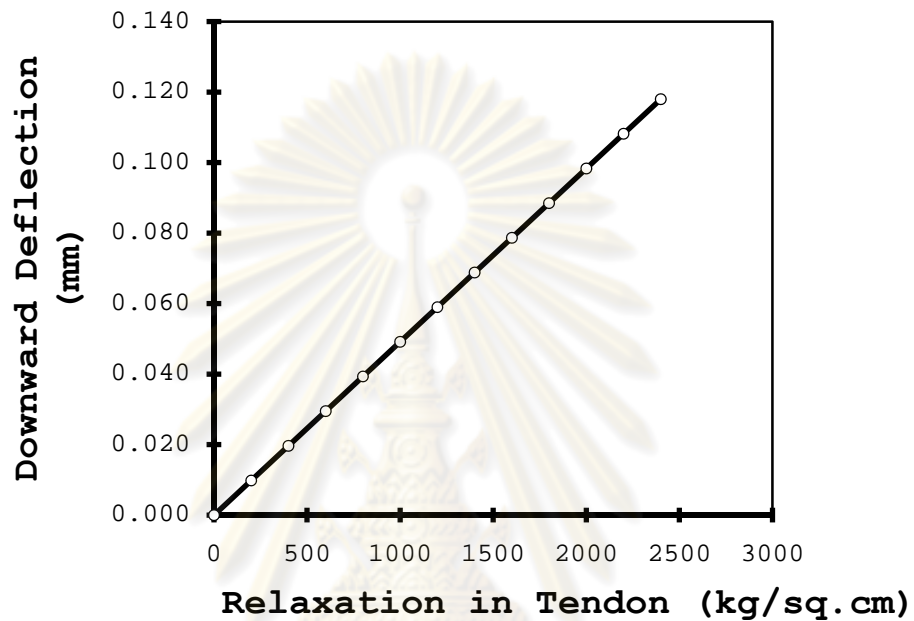


Figure 4.29 Downward deflection - relaxation in tendon curve.

Figure 4.27 shows the relation between the relaxation in the tendon and the downward deflection. The relaxation causes the truss to deflect downward due to the decrease in tendon force and as a result the precamber amount is decreased acc. causes the concrete and vertical members to be less highly compressed while the tension stress in the bottom chord and diagonal members experience a reduced tension stress.  $I_{\text{eff}}$

## CHAPTER 5

### STRUCTURAL MODEL

#### 5.1 Strength and Stability

##### 5.1.1 Flexural Strength

###### 5.1.1.1 Ultimate Moment Capacity

The ultimate moment capacity of a posttensioned composite truss can be computed as:

$$M_u = F_{\max} \left( h - \frac{a}{2} \right) \quad (2.37)$$

$$F_{\max} = \min \left[ \left( A_s \cdot f_y + A_{ps} \cdot f_{ps,\max} \right), \sum Q_u, 0.85 f_c' b t_c \right]$$

where  $F_{\max}$  is the maximum combined tensile force in the bottom chord and the tendon with the following limits: (1) the sum of the yielding force in the bottom chord and the tensile force in the tendon; (2) the forces in the shear stud connectors at maximum strength summed from the point of maximum moment to the point of zero moment along the length; (3) the maximum compressive strength that can be developed in the concrete slab of width  $b$  and thickness  $t$ . In Equation 2.37,  $h$  is the distance from the top surface of the concrete slab to the centroid of the resultant of the bottom chord and tendon forces;  $a$  is the depth of the concrete stress block at ultimate determined as follows;

$$a = \frac{F_{\max}}{0.85 f_c' b} \quad (2.18)$$

The tendon stress,  $f_{ps,\max}$ , can have one of the following three possible values: (1) the tendon stress at the time the bottom chord starting to yield from the external applied load,  $f_{ps,\text{yield}}$ ; (2) the yield strength of the tendon itself,  $f_{py}$ , or: (3) the tensile strength of the tendon,  $f_{pu}$ .

Based on analytical and experimental considerations for the current research as presented herein, these three values are different by an amount of less than 5% because of the relatively low percentage of reinforcement. For the conservative case, the appropriate value for  $f_{ps,max}$  corresponds to the tendon stress at yield,  $f_{ps,yield}$  as can be computed from:

$$f_{ps,max} = f_{ps,yield} = f_{pi} + \left( \frac{\Delta P}{A_{ps}} \right)$$

$$\Delta P = \frac{\left[ \sum_{i=1}^n (\delta F_{1,i}) \left( \frac{F_{1,si} \cdot L_i}{A_i E_i} \right) \right]}{\left[ \sum_{i=1}^n (\delta F_{2,i}) \left( \frac{F_{2,si} \cdot L_i}{A_i E_i} \right) + \sum_{j=1}^m (\delta F_{2,j}) \left( \frac{F_{2,sj} \cdot L_{Tj}}{A_{Tj} E_{Tj}} \right) \right]} \quad (5.1)$$

where  $f_{pi}$  is the initial tendon stress,  $\Delta P$  is the increase in tendon force at the beginning of yield of the bottom chord;  $\delta F_{1,i}$  is the virtual force in member  $i$  resulting from a unit virtual force acting on the composite truss at the same location as the tendon;  $F_{1,si}$  is the actual force in member  $i$  due to the external load that causes the bottom chord to begin yielding;  $L_i$ ,  $A_i$  and  $E_i$  are the length, cross sectional area, and modulus of elasticity of member  $i$ , respectively.  $\delta F_{2,i}$  is the virtual force in member  $i$  resulting from a unit virtual force acting on the composite truss at the same location as the tendon;  $F_{2,si}$  is the actual force in member  $i$  due to a unit force acting on the composite truss at the same location as the tendon.  $\delta F_{2,j}$  is the virtual force in tendon  $j$  resulting from a unit virtual force acting on the composite truss at the same location as the tendon;  $F_{2,sj}$  is the actual force in member  $j$  due to a unit force acting on the composite truss at the same location as the tendon;  $L_{Tj}$ ,  $A_{Tj}$  and  $E_{Tj}$  are the length, cross sectional area, and the modulus of elasticity of tendon  $j$ , respectively;  $n$  is the number of members and  $m$  is the number of the tendons;  $A_{ps}$  is the cross sectional area of the tendon and  $f_{pi}$  is the initial prestressing stress in the tendon.

### 5.1.1.2 Ultimate Shear Capacity

The ultimate shear capacity of the post-tensioned composite truss depends on the tensile strength of critical web members in tension and the buckling strength of critical web members in compression. The following expression applies:

$$\sigma_{Diagonal} = \frac{\left(\frac{5}{2}wa + wb\right)}{A_{Diagonal}} + \frac{\left(\frac{-P \sin \theta}{\sin \alpha}\right)}{A_{Diagonal}} + \frac{\left(\frac{P_{ext}}{\sin \alpha}\right)}{A_{Diagonal}} + \frac{\left(\frac{-\Delta P \sin \theta}{\sin \alpha}\right)}{A_{Diagonal}} \leq f_y$$

$$\sigma_{Vertical} = \frac{-(3wa + wb)}{A_{Vertical}} + \frac{(-P_{ext})}{A_{Vertical}} \leq f_y, f_{buckling} \quad (5.2)$$

where  $\sigma_{Diagonal}$  and  $\sigma_{Vertical}$  are the stresses in a critical diagonal member and a critical vertical member, respectively;  $A_{Diagonal}$  and  $A_{Vertical}$  are the cross sectional area of the diagonal member and the vertical member, respectively;  $w$  is the uniform dead load resulting from steel truss and concrete slab weights;  $a$  and  $b$  depend on the panel lengths of the truss;  $\alpha$  is the angle between the horizontal and the diagonal member;  $P$  is the tendon force;  $\theta$  is the angle between a horizontal member and the tendon;  $\Delta P$  is the increase in tendon force from the external load,  $P_{ext}$ , and  $f_y$  is the yield strength of the diagonal member.

### 5.1.1.3 Ultimate Shear Stud Connector Capacity

The ultimate shear stud connector capacity is based on consideration of three possible failure modes, concrete crushing, tensile rupture, and shear failure. The minimum strength resulting from these three modes is the maximum ultimate shear stud connector capacity;

For the concrete crushing mode;

$$Q_u = 0.5 \cdot A_s \cdot \sqrt{f_c' \cdot E_c} \quad (2.10)$$

where  $A_s$  is the cross sectional area of a shear stud connector,  $f'_c$  is the cylindrical concrete compressive strength, and  $E_c$  is the modulus of elasticity of the concrete material.

For the tensile rupture mode;

$$Q_u = A_s f_u \quad (5.3)$$

For direct shear at the base of the stud;

$$Q_u = 0.67 A_s f_y \quad (5.4)$$

where  $f_u$  and  $f_y$  are the tensile strength and the yield strength of the shear stud connector, respectively. The dimensions of the shear stud and the base material thickness affect the shear stud strength. The ratio of the stud diameter to the base material thickness,  $\tau$ , shall not exceed 4.0. If  $\tau$  exceeds 2.5, the stud strength shall be multiplied by a reduction factor,  $R_f$ , given by;

$$R_f = 2.67 - 0.67\tau \leq 1.0 \quad (2.14)$$

Studs shall not be placed closer than the height of the stud to the edge of the concrete slab otherwise it may exhibit a reduction in strength. Moreover, a uniform distribution of shear studs along the top chord is applicable for shear studs of length greater than 4 times it's the stud diameter. Such slender studs tend to deform and yield in an s- shape. The resulting flexibility leads to redistribution of the shear stress in all of the studs distributed along the point of the maximum moment to the zero moment and tends to be independent of the shape of the shear force diagram along the span length. The spacing should not be less than six times the stud shank diameter and should not be more than eight times the slab thickness. The stud head size should be at least 1.5 times the stud shank diameter. The stud head thickness should be at least half of the stud shank diameter. Concrete covering of at least 25mm should be provided all around the shear stud connector.

## 5.1.2 Maximum Tendon Capacity

### 5.1.2.1 Yielding of Bottom Chord

The tendon prestressing force causes a compressive stress in the bottom chord or at least a tendency to reduce any tension in that chord. If lateral bracing is adequate, the bottom chord stress may reach the yield level. The criteria of yielding of the bottom chord can be written as;

$$\sigma_{x(\text{bottom chord})} = -\frac{F(x)}{A_t(x)} - \frac{F(x) \cdot e(x) \cdot y_b(x)}{I_t} + \frac{M_{DL}(x) \cdot y_b(x)}{I_t} \leq f_y \quad (5.5)$$

where the transformed moment of inertia of the composite section can be computed from  $I_t = \sum (I_i + A_i d^2)$  and the transformed cross sectional area is calculated from  $A_t = \frac{b_c \cdot t_c}{n} + \sum A_s$

### 5.1.2.2 Yielding of Web Members

The tendon prestressing force induces tension in some web members and compression in other members. . If the lateral bracing is sufficient, the web member stress can reach the compressive yield strength and the criteria of yielding of the web member can be written as;

$$\sigma_{Diagonal} = \frac{\left( \frac{5}{2} wa + wb \right) + \left( \frac{-P \sin \theta}{\sin \alpha} \right)}{A_{Diagonal}} \leq f_y \quad (5.6)$$

where  $\sigma_{Diagonal}$  is the stress in a diagonal member,  $A_{Diagonal}$  is the cross sectional area of the member,  $w$  is the uniform dead weight from the truss and concrete slab;  $a$  and  $b$  depend on the panel dimensions at the member in question;  $\alpha$  is the angle between the horizontal member and the diagonal member;  $P$  is the tendon force;  $\theta$  is the angle between the horizontal member and the tendon and;  $f_y$  is the yield strength of the member.

### 5.1.2.3 Cracking at Concrete Tension Surface

The stress in the tension zone at the concrete surface due to the prestressing force is;

$$\sigma_{conc,top} = \left( \frac{1}{n} \right) \left( -\frac{P}{A_t} + \frac{M_{ps} \cdot y_{N.A.}}{I_t} \right) \quad (4.5)$$

where  $n$  is the ratio of the elastic modulus of steel to that of concrete,  $M$  is the moment from the prestressing tendon,  $e$  is the eccentricity of the tendon force with respect to the centroid of the transformed composite section, and  $y_t$  is the distance from the top surface concrete to the centroid of the transformed section.

To prevent the concrete from cracking, the maximum tensile stress must be less than the concrete modulus of rupture strength,  $f_r$ , which equals to  $2\sqrt{f'_c}$ . The maximum prestressing force to prevent the concrete top surface from cracking is computed from;

$$P_{max} = \frac{f_r \cdot n}{\left( +\frac{e \cdot y_{N.A.}}{I_t} - \frac{1}{A_t} \right)} \quad (4.6)$$

### 5.1.2.4 Buckling of Bottom Chord

In the absence of intermediate lateral bracing it is possible for a bottom chord compression member to buckle. Considering the possibility of buckling the upper limit of prestressing force, above which buckling may occur, is calculated from;

$$P_{max} = \frac{3 \cdot E_w \cdot I_w}{d_w^3} \left( \frac{L_u}{4} \right) \quad (5.7)$$

where  $E_w$ ,  $I_w$  and  $d_w$  are the elastic modulus, the moment of inertia and the member length respectively, of the compression member in question and  $L_u$  is the unbraced length of the compression chord between two adjacent vertical members.

### 5.1.2.5 Buckling of Web Members

Tendon prestressing forces may result in compression of certain web members. If the lateral bracing is inadequate, the web member may fail in a buckling mode and the stress criteria of buckling for either a diagonal web member or a vertical web member can be written as;

$$\sigma_{Diagonal} = \frac{\left( \frac{5}{2} \frac{wa + wb}{\sin \alpha} \right)}{A_{Diagonal}} + \frac{\left( -\frac{P \sin \theta}{\sin \alpha} \right)}{A_{Diagonal}} \leq f_{buckling}$$

$$\sigma_{Vertical} = \frac{-(3wa + wb)}{A_{Vertical}} + \frac{(-P_{ext})}{A_{Vertical}} \leq f_{buckling} \quad (5.8)$$

### 5.1.2.6 Top Chord Local and Overall Buckling

During the concrete casting procedure, the dead load of the steel truss and the dead load of the concrete results in compressive stress in the steel truss top chord and its possibility to fail in a buckling mode. The local buckling criterion for the top chord member is;

$$\sigma_{topchord} = \frac{\left( \frac{9}{2} \frac{wa + 3wb}{\tan \alpha} - \frac{1}{2} \frac{wb}{\tan \beta} \right)}{A_{topchord}} \leq f_{buckling} \quad (5.9)$$

In case there is inadequate lateral bracing for the steel truss, the overall buckling moment  $M_{x,cr}$  is calculated from;

$$M_{x,cr}^2 = C_b^2 \left( \frac{\pi^4}{(KL)^4} EI_y EC_w + \frac{\pi^2}{(KL)^2} EI_y GJ \right)$$

$$I_{y,truss} = 2I_{y,chord}$$

$$C_{w,truss} = \frac{d^2}{4} (I_{y,truss}) \quad (4.4)$$

$$J_{truss} = \frac{1}{3} \sum bt^3$$



For a simply supported span with two point loads, the value for  $C_b$  and  $K$  are 1.04 and 1.00, respectively. For  $C_{w, \text{truss}}$ , the value of 'd' is the distance between the top chord and the bottom chord.

#### 5.1.2.7 Tendon Strength

The total tendon internal force from the summation of the initial prestressing force,  $P$ , and the increase in tendon force,  $\Delta P$ , must remain less than or equal to the yield strength of the tendon material  $A_s$  defined by:

$$\frac{(P + \Delta P)}{A_{ps}} < f_{py} \quad (5.10)$$

#### 5.1.2.8 Pre Camber Criteria

The prestressing force results in an upward deflection, or precamber,  $\Delta$ , which is limited to the permissible serviceability limit of the structure and which depends on the type of structure. The precamber criterion is:

$$\Delta = \left( \frac{1}{\delta P} \right) \sum_{i=1}^n \int_0^L \left( \frac{F_i(x) \cdot \delta F_i(x)}{E_i(x) A_i(x)} \right) dx \leq \Delta_{LIMIT} \quad (5.11)$$

where  $\delta P$  is a virtual unit load at mid-span;  $\delta F_i(x)$  is the virtual internal force due to a virtual unit load at mid span;  $F_i(x)$ ,  $E_i(x)$ ,  $A_i(x)$  are the actual force in the real structure due to the tendon load, the modulus of elasticity and the cross sectional area of member  $i$ , respectively;  $n$  is the number of members in the post tensioned composite truss.

#### 5.1.2.9 Prestress Losses

Shrinkage and creep may cause the prestressing tendons to shorten which leads to a decreases,  $\Delta P_{sh}$  and  $\Delta P_{cr}$ , in tendon force. This results in downward deflection of the truss. To find  $\Delta P_{sh}$  and  $\Delta P_{cr}$ , the total elongation at the elevation of the tendon due shrinkage or creep,  $\delta_{1p}$ , and the total elongation at the same elevation of the

tendon due to a unit prestressing force,  $\delta_{11}$  are determined and,  $\Delta P_{sh}$  or  $\Delta P_{cr}$  equals  $\delta_{1p}/\delta_{11}$ . Thus,

$$\Delta P_{sh} = \frac{\left[ \sum_{i=1}^n (\delta R_i) \left( \frac{R_{si} \cdot L_i}{A_i E_i} \right) \right]}{\left[ \sum_{i=1}^n (\delta F_i) \left( \frac{F_{si} \cdot L_i}{A_i E_i} \right) + \sum_{j=1}^m (\delta F_j) \left( \frac{F_{sj} \cdot L_{Tj}}{A_{Tj} E_{Tj}} \right) \right]} \quad (5.12)$$

where  $\Delta P_{sh}$  is the decrease in tendon force due to shrinkage,  $\delta R_i$  is the virtual force in member  $i$  from the unit virtual force acting on the composite truss at the same location as the tendon,  $R_{si}$  is the actual force in member  $i$  due to the shrinkage moment,  $L_i$ ,  $A_i$  and  $E_i$  are the length, cross sectional area and the modulus of elasticity of member  $i$ , respectively.  $\delta F_i$  is the virtual force in member  $i$  resulting from a unit virtual force acting on the composite truss at the same location as the tendon,  $F_{si}$  is the actual force in member  $i$  due to the unit force acting on the composite truss at the same location as the tendon.  $\delta F_j$  is the virtual force in tendon  $j$  resulting from a unit virtual force acting on the composite truss at the same location as the tendon,  $F_{sj}$  is the actual force in member  $j$  due to a unit force acting on the composite truss at the same location as the tendon,  $L_{Tj}$ ,  $A_{Tj}$  and  $E_{Tj}$  are the length, cross sectional area, and the modulus of elasticity of tendon  $j$ , respectively,  $n$  is the number of members and  $m$  is the number of tendons.

$$\Delta P_{cr} = \frac{\left[ \sum_{i=1}^n (\delta R_i) \left( \frac{R_{si} \cdot L_i}{A_i E_i} \right) \right]}{\left[ \sum_{i=1}^n (\delta F_i) \left( \frac{F_{si} \cdot L_i}{A_i E_i} \right) + \sum_{j=1}^m (\delta F_j) \left( \frac{F_{sj} \cdot L_{Tj}}{A_{Tj} E_{Tj}} \right) \right]} \quad (5.13)$$

where  $\Delta P_{cr}$  is the decrease in tendon force due to creep,  $\delta R_i$  is the virtual force in member  $i$  resulting from a unit virtual force acting on the composite truss at the same location as the tendon,  $R_{si}$  is the actual force in member  $i$  due to the creep moment,

For the posttensioned composite truss, the anchorage seating loss and the relaxation are distributed uniformly over the entire length of the tendon between the two anchorage points because of the unbonded posttensioning property.

The loss of stress from the anchorage seating can be calculated from the following equations;

$$\Delta f_{anch} = \frac{\Delta}{L_T} E_{tendon} \quad (2.60)$$

Where  $\Delta$  is the anchorage movement,  $L_T$  is the total length of the tendon between two anchorage points and  $E_{tendon}$  is the elastic modulus of the tendon.

The loss of stress from relaxation can be calculated from the following equations;

$$\frac{f_p}{f_{pi}} = 1 - \left( \frac{\log t - \log t_1}{10} \right) \left( \frac{f_{pi}}{f_{py}} - 0.55 \right) \quad (2.61)$$

where  $f_p$  is the tendon stress at time  $t$ ,  $f_{pi}$  is the initial tendon stress at time  $t_1$ , and  $f_{py}$  is the yield strength of the tendon.

## 5.2 Ductility

The ductility of the posttensioned composite truss can be controlled by the percentage of reinforcement, and  $\rho_{total}$  is calculated from;

$$\rho_{total} = \rho_s + \rho_{ps}$$

$$\rho_{total} = \left( \frac{A_s}{b \cdot d} \right) + \eta \left( \frac{A_{ps}}{b \cdot d} \right) \quad (2.42)$$

$$\eta = \frac{f_{py}}{f_y}$$

where  $\eta$  is the yield strength ratio calculated from the ratio between the yield strength of the tendon,  $F_{py}$  corresponding to the yield strength of the bottom chord,  $F_y$ .

The limit percentage of  $\rho_{total}$  is to be not more than the  $\rho_b$  to ensure that the structure will fail in ductile behavior from yielding of the bottom chord prior to the crushing of the concrete at the ductility ratio equals to 4 or greater. The ductility criterion can be stated as;

$$\rho_{total} = \left( \frac{A_s}{b \cdot d} \right) + \left( \frac{f_{py}}{f_y} \right) \left( \frac{A_{ps}}{b \cdot d} \right) \leq \rho_b = 0.85 \frac{f_c'}{f_y} \beta_1 \frac{\epsilon_{cu}}{\left( \frac{f_y}{E} - \epsilon_{cu} \right)} \quad (5.14)$$

where  $\epsilon_{cu}$  is the ultimate compressive strain of the concrete material.

The minimum of the total percentage of reinforcement should not less than the minimum reinforcement required for the flexural member which is;

$$\rho_{min} = \frac{14}{f_y} \leq \rho_{total} = \left( \frac{A_s}{b \cdot d} \right) + \left( \frac{f_{py}}{f_y} \right) \left( \frac{A_{ps}}{b \cdot d} \right) \quad (5.15)$$

The maximum cross sectional area of the prestressing tendon that can be applied to the post-tensioned composite truss when the required rotation capacity is known can be find from the equation 5.16 and 5.17 below;

$$\left( \rho_{tendon} / \rho_{total} \right) = \frac{1}{(-266.9)} \left[ \left( \frac{\phi_u}{\phi_y} \right)_{required} - 72.447 \right] \quad (5.16)$$

$$A_{ps} = \frac{(\rho_{tendon} / \rho_{total})}{\left[ 1 - (\rho_{tendon} / \rho_{total}) \left( \frac{f_{py}}{f_y} \right) \right]} A_s \quad (5.17)$$

Where  $\phi_u$  is the ultimate curvature of the structure,  $\phi_y$  is the yield curvature of the structure. Please be noted that the equation 5.16 are applicable for the concrete strength of 60MPa only.

### 5.3 Serviceability

The deflection of the posttensioned composite truss can be computed from;

$$\Delta = \left( \frac{1}{\delta P} \right) \sum_{i=1}^n \int_0^L \left( \frac{F_i(x) \cdot \delta F_i(x)}{E_i(x) A_i(x)} \right) dx \quad (5.18)$$

where  $\delta P$  is the virtual unit load at mid span,  $\delta F_i(x)$  is the virtual internal force due to the virtual unit load at mid span,  $F_i(x)$ ,  $E_i(x)$ ,  $A_i(x)$  are the actual force in the real structure due to the tendon load, the dead load of steel and concrete, the external load and the increase in tendon force from the external load, the modulus of elasticity and the cross sectional area of member  $i$ , respectively, and  $n$  is the number of members of the post tensioned composite truss.

The other method to calculate the deflection is to use the effective transformed moment of inertia of the posttensioned composite section. The effective transformed moment of inertia is the moment of inertia of the transformed section considering the prestressing force from the tendon.

The relation between the percentage of relative prestressing ratio ( $A_{ps} F_{ps} / A_s F_y$ ) and the reduction factor for the calculated transformed moment of inertia is;

$$R_{I,eff} = 0.0044 \left( \frac{A_{ps} F_{ps}}{A_s F_y} \right) + 0.826 \quad (4.11)$$

Thus, the effective moment of inertia is the transformed moment of inertia times reduction factor  $R_{I,eff}$  as in the equation below,

$$I_{eff} = R_{I,eff} \cdot I_t \quad (4.12)$$

The simply supported posttensioned composite truss is subjected to two point loads of  $P$  at  $L/3$  and  $P$  at  $2L/3$  where  $L$  is the total span length of the beam. The mid-span deflection can be computed from;

$$\Delta_{midspan} = \frac{23PL^3}{648EI_{eff}} \quad (4.8)$$

For time dependent serviceability deflections related to shrinkage and creep, the effective transformed moment of inertia can be used to calculate the deflection. The deflection due to shrinkage,  $\Delta_{sh}$ , is calculated from;

$$\Delta_{SH} = \frac{ML^2}{8EI_t} \quad (2.55)$$

$$M = (\varepsilon_r E_c A_c)(e)$$

The following three equations may be solved for the restrained strain,  $\varepsilon_r$ , the strain in the bottom chord,  $\varepsilon_{bc}$  and the strain in the top chord member,  $\varepsilon_{tc}$ .

$$\varepsilon_{tc} EA_{tc} - \varepsilon_{bc} EA_{bc} = (\varepsilon_f - \varepsilon_r) E_c A_c$$

$$\varepsilon_{bc} EA_{bc} = \left(\frac{a}{b}\right) (\varepsilon_f - \varepsilon_r) A_c E_c \quad (2.54)$$

$$\left(\frac{a+b}{b}\right) \varepsilon_{tc} + \left(\frac{a}{b}\right) \varepsilon_{bc} = \varepsilon_r$$

where a is the distance from the centroid of concrete to the centroid of the transformed section, b is the distance from the centroid of the transformed section to the centroid of the bottom chord. The free shrinkage strain can be calculated from the shrinkage equation which is a function of the volume-to-surface ratio, (V/S) and the relative humidity (RH);

$$\varepsilon_f = 8.2 \times 10^{-6} \left(1 - 0.06 \left(\frac{V}{S}\right)\right) (100 - RH) \quad (4.13)$$

The deflection due to creep,  $\Delta_{cr}$ , is calculated from;

$$\Delta_{CR} = \frac{M_1 L^2}{162EI_t} + \frac{M_2 L^2}{54EI_t}$$

$$M_1 = [(\varepsilon_{cr,r} E_c A_c)(e)]_1 \quad (2.59)$$

$$M_2 = [(\varepsilon_{cr,r} E_c A_c)(e)]_2$$

where  $M_1$  and  $M_2$  are the moments from the forces equal to restrained creep strains times the elastic modulus and cross sectional areas of the concrete about the centroid of the transformed section for panel 1 and panel 2, respectively.

The restrained creep strain,  $\epsilon_{cr,r}$  is calculated the same way as in the case of shrinkage restrained strain by substituting the free creep strain,  $\epsilon_{cc}(t,t_0)$ , which is a function of the creep coefficient  $\phi(t,t_0)$ :

$$\epsilon_{cc}(t,t_0) = \frac{\sigma_c(t_0)}{E_c(28)} \phi(t,t_0) \quad (2.57)$$

where  $\sigma_c(t_0)$  is the initial elastic creep,  $E_c(28)$  is the concrete modulus of elasticity at 28 days, and  $\phi(t,t_0)$  is the creep coefficient. Using  $\phi_0$  as the basic creep;  $\beta_c(t,t_0)$  is a coefficient to account for the development of creep with time;  $h_e$  is the effective thickness in inches to account for the volume to surface ratio and equals two times the cross sectional area over the perimeter in inches of the cross section exposed to the atmosphere;  $h_0$  is the original thickness in inches; RH is the relative humidity of the ambient atmosphere in percent,  $RH_0$  is 100%,  $f_{cm}$  is the mean compressive strength at 28 days in psi;  $f_{cm0}$  equals 1450 psi;  $t_1$  equals one day, and;  $\beta_{RH}$  is the coefficient that accounts for the effect of relative humidity on shrinkage. Thus, the creep coefficient is computed from the following equations:

ศูนย์วิทยทรัพยากร  
จุฬาลงกรณ์มหาวิทยาลัย

$$\begin{aligned}
\phi(t, t_o) &= \phi_o \beta_c(t, t_o) \\
\phi_o &= \phi_{RH} \beta(f_{cm}) \beta(t_o) \\
\phi_{RH} &= 1 + \frac{1 - RH/RH_o}{0.46(h_e/h_o)^{1/3}} \\
\beta(f_{cm}) &= \frac{5.3}{(f_{cm}/f_{cmo})^{0.5}} \\
\beta(t_o) &= \frac{1}{0.1 + (t_o/t_1)^{0.2}} \\
\beta_c(t, t_o) &= \left[ \frac{(t - t_o)/t_1}{\beta_H + (t - t_o)/t_1} \right]^{0.3} \\
\beta_H &= 150 \left[ 1 + \left( 1.2 \frac{RH}{RH_o} \right)^{18} \right] \left( \frac{h_e}{h_o} \right) + 250 \leq 1500
\end{aligned} \tag{2.58}$$

The other time dependent serviceability is the deflection from the relaxation of the prestressing tendon which is calculated in a manner similar to the way precamber is calculated but in the opposite direction:

$$\Delta = \left( \frac{1}{\delta P} \right) \sum_{i=1}^n \int_0^L \left( \frac{F_i(x) \cdot \delta F_i(x)}{E_i(x) A_i(x)} \right) dx \tag{5.19}$$

where  $\delta P$  is the virtual unit load at mid span,  $\delta F_i(x)$  is the virtual internal force due to a virtual unit load at mid span,  $F_i(x)$ ,  $E_i(x)$ ,  $A_i(x)$  are the actual force in the real structure due to the change in the tendon force from the relaxation behavior, the modulus of elasticity and the cross sectional area of member  $i$ , respectively, and  $n$  is the number of members comprising the steel truss.



## CHAPTER 6

### CONCLUSIONS

#### 6.1 General Observations

Based on experimental results, posttensioned steel trusses with high performance concrete composite decks are believed to perform better than conventional composite trusses. With respect to this noticeably better performance, the following observations are presented;

(1) For the extra percentage of reinforcement ratio of the prestressing tendon ( $\rho_{\text{tendon}}/\rho_{\text{total}}$ ) or the partial prestress ratio (PPR) of 6.1%, the ultimate load capacity of the posttensioned composite truss was 68.4 tons which is 20.4% higher than the ultimate load of 56.8 tons as is the case for a similar conventional composite truss without prestressing tendons.

(2) The failure mode of the posttensioned composite truss occurs by yielding of the bottom chord while the tendon is still in the elastic zone. This behavior results in a ductile failure mode which displays detectable warning deformation and for that reason is preferred to sudden failure occurring without any noticeable ductile deformations. This favorable ductility is improved due to the presence of prestressing tendons.

(3) The level of prestressing affects the precamber amount of the posttensioned composite truss. Controlling the level of prestressing results in a controlled amount of precamber which advantageously compensates for dead and live load deflections.

(4) The level of prestressing improves the linearity of, and contributes to, a smoother more graphically stable load - deflection response. In contrast, the deflection determination of conventional composite trusses using transformed section analysis is increased by 20 per cent to account for incidentally increased deflection due to slippage, concrete cracking, and similar occurrences. By

applying prestressing forces, on the other hand, the effective transformed moment of inertia is improved by the function;  $I_{eff} = \left( 0.0044 \left( \frac{A_{ps} f_{ps}}{A_s F_y} \right) + 0.826 \right) \cdot I_t$ . Thus the effective transformed moment of inertia varies from a maximum of 17 per cent reduction to zero reduction when the ratio of  $\left( \frac{A_{ps} f_{ps}}{A_s F_y} \right)$  equals 39.55.

For a structural steel truss without a composite deck slab, the posttensioning technique has no advantage due to the likelihood of premature failure of the top chord prior to yielding of the bottom chord which usually governs maximum capacity of the truss.

## 6.2 Research Conclusions

Based on the analytical and experimental research as described herein, the following conclusions have been reached:

(1) The method of analysis based on an energy method, more specifically the principle of virtual work, and the principle of superposition, were used in the analysis. Analytically, it was found that the assumption of ideal pin joint connections resulted in better correlation with experimental results than was obtained using fixed joint assumptions. Pin joint analysis corresponded well with observed values of precamber, load - deflection response, and moment - curvature calculations.

(2) Considering the force,  $A_s F_y$ , required to yield the bottom chord, and the tensile force,  $A_{ps} f_{ps}$ , in the tendons, results in three possible levels of prestress,

$f_{ps}$ :

- i.  $f_{ps}$  is equal to the tendon stress at the yield load,  $f_{ps,yield}$ . The tendon force increases as external load is applied and the tendon force at the time the bottom chord begins to yield is called  $f_{ps,yield}$
- ii.  $f_{ps}$  equals the yield strength of the tendon,  $f_{py}$ , and;

- iii.  $f_{ps}$  equals the tensile strength of the tendon,  $f_{pu}$ , which differs by only 5% because of the relatively low percentage of the tendon area reinforcement.

The appropriate value of  $f_{ps}$  is  $f_{ps,yield}$  as based on the tendon stress at the yield load.

(3) Posttensioning improves the ultimate shear capacity of the truss with respect to web member yielding and buckling failures, but has no advantage for vertical web members located over the supports.

(4) The higher level of maximum tensile force from the summation of the yielding of the bottom chord and the tensile force in the tendon requires consideration for a higher level of shear stud design capacity.

(5) In design considerations related to the level of permissible posttensioning, yielding and buckling of the bottom chord as well as web member strength should be considered along with a consideration of concrete cracking at its tension surface. The prestressing force should also be limited in consideration of the total prestressing force combined with the effects of superimposed external loads. Forces should not exceed tendon strength and should not result in excessive precamber after considering the losses of the prestressing force. Ductility is also a criterion for determining maximum tendon forces. The total reinforcement ratio,  $\rho_{total}$ , must not be greater than  $\rho_b$ .

ศูนย์วิทยทรัพยากร  
จุฬาลงกรณ์มหาวิทยาลัย

## REFERENCES

- ACI Committee 318. Building Code Requirements for Structural Concrete (ACI 318-05) and Commentary (ACI 318R-05). Michigan : American Concrete Institute, 2005.
- American Institute of Steel Construction (AISC). Metric Load and Resistance Factor Design Specification for Structural Steel Buildings. Chicago, Illinois : American Institute of Steel Construction, INC., 1994.
- ASCE - ACI Joint Committee on Composite Construction. Tentative Recommendations for the Design and Construction of Composite Beams and Girders for Buildings. ASCE Journal of the Structural Division Vol. 86, No. ST12, (December, 1960).
- ASCE Task Committee on Design Criteria for Composite Structures in Steel and Concrete. Proposed Specification and Commentary for Composite Joists and Composite Trusses. ASCE Journal of Structural Engineering Vol. 122, No. 4, (April, 1996) : 350-358.
- Ayyub, M.B., Ibrahim, A. and Schelling, D. Posttensioned Trusses : Analysis and Design. ASCE Journal of Structural Engineering Vol. 116, No. 6, (June, 1990) : 1491-1506.
- Ayyub, M.B. and Ibrahim, A.. Posttensioned Trusses : Reliability and Redundancy. ASCE Journal of Structural Engineering Vol. 116, No. 6, (June, 1990) : 1507-1521.
- Ayyub, M.A. , Sohn, G.Y. and Saadatmanesh, H.. Prestressed Composite Girders under Positive Moment. ASCE Journal of Structural Engineering Vol. 116, No. 11, (November, 1990) : 2931-2951.
- Benson, S.. Stability of Open Web Steel Joists Subjected to Wind Uplift. Doctoral Dissertation, Department of Civil Engineering University of New Brunswick, 2009.
- Brattland, A. and Kennedy, D.J.. Shrinkage and Flexural Tests of Two Full-Scale Composite Trusses. Master's Thesis, Department of Civil Engineering University of Alberta, December, 1986.
- British Standards Institution (BSI). Design of Composite Steel and Concrete Structures. Part 1.1, General rules and rules for buildings (with U.K. National Application Document), DD ENV 1994-1-1. London : EC4, 1994.

- Canadian Institute of Steel Construction. Handbook of Steel Construction. Toronto, Ontario : Quadratone Graphics Ltd., 2003.
- Chinn, J.. Pushout Tests on Lightweight Composite Slabs. AISC Engineering Journal (October, 1965) : 129-134.
- Dywidag-Systems International (DSI). Dywidag Unbonded Monostrand Post-Tensioning Systems. [Online]. Available from : <http://www.dsiamerica.com> [2009, January].
- Easterling, W.S., Gibbings, D.R. and Murray, T.M.. Strength of Shear Studs in Steel Deck on Composite Beams and Joists. AISC Engineering Journal (April, 1993) : 44-55.
- Hiragi, H., Matsui, S., Sato, T., Alsakkaf, A., Ishizaki, S. and Ishihara, Y.. Pull-out and Shear Strength Equations for Headed Studs Considering Edge Distance. JSCE Structural Engineering Vol. 20, No. 1, (January, 2003) : 69-80.
- Hoadley, P.G.. Behavior of Prestressed Composite Steel Beams. ASCE Journal of Structural Division Vol. 89, No. ST3, (June, 1963) : 21-34.
- Klingner, R.E. and Mendonca, J.A.. Shear Capacity of Short Anchor Bolts and Welded Studs: A Literature Review. ACI Journal (September - October, 1982) : 339-343.
- Lam, D. and El-Lobody, E.. Behavior of Headed Stud Shear Connectors in Composite Beam. ASCE Journal of Structural Engineering Vol. 131, No. 1, (January, 2005) : 96-107.
- Li, W., Albrecht, P. and Saadatmanesh, H.. Strengthening of Composite Steel-Concrete Bridges. ASCE Journal of Structural Engineering Vol. 121, No. 12, (December, 1995) : 1842-1849.
- Lin, T.Y. and Burns, N.H.. Design of Prestressed Concrete Structures. Third Edition. New York : John Wiley & Sons, 1981.
- Lorenz, R.F. and Stockwell, F.W., JR. Concrete Slab Stresses in Partial Composite Beams and Girders. AISC Engineering Journal (July, 1984) : 185-188.
- Measurements Group. Student Manual for Strain Gage Technology. North Carolina : Measurement Group, Inc., 1992.
- Nethercot, D.A.. Composite Construction. New York : Spon Press, 2003.
- Oden, J.T.. Mechanics of Elastic Structures. New York : McGraw-Hill Book Company, 1967.

- Ollgaard, J.G., Slutter, R.G. and Fisher, J.W.. Shear Strength of Stud Connectors in Lightweight and Normal-weight Concrete. AISC Engineering Journal (April, 1971) : 55-64.
- Saadatmanesh, H., Albrecht, P. and Ayyub, B.M.. Analytical Study of Prestressed Composite Beams. ASCE Journal of Structural Engineering Vol. 115, No. 9, (September 1989) : 2364-2381.
- Saadatmanesh, H., Albrecht, P. and Ayyub, B.M.. Experimental Study of Prestressed Composite Beams. ASCE Journal of Structural Engineering Vol. 115, No. 9, (September 1989) : 2348-2363.
- Saadatmanesh, H., Albrecht, P. and Ayyub, B.M.. Guidelines for Flexural Design of Prestressed Composite Beams. ASCE Journal of Structural Engineering Vol. 115, No. 11, (November 1989) : 2944-2961.
- Salmon, C.G., Johnson, J.E.. Steel Structures Design and Behavior : Emphasizing Load and Resistance Factor Design. Fourth Edition. New York : HarperCollins College Publishers, 1996.
- Samuelson, D.. Composite Steel Joists. AISC Engineering Journal (July, 2002) : 111-120.
- Seri Kiatyuttachai. A Study to Propose Design Guide for High-Strength Concrete members. Master's Thesis Department of Civil Engineering Faculty of Engineering Chulalongkorn University, 1994.
- Slutter, R.G. and Driscoll, G.C.. Flexural Strength of Steel-Concrete Composite Beams. ASCE Journal of the Structural Division Vol. 91, No. ST2, (April, 1965).
- Task Group 5, Column Research Council. Classification of Steels for Structures. AISC Engineering Journal (July, 1971) : 99-109.
- Timoshenko, S.P. and Gere, J.M.. Theory of Elastic Stability. New York : McGraw-Hill Book Company, 1961.
- Topkaya, C., Yura, J.A. and Williamson, E.B.. Composite Shear Stud Strength at Early Concrete Ages. ASCE Journal of Structural Engineering Vol. 130, No. 6, (June, 2004) : 952-960.

- Uy, B. and Craine, S.. Static Flexural Behaviour of Externally Post-Tensioned Steel-Concrete Composite Beams. Advances in Structural Engineering Vol. 7 No. 1 (January, 2004) : 1-20.
- Vallenilla, C.R. and Bjorhovde, R.. Effective Width Criteria for Composite Beams. AISC Engineering Journal (October, 1985) : 169-175.
- Viest, I.M., Fountain, R.S. and Singleton, R.C.. Composite Construction in Steel and Concrete for Bridges and Buildings. New York : McGraw-Hill Book Company, Inc., 1958.
- Viest, I.M.. Review of Research on Composite Steel-Concrete Beams. ASCE Journal of the Structural Division Vol. 86, No. ST6, (June, 1960).
- Wang, Y.C.. Deflection of Steel –Concrete Composite Beams with Partial Shear Interaction. ASCE Journal of Structural Engineering Vol. 124, No. 10, (October, 1998)
- Watson, J., O'Neil, R., Barnoff, R. and Mead, E.. Composite Action without Shear Connectors. AISC Engineering Journal (April, 1974) : 29-31.



คุนยวทยทรพยากร  
จุพาลงกรณมหาวิทยาฬย



APPENDIX

ศูนย์วิทยทรัพยากร  
จุฬาลงกรณ์มหาวิทยาลัย



APPENDIX  
CALCULATION EXSAMPLES

Table A.1 Precamber from the prestressing force at 460MPa on composite truss

Member	Elastic Modulus (ksc)	Member force in Real Str. (F)	Member force ( $\delta F$ ) in Virt. Struct.	Cross Sectional Area ( $\text{cm}^2$ )	Length (cm)	Real Elongation (FL/EA), $\Delta_i$	$\delta U$ ( $\delta F \cdot \Delta_i$ )
TL4	2040000	-5874	-0.677	450.1	94.8	-0.00060644	0.000411
TL3	2040000	-2937	-1.354	450.1	94.8	-0.00030322	0.000411
TL2	2040000	0	-2.031	450.1	94.8	0	0
TL1	2040000	0	-3.047	450.1	142.2	0	0
TR1	2040000	0	-3.047	450.1	142.2	0	0
TR2	2040000	0	-2.031	450.1	94.8	0	0
TR3	2040000	-2937	-1.354	450.1	94.8	-0.00030322	0.000411
TR4	2040000	-5874	-0.677	450.1	94.8	-0.00060644	0.000411
BL4	2040000	0	0.000	24.8	94.8	0	0
BL3	2040000	-2937	0.677	24.8	94.8	-0.00550366	-0.003727
BL2	2040000	-5874	1.354	24.8	94.8	-0.01100732	-0.014907
BL1	2040000	-8811	2.031	24.8	142.2	-0.02476648	-0.050311
BR1	2040000	-8811	2.031	24.8	142.2	-0.02476648	-0.050311
BR2	2040000	-5874	1.354	24.8	94.8	-0.01100732	-0.014907
BR3	2040000	-2937	0.677	24.8	94.8	-0.00550366	-0.003727
BR4	2040000	0	0.000	24.8	94.8	0	0
VL4	2040000	0	-0.500	24.8	50.0	0	0
VL3	2040000	2169	-0.500	10.7	50.0	0.00496788	-0.002484
VL2	2040000	2169	-0.500	10.7	50.0	0.00496788	-0.002484
VL1	2040000	0	-0.500	10.7	50.0	0	0
VC	2040000	0	-1.000	10.7	50.0	0	0
VR1	2040000	0	-0.500	10.7	50.0	0	0
VR2	2040000	2169	-0.500	10.7	50.0	0.00496788	-0.002484
VR3	2040000	2169	-0.500	10.7	50.0	0.00496788	-0.002484
VR4	2040000	0	-0.500	24.8	50.0	0	0
DL4	2040000	-3651	0.842	10.7	107.2	-0.01792717	-0.01509
DL3	2040000	-3651	0.842	10.7	107.2	-0.01792717	-0.01509
DL2	2040000	-3651	0.842	10.7	107.2	-0.01792717	-0.01509
DL1	2040000	0	1.132	10.7	150.7	0	0
DR1	2040000	0	1.132	10.7	150.7	0	0
DR2	2040000	-3651	0.842	10.7	107.2	-0.01792717	-0.01509
DR3	2040000	-3651	0.842	10.7	107.2	-0.01792717	-0.01509
DR4	2040000	-3651	0.842	10.7	107.2	-0.01792717	-0.01509
$\Sigma \delta U$							-0.236723

The precamber is the total strain energy,  $\Sigma \delta U$ , from table 4.1 divided by the virtual load,  $\delta P$ , and therefore;  $\Delta = \left( \frac{1}{\delta P} \right) \sum_{i=1}^n \int_0^L \left( \frac{F_i(x) \cdot \delta F_i(x)}{E_i(x) A_i(x)} \right) dx = -0.237$

Table A.2 Precamber from the prestressing force at 690MPa on composite truss

Member	Elastic Modulus (ksc)	Member force in Real Str. (F)	Member force ( $\delta F$ ) in Virt. Struct.	Cross Sectional Area (cm <sup>2</sup> )	Length (cm)	Real Elongation (FL/EA), $\Delta_i$	$\delta U$ ( $\delta F \cdot \Delta_i$ )
TL4	2040000	-8811	-0.677	450.1	94.8	-0.00090966	0.000616
TL3	2040000	-4406	-1.354	450.1	94.8	-0.00045483	0.000616
TL2	2040000	0	-2.031	450.1	94.8	0	0
TL1	2040000	0	-3.047	450.1	142.2	0	0
TR1	2040000	0	-3.047	450.1	142.2	0	0
TR2	2040000	0	-2.031	450.1	94.8	0	0
TR3	2040000	-4406	-1.354	450.1	94.8	-0.00045483	0.000616
TR4	2040000	-8811	-0.677	450.1	94.8	-0.00090966	0.000616
BL4	2040000	0	0.000	24.8	94.8	0	0
BL3	2040000	-4406	0.677	24.8	94.8	-0.00825549	-0.00559
BL2	2040000	-8811	1.354	24.8	94.8	-0.01651098	-0.022361
BL1	2040000	-13217	2.031	24.8	142.2	-0.03714971	-0.075467
BR1	2040000	-13217	2.031	24.8	142.2	-0.03714971	-0.075467
BR2	2040000	-8811	1.354	24.8	94.8	-0.01651098	-0.022361
BR3	2040000	-4406	0.677	24.8	94.8	-0.00825549	-0.00559
BR4	2040000	0	0.000	24.8	94.8	0	0
VL4	2040000	0	-0.500	24.8	50.0	0	0
VL3	2040000	3253	-0.500	10.7	50.0	0.00745182	-0.003726
VL2	2040000	3253	-0.500	10.7	50.0	0.00745182	-0.003726
VL1	2040000	0	-0.500	10.7	50.0	0	0
VC	2040000	0	-1.000	10.7	50.0	0	0
VR1	2040000	0	-0.500	10.7	50.0	0	0
VR2	2040000	3253	-0.500	10.7	50.0	0.00745182	-0.003726
VR3	2040000	3253	-0.500	10.7	50.0	0.00745182	-0.003726
VR4	2040000	0	-0.500	24.8	50.0	0	0
DL4	2040000	-5477	0.842	10.7	107.2	-0.02689076	-0.022635
DL3	2040000	-5477	0.842	10.7	107.2	-0.02689076	-0.022635
DL2	2040000	-5477	0.842	10.7	107.2	-0.02689076	-0.022635
DL1	2040000	0	1.132	10.7	150.7	0	0
DR1	2040000	0	1.132	10.7	150.7	0	0
DR2	2040000	-5477	0.842	10.7	107.2	-0.02689076	-0.022635
DR3	2040000	-5477	0.842	10.7	107.2	-0.02689076	-0.022635
DR4	2040000	-5477	0.842	10.7	107.2	-0.02689076	-0.022635
$\Sigma \delta U$							-0.355085

The precamber is the total strain energy,  $\Sigma \delta U$ , from Table 4.2 divided by the virtual load,  $\delta P$ . Therefore;  $\Delta = \left( \frac{1}{\delta P} \right) \sum_{i=1}^n \int_0^L \left( \frac{F_i(x) \cdot \delta F_i(x)}{E_i(x) A_i(x)} \right) dx = -0.355$

Table A.3 Precamber from the prestressing force at 920MPa on composite truss

Member	Elastic Modulus (ksc)	Member force in Real Str. (F)	Member force ( $\delta F$ ) in Virt. Struct.	Cross Sectional Area ( $\text{cm}^2$ )	Length (cm)	Real Elongation (FL/EA), $\Delta_i$	$\delta U$ ( $\delta F \cdot \Delta$ )
TL4	2040000	-11749	-0.677	450.1	94.8	-0.00121287	0.000821
TL3	2040000	-5874	-1.354	450.1	94.8	-0.00060644	0.000821
TL2	2040000	0	-2.031	450.1	94.8	0	0
TL1	2040000	0	-3.047	450.1	142.2	0	0
TR1	2040000	0	-3.047	450.1	142.2	0	0
TR2	2040000	0	-2.031	450.1	94.8	0	0
TR3	2040000	-5874	-1.354	450.1	94.8	-0.00060644	0.000821
TR4	2040000	-11749	-0.677	450.1	94.8	-0.00121287	0.000821
BL4	2040000	0	0.000	24.8	94.8	0	0
BL3	2040000	-5874	0.677	24.8	94.8	-0.01100732	-0.007454
BL2	2040000	-11749	1.354	24.8	94.8	-0.02201465	-0.029814
BL1	2040000	-17623	2.031	24.8	142.2	-0.04953295	-0.100623
BR1	2040000	-17623	2.031	24.8	142.2	-0.04953295	-0.100623
BR2	2040000	-11749	1.354	24.8	94.8	-0.02201465	-0.029814
BR3	2040000	-5874	0.677	24.8	94.8	-0.01100732	-0.007454
BR4	2040000	0	0.000	24.8	94.8	0	0
VL4	2040000	0	-0.500	24.8	50.0	0	0
VL3	2040000	4338	-0.500	10.7	50.0	0.00993576	-0.004968
VL2	2040000	4338	-0.500	10.7	50.0	0.00993576	-0.004968
VL1	2040000	0	-0.500	10.7	50.0	0	0
VC	2040000	0	-1.000	10.7	50.0	0	0
VR1	2040000	0	-0.500	10.7	50.0	0	0
VR2	2040000	4338	-0.500	10.7	50.0	0.00993576	-0.004968
VR3	2040000	4338	-0.500	10.7	50.0	0.00993576	-0.004968
VR4	2040000	0	-0.500	24.8	50.0	0	0
DL4	2040000	-7302	0.842	10.7	107.2	-0.03585435	-0.03018
DL3	2040000	-7302	0.842	10.7	107.2	-0.03585435	-0.03018
DL2	2040000	-7302	0.842	10.7	107.2	-0.03585435	-0.03018
DL1	2040000	0	1.132	10.7	150.7	0	0
DR1	2040000	0	1.132	10.7	150.7	0	0
DR2	2040000	-7302	0.842	10.7	107.2	-0.03585435	-0.03018
DR3	2040000	-7302	0.842	10.7	107.2	-0.03585435	-0.03018
DR4	2040000	-7302	0.842	10.7	107.2	-0.03585435	-0.03018
$\Sigma \delta U$							-0.473447

The precamber is the total strain energy,  $\Sigma \delta U$ , from Table 4.3 divided

by the virtual load,  $\delta P$ , which is;  $\Delta = \left( \frac{1}{\delta P} \right) \sum_{i=1}^n \int_0^L \left( \frac{F_i(x) \cdot \delta F_i(x)}{E_i(x) A_i(x)} \right) dx = -0.473$

Table A.4 Vertical deformation from the steel dead load

Member	Elastic Modulus (ksc)	Member force in Real Str. (F)	Member force ( $\delta F$ ) in Virt. Struct.	Cross Sectional Area (cm <sup>2</sup> )	Length (cm)	Real Elongation (FL/EA), $\Delta_i$	$\delta U$ ( $\delta F \cdot \Delta_i$ )
TL4	2040000	-359	-0.948	24.8	94.8	-0.0006736	0.000639
TL3	2040000	-629	-1.896	24.8	94.8	-0.0011788	0.002235
TL2	2040000	-809	-2.844	24.8	94.8	-0.0015156	0.00431
TL1	2040000	-910	-4.266	24.8	142.2	-0.00255758	0.010911
TR1	2040000	-910	-4.266	24.8	142.2	-0.00255758	0.010911
TR2	2040000	-809	-2.844	24.8	94.8	-0.0015156	0.00431
TR3	2040000	-629	-1.896	24.8	94.8	-0.0011788	0.002235
TR4	2040000	-359	-0.948	24.8	94.8	-0.0006736	0.000639
BL4	2040000	0	0.000	24.8	94.8	0	0
BL3	2040000	359	0.948	24.8	94.8	0.0006736	0.000639
BL2	2040000	629	1.896	24.8	94.8	0.0011788	0.002235
BL1	2040000	809	2.844	24.8	142.2	0.00227341	0.006466
BR1	2040000	809	2.844	24.8	142.2	0.00227341	0.006466
BR2	2040000	629	1.896	24.8	94.8	0.0011788	0.002235
BR3	2040000	359	0.948	24.8	94.8	0.0006736	0.000639
BR4	2040000	0	0.000	24.8	94.8	0	0
VL4	2040000	-213	-0.500	24.8	50.0	-0.0002108	0.000105
VL3	2040000	-190	-0.500	10.7	50.0	-0.0004343	0.000217
VL2	2040000	-142	-0.500	10.7	50.0	-0.00032573	0.000163
VL1	2040000	-95	-0.500	10.7	50.0	-0.00021715	0.000109
VC	2040000	-71	-1.000	10.7	50.0	-0.00016286	0.000163
VR1	2040000	-95	-0.500	10.7	50.0	-0.00021715	0.000109
VR2	2040000	-142	-0.500	10.7	50.0	-0.00032573	0.000163
VR3	2040000	-190	-0.500	10.7	50.0	-0.0004343	0.000217
VR4	2040000	-213	-0.500	24.8	50.0	-0.0002108	0.000105
DL4	2040000	406	1.072	10.7	107.2	0.00199555	0.002139
DL3	2040000	305	1.072	10.7	107.2	0.00149666	0.001604
DL2	2040000	203	1.072	10.7	107.2	0.00099777	0.001069
DL1	2040000	107	1.507	10.7	150.7	0.00074008	0.001116
DR1	2040000	107	1.507	10.7	150.7	0.00074008	0.001116
DR2	2040000	203	1.072	10.7	107.2	0.00099777	0.001069
DR3	2040000	305	1.072	10.7	107.2	0.00149666	0.001604
DR4	2040000	406	1.072	10.7	107.2	0.00199555	0.002139
$\Sigma \delta U$							0.068074

The vertical downward deformation from the steel dead load is given by;

$$\Delta = \left( \frac{1}{\delta P} \right) \sum_{i=1}^n \int_0^L \left( \frac{F_i(x) \cdot \delta F_i(x)}{E_i(x) A_i(x)} \right) dx = +0.068$$

Table A.5 Vertical deformation from the concrete dead load

Member	Elastic Modulus (ksc)	Member force in Real Str. (F)	Member force ( $\delta F$ ) in Virt. Struct.	Cross Sectional Area ( $\text{cm}^2$ )	Length (cm)	Real Elongation (FL/EA), $\Delta_i$	$\delta U$ ( $\delta F \cdot \Delta_i$ )
TL4	2040000	-4659	-0.948	24.8	94.8	-0.00872988	0.008276
TL3	2040000	-8153	-1.896	24.8	94.8	-0.01527729	0.028966
TL2	2040000	-10482	-2.844	24.8	94.8	-0.01964222	0.055862
TL1	2040000	-11793	-4.266	24.8	142.2	-0.03314625	0.141402
TR1	2040000	-11793	-4.266	24.8	142.2	-0.03314625	0.141402
TR2	2040000	-10482	-2.844	24.8	94.8	-0.01964222	0.055862
TR3	2040000	-8153	-1.896	24.8	94.8	-0.01527729	0.028966
TR4	2040000	-4659	-0.948	24.8	94.8	-0.00872988	0.008276
BL4	2040000	0	0.000	24.8	94.8	0	0
BL3	2040000	4659	0.948	24.8	94.8	0.00872988	0.008276
BL2	2040000	8153	1.896	24.8	94.8	0.01527729	0.028966
BL1	2040000	10482	2.844	24.8	142.2	0.02946334	0.083794
BR1	2040000	10482	2.844	24.8	142.2	0.02946334	0.083794
BR2	2040000	8153	1.896	24.8	94.8	0.01527729	0.028966
BR3	2040000	4659	0.948	24.8	94.8	0.00872988	0.008276
BR4	2040000	0	0.000	24.8	94.8	0	0
VL4	2040000	-2764	-0.500	24.8	50.0	-0.00273202	0.001366
VL3	2040000	-2457	-0.500	10.7	50.0	-0.00562859	0.002814
VL2	2040000	-1843	-0.500	10.7	50.0	-0.00422144	0.002111
VL1	2040000	-1229	-0.500	10.7	50.0	-0.00281429	0.001407
VC	2040000	-921	-1.000	10.7	50.0	-0.00211072	0.002111
VR1	2040000	-1229	-0.500	10.7	50.0	-0.00281429	0.001407
VR2	2040000	-1843	-0.500	10.7	50.0	-0.00422144	0.002111
VR3	2040000	-2457	-0.500	10.7	50.0	-0.00562859	0.002814
VR4	2040000	-2764	-0.500	24.8	50.0	-0.00273202	0.001366
DL4	2040000	5267	1.072	10.7	107.2	0.02586232	0.027719
DL3	2040000	3950	1.072	10.7	107.2	0.01939674	0.020789
DL2	2040000	2634	1.072	10.7	107.2	0.01293116	0.013859
DL1	2040000	1389	1.507	10.7	150.7	0.00959147	0.014458
DR1	2040000	1389	1.507	10.7	150.7	0.00959147	0.014458
DR2	2040000	2634	1.072	10.7	107.2	0.01293116	0.013859
DR3	2040000	3950	1.072	10.7	107.2	0.01939674	0.020789
DR4	2040000	5267	1.072	10.7	107.2	0.02586232	0.027719
$\Sigma \delta U$							0.882239

The vertical downward deformation from the concrete dead load is;

$$\Delta = \left( \frac{1}{\delta P} \right) \sum_{i=1}^n \int_0^L \left( \frac{F_i(x) \cdot \delta F_i(x)}{E_i(x) A_i(x)} \right) dx = +0.882$$

Table A.6 Total elongation of the steel truss at the same level of the tendon due to the external load from the external ram loads of 58tons (yield load),  $\delta_{1p}$ .

Member	Elastic Modulus (ksc)	Member force in Real Str. (F)	Member force ( $\delta F$ ) in Virt. Struct.	Cross Sectional Area (cm <sup>2</sup> )	Length (cm)	Real Elongation (FL/EA), $\Delta_i$	$\delta U$ ( $\delta F \cdot \Delta$ )
TL4	2040000	-39288	0.647	249.9	94.8	-0.00730671	-0.00473
TL3	2040000	-78576	0.324	249.9	94.8	-0.01461342	-0.00473
TL2	2040000	-117863	0.000	249.9	94.8	-0.02192013	0
TL1	2040000	-117863	0.000	249.9	142.2	-0.0328802	0
TR1	2040000	-117863	0.000	249.9	142.2	-0.0328802	0
TR2	2040000	-117863	0.000	249.9	94.8	-0.02192013	0
TR3	2040000	-78576	0.324	249.9	94.8	-0.01461342	-0.00473
TR4	2040000	-39288	0.647	249.9	94.8	-0.00730671	-0.00473
BL4	2040000	0	0.000	24.8	94.8	0	0
BL3	2040000	39288	0.324	24.8	94.8	0.07361808	0.023828
BL2	2040000	78576	0.647	24.8	94.8	0.14723617	0.095313
BL1	2040000	117863	0.971	24.8	142.2	0.33128138	0.321681
BR1	2040000	117863	0.971	24.8	142.2	0.33128138	0.321681
BR2	2040000	78576	0.647	24.8	94.8	0.14723617	0.095313
BR3	2040000	39288	0.324	24.8	94.8	0.07361808	0.023828
BR4	2040000	0	0.000	24.8	94.8	0	0
VL4	2040000	-29010	0.000	24.8	50.0	-0.02867054	0
VL3	2040000	-29010	-0.239	10.7	50.0	-0.06645135	0.015882
VL2	2040000	-29010	-0.239	10.7	50.0	-0.06645135	0.015882
VL1	2040000	-29010	0.000	10.7	50.0	-0.06645135	0
VC	2040000	0	0.000	10.7	50.0	0	0
VR1	2040000	-29010	0.000	10.7	50.0	-0.06645135	0
VR2	2040000	-29010	-0.239	10.7	50.0	-0.06645135	0.015882
VR3	2040000	-29010	-0.239	10.7	50.0	-0.06645135	0.015882
VR4	2040000	-29010	0.000	24.8	50.0	-0.02867054	0
DL4	2040000	48838	0.402	10.7	107.2	0.2397975	0.096482
DL3	2040000	48838	0.402	10.7	107.2	0.2397975	0.096482
DL2	2040000	48838	0.402	10.7	107.2	0.2397975	0.096482
DL1	2040000	0	0.000	10.7	150.7	0	0
DR1	2040000	0	0.000	10.7	150.7	0	0
DR2	2040000	48838	0.402	10.7	107.2	0.2397975	0.096482
DR3	2040000	48838	0.402	10.7	107.2	0.2397975	0.096482
DR4	2040000	48838	0.402	10.7	107.2	0.2397975	0.096482
$\Sigma \delta U$							1.505145

Table A.7: Total elongation of the steel truss at the same level of the tendon due to the unit load in tendon,  $\delta_{11}$

Member	Elastic Modulus (ksc)	Member force in Real Str. (F)	Member force ( $\delta F$ ) in Virt. Struct.	Cross Sectional Area (cm <sup>2</sup> )	Length (cm)	Real Elongation (FL/EA), $\Delta_i$	$\delta U$ ( $\delta F \cdot \Delta$ )
TL4	2040000	-0.647	-0.647	249.9	94.8	-1.2039E-07	7.79E-08
TL3	2040000	-0.324	-0.324	249.9	94.8	-6.0196E-08	1.95E-08
TL2	2040000	0.000	0.000	249.9	94.8	0	0
TL1	2040000	0.000	0.000	249.9	142.2	0	0
TR1	2040000	0.000	0.000	249.9	142.2	0	0
TR2	2040000	0.000	0.000	249.9	94.8	0	0
TR3	2040000	-0.324	-0.324	249.9	94.8	-6.0196E-08	1.95E-08
TR4	2040000	-0.647	-0.647	249.9	94.8	-1.2039E-07	7.79E-08
BL4	2040000	0.000	0.000	24.8	94.8	0	0
BL3	2040000	-0.324	-0.324	24.8	94.8	-6.065E-07	1.96E-07
BL2	2040000	-0.647	-0.647	24.8	94.8	-1.213E-06	7.85E-07
BL1	2040000	-0.971	-0.971	24.8	142.2	-2.7293E-06	2.65E-06
BR1	2040000	-0.971	-0.971	24.8	142.2	-2.7293E-06	2.65E-06
BR2	2040000	-0.647	-0.647	24.8	94.8	-1.213E-06	7.85E-07
BR3	2040000	-0.324	-0.324	24.8	94.8	-6.065E-07	1.96E-07
BR4	2040000	0.000	0.000	24.8	94.8	0	0
VL4	2040000	0.000	0.000	24.8	50.0	0	0
VL3	2040000	0.239	0.239	10.7	50.0	5.4746E-07	1.31E-07
VL2	2040000	0.239	0.239	10.7	50.0	5.4746E-07	1.31E-07
VL1	2040000	0.000	0.000	10.7	50.0	0	0
VC	2040000	0.000	0.000	10.7	50.0	0	0
VR1	2040000	0.000	0.000	10.7	50.0	0	0
VR2	2040000	0.239	0.239	10.7	50.0	5.4746E-07	1.31E-07
VR3	2040000	0.239	0.239	10.7	50.0	5.4746E-07	1.31E-07
VR4	2040000	0.000	0.000	24.8	50.0	0	0
DL4	2040000	-0.402	-0.402	10.7	107.2	-1.9756E-06	7.95E-07
DL3	2040000	-0.402	-0.402	10.7	107.2	-1.9756E-06	7.95E-07
DL2	2040000	-0.402	-0.402	10.7	107.2	-1.9756E-06	7.95E-07
DL1	2040000	0.000	0.000	10.7	150.7	0	0
DR1	2040000	0.000	0.000	10.7	150.7	0	0
DR2	2040000	-0.402	-0.402	10.7	107.2	-1.9756E-06	7.95E-07
DR3	2040000	-0.402	-0.402	10.7	107.2	-1.9756E-06	7.95E-07
DR4	2040000	-0.402	-0.402	10.7	107.2	-1.9756E-06	7.95E-07
Tendon	1960000	1	1	1.96	862	0.00022437	0.000224
$\Sigma \delta U$							0.000237

Table A.8 Vertical deformation due to increase of tendon load,  $\Delta P$ .

Member	Elastic Modulus (ksc)	Member force in Real Str. (F)	Member force ( $\delta F$ ) in Virt. Struct.	Cross Sectional Area ( $\text{cm}^2$ )	Length (cm)	Real Elongation ( $(FL/EA), \Delta_i$ )	$\delta U$ ( $\delta F \cdot \Delta_i$ )
TL4	2040000	-3945	-0.677	249.9	94.8	-0.00073366	0.000497
TL3	2040000	-1972	-1.354	249.9	94.8	-0.00036683	0.000497
TL2	2040000	0	-2.031	249.9	94.8	0	0
TL1	2040000	0	-3.047	249.9	142.2	0	0
TR1	2040000	0	-3.047	249.9	142.2	0	0
TR2	2040000	0	-2.031	249.9	94.8	0	0
TR3	2040000	-1972	-1.354	249.9	94.8	-0.00036683	0.000497
TR4	2040000	-3945	-0.677	249.9	94.8	-0.00073366	0.000497
BL4	2040000	0	0.000	24.8	94.8	0	0
BL3	2040000	-1972	0.677	24.8	94.8	-0.00369596	-0.002503
BL2	2040000	-3945	1.354	24.8	94.8	-0.00739192	-0.010011
BL1	2040000	-5917	2.031	24.8	142.2	-0.01663182	-0.033786
BR1	2040000	-5917	2.031	24.8	142.2	-0.01663182	-0.033786
BR2	2040000	-3945	1.354	24.8	94.8	-0.00739192	-0.010011
BR3	2040000	-1972	0.677	24.8	94.8	-0.00369596	-0.002503
BR4	2040000	0	0.000	24.8	94.8	0	0
VL4	2040000	0	-0.500	24.8	50.0	0	0
VL3	2040000	1456	-0.500	10.7	50.0	0.00333616	-0.001668
VL2	2040000	1456	-0.500	10.7	50.0	0.00333616	-0.001668
VL1	2040000	0	-0.500	10.7	50.0	0	0
VC	2040000	0	-1.000	10.7	50.0	0	0
VR1	2040000	0	-0.500	10.7	50.0	0	0
VR2	2040000	1456	-0.500	10.7	50.0	0.00333616	-0.001668
VR3	2040000	1456	-0.500	10.7	50.0	0.00333616	-0.001668
VR4	2040000	0	-0.500	24.8	50.0	0	0
DL4	2040000	-2452	0.842	10.7	107.2	-0.01203891	-0.010134
DL3	2040000	-2452	0.842	10.7	107.2	-0.01203891	-0.010134
DL2	2040000	-2452	0.842	10.7	107.2	-0.01203891	-0.010134
DL1	2040000	0	1.132	10.7	150.7	0	0
DR1	2040000	0	1.132	10.7	150.7	0	0
DR2	2040000	-2452	0.842	10.7	107.2	-0.01203891	-0.010134
DR3	2040000	-2452	0.842	10.7	107.2	-0.01203891	-0.010134
DR4	2040000	-2452	0.842	10.7	107.2	-0.01203891	-0.010134
$\Sigma \delta U$							-0.158086

The vertical upward deformation from the increase in tendon load is;

$$\Delta = \left( \frac{1}{\delta P} \right) \sum_{i=1}^n \int_0^L \left( \frac{F_i(x) \cdot \delta F_i(x)}{E_i(x) A_i(x)} \right) dx = -0.158$$



Table A.9 Vertical deformation due to the external ram loads

Member	Elastic Modulus (ksc)	Member force in Real Str. (F)	Member force ( $\delta F$ ) in Virt. Struct.	Cross Sectional Area ( $\text{cm}^2$ )	Length (cm)	Real Elongation (FL/EA), $\Delta_i$	$\delta U$ ( $\delta F \cdot \Delta$ )
TL4	2040000	-39288	-0.677	249.9	94.8	-0.00730671	0.004948
TL3	2040000	-78576	-1.354	249.9	94.8	-0.01461342	0.019791
TL2	2040000	-117863	-2.031	249.9	94.8	-0.02192013	0.044529
TL1	2040000	-117863	-3.047	249.9	142.2	-0.0328802	0.100191
TR1	2040000	-117863	-3.047	249.9	142.2	-0.0328802	0.100191
TR2	2040000	-117863	-2.031	249.9	94.8	-0.02192013	0.044529
TR3	2040000	-78576	-1.354	249.9	94.8	-0.01461342	0.019791
TR4	2040000	-39288	-0.677	249.9	94.8	-0.00730671	0.004948
BL4	2040000	0	0.000	24.8	94.8	0	0
BL3	2040000	39288	0.677	24.8	94.8	0.07361808	0.04985
BL2	2040000	78576	1.354	24.8	94.8	0.14723617	0.1994
BL1	2040000	117863	2.031	24.8	142.2	0.33128138	0.672974
BR1	2040000	117863	2.031	24.8	142.2	0.33128138	0.672974
BR2	2040000	78576	1.354	24.8	94.8	0.14723617	0.1994
BR3	2040000	39288	0.677	24.8	94.8	0.07361808	0.04985
BR4	2040000	0	0.000	24.8	94.8	0	0
VL4	2040000	-29010	-0.500	24.8	50.0	-0.02867054	0.014335
VL3	2040000	-29010	-0.500	10.7	50.0	-0.06645135	0.033226
VL2	2040000	-29010	-0.500	10.7	50.0	-0.06645135	0.033226
VL1	2040000	-29010	-0.500	10.7	50.0	-0.06645135	0.033226
VC	2040000	0	-1.000	10.7	50.0	0	0
VR1	2040000	-29010	-0.500	10.7	50.0	-0.06645135	0.033226
VR2	2040000	-29010	-0.500	10.7	50.0	-0.06645135	0.033226
VR3	2040000	-29010	-0.500	10.7	50.0	-0.06645135	0.033226
VR4	2040000	-29010	-0.500	24.8	50.0	-0.02867054	0.014335
DL4	2040000	48838	0.842	10.7	107.2	0.2397975	0.201847
DL3	2040000	48838	0.842	10.7	107.2	0.2397975	0.201847
DL2	2040000	48838	0.842	10.7	107.2	0.2397975	0.201847
DL1	2040000	0	1.132	10.7	150.7	0	0
DR1	2040000	0	1.132	10.7	150.7	0	0
DR2	2040000	48838	0.842	10.7	107.2	0.2397975	0.201847
DR3	2040000	48838	0.842	10.7	107.2	0.2397975	0.201847
DR4	2040000	48838	0.842	10.7	107.2	0.2397975	0.201847
$\Sigma \delta U$							3.622469

The vertical downward deformation from the external load is;

$$\Delta = \left( \frac{1}{\delta P} \right) \sum_{i=1}^n \int_0^L \left( \frac{F_i(x) \cdot \delta F_i(x)}{E_i(x) A_i(x)} \right) dx = +3.622$$

Table A.10 Precamber from the prestressing force at 920MPa by fixed joint assumption.

Member	E (kg/cm <sup>2</sup> )	Member force in Real Str. (F)	Member force (δF) in Virt. Struct.	A (sq. cm.)	L (cm)	Real Elongation (FL/EA) Δ <sub>i</sub>	δU1 (δF*Δ <sub>i</sub> )	I <sub>x</sub> (cm <sup>4</sup> )	Member force in Real Str. (M) kg-cm		Member force (dM) in Virt. Struct. Kg-cm		δU2 (∫ MδMdx) /EI
									M1	M2	δM1	δM2	
TL4	2040000	-14338	-0.006	518	87	-0.001184	0.000007	13479	23593	-112523	-3.60	18.00	-0.002572
TL3	2040000	-11252	-0.011	518	87	-0.000929	0.000010	13479	-105263	-255898	16.70	38.40	-0.012666
TL2	2040000	-8167	-0.017	518	87	-0.000674	0.000011	13479	-250454	-399274	37.20	58.40	-0.041347
TL1	2040000	-6171	-0.021	518	135	-0.000786	0.000017	13479	-395644	-304900	57.40	105.70	-0.150898
TR1	2040000	-6171	-0.021	518	135	-0.000786	0.000017	13479	-395644	-304900	57.40	105.70	-0.150898
TR2	2040000	-8167	-0.017	518	87	-0.000674	0.000011	13479	-250454	-399274	37.20	58.40	-0.041347
TR3	2040000	-11252	-0.011	518	87	-0.000929	0.000010	13479	-105263	-255898	16.70	38.40	-0.012666
TR4	2040000	-14338	-0.006	518	87	-0.001184	0.000007	13479	23593	-112523	-3.60	18.00	-0.002572
BL4	2040000	-544	0.000	25	87	-0.000940	0.000000	477	9074	-5445	-1.70	1.00	-0.001457
BL3	2040000	-3811	0.006	25	87	-0.006577	0.000041	477	0	-3630	-0.10	0.90	-0.000109
BL2	2040000	-6897	0.012	25	87	-0.011900	0.000137	477	0	-7260	0.00	1.20	-0.000261
BL1	2040000	-9982	0.017	25	135	-0.026576	0.000449	477	-7260	-1815	0.50	1.40	-0.000729
BR1	2040000	-9982	0.017	25	135	-0.026576	0.000449	477	-7260	-1815	0.50	1.40	-0.000729
BR2	2040000	-6897	0.012	25	87	-0.011900	0.000137	477	0	-7260	0.00	1.20	-0.000261
BR3	2040000	-3811	0.006	25	87	-0.006577	0.000041	477	0	-3630	-0.10	0.90	-0.000109
BR4	2040000	-544	0.000	25	87	-0.000940	0.000000	477	9074	-5445	-1.70	1.00	-0.001457
VL4	2040000	-181	-0.005	25	50	-0.000179	0.000001	477	-9074	23593	1.70	-3.40	-0.002457
VL3	2040000	1633	-0.003	11	50	0.003742	0.000010	104	-5445	5445	2.00	-2.00	-0.003422
VL2	2040000	1633	-0.003	11	50	0.003742	0.000010	104	-3630	3630	1.00	-1.00	-0.001141
VL1	2040000	-1452	-0.003	11	50	-0.003326	0.000009	104	-1815	1815	0.70	-0.70	-0.000399
VC	2040000	1270	-0.003	11	50	0.002910	0.000009	104	0	0	0.00	0.00	0.000000
VR1	2040000	-1452	-0.003	11	50	-0.003326	0.000009	104	-1815	1815	0.70	-0.70	-0.000399
VR2	2040000	1633	-0.003	11	50	0.003742	0.000010	104	-3630	3630	1.00	-1.00	-0.001141
VR3	2040000	1633	-0.003	11	50	0.003742	0.000010	104	-5445	5445	2.00	-2.00	-0.003422
VR4	2040000	-181	-0.005	25	50	-0.000179	0.000001	477	-9074	23593	1.70	-3.40	-0.002457
DL4	2040000	-3448	0.005	11	107	-0.016931	0.000090	104	0	0	0.00	0.00	0.000000
DL3	2040000	-3267	0.006	11	107	-0.016040	0.000091	104	0	0	0.00	0.00	0.000000
DL2	2040000	-3267	0.006	11	107	-0.016040	0.000093	104	0	0	0.00	0.00	0.000000
DL1	2040000	-1996	0.005	11	151	-0.013786	0.000065	104	0	0	0.00	0.00	0.000000
DR1	2040000	-1996	0.005	11	151	-0.013786	0.000065	104	0	0	0.00	0.00	0.000000
DR2	2040000	-3267	0.006	11	107	-0.016040	0.000093	104	0	0	0.00	0.00	0.000000
DR3	2040000	-3267	0.006	11	107	-0.016040	0.000091	104	0	0	0.00	0.00	0.000000
DR4	2040000	-3448	0.005	11	107	-0.016931	0.000090	104	0	0	0.00	0.00	0.000000
ΣδU1							-0.00187	ΣδU2					-
													0.4349160 1

## BIOGRAPHY

Kanokpat Chanvaivit was born on August 3, 1979, in Bangkok Thailand. He earned his B.Eng. degree (2<sup>nd</sup> class honors) from the Department of Civil Engineering, Chulalongkorn University on April 26, 2000. He admitted into PhD. Candidate at the Department of Civil Engineering, Chulalongkorn University in 2003 with the financial support by the Royal Golden Jubilee Ph.D program (RGJ) scholarship from Thailand Research Fund (TRF). He married to Mrs. Karunee Chanvaivit on August 26, 2007 and got a baby daughter, Niya Chanvaivit on June 13, 2010.



ศูนย์วิทยทรัพยากร  
จุฬาลงกรณ์มหาวิทยาลัย